Zakia Hammouch
Mohamed Lahby
Dumitru Baleanu *Editors*

Mathematical Modeling and Intelligent Control for Combating Pandemics

🖋 Springer

Springer Optimization and Its Applications

Volume 203

Aims and Scope

Optimization has continued to expand in all directions at an astonishing rate. New algorithmic and theoretical techniques are continually developing and the diffusion into other disciplines is proceeding at a rapid pace, with a spot light on machine learning, artificial intelligence, and quantum computing. Our knowledge of all aspects of the field has grown even more profound. At the same time, one of the most striking trends in optimization is the constantly increasing emphasis on the interdisciplinary nature of the field. Optimization has been a basic tool in areas not limited to applied mathematics, engineering, medicine, economics, computer science, operations research, and other sciences.

The series **Springer Optimization and Its Applications (SOIA)** aims to publish state-of-the-art expository works (monographs, contributed volumes, textbooks, handbooks) that focus on theory, methods, and applications of optimization. Topics covered include, but are not limited to, nonlinear optimization, combinatorial optimization, continuous optimization, stochastic optimization, Bayesian optimization, optimal control, discrete optimization, multi-objective optimization, and more. New to the series portfolio include Works at the intersection of optimization and machine learning, artificial intelligence, and quantum computing.

Volumes from this series are indexed by Web of Science, zbMATH, Mathematical Reviews, and SCOPUS.

Zakia Hammouch • Mohamed Lahby •
Dumitru Baleanu
Editors

Mathematical Modeling and Intelligent Control for Combating Pandemics

Springer

Editors
Zakia Hammouch
Department of Medical Research
China Medical University Hospital
Taichung, Taiwan

Mohamed Lahby 🆔
University of Hassan II Casablanca
Casablanca, Morocco

Dumitru Baleanu
Department of Mathematics and Computer
Science
Cankaya University
Etimesgut, Türkiye

Preface

As of 2023, it has been 3 years since the emergence of the novel coronavirus (COVID-19) and the declaration of this virus as a global public health crisis by the World Health Organization (WHO). During these 3 years, the COVID-19 virus has caused significant disruptions to daily life, the economy, and healthcare systems, due to the rapid spread of the virus globally. Fortunately, statistics released by the WHO between January 2022 and January 2023 show that the number of confirmed cases and deaths due to the COVID-19 pandemic dropped significantly worldwide.

The improvement in health related to the COVID-19 pandemic is mainly due to the radical measures taken by the governments of each country affected by this pandemic. These measures include using face masks, promoting social distancing, and developing and distributing vaccines. Thanks to rapid scientific advancements of technological developments, smart tools have played active roles in developing and implementing these radical measures.

Accordingly, mathematical modeling and intelligent control techniques have captured the attention of every healthcare industry for providing quality care to patients. In this regard, mathematical modeling and intelligent control have emerged as powerful computational models and have shown significant success in combating the COVID-19 pandemic or new variants of this virus.

This book contains a total of 14 chapters classified into 2 main sections. The first part focuses on mathematical models that are useful in tackling the COVID-19 crisis. The second part provides some machine-learning techniques related to COVID-19. This book will be ideal for individuals new to the notion and application of mathematical modeling and intelligent control techniques in combating COVID-19 and for early career scholars. Additionally, advanced undergraduate- and graduate-level students who wish to learn and further extend their knowledge of data-driven informatics in COVID-19 diagnosis and management may find this book of use.

We want to take this opportunity to express our sincere thanks to the contributors to this volume and the reviewers for their outstanding efforts in reviewing and providing feedback to the authors of the chapters. The editors would like to thank Prof. Panos Pardalos (Series Editor), My Thai (Series Editor), Ms. Elizabeth Loew

(Executive Editor), and Ms. Kritheka Elango (Springer Project Coordinator) for the editorial assistance and support to help produce this important scientific work. Without this collective effort, this book would not have been possible.

Taichung, Taiwan   Zakia Hammouch
Casablanca, Morocco   Mohamed Lahby
Cankaya, Turkey   Dumitru Baleanu

Contents

COVID-19 Combating Strategies and Associated Variables for Its Transmission: An Approach with Multi-Criteria Decision-Making Techniques in the Indian Context 233

Debesh Mishra and Mohamed Lahby

Crisis Management, Internet, and AI: Information in the Age of COVID-19 and Future Pandemics 259

Karim Darban, Smail Kabbaj, and Khawla Esmaoui

About the Editors

Zakia Hammouch (https://orcid.org/0000-0002-7459-2438) is currently a full Professor at the Ecole Normale Supérieure of the University Moulay Ismail Meknès. She received her Master's in Applied Mathematics and her PhD in Numerical Analysis and Fluid Mechanics from the University of Picardie Jules Verne, Amiens, France. She is Researcher at the Division of Applied Mathematics of Thu Dau Mot University, Binh Duong, Vietnam, and Consultant at the Department of Medical Research, China Medical University Hospital, Taichung, Taiwan. She is a Member of the European Women in Mathematics (EWM) Association, a Permanent Member of the Organization for Women in Science for the Developing World (OWSD), and an Advisory Member of the Abdus Salam School of Mathematical Sciences, Pakistan. She has published more than 100 articles and chapters in indexed journals and reputable books (Springer, Elsevier, . . .). She is a member of editorial boards of several international indexed journals (*Scopus*, *WOS*, . . .).

Mohamed Lahby (https://orcid.org/0000-0002-8272-0487) is Associate Professor at the Higher Normal School (ENS) University Hassan II of Casablanca, Morocco. He was awarded a PhD in Computer Science from the Faculty of Sciences and Technology of Mohammedia, University Hassan II of Casablanca, in 2013. His research interests are wireless communication and network, mobility management, QoS/QoE, Internet of Things, smart cities, optimization, and machine learning. He has published more than 50 papers (book chapters, international journals, and conferences), 7 edited books, and 2 authored book. He has served and continues to serve on executive and technical program committees of numerous international conferences such as IEEE PIMRC, ICC, NTMS, IWCMC, WINCOM, and ISNCC. He also serves as a referee of many prestigious Elsevier journals: *Ad Hoc Networks*, *Applied Computing and Informatics*, and *International Journal of Disaster Risk Reduction*. He organized and participated in more than 40 conferences and workshops. He is the chair of many international workshops and special sessions such as MLNGSN'19, CSPSC'19, MLNGSN'20, MLNGSN'21, AI2SC'20 and WCTCP'20, CIOT'22. He has also edited many books published in Springer and Taylor & Francis.

Dumitru Baleanu (https://orcid.org/0000-0002-0286-7244) is a Professor at the Institute of Space Sciences, Magurele-Bucharest, Romania, and a visiting staff member at the Department of Mathematics, Cankaya University, Ankara, Turkey. Dumitru got his PhD from the Institute of Atomic Physics in 1996. His fields of interest include the fractional dynamics and its applications, fractional differential equations and their applications, discrete mathematics, image processing, bio-informatics, mathematical biology, mathematical physics, soliton theory, Lie symmetry, dynamic systems on time scales, computational complexity, and the wavelet method and its applications. Dumitru is a pioneer of the fractional variational principles and their applications in control theory. He is one of the co-authors of the seminal paper, entitled Anomalous diffusion expressed through fractional order differential operators in the Bloch-Torrey equation, published in the *Journal of Magnetic Resonance* (2008), which plays now a fundamental role within diffusion weighted MRI. Dumitru had an important role in developing the non-singular operators with Mittag-Leffler kernels and their applications in real-world phenomena. He is a co-author of 15 books and he published more than 1000 papers indexed in ISI journals. His H index is 61 and he is a highly cited researcher in Mathematics and Engineering in 2019. He organized several prestigious international conferences in various countries. He won the ICFDA2018 Award: Innovation in Fractional Calculus and 2019-Obada Prize. Dumitru is a co-author of a Chinese Patent No: ZL 2014 1 0033835.7 regarding chaotic maps and its important role in information encryption. He is the Editor in Chief of *Progress in Fractional Differentiation and Applications*, and he is a Co-Editor in Chief of *Discontinuity, Nonlinearity and Complexity*. Dumitru is an editorial board member of *Applied Numerical Analysis*, *Mathematics*, *Symmetry*, *Mathematical Methods in Applied Sciences*, *Fractional Calculus and Applied Analysis*, *Alexandria Journal of Engineering*, *Open Physics*, *Advances in Difference Equations*, and *Journal of Computational and Nonlinear Dynamics*.

Part I
Mathematical Modelling and Analysis for Covid-19 Pandemic

An Extended Fractional SEIR Model to Predict the Spreading Behavior of COVID-19 Disease using Monte Carlo Back Sampling

A. S. Khoojine, M. Shadabfar, H. Jafari, and V. R. Hosseini

1 Introduction

Modeling and forecasting of natural phenomena has long been of interest to scientists and researchers [1–4]. These phenomena typically have complex structures, making them difficult to model [5, 6]. The design and implementation of these models depend on many factors and require advanced techniques to understand their behavior and predict their dynamics [7–9].

Mathematical Modeling Infectious disease models can be used to project how outbreaks will progress in order to predict the likely outcomes of epidemics.

The objective of models is to estimate parameters for a variety of infectious diseases through the use of basic assumptions, collected statistics, and mathematics. These parameters are then used for calculating the impact of interventions like the programs proposed for mass vaccination programs, on the spread of the diseases [10–12]. Modeling the spread of infectious diseases is a challenging task as it requires sophisticated mathematical methods to accurately predict the course of the disease [13–16].

A. S. Khoojine
Faculty of economic and business administration, Yibin University, Yibin, China
e-mail: arashsioofy@yibinu.edu.cn

M. Shadabfar (✉)
Center for Infrastructure Sustainability and Resilience Research, Department of Civil Engineering, Sharif University of Technology, Tehran, Iran

H. Jafari
Department of Mathematical Sciences, University of South Africa, UNISA, South Africa

V. R. Hosseini
Institute for Advanced Study, Nanchang University, Nanchang, China

Forecasting of infectious diseases is a rapidly growing area of research, especially in light of the current COVID-19 pandemic [17–19]. Modeling the transmission structure of such diseases can aid in the implementation of effective monitoring and control measures, thereby reducing the number of fatalities and mitigating the negative economic and social impacts of their spread [20–22].

Mathematical modeling is involved crucially in predicting the spread of infectious diseases and shaping public health intervention strategies [23, 24]. There are various techniques used in mathematical modeling, including transmission, recovery, and mortality rate estimation, which help in visualizing the spread of the disease across different countries. The response of governments to outbreaks of infectious diseases can vary, and these responses are reflected in the transmission patterns of the disease [25, 26].

In the case of COVID-19, experts in the field developed and improved multiple modeling methods over time, taking into account real-world data and unique characteristics of the disease transmission. These models have been used to simulate the spread of the disease and to evaluate the impact of different intervention measures. Policymakers can then use the results from these models to predict the potential severity and magnitude of outbreaks and to plan for effective intervention measures. These models have proven to be a valuable tool for public health decision-making, enabling a more informed and proactive approach to disease control [27, 28].

Many researchers have attempted to use various methods of statistical analysis in order to estimate the numbers of the patients with COVID-19. Stochastic computations as well as numerical procedures have been presented for assessing diverse dimensions of the spread of COVID-19. Katoch et al., for example, applied an autoregressive integrated moving average (ARIMA) model for forecasting COVID-19 dynamics in India [29]. Malki et al. originally estimated the second rebound of this disease based on the ARIMA model and estimated the full recovery of the pandemic [30]. Furthermore, Kumar et al. analyzed the spreading profile of COVID-19 in ten infected countries [31]. Sioofy et al. develop one of the network autoregressive (NAR) models to estimate the numbers of the infected people suffering from COVID-19 in Iran with the view of the interaction of disease within the adjacent countries in the respective region [32].

A compartmental model is a commonly used method in infectious disease modeling. This model divides the population into different compartments, each represented by a label, such as S (Susceptible), I (Infectious), or R (Recovered). The labels indicate the flow pattern of the population from one compartment to another. The progression from one compartment to another is typically modeled as a set of differential equations.

Compartmental models have been widely used to simulate the spread of COVID-19, like susceptible–exposed–infected–recovered (SEIR) model and the respective modified variants. These models can further our knowledge of the spread dynamics of the disease and how it impacts different populations. By incorporating various assumptions and data on the transmission rate, recovery rate, and other factors, these models can provide a comprehensive picture of the disease spread.

Regarding COVID-19, the use of compartmental models has been instrumental in informing public health intervention strategies and decision-making. For example, the results of these models have been used to predict the potential impact of mass vaccination programs, social distancing measures, and other interventions on the spread of the disease. By providing a comprehensive view of the spread of the disease, compartmental models have proven to be a valuable tool in the fight against COVID-19 [33].

M. Nandhini et al. present a fractional-order model of COVID-19 with vaccination that considers both the efficacy and the ineffectiveness of vaccines. The model calculates the reproduction number, determines equilibrium points, and analyzes stability. Mathematical techniques such as fixed-point theory, Adomian decomposition, and Laplace integral transformation are used to find the solution and analyze the disease dynamics with different fractional orders. The study aims to improve understanding of COVID-19 transmission for better health outcomes [34].

Dawit Denu and Seth Kermausuor develop one of the mathematical models of COVID-19 with lockdown using the Caputo fractional-order derivative. The model establishes exclusiveness as well as the presence of the solutions and studies its local and global stability. The authors use a model known as residual power series to approximate a fractional power series of the solution and provide numerical and graphical results to validate their findings [35].

Hasib Khan et al. study a COVID-19 mathematical model in a fractal–fractional state to examine a solution, computational results, and stability. This model is converted to an equivalent integral form to be qualitatively analyzed using iterative convergent sequences and fixed-point approaches. The authors also use Lagrange's interpolation to create a numerical scheme for fractal–fractional model and test it with a case study, resulting in interesting findings [36, 37].

While mathematical models and compartmental approaches are useful in our knowledge of the speed and rates of the disease outbreak among society members, they come with some limitations. One significant drawback is that these models are deterministic, which raises two key concerns. Firstly, the accuracy of the models depends heavily on the quality and availability of data provided by governments and other organizations. The results generated by these models are only as credible as the data on which they are based. Secondly, the input variables, like recovery, infections, as well as the rate of mortalities, are often subject to uncertainty and variability, which can affect the accuracy of the results.

To address these concerns, it is crucial for governments and organizations to provide comprehensive and reliable data on the spread of the disease. Additionally, to reduce the impacts of variability in input variables, statistical methods, such as Bayesian modeling, can be used to incorporate prior knowledge and to account for uncertainty in the input data. By combining these techniques, practitioners may reach more precise and robust results from mathematical models and to make more informed decisions on public health interventions.

Assuming fixed input parameters in mathematical models can lead to unreliable results, as real-world disease transmission is inherently uncertain. A more rational approach to modeling the spread of infectious diseases is to incorporate this

uncertainty by treating the input parameters as random variables, rather than fixed quantities. This probabilistic approach acknowledges the inherent variability in disease transmission and provides a more nuanced view of the disease spread.

Additionally, this approach can be combined with other techniques, such as Bayesian inference, to incorporate prior knowledge and to account for additional sources of uncertainty in the input parameters. By taking a probabilistic approach to modeling the spread of infectious diseases, it is possible to generate more accurate and robust predictions of the disease trajectory and to inform decision-making with a more comprehensive understanding of the underlying uncertainty.

The fractional SIR model is a mathematical approach used in infectious disease modeling that allows for the sub-compartments of susceptible and infected populations to be raised by exponents less than unity. This is an exclusive feature of the fractional SIR model, as it recognizes the importance of susceptibility in the initial steps of an epidemic, when the disease is spreading through the infected population to larger susceptible populations.

In this context, it is more appropriate to scale the susceptible and infected populations as fractional powers, with susceptibility being given a higher weighting. This approach provides a more nuanced representation of the dynamics of disease spread during the initial stages of an outbreak and is in line with the observation that susceptibility is a key driver of the epidemic at this stage.

Studies have supported the effectiveness of the fractional SIR model in modeling infectious diseases, and its use has been shown to inform decision-making during the early stages of an outbreak [38]. By taking into account the importance of susceptibility in the early stages of an epidemic, the fractional SIR model provides a valuable tool for understanding and predicting the outbreak of infectious illnesses. The idea of the fractional exponents originates from the growth model known as Norton–Simon–Massague (NSM), which employs established energy principles for the explanation of the growth of the biological organisms. The governing differential equation in this model is as follows:

$$\frac{\mathrm{d}g(t)}{\mathrm{d}t} = l_1 g(t)^{\delta(t)} - l_1 g(t). \tag{1}$$

Anabolism growth and defuse are measured by l_1 and l_2, respectively, in which we observe the rate proportional to the growing volume $g(t)$ with a power function, whereas the rate of the former process is linear with $g(t)$. Researchers utilized various fractional compartmental models for several infectious illnesses [39, 40]:

This chapter proposes an innovative approach as follows:

1. This chapter proposes a more comprehensive and accurate model, as it takes into account various influential compartments beyond those considered in existing models.
2. The spread profile of COVID-19 is modeled using fractional differential equations, which accurately reflects the fractional nature of many natural phenomena.

3. The Monte Carlo back sampling technique is employed to estimate the unknown parameters in the model, which leads to a robust and reliable prediction of the spread of the disease.
4. Real-world data are used to calibrate the model, making it applicable to various real-world scenarios and providing valuable data into the COVID-19 spread dynamics.
5. Fractional nature of the spread of COVID-19 is evaluated, which adds to our understanding of the nature of the disease and provides a basis for future research.

The organization of the chapter is presented here: Sect. 2 defines the preliminary concepts of compartmental models and fractional derivatives. Section 3 provides an overview of the Extended SEIR model. The Monte Carlo-based back analysis procedure will be discussed in Sects. 4, and 5 describes the new model on real data. Finally, the chapter is summarized, and conclusions are drawn.

2 Preliminaries

2.1 Compartmental Models

Research has shown SIR model as an easy-to-use compartmental model so that numerous derivative models are derived from it. Three compartments are included in the model:

S: The number of individuals who are susceptible. An infectious individual contracts the disease when they come into "infectious contact" with a susceptible case.

I: The numbers of individuals infected with the disease. A susceptible individual is one who has been infected and can infect others.

R: The number of individuals who have been removed (and immune) or who have died. They have either recovered from the disease and included in the removed compartment, or they have died.

Practitioners usually omit death and birth from simple compartmental models due to the epidemic dynamic, such as influenza virus. Using the ordinary differential equations system, we can describe the SIR system with no vital dynamic as follows:

$$
\begin{cases}
\dfrac{dS}{dt} = -\dfrac{\beta I S}{N}, \\[2ex]
\dfrac{dI}{dt} = \dfrac{\beta I S}{N} - \gamma I, \\[2ex]
\dfrac{dR}{dt} = \gamma I,
\end{cases}
\tag{2}
$$

where S represents the stock of the susceptible individuals, I represents the stock of the infected individuals, and R represents the stock of the removed individuals (either recovery/or death). N represents the sum of the above 3 stocks. Although the system is nonlinear, we can derive its implicit analytic solution. The first thing to note is that

$$\frac{dS}{dt} + \frac{dI}{dt} + \frac{dR}{dt} = 0. \tag{3}$$

Therefore,

$S(t) + I(t) + R(t) = \text{constant} = N$, an expression of the constancy of the population N in mathematical terms. Considering the above relationship, we only need to study the equations for two variables.

In addition, the infectious class dynamics are governed by ratio (4):

$$R_0 = \frac{\beta}{\gamma}. \tag{4}$$

2.2 Fractional Derivatives

In this subsection, the basic definitions of fractional calculus are presented, which will be utilized later. A variety of definitions have been proposed for integrals and derivatives of non-integer order in the past. There are many definitions of integrals, but Riemann–Liouville is perhaps the most notable [41, 42].

Definition Having the integrable function $f : [a, b] \to R$ as well as a positive real number η, we can define the fractional integral of f of order η:

$$I_{a+}^{\eta} f(t) = \frac{1}{\Gamma(\eta)} \int_a^t (t - \tau)^{\eta-1} f(\tau) d\tau, \quad a < t < b \quad \text{and} \quad 0 < \eta < 1, \tag{5}$$

where Γ denotes the Gamma function.

Moreover, the Caputo fractional derivative, which is currently widely used, is determined via reformulation of the Riemann–Liouville fractional derivative to form a feasible solution for fractional initial value problems [43].

Definition The Caputo fractional derivative, so that $D = d/dt$, defined as

$$^C D_{a+}^{\eta} f(t) = D^n I_{a+}^{n-\eta} \left[f(t) - \sum_{k=0}^{n-1} \frac{f^{(k)}(a)}{k!} (t - a)^k \right]. \tag{6}$$

If we have f as the function of class C^n, hence, its fractional derivative will be determined:

$$^C D_{a+}^{\eta} f(t) = \frac{1}{\Gamma(n-\eta)} \int_a^t (t-\tau)^{n-\eta-1} f^{(n)}(\tau) d\tau, \quad n-1 < \eta < n. \qquad (7)$$

3 Extended SEIR Model

3.1 Model Formation

For developing one of the deterministic models for COVID-19 outbreak, we propose the use of an extended fractional SEIR model. In this model, the population will be grouped into 9 states, with the entire population initially as the susceptible (S). From there, individuals may either become insusceptible (P) or exposed (E), based on the level of social exposure. If exposed, they may then become infected (I). Upon diagnosis, individuals will enter quarantine (Q) and may eventually recover (R) or succumb to the disease and die (D). The relationships between these nine states are depicted in Fig. 1.

Thus, a deterministic model for COVID-19 outbreak is developed using an extended fractional SEIR model in which the population is grouped into 9 states. The mathematical relationships between these states are defined using a system of the fractional differential equations.

$$^C D_{a+}^{\eta} S(t) = -\beta \frac{S(t)I(t)}{N} - \alpha S(t) - \rho S(t) \qquad (8)$$
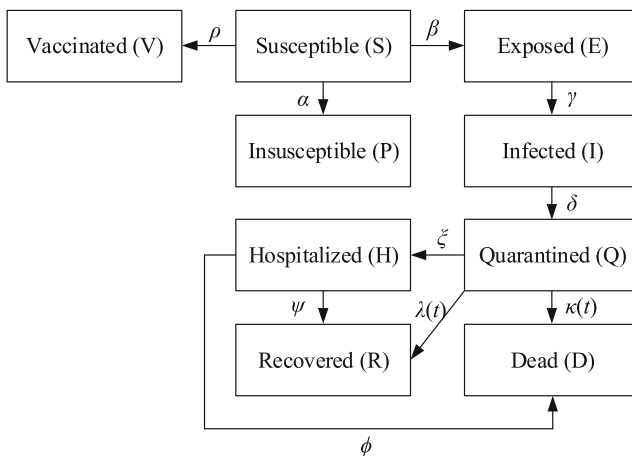
Fig. 1 The relationship between different compartments of extended SEIR model

$$^C D_{a+}^\eta E(t) = \beta \frac{S(t)I(t)}{N} - \gamma E(t) \tag{9}$$

$$^C D_{a+}^\eta I(t) = \gamma E(t) - \delta I(t) \tag{10}$$

$$^C D_{a+}^\eta Q(t) = \delta I(t) - Q(t)(\lambda(t) + \kappa(t) + \zeta) \tag{11}$$

$$^C D_{a+}^\eta H(t) = \zeta Q(t) - H(t)(\psi + \phi) \tag{12}$$

$$^C D_{a+}^\eta R(t) = \lambda(t)Q(t) + \psi H(t) \tag{13}$$

$$^C D_{a+}^\eta P(t) = \alpha S(t) \tag{14}$$

$$^C D_{a+}^\eta V(t) = \rho S(t) \tag{15}$$

$$^C D_{a+}^\eta D(t) = \kappa(t)Q(t) + \phi H(t) \tag{16}$$

$$S(0) = S_0, \; E(0) = E_0, \; V(0) = V_0, \; Q(0) = Q_0, \; I(0) = I_0, \; R(0) = R_0,$$
$$P(0) = P_0, \; V(0) = V_0, \; H(0) = H_0. \tag{17}$$

The parameters are defined as follows: α implies the rate of protection and β refers to the rate of infection. ρ stands for the rate of vaccination rate, γ represents the average latent time, δ presents the rate at which an infectious case enters quarantine, and λ refers to the time-dependent recovery rate. Finally, κ represents the time-dependent rate of deaths.

Also, $S + E + V + Q + I + R + P + S + H = N$, $(S, E, I, Q, H, R, P, V, D) \in \mathbb{R}^{+9}$, where N is the whole targeted population.

3.2 Numerical Solution

In order to solve the system of fractional differential equations of the extended SEIR, it is written as the general matrix form in this way:

$$^C D_{a+}^\eta Y(t) = A(t) \cdot Y + F(t) = f(t, Y) \quad where \quad 0 < \eta \le 1, \tag{18}$$

$$where \quad Y = [S, E, I, H, Q, R, P, V, D]^T, \tag{19}$$

$$A(t) = \begin{bmatrix} -\alpha - \rho & 0 & 0 & 0 & 0 & 0 & 0 & 0 & 0 \\ 0 & -\gamma & 0 & 0 & 0 & 0 & 0 & 0 & 0 \\ 0 & \gamma & -\delta & 0 & 0 & 0 & 0 & 0 & 0 \\ 0 & 0 & \delta & -\kappa(t) - \lambda(t) - \zeta & 0 & 0 & 0 & 0 & 0 \\ 0 & 0 & 0 & -\psi - \phi & \zeta & 0 & 0 & 0 & 0 \\ 0 & 0 & 0 & \phi & \lambda(t) & 0 & 0 & 0 & 0 \\ \alpha & 0 & 0 & 0 & 0 & 0 & 0 & 0 & 0 \\ \rho & 0 & 0 & 0 & 0 & 0 & 0 & 0 & 0 \\ 0 & 0 & 0 & \phi & \kappa(t) & 0 & 0 & 0 & 0 \end{bmatrix}, \tag{20}$$

$$\text{and} \quad F(t) = S(t)I(t)\left[\frac{-\beta}{N}, \frac{\beta}{N}, 0, 0, 0, 0, 0, 0, 0\right]^T. \tag{21}$$

Another method called Adams–Bashforth–Moulton predictor–corrector has been developed as a numerical method for solving the matrix form of a given system. This method consists of two steps: prediction and correction. In the prediction stage, therefore, an accurate approximation of the intended quantity is calculated. This initial approximation is then refined in the correction step, which involves the use of a second method, typically an implicit one. The general formula for the Adams–Bashforth–Moulton method can be written as follows:

$$y_{n+1} = y_n + \frac{h}{24}(55f_n - 59f_{n-1} + 37f_{n-2} - 9f_{n-3}) \tag{22}$$

$$y_{n+1} = y_n + \frac{h}{24}(9f_{n+1} + 19f_n - 5f_{n-1} + f_{n-2}), \tag{23}$$

where h is the step size, f_n is the function to be evaluated, and y_n is the estimated value of the solution at the nth step. The Adams–Bashforth–Moulton method is a highly efficient numerical method that can provide accurate solutions to a wide range of differential equation problems.

4 Monte Carlo Back Sampling

We have established the formulation of the extended SEIR model, including the fractional form of the differential equations and their solution. Our goal is the determination of the optimal values of unknown parameters in that model, namely β, α, γ, δ, λ_0, λ_1, κ_0, κ_1, ζ, ρ, ψ, and ϕ, so that the model accurately represents the observed data. In this section, we present a modern two-step optimization algorithm that leverages Monte Carlo-based back analysis to find the best values of the parameters when η is assumed to be 1.

Therefore, parameters of the problem are treated as random variables in order to complete the back analysis approach. This allows for the evaluation of various combinations of these parameters and consideration of a range of values for them. We conceptualize the parameter combinations as a lattice, where the parameters are arranged within a set of defined ranges and the x- and y-axes represent the parameters in this range. It is assumed that a random walk on the lattice results in a range of parameter values. Table 1 displays the ranges of changes specified in each of the random variables [44–46].

The next step is to generate 10,000 realizations for each random variable. After introducing each realization into the differential equation system, a new extended SEIR problem is created that can be solved using the previously described method. In this way, 10,000 distinct predictions can be made regarding how the disease will spread over time. It is employed as an input for the back analysis algorithm

Table 1 Random variables and the corresponding range of variations

No.	Parameters	Distribution function	Min	Max
1	β	Uniform	0.0	10.0
2	α	Uniform	0.0	0.5
3	γ	Uniform	0.0	0.05
4	δ	Uniform	0.0	0.5
5	λ_0	Uniform	0.0	0.5
6	λ_1	Uniform	0.0	0.5
7	κ_0	Uniform	0.0	0.5
8	κ_1	Uniform	0.0	0.5
9	ζ	Uniform	0.0	0.1
10	ρ	Uniform	0.0	0.1
11	ψ	Uniform	0.0	0.1
12	ϕ	Uniform	0.0	0.1

Fig. 2 Schema of the Monte Carlo sampling process

to calculate I, R, D, and V based on the database. A schematic representation of the Monte Carlo sampling process can be found in Fig. 2. It is necessary to collect the actual observations of COVID-19, including I, R, D, and V, before implementing the back analysis method. An interval of 15% above and below the observed data is then used as a filter to select the cases that are closest to the observed data among the 10,000 realizations of I, R, D, and V. Consequently, the allowable area is determined by a sample selection criterion which guides the algorithm toward finding the best fit. In Fig. 1, the selection and rejection of samples is schematically depicted in Fig. 3. It is necessary to collect true observations of COVID-19, including I, R, D, and V, before implementing the back analysis method. An interval of 15% above and below the observed data is then applied as one of the filters for selecting the cases that are closest to the data found among 10,000 realizations of I, R, D, and V. Consequently, the permissible region would be determined by a criterion for selecting the samples which guides the algorithm for discovering the best fit. In Fig. 1, the selection and rejection of samples is schematically depicted. When the proposed threshold is applied to the data, some of the 10,000 samples fall within the acceptable range. After that, a second-round selection is conducted using a new criterion to determine which sample is the best
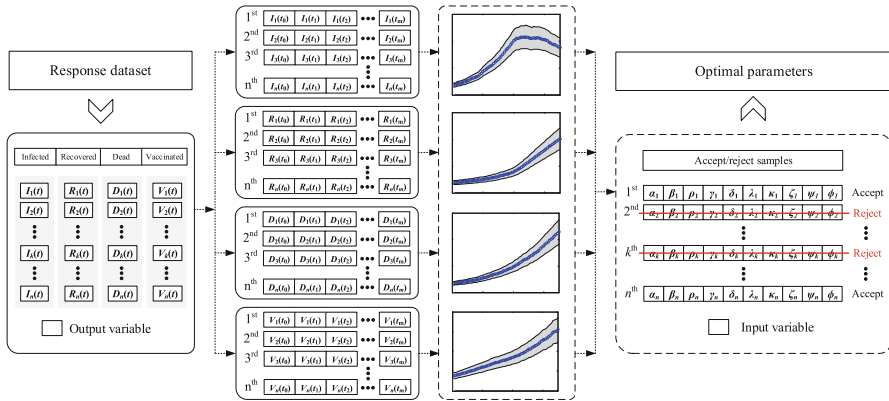
Fig. 3 Schematic diagram of the proposed back analysis method

from those previously selected. Accordingly, the root mean square error (RMSE) between the predicted and observed time series of I, R, D, and V is calculated of the sample, as follows:

$$\theta_{1,i} = \sqrt{\sum_{t=0}^{t_{now}} \left(I(t) - I_i^S(t) \right)^2}, \tag{24}$$

$$\theta_{2,i} = \sqrt{\sum_{t=0}^{t_{now}} \left(R(t) - R_i^S(t) \right)^2}, \tag{25}$$

$$\theta_{3,i} = \sqrt{\sum_{t=0}^{t_{now}} \left(D(t) - D_i^S(t) \right)^2}, \tag{26}$$

$$\theta_{4,i} = \sqrt{\sum_{t=0}^{t_{now}} \left(V(t) - V_i^S(t) \right)^2}, \tag{27}$$

where $\theta_{1,i}$, $\theta_{2,i}$, $\theta_{3,i}$, and $\theta_{4,i}$, respectively, stand for RMSE of the ith sample for the infected, recovered, dead, and vaccinated, and $I(t)$, $R(t)$, $D(t)$, and $V(t)$, respectively, refer to true measurements of the infected, recovered, dead, and vaccinated cases. Finally, $I_i^S(t)$, $R_i^S(t)$, $D_i^S(t)$, and $V_i^S(t)$, respectively, represent time series of the infected, recovered, dead, and vaccinated cases for the ith sample that are computed by the new extended SEIR model.

In order to define the final selection criterion, θ_t, we must combine the RMSEs of the variables I, R, D, and V, using a square root of the sum of squares.

$$\theta_t = \sqrt{\left(\theta_{1,i} \right)^2 + \left(\theta_{2,i} \right)^2 + \left(\theta_{3,i} \right)^2 + \left(\theta_{4,i} \right)^2}. \tag{28}$$

5 Application of the Fractional Extended SEIR Model

In this section, we apply the extended SEIR model to analyze Thailand COVID-19 data. The actual observations of I, R, D, and V in Thailand were collected from the online databases of the World Health Organization (WHO) and are plotted in Fig. 4. The figure also displays intervals 15% above and below the observed data. With the selected threshold, 40 samples are chosen as the best fit the θ_1, θ_2, and θ_3 are calculated. Columns 6 and 12 of Table 2 present θ_t results.

In Table 2, the sample with the lowest θ_t is selected as the best fit from the earlier assigned 40 samples. Table 3 presents optimal parameters of this sample. In addition, Fig. 5 is the time series of I, R, D, and V corresponding to the optimal parameters.

The Extended SEIR model is presented in fractional form, which enables it to handle differential equations of orders less than unity, i.e., $\eta \leq 1$. This capability is a distinct advantage for optimization and regression models, as it provides a new level of flexibility in fitting the data to the model. Therefore, the order of the differential equations is signified as a decision variable, which can assume values less than unity and fractional form of the problem is then solved, and thus the final fit is evaluated to determine improvements in prediction accuracy.

To investigate the effects of the decision variable on the performance of the model, eleven different values of η, including $\eta = 0$, 0.5, 0.6, 0.65, 0.7, 0.75, 0.8, 0.85, 0.9, 0.95, and 1, were considered. The fractional form of the extended SEIR problem was determined for each η value using the method outlined in Sect. 3. The resulting time series of I, R, and D were stored and presented in Table 4, which shows the values of θ_1, θ_2, and θ_3, as well as θ for each η. Additionally, the corresponding time series of I, R, and D are drawn against various values of η in Fig. 6.
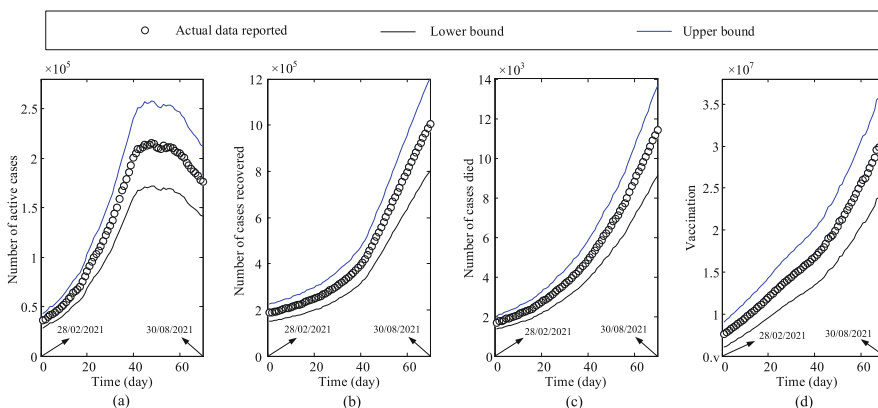
Fig. 4 Permissible interval presented above and below the observed data for (**a**) the infected, (**b**) recovered, (**c**) dead, and (**d**) vaccinated cases

Table 2 RMSE for 40 samples

No.	$\theta_1 \, (\times 10^4)$	$\theta_2 \, (\times 10^4)$	$\theta_3 \, (\times 10^6)$	$\theta_4 \, (\times 10^2)$	$\theta_t \, (\times 10^6)$	No.	$\theta_1 \, (\times 10^4)$	$\theta_2 \, (\times 10^4)$	$\theta_3 \, (\times 10^6)$	$\theta_4 \, (\times 10^2)$	$\theta_t \, (\times 10^6)$
1	3.96	2.05	4.69	3.09	4.69	21	9.45	1.87	4.35	2.86	4.35
2	5.07	2.26	4.63	2.90	4.63	22	3.09	2.38	4.60	3.49	4.60
3	10.30	2.31	4.39	2.77	4.40	23	8.36	2.47	3.85	3.25	3.85
4	2.50	1.83	3.52	1.39	3.52	24	5.60	2.44	4.16	3.50	4.16
5	5.15	2.02	4.25	3.20	4.25	25	10.70	2.26	4.44	2.74	4.45
6	5.19	1.99	4.65	2.84	4.65	26	8.33	2.08	4.59	2.36	4.59
7	6.77	2.45	4.55	2.03	4.55	27	2.51	2.38	4.07	3.28	4.07
8	4.11	2.42	4.58	2.70	4.58	28	3.86	2.51	4.17	2.28	4.17
9	4.79	2.00	4.44	3.22	4.44	29	7.62	2.52	4.09	3.10	4.09
10	7.83	2.44	3.83	2.47	3.83	30	9.81	2.29	4.54	2.53	4.54
11	4.27	2.45	4.23	2.94	4.23	31	6.65	2.31	4.67	1.95	4.67
12	10.00	2.15	4.44	2.64	4.44	32	7.08	2.53	4.17	1.82	4.17
13	8.13	2.02	4.66	2.36	4.66	33	7.84	2.52	4.18	1.95	4.18
14	2.53	2.34	4.45	2.79	4.45	34	3.48	2.46	4.22	2.59	4.22
15	4.17	2.39	4.38	2.42	4.38	35	6.65	2.35	3.90	3.44	3.90
16	9.64	2.07	4.52	3.19	4.52	36	4.50	2.25	4.56	3.06	4.56
17	5.36	2.28	4.61	3.08	4.61	37	9.45	2.33	4.48	3.47	4.48
18	5.41	2.11	4.46	1.69	4.46	38	9.44	2.06	4.73	2.63	4.73
19	7.52	2.38	4.61	3.34	4.61	39	10.00	2.42	4.62	3.03	4.62
20	4.36	2.31	4.17	3.19	4.17	40	5.81	2.13	4.54	1.93	4.54

Table 3 The optimal values of parameters

No.	Parameter	Value	No.	Parameter	Value
1	β	5.1769	7	κ_0	0.0360
2	α	0.1599	8	κ_1	0.1239
3	γ	0.0294	9	ζ	0.0061
4	δ	0.3246	10	ρ	0.0837
5	λ_0	0.1773	11	ψ	0.0010
6	λ_1	0.3034	12	ϕ	0.0015
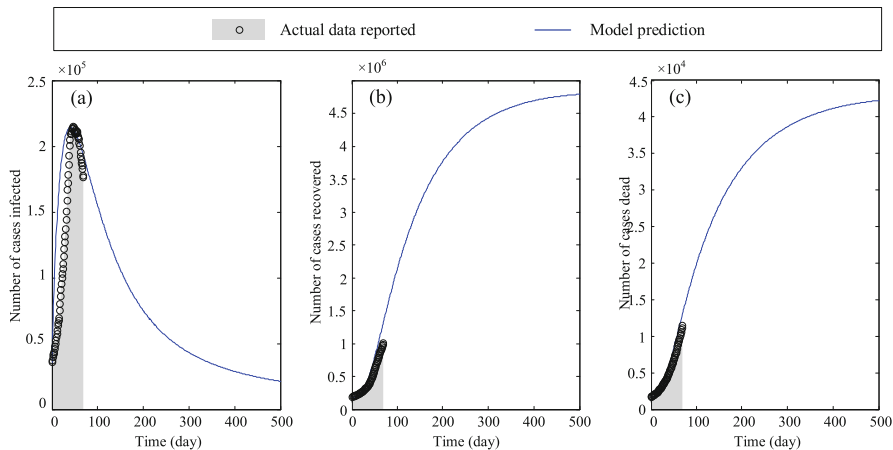
Fig. 5 Predictions of the model based on the optimal parameters

Table 4 RMSE values for different η

No.	η	θ_1 ($\times 10^4$)	θ_2 ($\times 10^4$)	θ_3 ($\times 10^6$)	θ_4 ($\times 10^2$)	θ_t ($\times 10^6$)
1	0.50	4.20	2.16	4.07	1.90	4.07
2	0.55	5.29	2.29	3.89	2.19	3.89
3	0.60	5.55	2.12	3.54	1.77	3.54
4	0.65	2.96	2.12	3.59	1.41	3.59
5	0.70	3.14	2.26	3.87	2.19	3.87
6	0.75	5.72	2.21	4.10	2.00	4.10
7	0.80	4.49	2.22	4.20	2.22	4.20
8	0.85	3.39	2.27	3.43	2.03	3.43
9	0.90	2.12	1.81	2.58	1.15	2.58
10	0.95	4.74	2.21	3.37	1.90	3.37
11	1.00	2.50	1.83	3.52	1.39	3.52
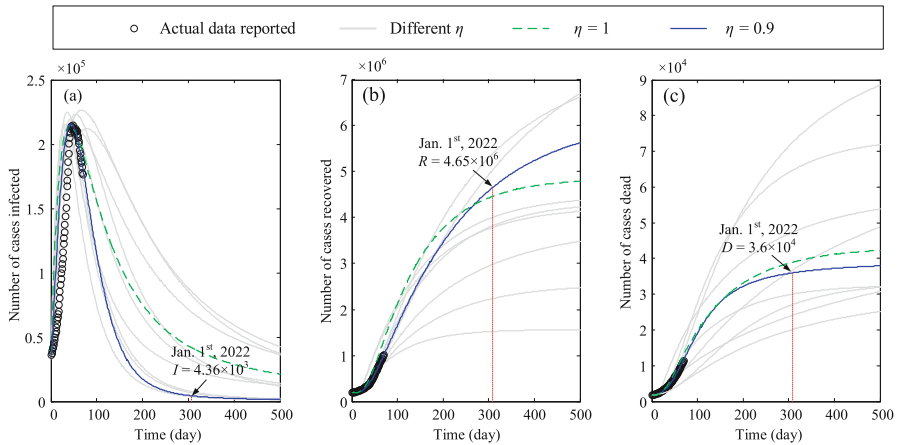
Fig. 6 The resulting fit on the data for different η

The most acceptable result is determined for $\eta = 0.9$. Put differently, if $\eta = 0.9$, a more acceptable fit to data is received, and θ_t will be minimized. In comparison to the assumption $\eta = 1$, θ_t value changes from 3.52 to 2.58, which is a 27% decrease in the error measured. A recent study indicates that at the beginning of 2022, roughly 4300 people will be infected, recovered, and dead in Thailand. Compared to the previous section, these results are based on a better and more reliable fit obtained using the fractional model.

6 Conclusion

As part of this chapter, a compartmental model is developed using a fractional extended SEIR model that is used for predicting the outbreak profile of Coronavirus disease. A Monte Carlo back analysis is conducted using the proposed model in which the parameters for the model are treated as random variables, namely β, α, γ, δ, λ_0, λ_1, κ_0, κ_1, ζ, ρ, and ψ. Hence, with the generation of a set of random samples for each of the random variables, we observe that the Monte Carlo back analysis can determine if the parameters' predictions are within a desired range around the observed values. In order to determine the best fit to the real data, therefore, the RMSE criterion would be utilized to the chosen samples. The accuracy of the fit is investigated using a sensitivity analysis. In addition, the proposed model is applied to Thailand's COVID-19 data, and the fractional-order results indicate a more acceptable fit with the actual data. In conclusion, fractional extended SEIR model has been used to successfully forecast the outbreak profile of Coronavirus disease. Through incorporating fractional-order results, we observe improvement in the model accuracy. Consequently, this research findings could be employed for

assisting in the design of effective control approaches to mitigate COVID-19 spread in the future. In addition, the proposed model can be extended to other diseases, such as influenza and malaria, and can be used to better understand the spread of these diseases and develop control strategies to reduce their impact. Furthermore, this study can be extended to include the effects of social distancing and other strategies on disease spread. Finally, this model can be applied for studying the impacts of various demographic characteristics on disease spread, such as age, gender, and socio-economic status.

References

1. Kretzschmar, M., Wallinga, J.: Mathematical Models in Infectious Disease Epidemiology. Statistics for Biology and Health. Springer, New York (2010). https://doi.org/10.1007/978-0-387-93835-6_12
2. Anderson, R.M., May, R.M.: Infectious Diseases of Humans: Dynamics and Control. Oxford University Press, Oxford (1992)
3. Keeling, M.J., Eames, K.T.: Networks and epidemic models. J. R. Soc. Interface **2**(4), 295–307 (2005)
4. Grundmann, H., Hellriegel, B.: Mathematical modelling: a tool for hospital infection control. Lancet Infect. Dis. **6**(1), 39–45 (2006)
5. Meerschaert, M.M.: Mathematical Modeling. Academic Press, London (2013)
6. Gershenfeld, N.A., Gershenfeld, N.: The Nature of Mathematical Modeling. Cambridge University Press, Cambridge (1999)
7. Heinz, S.: Mathematical Modeling. Springer, Heidelberg (2011)
8. Bender, E.A.: An Introduction to Mathematical Modeling. Courier Corporation, Chelmsford (2000)
9. Nogueira, P.J., de Araújo Nobre, M., Costa, A., Ribeiro, R.M., Furtado, C., Bacelar Nicolau, L., Camarinha, C., Luís, M., Abrantes, R., Vaz Carneiro, A.: The role of health preconditions on COVID-19 deaths in Portugal: evidence from surveillance data of the first 20293 infection cases. J. Clin. Med. **9**(8), 2368 (2020). https://doi.org/10.3390/jcm9082368
10. Grassly, N., Fraser, C.: Mathematical models of infectious disease transmission. Nat. Rev. Microbiol. **6**, 477–487 (2008). https://doi.org/10.1038/nrmicro1845
11. Odagaki, T.: Exact properties of SIQR model for COVID-19. Phys. A: Stat. Mech. Appl. **564**, 125564 (2021). https://doi.org/10.1016/j.physa.2020.125564
12. Liu, Q., Jiang, D., Shi, N.: Threshold behavior in a stochastic SIQR epidemic model with standard incidence and regime switching. Appl. Math. Comput. **316**, 310–325 (2018). https://doi.org/10.1016/j.amc.2017.08.042
13. Dietz, K., Schenzle, D.: Mathematical models for infectious disease statistics. In: A Celebration of Statistics, pp. 167–204, (1985)
14. Li, M.Y.: An Introduction to Mathematical Modeling of Infectious Diseases, vol. 2. Springer, Cham (2018)
15. Choisy, M., Guégan, J.F., Rohani, P.: Mathematical Modeling of Infectious Diseases Dynamics. Encyclopedia of Infectious Diseases: Modern Methodologies, vol. 379. Wiley, London (2007)
16. James, L.P., Salomon, J.A., Buckee, C.O., Menzies, N.A.: The use and misuse of mathematical modeling for infectious disease Policymaking: lessons for the COVID-19 pandemic. Med. Decis. Making **41**(4), 379–385 (2021)
17. Rahimi, I., Chen, F., Gandomi, A.H.: A review on COVID-19 forecasting models. Neural. Comput. Appl., 1–11 (2021)

18. Venkatramanan, S., Vullikanti, A.: Mathematical models for covid-19 pandemic: a comparative analysis. J. Indian Inst. Sci. **100**(4), 793–807 (2020)
19. Santosh, K.C.: COVID-19 prediction models and unexploited data. J. Med. Syst. **44**(9), 1–4 (2020)
20. Enserink, M., Kupferschmidt, K.: With COVID-19, modeling takes on life and death importance. Science **367**, 1414–1415 (2020)
21. Eker, S.: Validity and usefulness of COVID-19 models. Humanit. Soc. Sci. Commun. **7**(1), 1–5 (2020)
22. Bani Younes, A., Hasan, Z.: COVID-19: modeling, prediction, and control. Appl. Sci. **10**(11), 3666 (2020)
23. Adiga, A., Dubhashi, D., Lewis, B., Marathe, M., Venkatramanan, S., Vullikanti, A.: Mathematical models for covid-19 pandemic: a comparative analysis. J. Indian Inst. Sci. **100**(4), 793–807 (2020)
24. Samui, P., Mondal, J., Khajanchi, S.: A mathematical model for COVID-19 transmission dynamics with a case study of India. Chaos Solit. Fractals **140**, 110173 (2020)
25. Shankar, S., Mohakuda, S.S., Kumar, A., Nazneen, P.S., Yadav, A.K., Chatterjee, K., Chatterjee, K.: Systematic review of predictive mathematical models of COVID-19 epidemic. Med. J. Armed Forces India **77**, S385–S392 (2021)
26. Tang, Y., Wang, S.: Mathematics modeling of COVID-19 in the United States. Emerg. Microbes Infect. **9**(1), 827–829 (2020)
27. Wang, J.: Mathematical models for COVID-19: Applications, limitations, and potentials. J. Public Health Emerg. **4**, 9 (2020)
28. Khajanchi, S., Sarkar, K., Mondal, J., Nisar, K. S., Abdelwahab, S.F.: Mathematical modeling of the COVID-19 pandemic with intervention strategies. Results Phys. **25**, 104285 (2021)
29. Katoch, R., Sidhu, A.: An application of ARIMA model to forecast the dynamics of COVID-19 epidemic in India. Glob. Bus. Rev. 0972150920988653 (2021)
30. Malki, Z., Atlam, E.S., Ewis, A., Dagnew, G., Alzighaibi, A.R., ELmarhomy, G., Elhosseini, M.A., Hassanien, A.E., Gad, I.: ARIMA models for predicting the end of COVID-19 pandemic and the risk of second rebound. Neural Comput. Appl. **33**, 2929–2948 (2021). https://doi.org/10.1007/s00521-020-05434-0
31. Kumar, N., Susan, S.: COVID-19 Pandemic prediction using time series forecasting models. In: Proceedings of the 2020 11th International Conference on Computing, Communication and Networking Technologies, ICCCNT 2020, Kharagpur, India, 1–3 July 2020. https://doi.org/10.1109/ICCCNT49239.2020.9225319
32. Sioofy Khoojine, A., Shadabfar, M., Hosseini, V.R., Kordestani, H.: Network autoregressive model for the prediction of COVID-19 considering the disease interaction in neighboring countries. Entropy **23**, 1267 (2021). https://doi.org/10.3390/e23101267
33. Mohamadou, Y., Halidou, A., Kapen, P.T.: A review of mathematical modeling, artificial intelligence and datasets used in the study, prediction and management of COVID-19. Appl. Intell. **50**(11), 3913–3925 (2020). https://doi.org/10.1007/s10489-020-01770-9
34. Nandhini, M., Lavanya, R., Nieto, J.J.: A fractional COVID-19 model with efficacy of vaccination. Axioms **11**, 446 (2022). https://doi.org/10.3390/axioms11090446
35. Denu, D., Kermausuor, S.: Analysis of a fractional-order COVID-19 epidemic model with lockdown. Vaccines **10**, 1773 (2022). https://doi.org/10.3390/vaccines10111773
36. Khan, H., Ahmad, F., Tunç, O., Idrees, M.: On fractal-fractional Covid-19 mathematical model. Chaos Solit. Fractals **157**, (2022). https://doi.org/10.1016/j.chaos.2022.111937
37. Kudryashov, N.A., Chmykhov, M.A., Vigdorowitsch, M.: Analytical features of the SIR model and their applications to COVID-19. Appl. Math. Model. **90** (2021) 466–473. https://doi.org/10.1016/j.apm.2020.08.057
38. Sioofy Khoojine, A., Mahsuli, M., Shadabfar, M., Hosseini, V.R., Kordestani, H.: A proposed fractional dynamic system and Monte Carlo-based back analysis for simulating the spreading profile of COVID-19. Eur. Phys. J. Spec. Top. **231**, 1–11 (2022)
39. Gerlee, P.: The model muddle: in search of tumor growth laws. Can. Res. **73**, 2407–2411 (2013). https://doi.org/10.1158/0008-5472.CAN-12-4355

40. Gonzalez-Parra, G., Arenas, A.J., ChenCharpentier, B.M.: A fractional order epidemicmodel for the simulation of outbreaks of influenza A(H1N1). Math. Methods Appl. Sci. **37**, 2218–2226 (2014) https://doi.org/10.1002/mma.296
41. Babaei, A., Jafari, H., Banihashemi, S., Ahmadi, M.: Mathematical analysis of a stochastic model for spread of coronavirus. Chaos, Solit. Fractals **145**, 110788 (2021). https://doi.org/10.1016/j.chaos.2021.110788
42. Babaei, A., Jafari, H., Banihashemi, S., Ahmadi, M.: A stochastic mathematical model for COVID-19 according to different age groups. Appl. Comput. Math. **20**, 140–159 (2021)
43. Babaei, A., Ahmadi, M., Jafari, H., Liya, A., A mathematical model to examine the effect of quarantine on the spread of coronavirus. Chaos Solit. Fractals **142**, 110418 (2021). https://doi.org/10.1016/j.chaos.2020.110418
44. Shadabfar, M., Mahsuli, M., Khoojine, A.S., Hosseini, V.R.: Time-variant reliability-based prediction of COVID-19 spread using extended SEIVR model and Monte Carlo sampling, Results Phys. **26**, 104364 (2021). https://doi.org/10.1016/j.rinp.2021.104364. ISSN 2211–3797
45. Ebrahimpour, Z., Wan, W., Khoojine, A.S., Hou, L.: Twin hyper-ellipsoidal support vector machine for binary classification. IEEE Access **8**, 87341–87353 (2020), https://doi.org/10.1109/ACCESS.2020.2990611
46. Abbasi, A., MahmoudZadeh, S., Yazdani, A. et al.: Feasibility assessment of Kian-I mobile robot for autonomous navigation. Neural Comput. Applic. **34**, 1199–1218 (2022). https://doi.org/10.1007/s00521-021-06428-2

Dynamics and Optimal Control Methods for the COVID-19 Model

Saida Id ouaziz and Mohammed EL Khomssi

1 Introduction

In many different parts of the world, respiratory and gastrointestinal disorders are caused by a group of viruses known as coronaviruses. Respiratory conditions can include both the typical cold and more serious infections. Under a microscope, coronaviruses resemble coronas, hence their name. The virus's genetic core is encased in an injected envelope. As a result, it has the appearance of a crown. Latin's "corona" refers to the "diamond."

According to research on the Between Nations Disease Spread that was conducted using an approximative mathematical model of COVID-19, the most significant risk of importing an ill person from other affected regions is in the USA. The dynamics of COVID-19 have been studied using a variety of epidemic models. In [1], the authors explain in detail how to model COVID-19 using the omicron form and display their mathematical outcomes. In this study, they discuss the local and global steadiness of equilibria. They use the previously new digital procedure disclosed for solving fractional differential systems to show the digital representation of the model. A mathematical model was presented in [2] to examine the impacts of quarantine, self-isolation, and environmental load. The authors of [3] examined the mechanics of a fractional-order of a sample version of COVID-19. This fractional-order corona model is digitally resolved through an approach of efficient computation. In [4], the coronavirus is a single-stranded, positively stranded encapsulated virus that belongs to the Nidovirales order and family Coronaviridae. The authors replicate the transmission of a specific illness and describe global parts at risk utilizing the spatial and temporal epidemiological template to investigate

S. Id ouaziz (✉) · M. EL Khomssi
Department of Mathematics, Laboratory of Modeling and Mathematical Structures, Sidi Mohamed Ben Abdellah University, Fez, Morocco

the development of human infections over nations. The effect of immunization on COVID-19 transmission is examined by the authors of [5]. They perform a mathematical analysis to prove the positivity, the delimitation, the equilibrium of the free disease point, and the basic reproductive rate of the template. Also, they incorporate the COVID-19 data into the model results and investigate the impact of vaccination on the expansion of the pandemic, indicating a considerable diminution of the number of instances while accounting for uncertainties in all model states and factors that are not satisfactorily evident. The use of the fractional mathematical modeling approach may be found in [6] and offers a greater understanding of the dynamics of a variety of phenomena including infectious illnesses. The authors of [7] investigated the connection between corruption and the media, and they offered a brand-new nonlinear mathematics media effect model. Only when $\mathcal{R}_0 > 1$, the endemic equilibrium does exist. The authors of [8] showed that the bioflavonoid rutin and the infectious drug doxycycline are the most effective inhibitors of the coronavirus genre linked to chronic strict respiratory syndrome (SARS). Seven distinct sections make up the entire chapter. The introduction is in Sect. 1. The template is provided in Sect. 2. A qualitative study of the model is discussed in Sect. 3. Model sensitivity is completed in Sect. 4. The regulated mathematical model is covered in Sect. 5. Section 6 gives a detailed explanation of the digital validation of the suggested template and offers ideas on the essential parameters that affect the COVID-19 dynamic. Section 7 concludes the chapter.

2   Description of the Model

The subordinate model divides the entire population denoted by N(t) into five categories: susceptible S_I, exposed E_I, infected or exhibiting symptoms I, people who are ill but not yet declared U_d recovered R. The total population is correspondingly written as $N = S_I + E_I + I + U_d + R$. Models based on this kind of structure just represent the behavior of the population of sick people without measuring the quantity of germs present within each individual. Figure 1, which illustrates the biological mechanism of coronavirus in humans, serves as the foundation for our model. Since it is a representation of the COVID-19 model, it contains all of the specifications of the variables included in Table 1.

To investigate the effects of a phenomenon on a particular mathematical model, one must always adopt a set of circumstances. We list these conditions below as specified in the citation for [9]:

1) According to the model, a net intake of vulnerable individuals occurs at Π per unit of time.
2) It does not take zoonotic coronavirus infections into account and solely looks at how the pandemic spreads through people.
3) There are no practical safeguards in place before April 10, 2020.
4) The model allows for proportional natural mortality in every subpopulation which has some demographic repercussions.
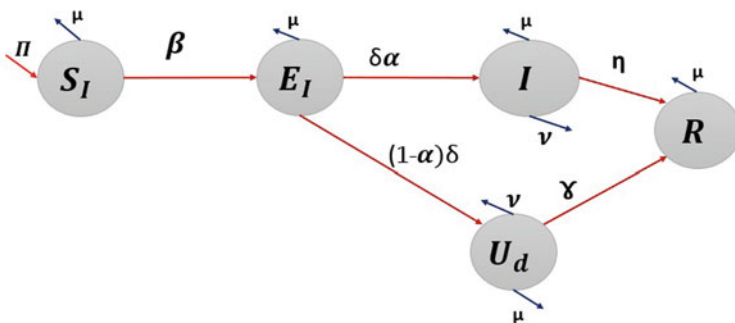
Fig. 1 Diagram of the COVID-19 transmission model

Table 1 Parameters of the model

Parameters	Description
$S_I(t)$	Quantity of susceptible individuals that are in contact with an infected person
$E_I(t)$	Quantity of individuals who are exposed to I but do not execute them
$I(t)$	Quantity of infected individuals
$\mathcal{U}_d(t)$	Quantity of infected person but undeclared
$R(t)$	Quantity of recovered individuals
Π	Recruitment number
μ	Natural death rate
ν	Death rate from disease
β	The interaction of S_I and E_I
α	Proportion of individuals that joins the infected subpopulation from the exposed compartment
δ	The infection rate of exposed individuals
η	Rate of recovered individuals from COVID-19
γ	The interaction between U_d and R

The next set of five equations represents the interaction between the transmission of the infection and the population and can be written as follows:

$$\begin{cases} \dfrac{dS_I}{dt} = \Pi - \beta S_I I - \mu S_I, \\[2mm] \dfrac{dE_I}{dt} = \beta S_I I - \delta E_I - \mu E_I, \\[2mm] \dfrac{dI}{dt} = \alpha \delta E_I - \eta I - (\mu + \nu)I, \\[2mm] \dfrac{dU_d}{dt} = (1-\alpha)\delta E_I - \gamma U_d - (\mu + \nu)U_d, \\[2mm] \dfrac{dR}{dt} = \eta I + \gamma U_d - \mu R, \end{cases} \qquad (1)$$

with the initial condition

$S_I(0) = S_{I,0} \geq 0, E_I(0) = E_{I,0} \geq 0, I(0) = I_0 \geq 0, U_d(0) = U_{d,0} \geq 0, R(0) = R_0 \geq 0.$

3   Qualitative Analysis of the Model

Let N be the total population, then

$$N = S_I + E_I + I + U_d + R.$$

We have

$$\frac{dN}{dt} = \Pi - \mu(S_I(t) + E_I(t) + I(t) + U_d(t) + R(t)) - \nu(I + U_d)$$

$$= \Pi - \mu N(t) - \nu(I + U_d),$$

and then

$$\frac{dN}{dt} = \Pi - \mu N(t) - \nu(I + U_d) \leq \Pi - \mu N(t),$$

$$\Rightarrow N(t) \leq \frac{\Pi}{\mu} + N(0)e^{-\mu t},$$

followed by $N(t) \leq \frac{\Pi}{\mu}$ if we take $t \to +\infty$.

The feasible region for the model (1) is given by

$$\Omega = \left\{ (S_I, E_I, I, U_d, R) \in R_+^5; \left| S_I, E_I, I, U_d, R \geq 0, N \leq \frac{\Pi}{\mu} \right. \right\}.$$

Clearly, Ω is positively invariant with the system presented by Eq. (1) in which the model is identified as mathematically valid and epidemiologically reliable. The transition plot for this model is presented in Fig. 1.

3.1   The Solution's Existence and Singularity

The existence of the solution system is demonstrated by applying the fixed point theorem.

Consider $\mathcal{H} = (C(J))^5$, and $C(J)$ is a Banach field of continuous functions on the interval $J \subset R \to R$ with the norm

$$\|(S_I(t), E_I(t), I(t), U_d(t), R(t))\| = \|S_I\|_\infty + \|E_I\|_\infty + \|I\|_\infty + \|U_d\|_\infty + \|R\|_\infty,$$

where $\|.\|_\infty$ indicates the standard of the supremum in $C(J)$.

For simplicity, we consider

$$\Theta_1(t, S_N) = \Pi - \beta S_I I - \mu S_I,$$

$$\Theta_2(t, E_I) = \beta S_I I - \delta E_I - \mu E_I,$$

$$\Theta_3(t, I) = \alpha \delta E_I - \eta I - (\mu + \nu)I,$$

$$\Theta_4(t, U_d) = (1 - \alpha)\delta E_I - \gamma U_d - (\mu + \nu)U_d,$$

$$\Theta_5(t, R) = \eta I + \gamma U_d - \mu R.$$

For proving the above theorems, we shall assume that $\|S_I\| \leq c_1, \|E_I\| \leq c_2, \|I\| \leq c_3, \|U_d\| \leq c_4, \|R\| \leq c_5$, where $c_i, i = 1, ..., 5$, are positive constants. Thus, we note $\kappa_1 = \beta c_3 + \mu, \kappa_2 = \alpha \delta + \delta + \mu, \kappa_3 = \eta + \mu + \nu, \kappa_4 = \gamma + \mu + \nu$, and $\kappa_5 = \mu$.

Theorem 3.1 *The kernels,* $\Theta_{i=1,...5}$*, are valid for the condition of Lipschitz and contraction if the presented inequality stands:*

$$0 \leq \kappa_i < 1 \quad for \; i = 1, ..., 5.$$

Proof Let S_{I_1} and S_{I_2} be two functions, then
$\|\Theta_1(t, S_{I_1}) - \Theta_1(t, S_{I_2})\| = \| - (\beta I + \mu)(S_{I_1} - S_{I_2})\| \leq (\beta c_3 + \mu)\|S_{N_1}(t) - S_{N_2}(t)\|$.

Thus,

$$\|\Theta_1(t, S_{I_1}) - \Theta_1(t, S_{I_2})\| \leq \kappa_1 \|S_{I_1}(t) - S_{I_2}(t)\|.$$

Hence, for Θ_1, the Lipschitz condition is obtained. Likewise, for Θ_2, Θ_3, Θ_4, and Θ_5, the Lipschitz condition can be conveniently verified and is the same as given above:

$$\|\Theta_2(t, E_{I_1}) - \Theta_2(t, E_{I_2})\| \leq \kappa_2 \|E_{I_1}(t) - E_{I_2}(t)\|.$$

$$\|\Theta_3(t, I_1) - \Theta_3(t, I_2)\| \leq \kappa_3 \|I_1(t) - I_2(t)\|.$$

$$\|\Theta_4(t, U_{d_1}) - \Theta_4(t, U_{d_2})\| \leq \kappa_4 \|U_{d_1}(t) - U_{d_2}(t)\|.$$

$$\|\Theta_5(t, R_1) - \Theta_5(t, R_2)\| \leq \kappa_5 \|R_1(t) - R_2(t)\|.$$

$\square$

Since model (1) follows the population of humans, all its variables of state and the relative parameters must be positive for the coming time. This shall be demonstrated by the theorem below:

Theorem 3.2 *All solutions* (S_I, E_I, I, U_d, R) *are positive whenever* $t \geq 0$.

Proof Since the state variables are all continuous, it is simple to determine from the system (1) that

$\frac{dS_I}{dt} \geq S_I(0) \exp(-(\beta I + \mu)t) \geq 0.$

$\frac{dE_I}{dt} \geq E_I(0) \exp(-(\delta + \mu)t) \geq 0.$

$\frac{dI}{dt} \geq I_0(0) \exp(-(\eta + \mu + \nu)t) \geq 0.$

$\frac{dU_d}{dt} \geq U_d(0) \exp(-(\gamma + \mu + \nu)t) \geq 0.$

$\frac{dR}{dt} \geq R_0(0) \exp(-\mu t) \geq 0.$

Consequently, the entire solution sets are positive for $t \geq 0$. □

The stability of the two points, the illness-free point, and the point where the infection persists in the COVID-19 epidemic model (1) are distinct and provided by $\mathcal{E}_0 = (S_I^0, 0, 0, 0, 0)$ and $(S_I^*, E_I^*, I^*, U_d^*, R^*)$, where

$$\begin{cases} S_I^* = \dfrac{(\eta + \mu + \nu)(\delta + \mu)}{\alpha \delta \beta}, \\[3mm] E_I^* = \dfrac{\Pi(\eta + \mu)\mu(\mathcal{R}_0 - 1)}{\alpha \delta \beta(\delta + \mu)}, \\[3mm] I^* = \dfrac{\mu(\mathcal{R}_0 - 1)}{\beta}, \\[3mm] U_d^* = \dfrac{(1 - \alpha)(\eta + \mu + \nu)}{(\gamma + \mu + \nu)}, \\[3mm] R^* = \dfrac{\eta\mu(\gamma + \mu)(\mathcal{R}_0 - 1) + \beta\gamma(1 - \alpha)(\eta + \mu + \nu)}{\beta\mu(\gamma + \mu + \nu)}. \end{cases}$$

3.2 Local Dynamic of the Covid-19 Free Equilibrium

The model's illness-free steady state (DFE) comes from setting all formulas of the template (1) to zero and allowing $E_I = 0$, $I = 0$, $U_d = 0$, and $R = 0$.

We then obtain $\mathcal{E}_0 = (S_I^0, 0, 0, 0, 0)$, where $S_I^0 = \frac{\Pi}{\mu}$.

3.3 The Effective Reproduction Number $\mathcal{R}_0$

The effective reproduction number of the model is important for analyzing the stability of the equilibrium points. Furthermore, $\mathcal{R}_0$ is used to estimate the anticipated number of secondary connections arising from the introduction of a newly detected individual among a sensitive community. Based on the generation matrix method, we obtain $\mathcal{R}_0$ directly from the model. As a first step to get $\mathcal{R}_0$, we rewrite the equations of the model beginning with the recently infected categories:

$$\begin{cases} \dfrac{dE_I}{dt} = \beta S_I I - (\delta + \mu)E_I, \\[2mm] \dfrac{dI}{dt} = \alpha\delta E_I - (\eta + \mu)I, \\[2mm] \dfrac{dU_d}{dt} = (1-\alpha)\delta E_I - (\gamma + \mu)U_d, \\[2mm] \dfrac{dR}{dt} = \eta I + \gamma U_d - \mu R. \end{cases}$$

The rate $\mathcal{R}_0$ is measured as the spectrum ρ of the matrix FV^{-1} (the generation matrix).

The matrices of F and V are the result of the infected classes (i.e., E_I, I, U_d and R) at the equilibrium point $\mathcal{E}_0$ and so we have

$$F = \begin{pmatrix} 0 & \beta S_I^0 & 0 & 0 \\ 0 & 0 & 0 & 0 \\ 0 & 0 & 0 & 0 \\ 0 & 0 & 0 & 0 \end{pmatrix} \text{ and } V = \begin{pmatrix} (\delta + \mu) & 0 & 0 & 0 \\ -\alpha\delta & (\eta + \mu + v) & 0 & 0 \\ -(1-\alpha)\delta & 0 & (\gamma + \mu + v) & 0 \\ 0 & -\eta & -\gamma & \mu \end{pmatrix}.$$

Then,

$$FV^{-1} = \frac{1}{|V|} \begin{pmatrix} \beta S_I^0 c_{12} & \beta S_I^0 c_{22} & \beta S_I^0 c_{32} & \beta S_I^0 c_{42} \\ 0 & 0 & 0 & 0 \\ 0 & 0 & 0 & 0 \\ 0 & 0 & 0 & 0 \end{pmatrix},$$

where $c_{32} = -\mu$, $c_{22} = \mu(\delta + \mu)(\gamma + \mu + v)$, $c_{12} = \mu(\gamma + \mu + v)\alpha\delta$, and $c_{42} = 0$.

Hence, the effective number of breeders $\mathcal{R}_0$ is given as follows: $\mathcal{R}_0 = \rho(FV^{-1}) = \dfrac{\beta \Pi \alpha \delta}{\mu(\eta + \mu + v)(\delta + \mu)}$

Theorem 3.3 *If $\mathcal{R}_0 < 1$, the illness equilibrium state is locally asymptotically stable; otherwise, it becomes unsteady.*

Proof Evaluating the Jacobean matrix at the equilibrium $\mathcal{E}_0$, we obtain

$$J(\mathcal{E}_0) = \begin{pmatrix} -\mu & 0 & -\dfrac{\beta \Pi}{\mu} & 0 & 0 \\ 0 & -(\delta + \mu) & \dfrac{\beta \Pi}{\mu} & 0 & 0 \\ 0 & \alpha\delta & -(\eta + \mu + v) & 0 & 0 \\ 0 & (1-\alpha)\delta & 0 & -(\gamma + \mu + v) & 0 \\ 0 & 0 & \eta & \gamma & -\mu \end{pmatrix}.$$

Based on the Jacobian matrix, a characteristic polynomial was attained in the following form:

$$\mathcal{P}(\lambda) = -(\mu + \lambda)^2(\gamma + \mu + \nu + \lambda)(\lambda)$$

$$= (\delta + \mu + \lambda)(\eta + \mu + \nu + \lambda) - \frac{\alpha\delta\beta\Pi(\mu + \lambda)}{\mu}, \tag{2}$$

$\lambda_1 = -\mu < 0$, $\lambda_2 = -(\gamma + \mu + \nu) < 0$, $\lambda_3 = -\frac{(\eta+\mu+\nu+\delta+\mu)+\sqrt{\Delta}}{2} < 0$, and $\lambda_4 = \frac{-(\eta+\mu+\nu+\delta+\mu)+\sqrt{\Delta}}{2}$,

$\lambda_4 < 0$ for $\mathcal{R}_0 < 1$. So that the virus can be removed to some extent if the starting population size of the infected members is in the bottom set of the point $\mathcal{E}_0$. □

3.4 Global Dynamic of DFE

Theorem 3.4 *The DFE, $\mathcal{E}^*$ of the model (1) is globally asymptotically stable if $\mathcal{R}_0 < 1$.*

Proof We shall consider the Lyapunov function as

$$V = \chi_1 E_I + \chi_2 I, \tag{3}$$

where χ_1 and χ_2 are two positive values. If we differentiate Eq. (3) concerning t, we discover that

$$\frac{dV}{dt} = \chi_1 \frac{dE_I}{dt} + \chi_2 \frac{dI}{dt}$$

we get $\frac{dV}{dt} < (\mathcal{R}_0 - 1)I$ well then, from $I < I^0$ and $\frac{dV}{dt} \leq 0$ for $\mathcal{R}_0 < 1$ and $\frac{dV}{dt} = 0$ if and only if $I = 0$.

Hence, according to the principle of invariance of LaSalle, $\mathcal{E}_0$ becomes globally asymptotically stable in Ω. □

3.5 Equilibrium Endemic Stability

Theorem 3.5 *The endemic point $\mathcal{E}^*$ becomes locally asymptotically stable if the basic reproductive rate is less than one, and $\mathcal{E}^*$ is unstable anyway, in addition.*

Proof The system (1)'s Jacobian at $\mathcal{E}^*$ seems to be

$$J(\mathcal{E}_0) = \begin{pmatrix} -(\beta I^* + \mu) & 0 & \beta S_I^* & 0 & 0 \\ \beta I^* & -(\delta + \mu) & \beta S_I^* & 0 & 0 \\ 0 & \alpha\delta & -(\eta + \mu + \nu) & 0 & 0 \\ 0 & (1-\alpha)\delta & 0 & -(\gamma + \mu + \nu) & 0 \\ 0 & 0 & \eta & \gamma & -\mu \end{pmatrix}.$$

Here is the equation for the equivalent characteristics: $\mathcal{P}(\lambda) = (\mu + \lambda)(\gamma + \mu + \lambda)[\zeta_0 + \lambda\zeta_1 + \zeta_2\lambda^2 - \lambda^3]$,

where

$\zeta_0 = -(\beta I^* + \mu)(\delta + \mu)(\eta + \mu + \nu) - (\beta^2\alpha\delta I^* + \alpha\delta\beta(\beta I^* + \mu))S_I^*.$

$\zeta_1 = -((\beta I^* + \mu)(\delta + \mu) + (\delta + \mu + \beta I^*)(\eta + \mu + \nu) - \alpha\delta\beta S_I^*).$

$\zeta_2 = -(\delta + \mu + \beta I^* + \eta + \mu + \nu) < 0.$

Moreover, it is straightforward to show that the requirements of the Routh–Hurwitz stability criterion for a polynomial of degree three are satisfied IF $\mathcal{R}_0 > \frac{\Pi(\beta I^* + \delta + \mu)(2\beta I^* + 3\mu + \delta)}{(\mu + \eta + \nu)(\delta + \mu)(\beta I^* + \eta + \delta + \mu)S_I^*} > 1.$ In light of this, the point $\mathcal{E}$ is locally in a stable state. □

Theorem 3.6 *In the event that $\mathcal{R}_0 > 1$, the endemic equilibrium point is globally asymptotically stable.*

Proof Take into account the suitable Lyapunov function provided by (4)

$$\frac{dL(S_I, I)}{dt} = \chi_1(1 - \frac{\tilde{S}_I}{S_I})\frac{dS_I}{dt} + \chi_2(1 - \frac{\tilde{I}}{I})\frac{dI}{dt}. \tag{4}$$

By substituting $\frac{dS_I}{dt}$ and $\frac{dI}{dt}$ of model (1), we obtain

$$\frac{dL}{dt} = \frac{\chi_1}{S_I}(S_I - \tilde{S}_I)(\Pi - (\beta I + \mu)S_I) + \frac{\chi_2}{I}(I - \tilde{I})(\alpha\delta E_I - (\eta + \mu + \nu)I)$$

$$< \chi_1\frac{(S_I - \tilde{S}_I)}{S_I}\Pi - \chi_1(\beta I + \mu)(S_I - \tilde{S}_I) + \frac{\chi_2(I - \tilde{I})\alpha\delta E_I}{I}.$$

For $\chi_1 = \frac{S_I(I - \tilde{I})}{(S_I - \tilde{S}_I)}$ and $\chi_2 = 1$, we have

$$\frac{dL}{dt} < (\Pi - \frac{\mathcal{R}_0(\eta + \mu + \nu)(\delta + \mu)(\theta + \mu)S_I}{\alpha\delta\Pi} - (\theta + \mu)S_I + \frac{\alpha\delta E_I}{I})(I - \tilde{I}),$$

$$< (\Pi - \frac{\mathcal{R}_0(\eta + \mu + \nu)(\delta + \mu)(\theta + \mu)S_I}{\alpha\delta\Pi} + \frac{\alpha\delta E_I}{I})(I - \tilde{I}).$$

Thus, $\frac{dL}{dt} < 0$ only if $\mathcal{R}_0 > \frac{\Pi^2\alpha\delta}{(\eta + \mu + \nu)(\delta + \mu)(\theta + \mu)}$, and $\frac{dL}{dt} \leq 0$ if $I = \tilde{I}$, and then the point $\mathcal{E}^*$ is globally asymptotically stable. □

4 Model Sensibility

The fundamental purpose of sensitivity analysis is to describe how resilient the reproduction number $\mathcal{R}_0$ is to changes in the system characteristics. Moreover, it enables us to determine how a state variable has changed proportionally when a

Table 2 Sensitivity index table

Symbol of the parameter	Index of sensitivity
μ	-0.8121
ν	-0.2472
δ	$+0.1324$
Π	$+1$
β	$+1$
η	-0.8653
α	$+1$

system parameter changes, and it is crucial to understand the relative importance of the many elements involved for the novel coronavirus's transmission in order to suggest the best ways to reduce human impermanence and morbidity. We determine the sensitivity indices with respect to $\mathcal{R}_0$, to the parameters of the system (1) since the first illness transmission is entirely related to the reproduction number $\mathcal{R}_0$. As a result, we formulate a sensitivity coefficient as such:

$$\Lambda_x^{\mathcal{R}_0} = \frac{\partial \mathcal{R}_0}{\partial x} \frac{x}{\mathcal{R}_0}.$$

$$\Lambda_\mu^{\mathcal{R}_0} = -\frac{\delta(\eta + \mu) + 2\mu(\eta + \delta + 1) + 3\mu^2 + 3\mu^2}{(\delta + \mu)(\eta + \mu + \nu)}.$$

$$\Lambda_\eta^{\mathcal{R}_0} = -\frac{\eta}{\eta + \mu + \nu}.$$

$$\Lambda_\delta^{\mathcal{R}_0} = \frac{\mu}{(\delta + \mu)}.$$

$$\Lambda_\nu^{\mathcal{R}_0} = -\frac{nu}{\eta + \mu + \nu}.$$

$$\Lambda_\beta^{\mathcal{R}_0} = 1.$$

$$\Lambda_\Pi^{\mathcal{R}_0} = 1.$$

$$\Lambda_\alpha^{\mathcal{R}_0} = 1.$$

We have $\Lambda_\delta^{\mathcal{R}_0}, \Lambda_\Pi^{\mathcal{R}_0}, \Lambda_\beta^{\mathcal{R}_0}, \Lambda_\alpha^{\mathcal{R}_0} > 0$, while $\Lambda_\mu^{\mathcal{R}_0}, \Lambda_\eta^{\mathcal{R}_0}, \Lambda_\nu^{\mathcal{R}_0} < 0$.
This means that $\mathcal{R}_0$ increased in δ, Π, β, and α, when $\mathcal{R}_0$ decreases in μ, ν, and η.
$\mathcal{R}_0$ does not depend on γ, and then $\Lambda_\gamma^{\mathcal{R}_0} = 0$ (Table 2).

5   The Controlled Mathematical Model

In the following part, a COVID-19 minimization problem based on the introduction of two time-dependent controls designated by $u_1(t)$ and $u_2(t)$ in the model is formulated (5). These time-dependent controls are being used to examine the impact

of their fluctuation through time on the dynamics of COVID-19. The previously maintained constant stay-at-home order is recommended using the control variable $u_1(t)$. The time-dependent control $u_2(t)$ is developed to examine the effectiveness of an improvement in detention and a travel ban. The abovementioned control variables are thus added in the following manner to produce the COVID-19 control model:

$$
\begin{cases}
\dfrac{dS_I}{dt} = \Pi - \beta(1 - u_1)S_I I - \mu S_I, \\[2mm]
\dfrac{dE_I}{dt} = \beta(1 - u_1)S_I I - \delta E_I - \mu E_I, \\[2mm]
\dfrac{dI}{dt} = \alpha\delta E_I - (\eta + \mu + v)I - u_2 I, \\[2mm]
\dfrac{dU_d}{dt} = (1 - \alpha)\delta E_I - (\gamma + \mu + v)U_d - u_2 U_d, \\[2mm]
\dfrac{dR}{dt} = \eta I + \gamma U_d - \mu R + u_2(I + u_d).
\end{cases}
\tag{5}
$$

5.1 The Optimal Control Problem

Minimizing the objective functional $J(u_1, u_2) = \int_0^t (I(t) + U_d(t) + \frac{A_1}{2}u_1^2(t) + \frac{A_2}{2}u_2^2(t))dt$ is the challenge.

When the cost coefficients $A_1 > 0$ and $A_2 > 0$ are present, they are chosen in order to compare the relative weights of $u_1(t)$ and $u_2(t)$ at time t, and T is the last instance. To put it another way, we aim to find the optimal controls u_1^* and u_2^* such that $J(u_1^*, u_2^*) = \min_{u_1, u_2 \in U} J(u_1, u_2)$,
where U is the set of admissible controls defined by

$$
U = \left\{u_1, u_2 \in U \,\middle|\, 0 \le u_1(t) \le 1 \text{ and } 0 \le u_1(t) \le 1, \ t \in [0, T]\right\}.
$$

5.2 Characterization of the Optimal Control

We utilize the Hamiltonian at time t specified by and apply Pontryagin's maximum principle to obtain the essential conditions for optimal control.

$$
\tilde{H} = I(t) + U_d(t) + \frac{A_1}{2}u_1^2(t) + \frac{A_2}{2}u_2^2(t) + \sum_{i=1}^{5} \lambda_i(t) f_i(S_I, E_I, I, U_d, R),
$$

where f_i represents the front of the difference equation (5) of the ith parameter value.

Theorem 5.1 *Considering that we have state system solutions that minimize J on U and optimum controls u_1^*, u_2^* and S_I, E_I, I, U_d, and R, lambda1,dots, and lambda5, respectively, adjacent variables, such as $\lambda_1, \ldots,$ and λ_5, are used.*

$$\frac{d\lambda_1}{dt} = \lambda_1(\beta(1-u_1)I - \mu) - \lambda_2\beta(1-u_1)I.$$

$$\frac{d\lambda_2}{dt} = \lambda_2(\delta + \mu) - \lambda_3\alpha\delta - \lambda_4(1-\alpha)\delta.$$

$$\frac{d\lambda_3}{dt} = -1 + \lambda_1\beta(1-u_1)S_I - \lambda_2\beta(1-u_1)S_I + \lambda_3(\eta + \mu + v + u_2)$$
$$- \lambda_5(\eta + u_2).$$

$$\frac{d\lambda_4}{dt} = -1 + \lambda_4(\gamma + \mu + v + u_2) - \lambda_5(\gamma + u_2).$$

$$\frac{d\lambda_5}{dt} = \lambda_5\mu.$$

Including transversality conditions $\lambda_1(t_f) = 0, \lambda_2(t_f) = 0, \lambda_3(t_f) = -1, \lambda_4(t_f) = -1,$ and $\lambda_5(t_f) = 0.$

Proof In addition,

$$\tilde{H} = I(t) + U_d(t) + \frac{A_1}{2}u_1^2(t) + \frac{A_2}{2}u_2^2(t) + \sum_{i=1}^{5}\lambda_i(t)f_i(S_I, E_I, I, U_d, R),$$

where $f_1 = \Pi - \beta(1-u_1)S_I I - \mu S_I$ $f_2 = \beta(1-u_1)S_I I - \delta E_I - \mu E_I$, $f_3 = \alpha\delta E_I - (\eta + \mu + v)I - u_2 I$, $f_4 = (1-\alpha)\delta E_I - (\gamma + \mu + v)U_d - u_2 U_d$, and $f_5 = \eta I + \gamma U_d - \mu R + u_2(I + u_d)$.

Then, by using Pontryagin's maximum principle [ref], we have

$$\frac{d\lambda_1}{dt} = -\frac{\partial\tilde{H}}{\partial S_I} = \lambda_1(\beta(1-u_1)I - \mu) - \lambda_2\beta(1-u_1)I.$$

$$\frac{d\lambda_2}{dt} = -\frac{\partial\tilde{H}}{\partial E_I} = \lambda_2(\delta + \mu) - \lambda_3\alpha\delta - \lambda_4(1-\alpha)\delta.$$

$$\frac{d\lambda_3}{dt} = -\frac{\partial\tilde{H}}{\partial I} = -1 + \lambda_1\beta(1-u_1)S_I - \lambda_2\beta(1-u_1)S_I + \lambda_3(\eta + \mu + v + u_2)$$
$$- \lambda_5(\eta + u_2).$$

$$\frac{d\lambda_4}{dt} = -\frac{\partial\tilde{H}}{\partial U_d} = -1 + \lambda_4(\gamma + \mu + v + u_2) - \lambda_5(\gamma + u_2).$$

$$\frac{d\lambda_5}{dt} = -\frac{\partial\tilde{H}}{\partial R} = \lambda_5\mu.$$

Therefore, from $\frac{\partial\tilde{H}}{\partial u_1} = 0$ and $\frac{\partial\tilde{H}}{\partial u_2} = 0$, the associated optimal controls u_1^* and u_2^* are determined. As a result, we established the characteristic equation involving the boundaries on the controls in the kind of proposed control argument as regards:

$$u_1^* = \min\left\{1, \max(0, \frac{\beta S_I I(\lambda_2 - \lambda_1)}{A_1})\right\}.$$
$$u_2^* = \min\left\{1, \max(0, \frac{\lambda_3 I + \lambda_4 U_d - \lambda_5(I + U_d)}{A_2})\right\}. \qquad \square$$

6 Numerical Simulation and Discussions

Analytical research will never be complete without numerical validation of the data. In the present section, we have presented some numerical simulations to follow the dynamics of the system (1) for various initial conditions and parameters given in Tables 3 and 4. Thus, to solve this system, we have used the fourth-order Runge–Kutta method in Matlab software. We took into account the parameters listed in Table 3 as well as the different values of the initial conditions given in Table 4.

By using these parameters, we have calculated the reproduction number, and we find that $\mathcal{R}_0 = 0.3865$. It is seen clearly from Fig. 2 that the solution profiles of system (1) converge to the COVID-19-free equilibrium $\mathcal{E}_0 = (0.059 \times 10^7, 1.0535 \times 10^7, 0, 0, 0)$. Furthermore, it is seen from Fig. 3 that the solution of (1) converges to the endemic equilibrium $\mathcal{E}^* = (1.4978 \times 10^7, 0.9096 \times 10^7, 2.6159 \times 10^7, 2.6581 \times 10^7, 3.8366 \times 10^7, 2.5910 \times 10^7)$ in all the three different initial values of $S_E(0)$ and $S_N(0)$. Figure 4 shows the stability of the solution of (1) in the three different values of $E_I(0)$ and $I(0)$, while Fig. 5 shows that the solution converges to the $\mathcal{E}_0$ in the same three initial values of $U_d(0)$ with $\alpha = 0.0002$. It is clear from Fig. 6 that the solution of (1) is stable and converges to the COVID-19-free equilibrium in all the three different initial values of individuals $U_d(0) = I(0)$. It implies that

Table 3 Basic values for parameters of system (1)

Parameter	Value	Source
β	0.8326	Presumption
α	0.4110	[9]
Π	30.000	Presumption
δ	$1/7 day^{-1}$	[9]
η	0.1430	Presumption
μ	$0.0062 day^{-1}$	[9]
ν	$0.022 day^{-1}$	[10]
θ	0.013	Presumption

Table 4 Initial values of variables of system (1)

Initial values	Case 1	Case 2	Case 3
N	2,330,769	2,330,769	2,330,769
$S_I(0)$	2,229,903	2,082,863	1,104,763
$E_I(0)$	100	500	1000
$I(0)$	10	3000	400,000
$U_d(0)$	100	1000	7000
$R(0)$	50	400	2000
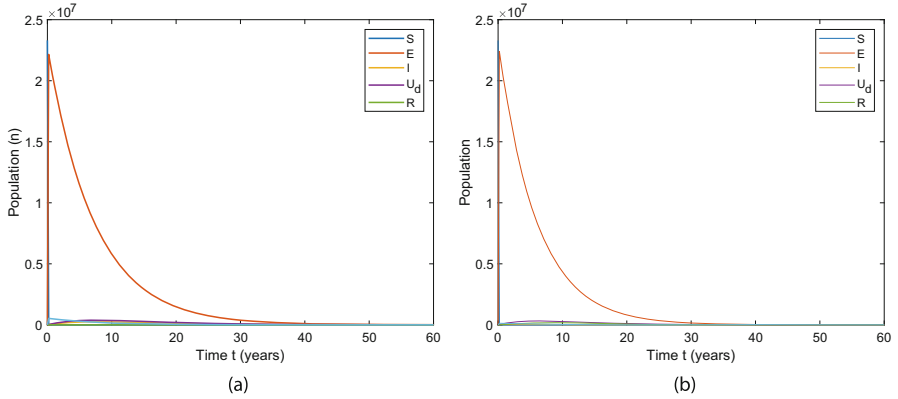
Fig. 2 This graph indicates that system (1)'s illness equilibrium is equal to $(0.059 \times 10^7, 1.0535 \times 10^7, 0, 0)$. (**a**) Case 1. (**b**) Case 2
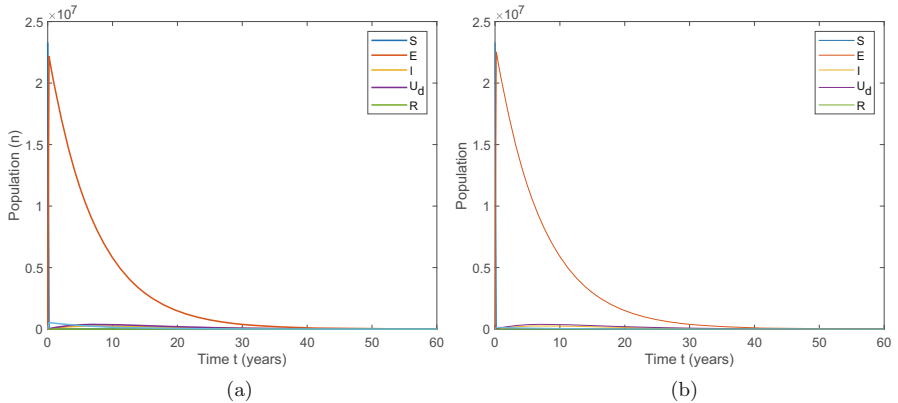
Fig. 3 This plot displays how the state of the endemic system (1) is $(1.4978 \times 10^7, 0.9096 \times 10^7, 2.6159 \times 10^7, 2.6581 \times 10^7, 3.8366 \times 10^7)$. (**a**) Case 3. (**b**) Case 4

as these listed parameters are raised (or lowered), the reproduction number values increase or decrease accordingly. The parameters ν, μ, and η, on the other hand, have negative indices. It denotes an inverse relationship with $\mathcal{R}_0$, and, as a result, raising these parameters will lower $\mathcal{R}_0$'s value and vice versa. We see a decline in the number of diseased and infected but undeclared people in Fig. 7, so following the realization of this approach, all citizens will be established to inform them of the seriousness of the COVID-19 virus. Figure 8 displays the value of sensitivity indices of the chosen parameters in graphical form. Finally, all outcomes of this section
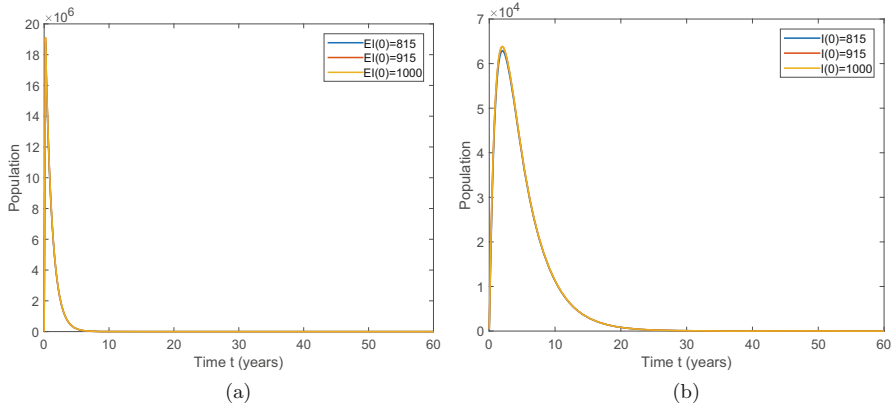
Fig. 4 Numerical solutions of the model (1) for parameters and different initial conditions of E_I and I given in Tables 3 and 4, here $\mathcal{R}_0 = 0.3865$, and the stability is for the COVID-19-free equilibrium. (**a**) Case 5. (**b**) Case 6
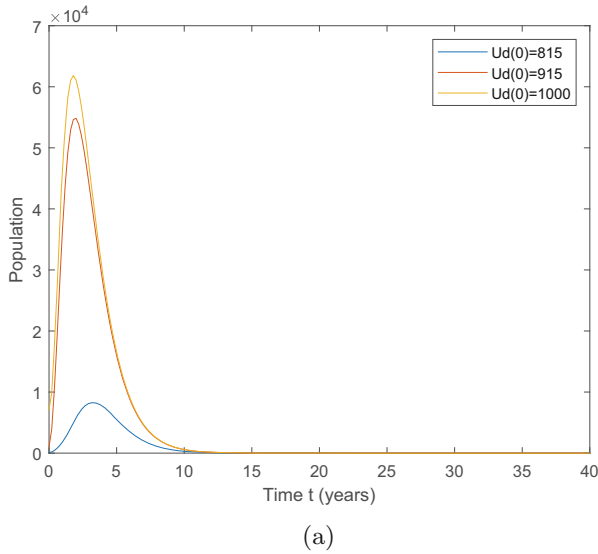
Fig. 5 Numerical solutions of the model (1) for parameters and different initial conditions of U_d given in Tables 3 and 4, here $\mathcal{R}_0 = 0.3865$, and the stability is for the COVID-19-free equilibrium. (**a**) 7

support the theoretical results of the local and the overall asymptotic stability of the undiseased and endemic state presented in the previous sections.
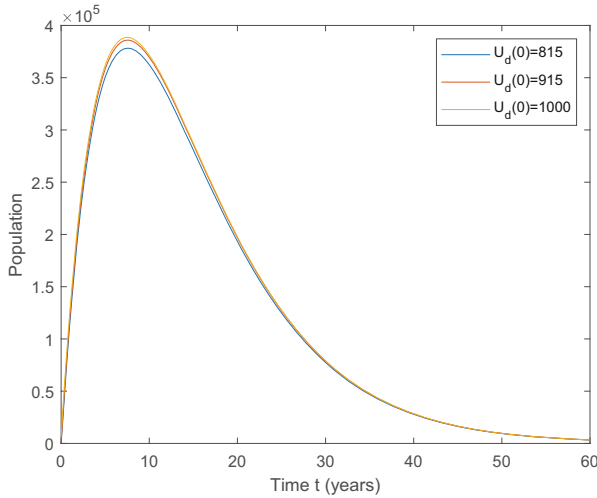
(a)

Fig. 6 Numerical solutions of the model (1) for parameters and different initial conditions of $U_d = U_d(0)$ given in Tables 3 and 4, here $\mathcal{R}_0 = 1.8662$, and the stability is for the endemic equilibrium. (**a**) 8

(a)   (b)
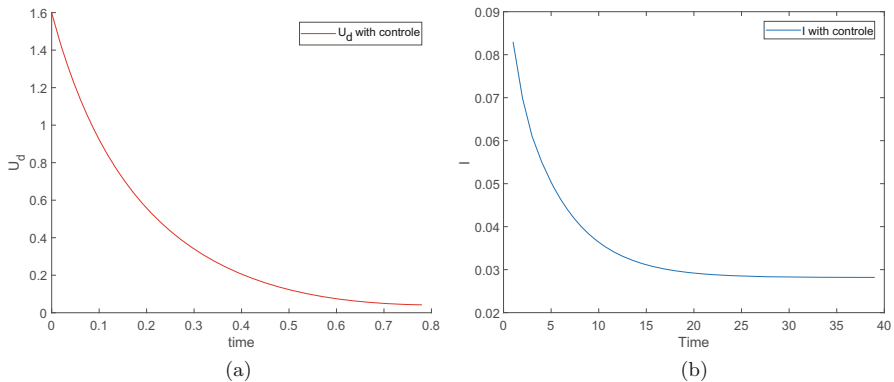
Fig. 7 Numerical solutions of the infected individuals and contaminated individuals but undeclared with controls. (**a**) Case 9. (**b**) Case 10

7   Conclusion

In this chapter, we construct a nonlinear mathematical model and analyze actual and estimated data to determine the impact of COVID-19 on society. A system of five ODEs mathematically captures the dynamics of the interaction between the compartments. The fixed point theorem is used in this essay to attempt to demonstrate the existence and originality of the solution to our issue. The fundamental reproduction
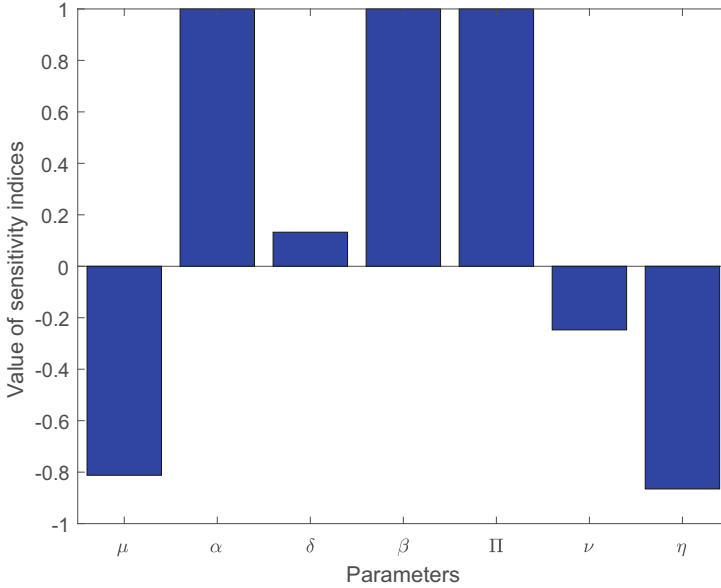
Fig. 8 The result displays the basic reproduction number $\mathcal{R}_0$'s normalized forward sensitivity indices relative to each of the standard parameter values used Table 3

number, $\mathcal{R}_0$ can be found using the generation matrix. Additionally, we calculated the equilibria and mentioned their local and global stability. Furthermore, by using the idea of normalized forward sensitivity, the research emphasizes the significance of each parameter to examine the role of approach factors in illness propagation and then to determine the most significant factors that raise or lower $\mathcal{R}_0$. By putting the control theory findings to use, we were able to identify the appropriate controllers. We conduct numerical simulations describing the impact of various situations such as the stay-at-home order, a travel ban, and solitary confinement to study the effects of modeling essential factors on the mediation and control of the illness. Besides, by including time-dependent factors $u_1(t)$ for staying at home and $u_2(t)$ for travel restrictions and solitary confinement, the suggested model is reorganized to achieve the optimal control model. The model is tuned, and the relevant optimality requirements are deduced using optimal control theory and Pontryagin's maximum principle. Eventually, with the parameter values derived from the data fit, the digital approximation is applied to develop the graphical output of the template. Various plots represent the model parameters and how they affect disease eradication, and these numerical simulations are used to confirm the analytical result. Similarly, sample diagram outputs of the model with the appropriate parameters suggest that adherence to World Health Organization (WHO) guidelines can help reduce disease in the community.

References

1. Padmanabhan, P., Desikan, R., Dixit, N.M.: Modeling how antibody responses may determine the efficacy of COVID-19 vaccines. Nat. Comput. Sci. **2**, 123–131 (2022). https://doi.org/10.1038/s43588-022-00198-0
2. Aba Oud, M.A., Ali, A., Alrabaiah, H. et al.: A fractional order mathematical model for COVID-19 dynamics with quarantine, isolation, and environmental viral load. Adv. Differ. Equ. **2021**, 106 (2021). https://doi.org/10.1186/s13662-021-03265-4
3. Singh, H., Srivastava, H.M., Hammouch, Z., Nisar, K.S.: Numerical simulation and stability analysis for the fractional-order dynamics of COVID-19. Results Phys. **20** (2021): 103722. https://doi.org/10.1016/j.rinp.2020.103722
4. Ivorra, B., Ramos, A.M.: Application of the Be-CoDiS mathematical model to forecast the international spread of the 2019–20 Wuhan coronavirus outbreak. ResearchGate Preprints. **9**, 1–13 (2020)
5. Ghostine, R., Gharamti, M., Hassrouny, S., Hoteit, I.: An extended seir model with vaccination for forecasting the COVID-19 pandemic in Saudi Arabia using an ensemble Kalman filter. Mathematics **9**(6), 636 (2021).
6. Khan, M.A., Ullah, S., Kumar, S.: A robust study on 2019-nCOV outbreaks through non-singular derivative. Eur. Phy. J. Plus **136**, 168 (2021)
7. Ouaziz, S.I., Hamou, A.A., El Khomssi, M.: Dynamics and optimal control strategies of Corruption model. Results Nonlinear Anal. **5**(4), 423–451 (2022)
8. Bhowmik, D., Nandi, R., Jagadeesan, R., Kumar, N., Prakash, A., Kumar, D.: Identification of potential inhibitors against SARS-CoV-2 by targeting proteins responsible for envelope formation and virion assembly using docking based virtual screening, and pharmacokinetics approaches. Infect. Genet. Evol. **84**, 104451 (2020). https://doi.org/10.1016/j.meegid.2020.104451
9. Khajanchi S., Sarkar K., Mondal J., Perc M.: Dynamics of the COVID-19 pan- demic in India. (2020). ArXiv: 2005.06286
10. COVID-19 Coronavirus Pandemic in Pakistan. Accessed 29 May 2020. https://covid.gov.pk/stats/pakistan

Optimal Strategies to Prevent COVID-19 from Becoming a Pandemic

Beyza Billur İskender Eroğlu and Dilara Yapışkan

1 Introduction

At the end of 2019, it was announced by the World Health Organization (WHO) that a new coronavirus (2019-nCoV) leading to pneumonia was identified in Wuhan City, Hubei Province of China [1]. This coronavirus, which is thought to be caused by bats [2], is also called Severe Acute Respiratory Syndrome Coronavirus 2 (SARS-CoV-2). The findings suggest that transmission may have started from the Huanan seafood wholesale market [3, 4] and then the virus spread rapidly among people, reaching all provinces of China. Therefore, the dynamics of the virus had to be revealed immediately to the prediction of the course of the epidemic. As is known, this can be achieved by mathematical models which have critical in comprehending the dynamics of transmissible illnesses and examining the process of the epidemic [5–7]. For this reason, the first spreading of coronavirus in Wuhan City was designed according to varied dynamics using ordinary differential equations (ODEs) [8–10]. Besides, the researchers examined the propagation of COVID-19 in various nations proposing different ODE models [11–14]. However, recent studies indicate that the spread of COVID-19 shows both power law and exponential law distributions [15]. Such complex behavior can be fitted by fractional calculus thanks to the singular and non-singular operators. Hence, fractional calculus has contributed to the effective resolution of many open problems in the literature [16–18]. In addition, many epidemiological models have been defined with fractional derivatives because fractional derivatives can properly reflect the characters of the epidemic [19–21]. On the other hand, epidemiological models have a critical threshold parameter that

B. B. İskender Eroğlu (✉) · D. Yapışkan
Department of Mathematics, Balıkesir University, Balıkesir, Turkey
e-mail: biskender@balikesir.edu.tr

provides information about whether the disease will turn into an epidemic. Suppose this parameter indicates that the disease has turned into a pandemic. In that case, various methods should be proposed to control and treat the epidemic. In this meaning, optimal control is one of the most effective control techniques because, while optimal control calculates the optimal value of the control variables, it takes into account their costs [22–25]. In addition, fractional optimal control [26, 27], which is an optimal control technique that includes fractional derivative terms in dynamic system or performance indexes, has recently taken its place among these techniques. However, the difference in the definition of derivative operators affects the necessary optimality and transversality conditions [28–30]. Since different types of fractional operators occur in modeling real-life phenomena to be compatible with their nature, various FOCPs have been proposed to control these phenomena [31–35]. Moreover, comparatively analyzing how fractional derivatives represent controlled dynamics has taken its place among the attractive topics in recent years [36, 37].

Various optimal control strategies have been proposed to prevent the spread of COVID-19 [38, 39]. In this chapter, the question of what measures could have been taken before the epidemic turned into a pandemic is replied. Therefore, we focus on a Reservoir–People model which is the starting point of the pandemic. In this meaning, we investigate the model created with real data proposed by [8] under power law and exponential law distributions compatible with the spreading of the virus. Thus, the organization of the chapter is planned as below. Firstly, in Sect. 1, the essential mathematical concepts are given. In Sect. 2, the Reservoir–Human model is introduced and then modified in terms of the Caputo derivative to examine it according to the distribution among people. In Sect. 3, the FOCP is formulated, and the optimality system is reached by the Pontryagin Maximum principle. In Sect. 4, Adam's type PCM combined with the FBSA is used to achieve the numerical solution. The FOCP is also formulated with the ABC derivative in this section. Then, it is solved numerically following the similar steps. Finally, all graphical results belonging to both FOCPs are shown comparatively using MATLAB.

1.1 Preliminaries

The traditional and new generation fractional derivatives and some of their properties are introduced below.

Definition 1 ([40]) The left and the right Caputo derivatives are, respectively, defined as

$$^C_a D^\alpha_t f(t) = \frac{1}{\Gamma(1-\alpha)} \int_a^t (t-\theta)^{-\alpha} \left(\frac{d}{d\theta}\right) f(\theta) \, d\theta, \ 0 < \alpha < 1,$$

$$^C_t D^\alpha_b f(t) = \frac{1}{\Gamma(1-\alpha)} \int_t^b (\theta-t)^{-\alpha} \left(-\frac{d}{d\theta}\right) f(\theta) \, d\theta, \ 0 < \alpha < 1,$$

where $0 < \alpha < 1$.

Definition 2 ([41]) The left and the right ABC derivatives are, respectively, defined as

$$^{ABC}_{a}D^\alpha_t f(t) = \frac{B(\alpha)}{1-\alpha} \int_a^t \frac{df(\theta)}{d\theta} E_\alpha \left[-\frac{\alpha}{1-\alpha}(t-\theta)^\alpha \right] d\theta,$$

$$^{ABC}_{t}D^\alpha_b f(t) = \frac{-B(\alpha)}{1-\alpha} \int_t^b \frac{df(\theta)}{d\theta} E_\alpha \left[-\frac{\alpha}{1-\alpha}(\theta-t)^\alpha \right] d\theta,$$

where $0 < \alpha < 1$, $B(\alpha)$ is the normalization function such that $B(0) = B(1) = 1$ and E_α is the Mittag–Leffler function.

Definition 3 ([40]) For $x \in \mathbb{R}$, the generalized Mittag–Leffler function is

$$E_{\upsilon,\omega}(x) = \sum_{m=0}^{\infty} \frac{x^m}{\Gamma(\upsilon m + \omega)}, \upsilon > 0, \omega > 0.$$

1.2 Reservoir–People Transmission Biological Network Model

The spread model of COVID-19 originated by Chen et al. [8] is evoked in this section. The model details the spread between people and the reservoir (the seafood market) in Wuhan City. The parameters at time t are represented as susceptible people with $S_p(t)$, exposed people with $E_p(t)$, symptomatic infected with $I_p(t)$, asymptomatic infected people with $A_p(t)$, and recovered people with $R_p(t)$. Then, the total people population represented by $N_p(t)$ corresponds to $N_p(t) = S_p(t) + E_p(t) + I_p(t) + A_p(t) + R_p(t)$. Additionally, the reservoir expressed as $W(t)$ is considered the source of COVID-19. The model is given by six compartment ODEs as follows:

$$\begin{cases} \frac{dS_p(t)}{dt} = \Lambda_p - m_p S_p(t) - \beta_p S_p(t)\left(I_p(t) + \kappa A_p(t)\right) - \beta_w S_p(t) W, \\ \frac{dE_p(t)}{dt} = \beta_p S_p(t)\left(I_p(t) + \kappa A_p(t)\right) + \beta_w S_p(t) W - \left(1 - \delta_p\right)\omega_p E_p(t) \\ \qquad\quad - \delta_p \bar{\omega}_p E_p(t) - m_p E_p(t), \\ \frac{dI_p(t)}{dt} = \left(1 - \delta_p\right)\omega_p E_p(t) - \left(\gamma_p + m_p\right)I_p(t), \\ \frac{dA_p(t)}{dt} = \delta_p \bar{\omega}_p E_p(t) - \left(\bar{\gamma}_p + m_p\right)A_p(t), \\ \frac{dR_p(t)}{dt} = \gamma_p I_p(t) + \bar{\gamma}_p A_p(t) - m_p R_p(t), \\ \frac{dW(t)}{dt} = \mu_p I_p(t) + \bar{\mu}_p A_p(t) - \varepsilon W. \end{cases}$$

$$(1)$$

Since COVID-19 behaves compatibly with the power law and exponential law in a heterogeneous biological network, the model suggested by Chen et al. [8] is discussed in sense of the Caputo derivative. Taking account of unit consistency, only the people-to-people spread of COVID-19 is studied in this chapter. COVID-19 is transmitted through direct or indirect contact. Droplets caused by sneezing, breath, speak or sing at a very close range, and airborne such as aerosol at long distances [42] can be given as examples. If vaccines are still missing in viral epidemics, non-pharmaceutical interventions such as mask usage, distance, and hygiene are effective ways to prevent the infection. If people have mild or no symptoms, pharmaceutical intervention can be accomplished with antiviral medications. However, if antiviral medications are unavailable or cannot be effective, plasma transfusion therapy is used as an effective method in severe viral epidemics [43]. The proposed preventive control strategies are adapted to the system (1) to avoid the spread of COVID-19 in Wuhan City from becoming a pandemic. Control function $u_1(t)$ stands for non-pharmaceutical intervention to protect susceptible people from infection. The control functions $u_2(t)$ and $u_3(t)$ also signify pharmaceutical intervention and plasma transfusion therapy, respectively, leading to the recovery of symptomatic infected and asymptomatic infected people. Thus, the controlled fractional-order model of COVID-19 is given as

$$
\begin{cases}
{}^{C}_{0}D^{\alpha}_{t} S(t) = \Lambda^{\alpha} - (1 - u_1(t))\,\beta^{\alpha} S(t)\,(I(t) + \kappa A(t)) - m^{\alpha} S(t), \\[6pt]
{}^{C}_{0}D^{\alpha}_{t} E(t) = (1 - u_1(t))\,\beta^{\alpha} S(t)\,(I(t) + \kappa A(t)) - (1 - \delta)\,\omega^{\alpha} E(t) \\[3pt]
\qquad\qquad - \delta\bar{\omega}^{\alpha} E(t) - m^{\alpha} E(t), \\[6pt]
{}^{C}_{0}D^{\alpha}_{t} I(t) = (1 - \delta)\,\omega^{\alpha} E(t) - (\gamma^{\alpha} + m^{\alpha}) I(t) - u_2(t) R(t) I(t), \qquad (2) \\[6pt]
{}^{C}_{0}D^{\alpha}_{t} A(t) = \delta\bar{\omega}^{\alpha} E(t) - (\bar{\gamma}^{\alpha} + m^{\alpha}) A(t) - u_3(t) A(t), \\[6pt]
{}^{C}_{0}D^{\alpha}_{t} R(t) = \gamma^{\alpha} I(t) + \bar{\gamma}^{\alpha} A(t) - m^{\alpha} R(t) + u_2(t) R(t) I(t) \\[3pt]
\qquad\qquad + u_3(t) A(t),
\end{cases}
$$

where the preventive control strategies are implemented to the system (1) during the period $[0, t_f]$, and the admissible set of control functions $u_1(t)$, $u_2(t)$, and $u_3(t)$ are given as

$$
U_{ad} = \left\{ (u_1, u_2, u_3) \mid 0 \le u_1 u_2,\, u_3 \le 1,\ 0 \le t \le t_f \right\}. \qquad (3)
$$

2 Formulation of FOCPs and Its Optimality Systems

In this section, an FOCP is considered to prevent the spread of COVID-19 from becoming a pandemic. For this aim, optimal preventive strategies are enhanced in accordance with the dynamics of system (2). The purpose of the objective functional is to minimize both the rate of exposed, symptomatic infected, and asymptomatic infected and the cost of non-pharmaceutical and pharmaceutical intervention, and plasma transfusion therapy. Thus, the objective functional is given by

$$
\min J\left(E, I, A, u_{1}, u_{2}, u_{3}\right) = \int_{0}^{t_f} \Big(\epsilon_1 E\left(t\right) + \epsilon_2 I\left(t\right) + \epsilon_3 A\left(t\right) + \eta_1 u_1^2\left(t\right) + \eta_2 u_2^2\left(t\right)
$$
$$
+ \eta_3 u_3^2\left(t\right)\Big) dt, \tag{4}
$$

where ϵ_1, ϵ_2, ϵ_3, η_1, η_2, and η_3 are the positive weight coefficients.

To solve the consist problem Eqs. (2–4), the Hamiltonian formulation $\mathcal{H}$ of the FOCP is produced as

$$
\begin{aligned}
\mathcal{H} &= \epsilon_1 E\left(t\right) + \epsilon_2 I\left(t\right) + \epsilon_3 A\left(t\right) + \eta_1 u_1^2\left(t\right) + \eta_2 u_2^2\left(t\right) + \eta_3 u_3^2\left(t\right) \\
&\quad + \lambda_1\left(t\right)\left(\Lambda^\alpha - \left(1 - u_1\left(t\right)\right)\beta^\alpha S\left(t\right)\left(I_p\left(t\right) + \kappa A\left(t\right)\right) - m^\alpha S\left(t\right)\right) \\
&\quad + \lambda_2\left(t\right)\left(\left(1 - u_1\left(t\right)\right)\beta^\alpha S\left(t\right)\left(I\left(t\right) + \kappa A\left(t\right)\right) - \left(1 - \delta\right)\omega^\alpha E\left(t\right)\right. \\
&\quad \left. - \delta\bar{\omega}^\alpha E\left(t\right) - m^\alpha E\left(t\right)\right) \\
&\quad + \lambda_3\left(t\right)\left(\left(1 - \delta\right)\omega^\alpha E\left(t\right) - \left(\gamma^\alpha + m^\alpha\right)I\left(t\right) - u_2\left(t\right)R\left(t\right)I\left(t\right)\right) \\
&\quad + \lambda_4\left(t\right)\left(\delta\bar{\omega}^\alpha E\left(t\right) - \left(\bar{\gamma}^\alpha + m^\alpha\right)A\left(t\right) - u_3\left(t\right)A\left(t\right)\right) \\
&\quad + \lambda_5\left(t\right)\left(\gamma^\alpha I\left(t\right) + \bar{\gamma}^\alpha A\left(t\right) - m^\alpha R\left(t\right) + u_2\left(t\right)R\left(t\right)I\left(t\right)\right. \\
&\quad \left. + u_3\left(t\right)A\left(t\right)\right).
\end{aligned} \tag{5}
$$

Now, the fractional necessary optimality conditions are revealed by Pontryagin's Maximum Principle [44].

2.1 Optimality Systems

Theorem 1 *Let $\left(u_1^*, u_2^*, u_3^*\right) \in U_{ad}$ be the optimal controls that minimize the objective functional (4) and $(S^*, E^*, I^*, A^*, R^*)$ is the optimal solution for the system (2). Thus, there are costate variables $\left(\lambda_1, \lambda_2, \lambda_3, \lambda_4, \lambda_5\right)$ that provide*

$$
\begin{cases}
{}^{C}_{t}D^{\alpha}_{t_f}\lambda_1(t) = -\lambda_1(t)\left(\left(1-u_1^*(t)\right)\beta^{\alpha}\left(I^*(t)+\kappa A^*(t)\right)+m^{\alpha}\right) \\
\qquad\qquad +\lambda_2(t)\left(\left(1-u_1^*(t)\right)\beta^{\alpha}\left(I^*(t)+\kappa A^*(t)\right)\right), \\
{}^{C}_{t}D^{\alpha}_{t_f}\lambda_2(t) = \epsilon_1 - \lambda_2(t)\left((1-\delta)\omega^{\alpha}+\delta\bar{\omega}^{\alpha}+m^{\alpha}\right)+\lambda_3(t)(1-\delta)\omega^{\alpha} \\
\qquad\qquad +\lambda_4(t)\delta\bar{\omega}^{\alpha}, \\
{}^{C}_{t}D^{\alpha}_{t_f}\lambda_3(t) = \epsilon_2 - \lambda_1(t)\left(\left(1-u_1^*(t)\right)\beta^{\alpha}S^*(t)\right) \\
\qquad\qquad +\lambda_2(t)\left(\left(1-u_1^*(t)\right)\beta^{\alpha}S^*(t)\right) \\
\qquad\qquad -\lambda_3(t)\left(\gamma^{\alpha}+m^{\alpha}+u_2^*(t)R^*(t)\right)+\lambda_4(t)\left(\gamma^{\alpha}+u_2^*(t)R^*(t)\right), \\
{}^{C}_{t}D^{\alpha}_{t_f}\lambda_4(t) = \epsilon_3 - \lambda_1(t)\left(\left(1-u_1^*(t)\right)\beta^{\alpha}S^*(t)\kappa\right) \\
\qquad\qquad +\lambda_2(t)\left(\left(1-u_1^*(t)\right)\beta^{\alpha}S^*(t)\kappa\right) \\
\qquad\qquad -\lambda_4(t)\left(\bar{\gamma}^{\alpha}+m^{\alpha}+u_3^*(t)\right)+\lambda_5(t)\left(\bar{\gamma}^{\alpha}+u_3^*(t)\right), \\
{}^{C}_{t}D^{\alpha}_{t_f}\lambda_5(t) = -\lambda_4(t)u_2^*(t)I^*(t)+-\lambda_5(t)\left(u_2^*(t)I^*(t)-m^{\alpha}\right),
\end{cases}
\tag{6}
$$

with transversality conditions $\lambda_i\left(t_f\right)=0$ $(i=1,2,3,4,5)$. Furthermore, the optimal control variables $\left(u_1^*, u_2^*, u_3^*\right)$ are achieved as

$$
\begin{cases}
u_1^*(t) = \max\left\{\min\left\{\frac{(\lambda_2(t)-\lambda_1(t))\beta^{\alpha}\left(I^*(t)+\kappa A^*(t)\right)}{2\eta_1}, 1\right\}, 0\right\}, \\
u_2^*(t) = \max\left\{\min\left\{\frac{(\lambda_3(t)-\lambda_5(t))I^*(t)R^*(t)}{2\eta_2}, 1\right\}, 0\right\}, \\
u_3^*(t) = \max\left\{\min\left\{\frac{(\lambda_4(t)-\lambda_5(t))A^*(t)}{2\eta_3}, 1\right\}, 0\right\}.
\end{cases}
\tag{7}
$$

Proof Since the state variables S, E, I, A, and R in the system (2) satisfy the Lipschitz condition, the existence of optimal control variables (u_1, u_2, u_3) is provided [45, 46]. For the solution of the formulated FOCP, the necessary optimality conditions proposed by Agrawal in terms of the Caputo derivative are benefited [27]. Thus the fractional Euler–Lagrange equations are given as follows:

$$
\begin{cases}
\text{State system:} \\
{}^{C}_{0}D^{\alpha}_{t}S = \frac{\partial\mathcal{H}}{\partial\lambda_1}, \ {}^{C}_{0}D^{\alpha}_{t}E = \frac{\partial\mathcal{H}}{\partial\lambda_2}, \ {}^{C}_{0}D^{\alpha}_{t}I = \frac{\partial\mathcal{H}}{\partial\lambda_3}, \\
{}^{C}_{0}D^{\alpha}_{t}A = \frac{\partial\mathcal{H}}{\partial\lambda_4}, \ {}^{C}_{0}D^{\alpha}_{t}R = \frac{\partial\mathcal{H}}{\partial\lambda_5}. \\
\text{Costate system:} \\
{}^{C}_{t}D^{\alpha}_{t_f}\lambda_1 = \frac{\partial\mathcal{H}}{\partial S}, \ {}^{C}_{t}D^{\alpha}_{t_f}\lambda_2 = \frac{\partial\mathcal{H}}{\partial E}, \ {}^{C}_{t}D^{\alpha}_{t_f}\lambda_3 = \frac{\partial\mathcal{H}}{\partial I}, \\
{}^{C}_{t}D^{\alpha}_{t_f}\lambda_4 = \frac{\partial\mathcal{H}}{\partial A}, \ {}^{C}_{t}D^{\alpha}_{t_f}\lambda_5 = \frac{\partial\mathcal{H}}{\partial R}. \\
\text{Control system:} \\
\frac{\partial\mathcal{H}}{\partial u_1} = 0, \ \frac{\partial\mathcal{H}}{\partial u_2} = 0, \ \frac{\partial\mathcal{H}}{\partial u_3} = 0.
\end{cases}
$$

The costate system is acquired by using the fractional Euler–Lagrange equations as

$$\begin{cases} {}^{C}_{t}D^{\alpha}_{t_f}\lambda_1(t) = -\lambda_1(t)\left(\left(1-u^*_1(t)\right)\beta^{\alpha}\left(I^*(t)+\kappa A^*(t)\right)+m^{\alpha}\right) \\ \qquad\quad +\lambda_2(t)\left(\left(1-u^*_1(t)\right)\beta^{\alpha}\left(I^*(t)+\kappa A^*(t)\right)\right), \\ {}^{C}_{t}D^{\alpha}_{t_f}\lambda_2(t) = \epsilon_1 - \lambda_2(t)\left((1-\delta)\omega^{\alpha}+\delta\bar{\omega}^{\alpha}+m^{\alpha}\right) \\ \qquad\quad +\lambda_3(t)(1-\delta)\omega^{\alpha}+\lambda_4(t)\delta\bar{\omega}^{\alpha}, \\ {}^{C}_{t}D^{\alpha}_{t_f}\lambda_3(t) = \epsilon_2 - \lambda_1(t)\left(\left(1-u^*_1(t)\right)\beta^{\alpha}S^*(t)\right) \\ \qquad\quad +\lambda_2(t)\left(\left(1-u^*_1(t)\right)\beta^{\alpha}S^*(t)\right) \\ \qquad\quad -\lambda_3(t)\left(\gamma^{\alpha}+m^{\alpha}+u^*_2(t)R^*(t)\right)+\lambda_4(t)\left(\gamma^{\alpha}+u^*_2(t)R^*(t)\right) \\ {}^{C}_{t}D^{\alpha}_{t_f}\lambda_4(t) = \epsilon_3 - \lambda_1(t)\left(\left(1-u^*_1(t)\right)\beta^{\alpha}S^*(t)\kappa\right) \\ \qquad\quad +\lambda_2(t)\left(\left(1-u^*_1(t)\right)\beta^{\alpha}S^*(t)\kappa\right) \\ \qquad\quad -\lambda_4(t)\left(\bar{\gamma}^{\alpha}+m^{\alpha}+u^*_3(t)\right)+\lambda_5(t)\left(\bar{\gamma}^{\alpha}+u^*_3(t)\right), \\ {}^{C}_{t}D^{\alpha}_{t_f}\lambda_5(t) = -\lambda_4(t)u^*_2(t)I^*(t)+-\lambda_5(t)\left(u^*_2(t)I^*(t)-m^{\alpha}\right) \end{cases}$$

with transversality conditions $\lambda_i\left(t_f\right)=0$ $(i=1,2,3,4,5)$. Similarly, the control system is arrived as

$$\begin{cases} \frac{\partial\mathcal{H}}{\partial u_1}\big|_{u_1=u^*_1(t)} = 2\eta_1 u^*_1(t)+(\lambda_1(t)-\lambda_2(t))\beta^{\alpha}(t)(I^*(t)+\kappa A^*(t))=0, \\ \frac{\partial\mathcal{H}}{\partial u_2}\big|_{u_2=u^*_2(t)} = 2\eta_2 u^*_2(t)+(-\lambda_3(t)+\lambda_5(t))I^*(t)R^*(t)=0, \\ \frac{\partial\mathcal{H}}{\partial u_3}\big|_{u_3=u^*_3(t)} = 2\eta_3 u^*_3(t)+(-\lambda_4(t)+\lambda_5(t))A^*(t)=0. \end{cases}$$

According to admissible set U_{ad}, the optimal control values of the control system are attained as in Eq. (7).

3   Numerical Results and Discussion

In this section, the impact of the proposed triple preventive control strategy on the spread of COVID-19 is shown with numerical results. Adam's type PCM [47] combined with the FBSA is applied to the optimality system formed by (2), (6), and (7). The parameter values used are the values of the epidemics in the city of Wuhan given in Table 1. For numerical results, the final time is taken $t_f=50$, and the initial conditions are assumed as $S(0)=0.80$, $E(0)=0.07$, $I(0)=0.10$, $A(0)=0.03$, and $R(0)=0$. Additionally, the weight coefficients are $\epsilon_1=\epsilon_2=\epsilon_3=10$, $\eta_1=0.05$, and $\eta_2=\eta_3=0.25$. According to the values, the state, costate, and control systems are solved using MATLAB. The proposed FOCP for the initial spread of COVID-19 in the city of Wuhan is graphically discussed below, with single, double, and triple control strategies.

Table 1 Interpretation of parameters in system (2)

Parameter	Description	Value	Unit
Λ^{α}	The birth rate of people in the total population	$(0.0018)^{\alpha}$ [8]	day$^{-\alpha}$
β^{α}	The infection rate from I and A to S	$(0.6870)^{\alpha}$ [8]	day$^{-\alpha}$
κ	The transmissibility of A is κ times that of I.	0.5 [8]	unitless
m^{α}	The death rate of people	$(0.0018)^{\alpha}$ [8]	day$^{-\alpha}$
δ	The proportion of asymptomatic infection rate of people	0.5 [8]	unitless
ω^{α}	The incubation period of people	$(0.1923)^{\alpha}$ [8]	day$^{-\alpha}$
$\bar{\omega}^{\alpha}$	The latent period of people	$(0.1923)^{\alpha}$ [8]	day$^{-\alpha}$
γ^{α}	The infectious period of symptomatic infection of people	$(0.1724)^{\alpha}$ [8]	day$^{-\alpha}$
$\bar{\gamma}^{\alpha}$	The infectious period of asymptomatic infection of people	$(0.1724)^{\alpha}$ [8]	day$^{-\alpha}$
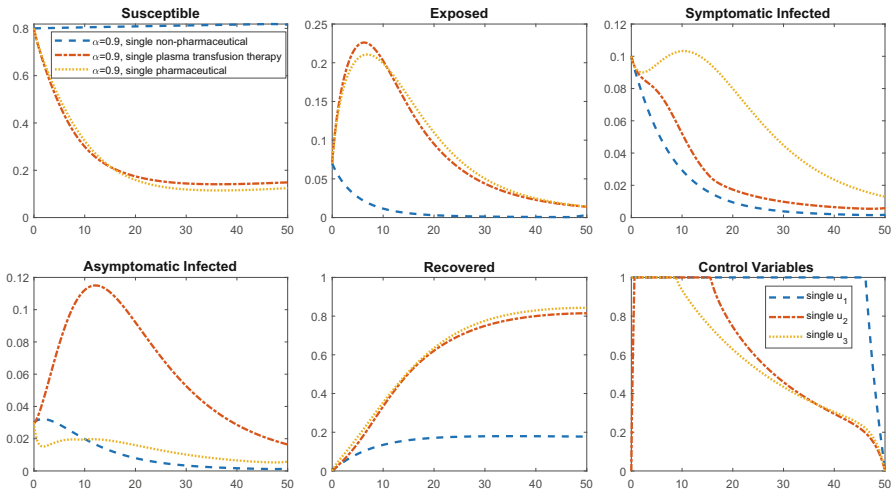
Fig. 1 Graphical comparison of single control strategies with Caputo derivative for $\alpha = 0.90$

3.1 Single Control Strategy

In a single control strategy, appropriate objective functionals for non-pharmaceutical intervention, plasma transfusion therapy, and pharmaceutical intervention controls are determined and minimized. Figure 1 displays the effectiveness of these strategies for $\alpha = 0.90$. Non-pharmaceutical intervention control adapted to susceptible people reduces medication and hospitalizations as it protects against infection. Furthermore, it is shown that plasma transfusion therapy and pharmaceutical intervention for symptomatic and asymptomatic infected people are influential. Although both controls treat infected people separately, pharmaceutical intervention displays a higher recovery rate. Compared to single control strategies, non-pharmaceutical intervention gives the most satisfactory result not only for susceptible people but also for the total population.

3.2 Double Control Strategy

Double control strategies are examined in different combinations.

3.2.1 Strategy 1

In this strategy, non-pharmaceutical intervention and plasma transfusion therapy controls are imposed to minimize the objective functional. Figure 2 exhibits the impact of the strategy with controlled and uncontrolled situations for $\alpha = 0.90$. According to this figure, symptomatic infected people recover with plasma transfusion therapy, and exposed people are also reduced rapidly by non-pharmaceutical intervention. Thus, it is observed that the emergence of new infections is prevented. This strategy is observed to drop exposed people rapidly, thus preventing the emergence of new infections.

3.2.2 Strategy 2

In this strategy, the objective functional is minimized by utilizing non-pharmaceutical intervention and pharmaceutical intervention controls. As can be seen in Fig. 3, Strategy 2 for $\alpha = 0.90$ also effectively reduces the exposed people, greatly eliminating the infection. Strategy 1 and Strategy 2 are compared in Fig. 4 for $\alpha = 0.90$ to decide which strategy yields more impact results. Although different medicines for symptomatic and asymptomatic people may make little difference, the
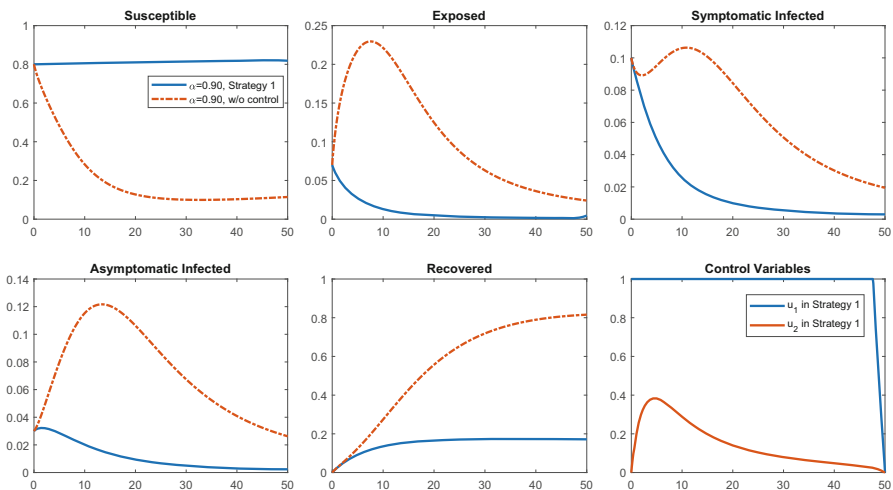
Fig. 2 The effects of Strategy 1 with Caputo derivative for $\alpha = 0.90$
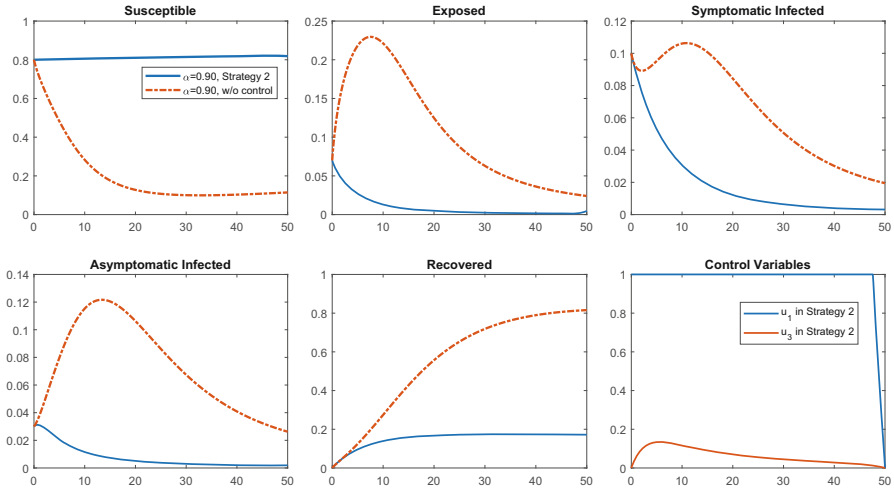
Fig. 3 The effects of Strategy 2 with Caputo derivative for $\alpha = 0.90$
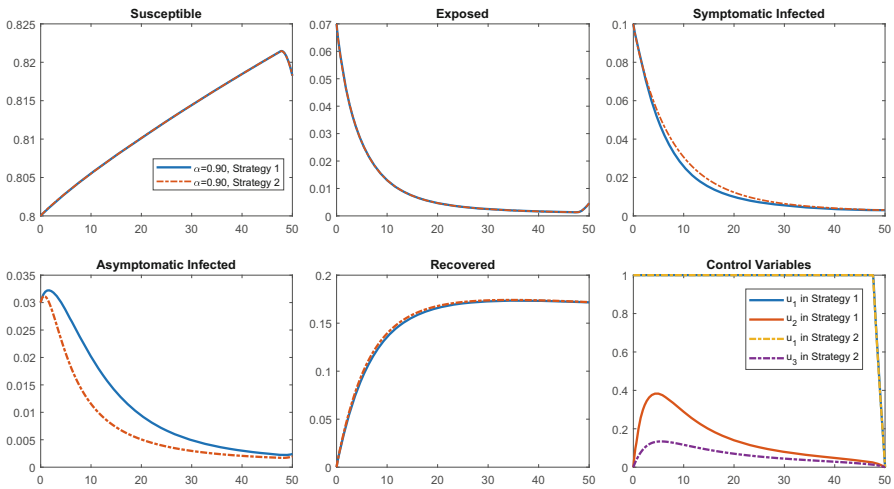
Fig. 4 Graphical comparison of Strategy 1 and Strategy 2 with Caputo derivative for $\alpha = 0.90$

strategies produce almost the same response for susceptible, exposed, and recovered people. Thus, it is concluded that both strategies are beneficial in controlling the infection.
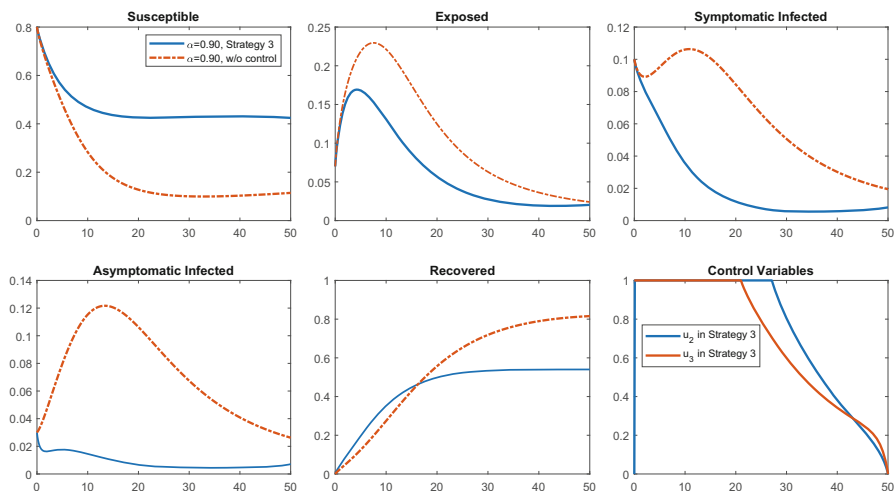
Fig. 5 The effects of Strategy 3 with Caputo derivative for $\alpha = 0.90$

3.2.3 Strategy 3

In this strategy, plasma transfusion therapy and pharmaceutical intervention controls are implemented to minimize the objective functional. Figure 5 illustrates the effect of Strategy 3 for $\alpha = 0.90$. The infection rate gradually fades in that infected people are treated with plasma transfusion therapy and pharmaceutical intervention controls. But unfortunately, people are vulnerable to the infection without non-pharmaceutical intervention. Hence, the rate of susceptible people stays low compared to Strategy 1 and Strategy 2.

3.3 Triple Control Strategy

In the triple control strategy, non-pharmaceutical intervention, plasma transfusion therapy, and pharmaceutical intervention controls are performed in order to minimize the objective functional. In Fig. 6, it is inferred that the implementing triple control strategy is fairly effective for $\alpha = 0.90$ because this control strategy protects susceptible people against infection, decreases exposed people, and resets symptomatic and asymptomatic infected people after the twentieth day. Thus, recovered people remain at a lower rate. The infection is almost eradicated, as the cases damping quickly. Therefore, the spread of COVID-19 is taken contain. As seen in Fig. 6, control $u_1(t)$ exerts more effort than controls $u_2(t)$ and $u_3(t)$ in the triple control strategy. As a result, it is deduced from Fig. 7 that the triple control strategy is the most satisfactory.
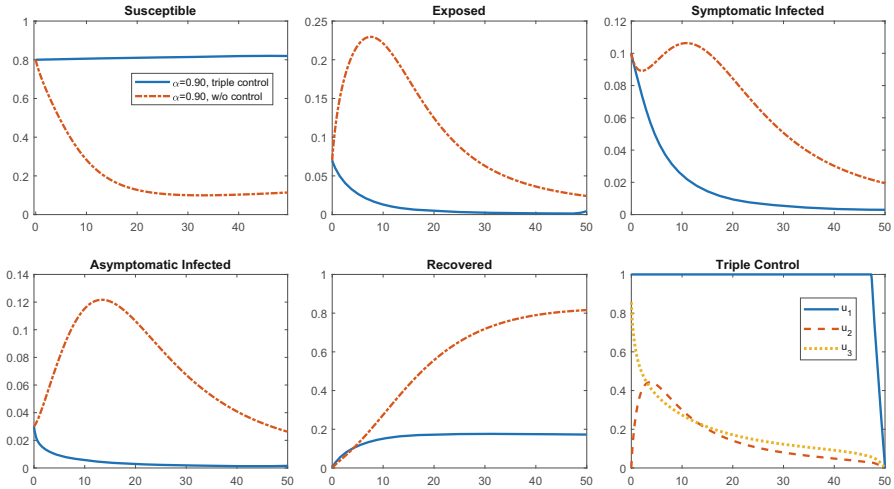
Fig. 6 The effects of triple control strategy with Caputo derivative for $\alpha = 0.90$
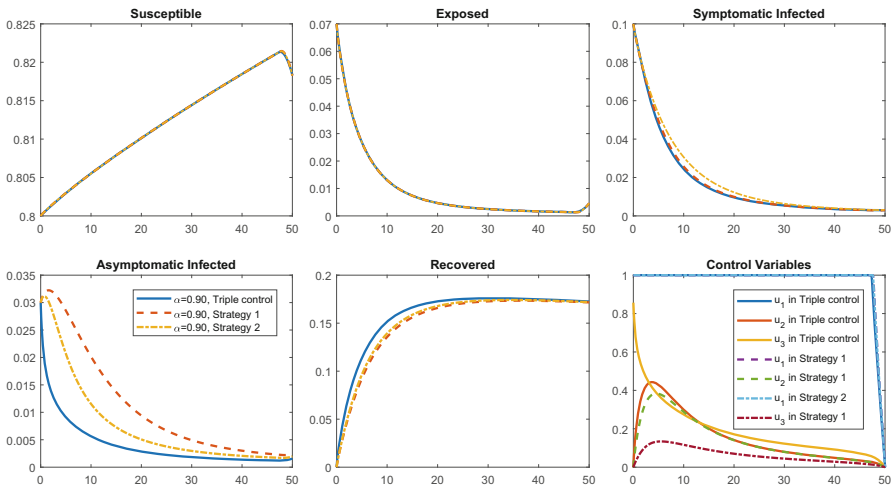
Fig. 7 Graphical comparison of triple control strategy, Strategy 1, and Strategy 2 with Caputo derivative for $\alpha = 0.90$

3.4 Comparative Analysis

Considering COVID-19 has an exponential law in a heterogeneous biological network, the first spread model of COVID-19 is also appropriate to discuss with the ABC derivative. In line with this objective, the optimality system of the problem is achieved and the numerical method presented in [48] in terms of ABC derivative
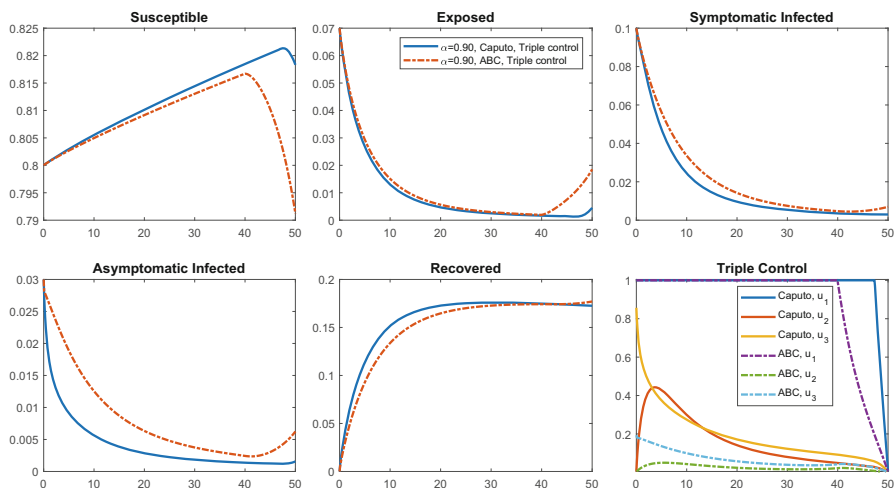
Fig. 8 Comparative analysis of Caputo and ABC derivatives with triple control strategy for $\alpha = 0.90$

is benefited in the solution. In addition, since the triple control strategy gives the best impact, all comparative results are analyzed with this strategy.

Figure 8 demonstrates the triple preventive control strategy for $\alpha = 0.90$ in comparison with Caputo and ABC derivatives. Both fractional derivatives show similar behavior, reducing the infection until the fortieth day. However, after that day, the strategy proposed with the ABC derivative loses its effect and decreases at the rate of the susceptible people. So, there is an increase in exposed, symptomatic, and asymptomatic infected people compared to the Caputo derivative. The reason is that the controls display different behaviors according to the fractional operators. In particular, although the control $u_1(t)$ exerts the same effort for both derivatives until the fortieth day, the ABC derivative starts to wield less effort after that day. Therefore, it is concluded that the fractional operator affects the control behavior and changes the course of the disease.

Figure 9 comparatively shows the triple preventive strategy of both derivatives for $\alpha = 0.80$. Compared to Fig. 8, the reduction in derivative order alters the spread of the infection. For $\alpha = 0.80$, the effort of the controls in the ABC derivative is still less than in the Caputo derivative, and however its effect fades after a few days compared to $\alpha = 0.90$. Such infections are required to destroy in that these infections are a burden to society in terms of health and the economy. For this reason, control measures are governed to eradicate the disease. Yet, Fig. 9 shows that the strategy with the ABC derivative increases toward the final time in exposed, symptomatic, and asymptomatic infected people.

As a result, the proposed preventive control strategies provide the desired result in dealing with COVID-19 in a short period, allowing the epidemic in Wuhan City to fade quickly. It means that it does not produce a burden on the world in terms of
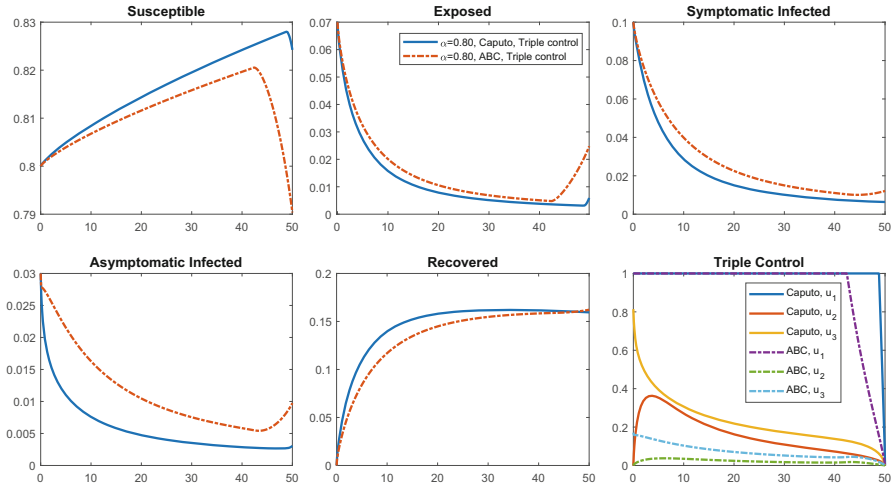
Fig. 9 Comparative analysis of Caputo and ABC derivatives with triple control strategy for $\alpha = 0.80$

health and economy. Moreover, it is concluded that although the proposed strategies with both derivative operators control the spread, the Caputo derivative exhibits more stable behavior.

4 Conclusions

This chapter explores optimal preventive strategies that, if implemented, would prevent the COVID-19 epidemic from becoming a pandemic. For this purpose, an FOCP has been proposed for the model representing COVID-19 that started in Wuhan City, Hubei Province, China. First, the model has been modified in sense of the Caputo derivative to appropriately study the spread of COVID-19 in a heterogeneous biological network. Afterward, preventive control strategies have been adapted representing non-pharmaceutical intervention for susceptible people, plasma transfusion therapy for symptomatic infected people, and pharmaceutical intervention for asymptomatic infected people. The FOCP has been numerically solved using Adam's type PCM combined with the FBSA with help of the MATLAB. Single, double, and triple control strategies have been compared with the graphical results. It has been observed that the triple control strategy delivered the most efficient result in the shortest period. Moreover, since COVID-19 also shows exponential law distribution, the model has been discussed in terms of ABC derivative and solved with the same numerical approach by implementing the triple control strategy. Caputo and ABC derivatives have been analyzed comparatively in different orders for the best response triple preventive control strategy. It has

been examined from the graphs that this strategy quickly damped and contained the infection for both fractional derivatives. However, the Caputo derivative has been more suitable for this strategy as it more consistently reflected the expected result. As a result, it has been concluded that the triple control strategy is effective in controlling the aggressive spread in Wuhan City, thus preventing it from becoming a pandemic.

References

1. World Health Organization: Coronavirus. World Health Organization, https://www.who.int/health-topics/coronavirus. Accessed 5 Nov 2022
2. Zhou, P., et al.: A pneumonia outbreak associated with a new coronavirus of probable bat origin. Nature **579**(7798), 270–273 (2020)
3. Li, Q., et al.: Early transmission dynamics in Wuhan, China, of novel coronavirus–infected pneumonia. New Eng. J. Med. **382**, 1199–1207 (2020)
4. Huang, C., et al.: Clinical features of patients infected with 2019 novel coronavirus in Wuhan, China. Lancet **395**(10223), 497–506 (2020)
5. Sharma, S., Samanta, G.P.: Analysis of a hand–foot–mouth disease model. Int. J. Biomath. **10**(02), 1750016 (2017)
6. Bonyah, E., Khan, M.A., Okosun, K.O., Islam, S.: A theoretical model for Zika virus transmission. PloS one **12**(10), e0185540 (2017)
7. Egonmwan, A.O., Okuonghae, D.: Analysis of a mathematical model for tuberculosis with diagnosis. J. Appl. Math. Comput. **59**, 129–162 (2019)
8. Chen, T.M., Yin, L.A., et al.: Mathematical model for simulating the phase-based transmissibility of a novel coronavirus. Infect. Dis. Poverty **9**(1), 1–8 (2020)
9. Hou, C., et al.: The effectiveness of quarantine of Wuhan City against the Corona Virus Disease 2019 (COVID-19): a well-mixed SEIR model analysis. J. Med. Virol. **92**(7), 841–848 (2020)
10. Ndaïrou, F., Area, I., Nieto, J.J., Torres, D.F.: Mathematical modeling of COVID-19 transmission dynamics with a case study of Wuhan. Chaos Solit. Fractals **135**, 109846 (2020)
11. Lemos-Paião, A.P., Silva, C.J., Torres, D.F.: A new compartmental epidemiological model for COVID-19 with a case study of Portugal. Ecol. Complex. **44**, 100885 (2020)
12. Samui, P., Mondal, J., Khajanchi, S.: A mathematical model for COVID-19 transmission dynamics with a case study of India. Chaos Solit. Fractals 140, 110173 (2020)
13. López, L., Rodo, X.: A modified SEIR model to predict the COVID-19 outbreak in Spain and Italy: simulating control scenarios and multi-scale epidemics. Results Phys. **21**, 103746 (2021)
14. Hamou, A.A., Rasul, R.R., Hammouch, Z., Özdemir, N.: Analysis and dynamics of a mathematical model to predict unreported cases of COVID-19 epidemic in Morocco. Comput. Appl. Math. **41**(6), 1–33 (2022)
15. Khojasteh, H., Khanteymoori, A., Olyaee, M.H.: Comparing protein–protein interaction networks of SARS-CoV-2 and (H1N1) influenza using topological features. Sci. Rep. **12**(1), 1–11 (2022)
16. Eroğlu, B.B.İ., Avcı, D.: Separable solutions of Cattaneo-Hristov heat diffusion equation in a line segment: Cauchy and source problems. Alex. Eng. J. **60**(2), 2347–2353 (2021)
17. Povstenko, Y., Avcı, D., Eroğlu, B.B.İ., Özdemir, N.: Control of thermal stresses in axisymmetric problems of fractional thermoelasticity for an infinite cylindrical domain. Therm. Sci. **21**(1 Part A), 19–28 (2017)
18. Hristov, J.: Magnetic field diffusion in ferromagnetic materials: fractional calculus approaches. Int. J. Optim. Control: Theor. Appl. (IJOCTA) **12**, 20–38 (2022)
19. Singh, J., Kumar, D., Hammouch, Z., Atangana, A.: A fractional epidemiological model for computer viruses pertaining to a new fractional derivative. Appl. Math. Comput. **316**, 504–515 (2018)

20. Naik, P.A., Owolabi, K.M., Zu, J., Naik, M.U.D.: Modeling the transmission dynamics of COVID-19 pandemic in Caputo type fractional derivative. J. Multiscale Model. **12**(03), 2150006 (2021)
21. Joshi, H., Jha, B.K., Yavuz, M.: Modelling and analysis of fractional-order vaccination model for control of COVID-19 outbreak using real data. Math. Biosci. Eng. **20**(1), 213–240 (2023)
22. Lemos-Paião, A.P., Silva, C.J., Torres, D.F.: An epidemic model for cholera with optimal control treatment. J. Comput. Appl. Math. **318**, 168–180 (2017)
23. Baba, I. A., Abdulkadir, R.A., Esmaili, P.: Analysis of tuberculosis model with saturated incidence rate and optimal control. Physica A. **540**, 123237 (2020)
24. Zine, H., El Adraoui, A., Torres, D.F.: Mathematical analysis, forecasting and optimal control of HIV/AIDS spatiotemporal transmission with a reaction diffusion SICA model. AIMS Math. **7**(9), 16519–16535 (2022)
25. Baleanu, D., Shekari, P., Torkzadeh, L., Ranjbar, H., Jajarmi, A., Nouri, K.: Stability analysis and system properties of Nipah virus transmission: a fractional calculus case study. Chaos Solit. Fractals **166**, 112990 (2023)
26. Agrawal, O.P.: A general formulation and solution scheme for fractional optimal control problems. Nonlinear Dyn. **38**, 323–337 (2004)
27. Agrawal, O.P.: A formulation and numerical scheme for fractional optimal control problems. J. Vib. Control **14**(9–10), 1291–1299 (2008)
28. Eroğlu, B.B.İ., Yapışkan, D.: Local generalization of transversality conditions for optimal control problem. Math. Model. Nat. Phenom. **14**(3), 310 (2019)
29. Yildiz, T.A., Jajarmi, A., Yildiz, B., Baleanu, D.: New aspects of time fractional optimal control problems within operators with nonsingular kernel. Discrete Contin. Dyn. Syst. -S. **13**(3), 407–428 (2020)
30. Eroğlu, B.B.İ., Yapışkan, D.: Generalized conformable variational calculus and optimal control problems with variable terminal conditions. AIMS Math. **5**(2), 1105–1126 (2020)
31. Avcı, D., Eroğlu, B.B.İ.: Optimal control of the Cattaneo–Hristov heat diffusion model. Acta Mech. **232**(9), 3529–3538 (2021)
32. Tajadodi, H., Jafari, H., Ncube, M.N.: Genocchi polynomials as a tool for solving a class of fractional optimal control problems. Int. J. Optim. Control: Theor. Appl. **12**(2), 160–168 (2022)
33. Sweilam, N.H., Assiri, T.A., Abou Hasan, M.M.: Optimal control problem of variable-order delay system of advertising procedure: numerical treatment. Discrete Contin. Dyn. Syst.-S. **15**(5), 1247–1268 (2022)
34. Avcı, D., Soytürk, F.: Optimal control strategies for a computer network under virus threat. J. Comput. Appl. Math. **419**, 114740 (2023)
35. Bonyah, E.: Fractional Optimal Control Model for Nutrients, Phytoplankton, and Zooplankton. In: Applications of Fractional Calculus to Modeling in Dynamics and Chaos, pp. 429–452. Chapman and Hall/CRC, New York (2023)
36. Panwar, V.S., Uduman, P.S., Gómez-Aguilar, J.F.: Mathematical modeling of coronavirus disease COVID-19 dynamics using CF and ABC non-singular fractional derivatives. Chaos Solit. Fractals **145**, 110757 (2021)
37. Eroğlu, B.B.İ., Yapışkan, D.: Comparative analysis on fractional optimal control of an SLBS model. J. Comput. Appl. Math. **421**, 114840 (2023)
38. Shen, Z.H., et al.: Mathematical modeling and optimal control of the COVID-19 dynamics. Results Phys. **31**, 105028 (2021)
39. Eroğlu, B.B.İ., Yapışkan, D.: An optimal control strategy to prevent the spread of COVID-19. In: Conference Proceedings of Science Technology, vol. 5(1), pp. 182–186 (2022)
40. Podlubny, I.: Fractional Differential Equations. Academic Press, San Diego (1999)
41. Atangana, A., Baleanu, D.: New fractional derivatives with nonlocal and non-singular kernel: theory and application to heat transfer model. Therm. Sci. **20**(2) 763–769 (2016)
42. Moriyama, M., Hugentobler, W.J., Iwasaki, A.: Seasonality of respiratory viral infections. Annu. Rev. Virol. **7**(1), 83–101 (2020)
43. Focosi, D., Anderson, A.O., Tang, J.W., Tuccori, M.: Convalescent plasma therapy for COVID-19: state of the art. Clin. Microbiol. Rev. **33**(4), e00072-20 (2020)

44. Ali, H.M., Pereira, F.L., Gama, S.M.: A new approach to the Pontryagin maximum principle for nonlinear fractional optimal control problems. Math. Methods Appl. Sci. **39**(13), 3640–3649 (2016)
45. Birkhoff, G., Rota, G.C.C.: Ordinary Differential Equations. John Wiley & Sons, New York (1989)
46. Lukes, D.L.: Differential equations: classical to controlled. Math. Sci. Eng. **162**, 335 (1982). Academic Press, New York
47. Diethelm, K., Ford, N.J., Freed, A.D.: A predictor-corrector approach for the numerical solution of fractional differential equations. Nonlinear Dyn. **29**(1), 3–22 (2002)
48. Baleanu, D., Jajarmi, A., Sajjadi, S.S., Mozyrska, D.: A new fractional model and optimal control of a tumor-immune surveillance with non-singular derivative operator. Chaos **29**(8), 083127 (2019)

Modeling and Analysis of COVID-19 Based on a Deterministic Compartmental Model and Bayesian Inference

Touria Jdid, Mohammed Benbrahim, Mohammed Nabil Kabbaj, and Mohamed Naji

1 Introduction

COVID-19 has been spreading worldwide, affecting every aspect of our lives and resulting in over 6 million deaths as of December 13, 2022 [1]. The spread of COVID-19 has prompted several countries to undertake urgent non-pharmaceutical interventions and vaccination programs to contain the expansion of the outbreak and return to pre-pandemic life [2]. Understanding how COVID-19 spreads [3], evaluating the effectiveness of contingency plans [4], and predicting infection and death rates [5] in addition to intensive care unit admissions [6] are of great interest to policymakers and society. Over the past three years, mathematical models have been instrumental in mitigating the COVID-19 pandemic, so they have helped decision-makers to take public health actions with greater efficiency [7].

In modeling COVID-19 dynamics, we used deterministic compartmental models [8], in which one can stratify the entire population into homogeneous groups known as compartments, classes, or categories. In a compartment, individuals are regarded to be in the same infectious state. The transition of individuals from one state to another is modeled using a system of ordinary differential equations. These models have been widely used in modeling, controlling, and forecasting COVID-19 [9] and [10]. In [11], a study has been conducted to evaluate the influence of a vaccine on controlling the pandemic of COVID-19 in the United States. In [12], the authors

T. Jdid (✉) · M. Benbrahim · M. N. Kabbaj
LIMAS, Faculty of Sciences, Sidi Mohamed Ben Abdellah University, Fez, Morocco
e-mail: touria.jdid@usmba.ac.ma; mohammed.benbrahim@usmba.ac.ma;
n.kabbaj@usmba.ac.ma

M. Naji
LPAIS, Faculty of Sciences, Sidi Mohamed Ben Abdellah University, Fez, Morocco
e-mail: mohamed.naji3@usmba.ac.ma

introduced a compartmental framework for COVID-19 to assess vaccine efficacy and coverage required to stop the outbreak if social contact were to turn back to the levels before the pandemic and face mask usage was reduced.

The robustness of the results produced by an epidemic model relies on the accuracy of its parameter estimates. Therefore, the number of research that performs inference techniques of COVID-19 spread within societies using mathematical models (compartmental and agent-based models) increases exponentially. In epidemiology, the commonly used approaches to estimate model parameters are the classical approach (curve fitting), where the parameters are fixed quantities and their values inferred from infectious disease count data using estimators, and the Bayesian inference, where the parameters are random variables sampled from the posterior distribution. The Bayesian statistical inference has some advantages compared to curve fitting. First, the foundation of the Bayesian framework on Markov Chain Monte Carlo (MCMC) algorithms makes it easier to obtain accurate estimates of model parameters and their percentiles and quantify uncertainties. Second, the sampling process in this framework explores both the posterior and marginal posterior density of the quantities of interest and the functions of these quantities, like threshold parameters. For illustration, in epidemiology, we are usually interested in a quantity called the basic reproduction number (R_0) [13]. This quantity behaves as a threshold parameter whose value is estimated from a mathematical model and tells whether an outbreak is likely to persist if R_0 has a value >1 and to die out if R_0 is <1. Third, in complex epidemic models with many parameters, the nonlinear correlations between parameters increase. So, in this case, using Bayesian inference helps us to identify the quantities of interest.

In the literature, there are two fundamental types of MCMC algorithms: classical or standard MCMC algorithms [14], in which searching the parameter space is performed according to the random walk, and the HMC algorithm [15], whose foundation is based on differential geometry and Hamiltonian dynamics. We provide a detailed explanation of these algorithms in Sect. 3. Recently, many studies have used these algorithms to identify model parameters from the data [16] and [17]. In [18], Acuña-Zegarra et al. investigated the impact of behavior changes needed to diminish community transmission of COVID-19 based on a modified SEIR modeling. They simulated the model using the t-walk algorithm, an MCMC algorithm. Andrade et al. examined the performance of the HMC algorithm by fitting an SEIR epidemic model structured by age to synthetic data [19]. In doing so, they compared the performance of the HMC with the Nelder–Mead algorithm.

In this study, we formulate a deterministic epidemiological model that contains nine compartments to study the evolution of COVID-19 propagation. The model accounts for the COVID-19 incubation time and the transmission of the infection by asymptomatic carriers. It allows tracking of infected patients quarantined at home and in the hospital. Furthermore, it provides the possibility to implement a vaccination strategy as it contains a compartment for the vaccinated individuals. We calibrate our model in the absence of vaccination on the Moroccan data, corresponding to the first wave of the outbreak, from March 2 to June 10, 2020. For this purpose, we apply two methods: curve fitting and Bayesian statistical

inference using the HMC algorithm. Numerical simulations from fitting the model to the data for both methods showed that our model is consistent with the data and more accurately reproduces the COVID-19 epidemic in Morocco. The parameter estimates obtained by Bayesian inference using HMC are, on average, similar to those obtained by curve fitting using the Nelder–Mead optimization method. We further account for the dynamics of vaccination in the model by assuming a daily baseline vaccination rate of 0.008, a baseline vaccine characterized by 79% efficacy, and an immunity period of 183 days and simulate the model to assess vaccination programs. Results showed that we should increase the daily vaccination rate from its baseline and use a high-efficacy vaccine, greater than 79%, to protect people from COVID-19 infection.

This chapter is organized as follows. A detailed description of our modeling framework is presented in Sect. 2. The methodology followed to calibrate the model using curve fitting and the HMC algorithm and the obtained numerical results are given in Sect. 3. Then, in Sect. 4, we introduce two scenarios to assess the effect of vaccination programs on the evolution of daily confirmed cases in Morocco. Section 5 contains a summary of the relevant findings and some discussions.

2   Modeling Framework

We propose a deterministic epidemic model (Fig. 1) for the COVID-19 dynamics stratified by infection state into nine classes, namely, Susceptible (S), Exposed (E), Symptomatic Infectious (I_S), Asymptomatic Infectious (I_A), Hospitalized (H), Quarantined (Q), Recovered (R), Dead (D), and Vaccinated (V). The population is assumed to be constant of size N ($N(t) = S(t) + E(t) + I_S(t) + I_A(t) + H(t) + Q(t) + R(t) + V(t)$), where S(t), E(t), $I_S(t)$, $I_A(t)$, H(t), Q(t), R(t), and V(t) stand for
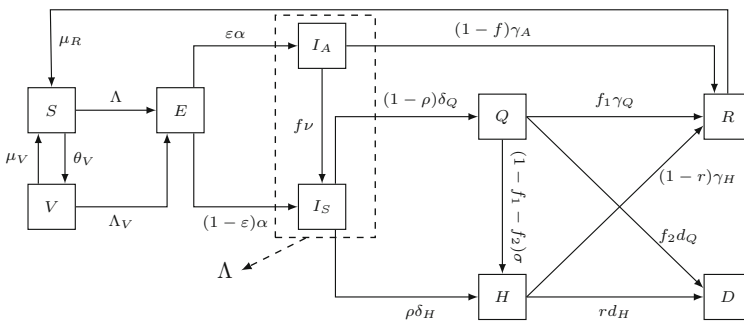
Fig. 1 Flow chart of the epidemic model. Classes S, E, I_S, I_A, H, Q, R, D, and V stand for the populations of susceptible, exposed, Symptomatic Infectious, Asymptomatic Infectious, hospitalized, quarantined, recovered, dead, and vaccinated individuals, respectively

the number of individuals within each compartment at time t. The model assumes that all individuals are initially equally susceptible and become exposed upon effective contact with an infectious class (symptomatic or asymptomatic). Once the incubation period ends, exposed individuals become contagious and progress to either symptomatic or asymptomatic classes with a rate of α. Depending on the severity of COVID-19 disease, symptomatic individuals move to hospitalized or quarantined classes at the transition rates δ_H and δ_Q, respectively. Asymptomatic individuals were supposed to have naturally recovered from the disease at a rate of γ_Q. A proportion f of them is assumed to develop clinical symptoms with a delay of $1/\nu$ day and move into the symptomatic compartment. We assume that hospitalized patients are in isolation, receive treatment, and cannot transmit the disease to the susceptible population. They are recovering from COVID-19 at a rate of γ_H or moving to the deceased category at a rate of d_H. Individuals quarantined at home are followed and admitted to the hospital immediately as their condition progresses, at a rate of σ. People in quarantine who refuse to be admitted to the hospital are likely to die from COVID-19 at a rate of d_Q. A fraction of them recover from COVID-19 at a rate of γ_Q. Individuals who recovered from natural COVID-19 infection are losing immunity at a rate of μ_R and joining the susceptible population. People who die from the disease are not involved in the COVID-19 dynamics. Due to the short simulation time frame, the model does not include vital dynamics.

In vaccination strategy, we consider the following assumptions:

– Only susceptible, exposed, asymptomatic infectious, and recovered individuals can receive the vaccine. Infectious people with clinical symptoms and hospitalized and quarantined patients are not eligible for vaccination.
– Only the COVID-19 variant is considered.
– The effects of the vaccine are only seen in susceptible people.
– A fraction of the susceptible population becomes vaccinated against COVID-19 at a rate of θ_V.
– Depending on the vaccine profile, a candidate for vaccination is assumed to receive one or two doses.
– The vaccine is assumed imperfect and has an efficacy, denoted by E_V, with $0 < E_V < 1$.
– A fraction of those vaccinated are likely to be infected with COVID-19 with a probability $(1 - E_V)$.
– Vaccinated people will lose immunity at the rate of μ_V.
– The induced immunity from the vaccine is equal to the natural immunity.

The model parameters implicated are positive, and Table 1 summarizes them. The differential system that governs the dynamics of COVID-19 is described as follows:

Table 1 Describing the parameters involved in Eq. (1)

Parameter	Description
N	Population size
β_S	The rate at which a susceptible individual has effective contact with a symptomatic person
β_A	The rate at which a susceptible individual has effective contact with an asymptomatic person
α	Incubation rate
ε	Fraction of asymptomatic people
f	Fraction of asymptomatic people who progress to the symptomatic class
ν	Transfer rate from asymptomatic to symptomatic classes.
ρ	Fraction of symptomatic people hospitalized due to COVID-19
δ_Q	Transition rate from symptomatic class to quarantine class
δ_H	Transition rate from symptomatic to hospitalized class
σ	Transition rate from quarantined to hospitalized class
f_1	Proportion of quarantined individuals recovering from COVID-19
f_2	Proportion of quarantined people who die from COVID-19
γ_A	Rate at which asymptomatic carriers remediate from the disease
γ_Q	Rate at which quarantined people remediate from the disease
γ_H	Rate at which hospitalized patients remediate from the disease
d_Q	Mortality rate induced by the disease caused by the quarantine class
d_H	Mortality rate induced by the disease caused by the hospitalized class
r	Proportion of patients hospitalized who die of COVID-19
μ_R	Rate of natural immunity loss
θ_V	Vaccination rate
E_V	Vaccine efficacy
μ_V	Waning rate of the vaccine

$$
\begin{cases}
\dfrac{dS(t)}{t} = \mu_R R(t) + \mu_V V(t) - (\Lambda + \theta_V)S(t) \\
\dfrac{dE(t)}{t} = \Lambda S(t) + \Lambda_V V(t) - \alpha E(t) \\
\dfrac{dI_S(t)}{t} = (1-\varepsilon)\alpha E(t) + f\nu I_A(t) - (\rho\delta_H + (1-\rho)\delta_Q)I_S(t) \\
\dfrac{dI_A(t)}{t} = \varepsilon\alpha E(t) - (f\nu + (1-f)\gamma_A)I_A(t) \\
\dfrac{dH(t)}{t} = \rho\delta_H I_S(t) + (1 - f_1 - f_2)\sigma Q(t) - (rd_H + (1-r)\gamma_H)H(t) \quad (1) \\
\dfrac{dQ(t)}{t} = (1-\rho)\delta_Q I_S(t) - (f_1\gamma_Q + f_2 d_Q + (1 - f_1 - f_2)\sigma)Q(t) \\
\dfrac{dR(t)}{t} = (1-f)\gamma_A I_A(t) + f_1\gamma_Q Q(t) + (1-r)\gamma_H H(t) - \mu_R R(t) \\
\dfrac{dD(t)}{t} = rd_H H(t) + f_2 d_Q Q(t) \\
\dfrac{dV(t)}{t} = \theta_V S(t) - (\mu_V + \Lambda_V)V(t).
\end{cases}
$$

In the system of Eq. (1), Λ and Λ_V refer to the forces of infection for susceptible and vaccinated individuals and are expressed, respectively, in the following equations:

$$
\Lambda = \frac{\beta_S I_S(t) + \beta_A I_A(t)}{N(t)}. \tag{2}
$$

$$
\Lambda_V = (1 - E_V)\Lambda. \tag{3}
$$

3   Model Calibration

In the present section, we applied our epidemiological model to Morocco's publicly available data on COVID-19 [20]. Daily confirmed count data on COVID-19 are analyzed from March 2 to June 10, 2020. Our primary objective is to identify from the data the effective contact rates (β_S, β_A) for symptomatic and asymptomatic individuals, the population fractions (f, ρ, f_1, f_2, r), and the transition rate δ_Q from symptomatic to quarantine class. For the sake of reducing the complexity of the model (1), the remaining parameters (α, ε, γ_A, γ_Q, γ_H) are taken from the literature, and (μ_R, ν, σ, δ_H, d_Q, d_H) are assumed on the basis of public information about COVID-19 (see Table 2). Because, as of March 2, 2020, the Moroccan authority reported the first confirmed case of COVID-19; we set the initial number of symptomatic individuals at one ($I_S(0) = 1$). And as this first case was hospitalized, we put the initial number of hospitalized people at one ($H(0) = 1$). We set the initial number of deaths, recovered, and vaccinated people at zero ($R(0) = D(0) = V(0) = 0$), as SARS-CoV2 has never appeared before, and no vaccine was available. We fixed the initial size of individuals quarantined at home to zero ($Q(0) = 0$). We assumed that the initial number of asymptomatic people equals one ($I_A(0) = 1$) and the initial number of exposed individuals is equal to four ($E(0) = 4$). We then established the initial size of individuals susceptible to $S(0) = (N - E(0) - I_S(0) - I_A(0) - H(0) - Q(0) - R(0) - D(0) - V(0))$, where N represents the size of the Moroccan population. According to [24], as of Monday, December 26, 2022, the Moroccan population is estimated at 37,994,215 million. In the identification process of model parameters, we employ a classical method known as curve fitting and a Bayesian inference method via the HMC algorithm. We explain both approaches in detail and provide numerical results obtained from each of them below.

Table 2 Fixed and assumed parameter values in Eq. (1)

Parameter	Mean value	95% CI	Source
α	0.1923	[0.1429, 0.2439]	[21]
ε	0.1790	[0.1550, 0.2020]	[22]
γ_A	0.1398	[0.0701, 0.2094]	[23]
γ_Q	0.1162	[0.0388, 0.1937]	[23]
γ_H	0.0714	[0.0476, 0.0909]	[23]
μ_R	0.0050	–	Assumed
ν	0.5000	–	Assumed
σ	0.1429	–	Assumed
δ_H	0.0314	–	Assumed
d_Q	0.0001	–	Assumed
d_H	0.0010	–	Assumed

3.1 Curve Fitting Method

In the curve fitting approach, we consider the parameters of the model to be fixed quantities and estimate their values using estimators. To identify the set of parameters β_S, β_A, f, ρ, f_1, f_2, r, and δ_Q, we calibrate model (1) without vaccination ($\theta_V = 0$ and $V(0) = 0$) to the daily COVID-19 count data; the data are smoothed using a moving average based on convolution. To do so, we used the Nelder–Mead (NM) Simplex method to minimize the sum of squares of the differences between the observed daily infections from the COVID-19 data and the daily infection estimates provided by the model (1). The NM Simplex Method is a direct local search method conceived for unconstrained minimization with no need to compute derivatives. It is simple to be applied as it does not calculate gradients and can be used to address nonlinear least-squares (NLS) problems. Due to its high sensitivity to the selected initial points, the NM Simplex method does not guarantee the global optimum. We denote the sum of the squared residuals by $SS_R(\Theta)$ and has the following expression:

$$SS_R(\Theta) = \sum_{i=1}^{n}(d_i - M_i(\Theta))^2. \tag{4}$$

In Eq. (4), d_i represents the actual value of COVID-19 data, n denotes the data size, $M_i(\Theta)$ is the model output for observation d_i as generated from the system (1), and Θ represents the set of unknown p parameters such that $\Theta = \{\beta_S, \beta_A, f, \rho, f_1, f_2, r, \delta_Q\}$.

We perform numerical simulations via the LMFIT package in Python, and the result is illustrated in Fig. 2. The mean values of the estimated parameters with their 95% confidence intervals (CI) are presented in Table 3.

To quantify the accuracy of fit between observed data and model predictions, we computed the root mean squared error (RMSE) metric. The RMSE is a measure of the standard deviation of the residuals. In addition, for the selection of a good statistical model purpose, we calculated two criteria based on information theory, the Akaike information criterion (AIC), and the Bayesian information criterion (BIC). AIC is a mathematical technique for evaluating the fit of a statistical model to the underlying data from which it was generated compared to different possible models. These three criteria are increasing functions of the residual. Therefore, a statistical model with the smallest value for RMSE, AIC, and BIC can be selected for inference. We define these criteria in Eqs. (5), (6), and (7), respectively, and their score values are given in Table 4.

$$RMSE = \sqrt{SS_R/(n-p)} \tag{5}$$

$$AIC = nln(SS_R/n) + 2p \tag{6}$$

$$BIC = nln(SS_R/n) + pln(n). \tag{7}$$
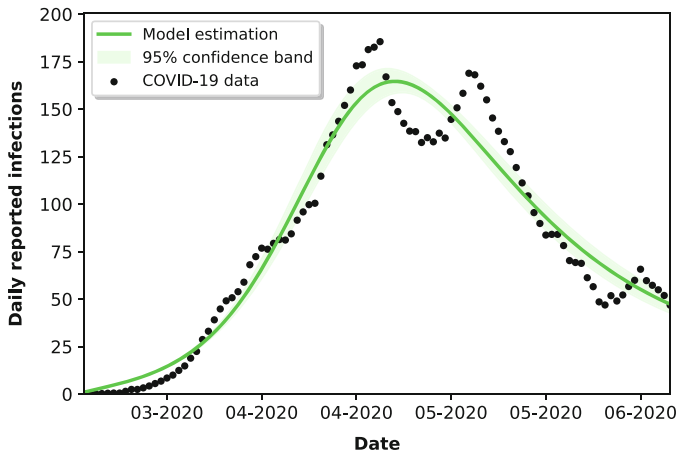
Fig. 2 Calibrating system (1) to daily reported infection counts in Morocco. The black dots represent reported infections, the solid green curve shows the model estimation, and the green area represents 95% CI

Table 3 Mean parameter estimates, standard deviations, and 95% confidence intervals

Parameter	Mean value	Standard deviation	95% CI
β_S	0.2052	0.0128	[0.1795, 0.2309]
β_A	0.8962	0.1101	[0.6761, 1.1164]
f	0.2985	0.0403	[0.2179, 0.3792]
ρ	0.3325	0.0463	[0.2399, 0.4251]
f_1	0.4008	0.0526	[0.2956, 0.5061]
f_2	0.0999	0.0163	[0.0673, 0.1326]
r	0.0976	0.0098	[0.0781, 0.1171]
δ_Q	0.0509	0.0001	[0.0507, 0.0511]

Table 4 Score values for RMSE, AIC, and BIC

Metric	Score value
RMSE	13.587
AIC	529.493
BIC	550.335

In analyzing the results, Table 4 shows that the statistical metrics RMSE, AIC, and BIC have low values. In addition, the estimated values of the quantities of interest in Table 3 have scientific sense, and their 95% confidence intervals are reasonably close. Therefore, our modeling framework is consistent with the data and more accurately reproduces the COVID-19 outbreak in Morocco.

From Table 3, we observe that the effective contact rate among symptomatic infected individuals (β_S) has a mean value of 0.205, while the effective contact rate among asymptomatic infected individuals (β_A) has a mean value of 0.896; β_A is higher than β_S. This result implies that asymptomatic carriers represent the primary

drivers of the epidemic of COVID-19 in Morocco. However, in [25], the authors estimated that the viral load of COVID-19 in symptomatic and asymptomatic individuals was in the same range. This finding is therefore outlined mainly from the fact that asymptomatic people are unaware of their infection state, so they cannot be avoided by the susceptible population, in contrast to symptomatic people, who can be detected, admitted to the hospital, or tracked in quarantine at home.

3.2 Bayesian Inference Method

An alternative approach for identifying model parameters, given measurements, is to consider the unknown model parameters as random variables. To achieve this, we apply Bayesian statistical inference to the model update [26]. The model update can combine prior knowledge of the unknown quantities with observed data to generate a posterior probability distribution. This distribution is also called the target distribution. Thus, in a Bayesian identification procedure, we first assign for each unknown parameter a prior distribution that reflects the starting assumption on the parameter to be estimated before collecting the data. Then, given n independent and identically distributed data points $d_1, d_2, ..., d_n$, we update the prior knowledge by using a likelihood function according to Bayes' theorem, resulting in a target distribution that contains all the information about the inferred parameters. Bayes' theorem is given by

$$P(\Theta \mid d) = \frac{P(d \mid \Theta) \cdot P(\Theta)}{P(d)},\tag{8}$$

where Θ is the vector of the parameters to be inferred, d is data points, $P(d \mid \Theta)$ is the likelihood function, $P(\Theta)$ denotes the distribution of priors, $P(d)$ indicates the evidence, and $P(\Theta \mid d)$ denotes the posterior probability distribution.

In Bayesian inference problems, the standard MCMC algorithms are used to compute the posterior distribution. As an example of these algorithms, we can cite the Metropolis–Hastings and Gibbs sampling algorithms. These algorithms aim to search the parameter space and generate samples from a posterior probability distribution. In doing so, the algorithm makes a random jump in the parameter space based on the current sample and then accepts or rejects the jump, probabilistically, based on prior beliefs and observed data. For complex statistical models involving many parameters, these algorithms have the challenge of requiring a sufficiently long runtime to converge to the stationary distribution because they tend to search the parameter space through non-efficient random walks.

Here, to calculate the target distribution, we employ an alternative algorithm, the HMC. The theoretical background of the HMC algorithm comes from physics, particularly from fields of differential geometry and Hamiltonian dynamics. The computation effort in the HMC algorithm is more demanding at each stage compared to the random walk algorithms due to the gradient calculations. Nev-

ertheless, this property makes the HMC more robust and efficient in exploring high-dimensional posterior distributions even though the parameters are highly correlated. So, the HMC estimation process takes a few iterations to estimate the quantities of interest and quantify their uncertainties. To enhance the performance of the HMC, which is very sensitive to manual adjustment of some parameters by the user, Hoffman and Gelman introduced in [27] the No-U-Turn Sampler (NUTS) algorithm to implement the HMC. The NUTS algorithm, an extension of HMC, can efficiently carry out Bayesian statistical inference for complex models, including epidemic models, with minimal user intervention. To realize HMC, a team of researchers [28] developed an automatic system for Bayesian inference modeling called Stan, which employs NUTS as the default inference algorithm for parameters with continuous values. Stan's algorithms are written in C++ with various user interfaces such as R, Python, and MATLAB.

3.2.1 Observation Model

In practice, the first step in inference modeling is to determine the observational model because the obtained data are not directly linked to the output derived from the mathematical model. Thus, we need to specify a link function $P(d \mid \Theta)$, the so-called likelihood function, which must be proportional to the target distribution $P(\Theta \mid d)$. The resultant proportionality relation up to a normalization constant is expressed in Eq. (9). The evidence, $P(d)$, acts as a normalization constant for Bayes' theorem to assure that the target distribution integrates with 1.

$$P(\Theta \mid d) \propto P(d \mid \Theta) \cdot P(\Theta). \tag{9}$$

In statistics, we generally model count data with a Poisson probability distribution. However, to consider variability in the observed COVID-19 data, the likelihood function relating daily observed symptomatic infections to the evolution in compartment counts in the deterministic model (1) is assumed to follow a negative binomial distribution. The Negative Binomial probability distribution models over-dispersion in a Poisson distribution when the variance of count data is higher than the mean. We provide the observation model by the following equation:

$$d_i \sim NB(M_i(\Theta), \phi), \tag{10}$$

where NB(.) stands for the Negative Binomial distribution, d_i represents daily reported infections of COVID-19 in Morocco, $M_i(\Theta)$ is the model output generated from the system of Eq. (1), and ϕ refers to the dispersion parameter.

3.2.2 Prior Specification

We incorporate our epidemiological beliefs into the model parameters by assigning to each unknown quantity a prior probability distribution. So, from the previous results (Table 3), the estimated mean values of the transmission rates β_S and β_A are 0.205 and 0.896, respectively. Thus, we assume that the effective contact rates β_S and β_A follow a Gaussian distribution $N(1.0, 0.2)$ ($\beta_S \sim N(1.0, 0.2)$, $\beta_A \sim N(1.0, 0.2)$). Then, we suppose that the population fractions (f, ρ, f_1, f_2, r) and the transition rate δ_Q from symptomatic to quarantine class follow a uniform distribution such that $f \sim U(0.0, 0.4)$, $\rho \sim U(0.3, 1.0)$, $f_1 \sim U(0.4, 1.0)$, $f_2 \sim U(0.0, 0.1)$, $r \sim U(0.0, 0.1)$, and $\delta_Q \sim U(0.0, 0.05)$. The dispersion parameter is an unknown quantity that must be inferred from the data, so we assume that its inverse is exponentially distributed ($1/\phi \sim exp(5)$). Thus, the vector of parameters we want to infer from the data becomes $\Theta = \{\beta_S, \beta_A, f, \rho, f_1, f_2, r, \delta_Q, \phi\}$.

3.2.3 Simulations

We used the NUTS algorithm through the RStan package in R version 4.2.1 to identify the parameters of interest from the data. We run the NUTS algorithm using four parallel chains, each with 2000 iterations. We fixed the number of iterations in the warm-up phase at 1000. As a result, the sampling process leads to 4000 samples for each parameter of interest. These samples are used to calculate summary statistics for each parameter (mean, standard deviation, and quantiles) and provide probabilistic predictions. Table 5 shows the posterior mean estimates, standard deviations (sd), and percentiles of 5%, 25%, 50%, 75%, and 95% for each quantity of interest as obtained from the posterior distribution.

In assessing the goodness of fit, we first test whether our model (1) converges to the posterior distribution. By model convergence, we mean that the NUTS algorithm will eventually attain a stationary distribution. To do so, we plot the trace for the four MCMC chains for each model parameter, dispersion parameter and its inverse,

Table 5 Mean posterior estimates, standard deviations, and percentiles

Parameter	Posterior mean	sd	5%	25%	50%	75%	95%
β_S	0.2322	0.0346	0.1743	0.2082	0.2317	0.2561	0.2900
β_A	0.5125	0.1936	0.1973	0.3759	0.5114	0.6450	0.8360
f	0.0552	0.0604	0.0027	0.0139	0.0353	0.0743	0.1821
ρ	0.4349	0.0993	0.3122	0.3561	0.4161	0.4905	0.6288
f_1	0.6980	0.1730	0.4283	0.5488	0.6989	0.8478	0.9682
f_2	0.0503	0.0291	0.0055	0.0251	0.0499	0.0757	0.0952
r	0.0497	0.0298	0.0045	0.0235	0.0498	0.0760	0.0958
δ_Q	0.0471	0.0028	0.0417	0.0455	0.0477	0.0494	0.0506
ϕ	5.0307	0.9560	3.6041	4.3332	4.9605	5.6503	6.7314
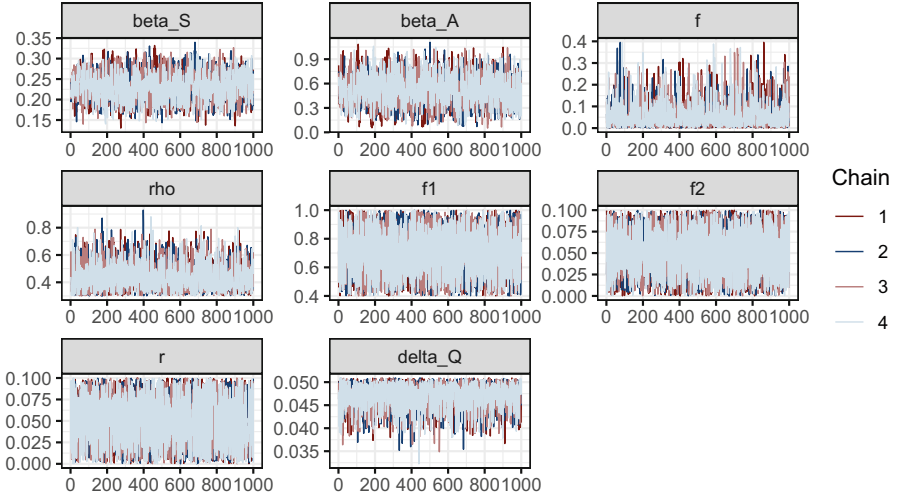
Fig. 3 Trace plots of the four MCMC chains at each iteration of the stationary phase for parameters β_S (beta_S), β_A (beta_A), f, ρ (rho), f_1, f_2, r, and δ_Q (delta_Q). A line (sequence of samples) represents each MCMC chain
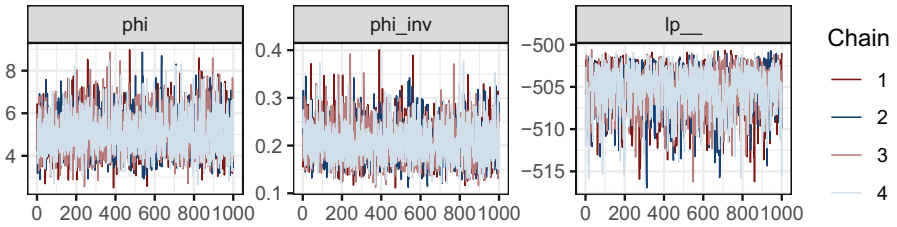
Fig. 4 Trace plots of the four MCMC chains at each iteration of the stationary phase for the dispersion parameter (ϕ or phi), the inverse of the dispersion parameter ($1/\phi$ or phi_inv), and the log-posterior (`lp__`). A line (sequence of samples) represents each MCMC chain

and log-posterior in Figs. 3 and 4. Then, we plot the model estimation against the raw COVID-19 data and the 95% credible interval (CrI) in Fig. 5. Additionally, to test whether model (1), once calibrated, produces consistent simulations with actual COVID-19 data and the extent to which the model predictions are uncertain, we calculated the median predicted cases per day from this model and plotted them against the data points. The numerical simulations are illustrated in Fig. 6.

3.2.4   Results

From Figs. 3 and 4, we see that the plots of the four parallel MCMC chains are mixed and in agreement with each other for each parameter. This result demonstrates that the NUTS algorithm is robust and efficient in identifying model parameters. It also
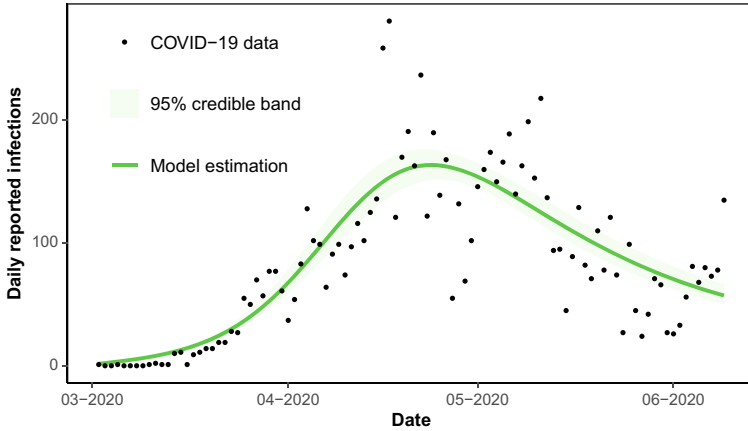
Fig. 5 Actual and estimated daily cases of COVID-19 in Morocco. The black dots represent observed confirmed cases, the solid green curve shows the model estimation, and the green area represents 95% CrI
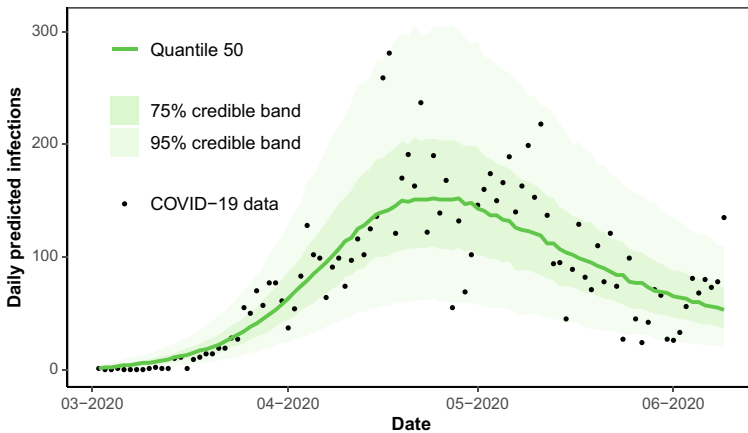
Fig. 6 Actual and predicted daily cases of COVID-19 in Morocco. The black dots represent observed confirmed cases, the solid green curve shows the predicted median cases, the dark green area represents 75% CrI, and the light green area represents 95% CrI

means that by running the algorithm only for 2000 iterations, model (1) converges to the stationary distribution. By analyzing Figs. 5 and 6, we observe that the model uncertainty (75% (CrI) and 95% (CrI)) matches the variation of the data points, and both the best fit curve (Fig. 5) and the median predicted line (Fig. 6) fall inside the credible intervals. This implies that our model fits the COVID-19 data and can reproduce the COVID-19 epidemic in Morocco. Also, from the summary statistics (Table 5), we provide the mean posterior estimates for the dispersion parameter ϕ as 5.03. This value indicates that the variance of the COVID-19 count data is greater

than the mean, which confirms our assumption that the likelihood function follows a Negative Binomial distribution.

Analyzing Table 5, we observe that the effective contact rate among symptomatic infected individuals (β_S) has a mean value of 0.232, whereas the effective contact rate among asymptomatic infected individuals (β_A) has a mean value of 0.513; β_A is greater than β_S. In other words, the estimated values of β_S and β_A are, on average, close to those in Table 3. Comparing the other parameters, we find that the estimated values obtained from Bayesian inference are, on average, close to those obtained from curve fitting. Therefore, estimating the model parameters using curve fitting and the HMC algorithm provides similar results that are coherent and illustrate the utility of our proposed modeling framework to investigate how COVID-19 propagates.

Identifying the parameters of an HMC-based mathematical model seems to be a good choice, especially when the number of quantities we want to estimate increases. Because in Bayesian inference, the parameters are considered random variables, and if we have the distribution of a parameter, then we have all the information about it.

4 Vaccination Impacts

One of the effective measures we can take to prevent the spread of COVID-19 from an infectious person is to vaccinate a fraction of the susceptible population once an efficient vaccine is available. Thus, accelerating vaccine rollout remains crucial to slow down COVID-19 propagation and contain the pandemic. To assess how vaccination programs affect the evolution of the COVID-19 outbreak in Morocco, we simulated our epidemiological model (1) by accounting for vaccination from March 2, 2020 to July 20, 2020. We, therefore, assumed a daily baseline vaccination rate of 0.008, a baseline vaccine characterized by 79% efficacy, and an immunity period of 183 days. We used the estimated parameter values from Table 5 and the other fixed parameters from Table 2.

In the first scenario, we used the reference vaccine with 79% efficacy ($E_V = 0.79$) and changed the vaccination rate. To do so, we simulated model (1) first without considering vaccination ($\theta_V = 0$ and $V(0) = 0$), then setting the vaccination rate to its baseline value ($\theta_V = 0.008$), and then increasing the vaccination rate from its baseline value by 30% and 60%, respectively. In Fig. 7a, we give the simulation results of this scenario. In the second scenario, we set the vaccination rate at 0.008 and examined three types of COVID-19 vaccines approved for use in Morocco: Sinopharm, AstraZeneca, and Pfizer. The efficacy of these vaccines is 79%, 70%, and 95%, respectively [29]. The result obtained is shown in Fig. 7b. From Fig. 7a, we see that vaccination with a baseline rate of 0.008 could protect the susceptible population from COVID-19 infection by reducing the epidemic peak of daily confirmed cases from 164 to 130. Additionally, by increasing the value of the vaccination rate from its baseline by 30% and 60%,
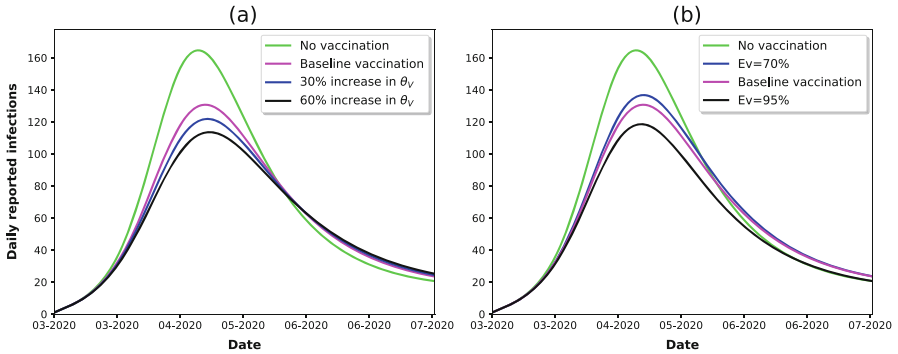
Fig. 7 The impact of vaccination against COVID-19 outbreak in Morocco. Daily evolution in confirmed cases (**a**) as a function of vaccination rate θ_V and (**b**) as a function of vaccine efficacy E_V

we could reduce the peak incidence to 121 and 113, respectively. Similarly, Fig. 7b indicates that vaccinating a susceptible population using a vaccine of 79% efficacy by keeping constant the vaccination rate at 0.008 could result in a reduction in the peak incidence from 164 to 130. If the same population is vaccinated with a vaccine of 95% efficacy, the maximum number of people infected drops from 164 to 118. In contrast, using a 70% effective vaccine to vaccinate the vulnerable population is expected to decrease the maximum number of infected people to only 136.

Assessment of the impact of vaccination on the evolution of daily reported cases in Morocco shows that the portion of the susceptible population to be immunized to flatten the epidemic curve is related to the rate of vaccination per day and vaccine efficacy. Consequently, the higher the rate of vaccination and vaccine effectiveness, the better the vaccination program will protect people from catching COVID-19 infection.

5   Conclusion

We proposed a deterministic population-based model for COVID-19 transmission dynamics that includes nine compartments. This compartmental model accounts for the COVID-19 incubation time and the transmission of the infection by asymptomatic carriers. It allows tracking of infected patients quarantined at home and in the hospital. Furthermore, it provides the possibility to implement a vaccination strategy as it contains a compartment for the vaccinated individuals. We parameterized the model developed here on the data of COVID-19 for Morocco from March 2 to June 10, 2020.

To identify the epidemiological parameters, we calibrated the model on daily reported infections of COVID-19 data using two methods, curve fitting and Bayesian statistical inference through the HMC algorithm. We evaluated whether

the model fits the data in the case of curve fitting by computing three metrics, the mean square error, the Akaike information criterion, and the Bayesian information criterion. The calculation results of these metrics gave lower values (13.587 for RMSE, 529.493 for AIC, and 550.335 for BIC). For Bayesian inference, we plotted the trace of the MCMC chains for each separate parameter. These plots showed that the four parallel MCMC chains are mixed and in agreement with one another. This result demonstrated that the algorithm (NUTS) we used in identifying model parameters is robust and efficient. We also calculated the median predicted cases by our model to test whether the model, once calibrated, produces consistent simulations with actual COVID-19 data. Numerical simulations indicated that the predicted median curve falls within the 75% credible interval and that the credible bands (75% (CrI) and 95% (CrI)) capture the structure of the observed data.

In addition, numerical simulations of fitting the model to the data in both methods showed that the model uncertainty (95% CI or 95% CrI) matches the variation of the measurements, and the best fit line falls inside the confidence/credible interval. We also found that the parameter estimates obtained by Bayesian inference using HMC are, on average, close to those obtained by curve fitting using the NM optimization method.

We further performed numerical simulations to assess how vaccination programs may affect the course of the epidemic if a vaccine were available. To this end, we incorporated vaccination dynamics into the model by assuming a daily baseline vaccination rate of 0.008, a baseline vaccine characterized by 79% efficacy, and an immunity period of 183 days. Simulations showed that we should increase the daily vaccination rate from its baseline and use a high-efficacy vaccine, greater than 79%, to protect people from COVID-19 infection.

This research does have some limitations. In calibrating our model, we used data on confirmed COVID-19 cases, but death statistics are more reliable, and using them to fit the model could lead to more accurate results. Furthermore, we did not consider the preventive measures implemented by the authority of Morocco in the model. So, combining vaccination programs and non-pharmaceutical interventions could be leveraged under different scenarios to reach the best control strategy for COVID-19. The framework developed here is particularly suited to analyze the spread of COVID-19 among homogeneous populations, but human communities are more complex given certain heterogeneous factors. Consequently, population heterogeneity influences the transmission dynamics of infectious diseases and must be addressed in mathematical modeling. In future work, we will extend the current modeling framework to study COVID-19 in heterogeneous communities.

References

1. WHO Coronavirus (COVID-19) Dashboard. https://covid19.who.int
2. Zhou, F., Hu, T.J., Zhang, X.Y., Lai, K., Chen, J.H., Zhou, X.H.: The association of intensity and duration of non-pharmacological interventions and implementation of vaccination with COVID-19 infection, death, and excess mortality: Natural experiment in 22 European countries. J. Infect. Public Health **15**(5), 499–507 (2022)
3. Randolph, H.E., Barreiro, L.B.: Herd immunity: understanding COVID-19. Immunity **52**(5), 737–741 (2020)
4. Cumbler, E., Wittig, M., Jacobson, N., McClain, H., Treat, A., Radin, J., Harry, E.: Contingency planning for health care worker masks in case of medical supply chain failure: lessons learned in novel mask manufacturing from COVID-19 pandemic. Amer. J. Infect. Control **49**(10), 1215–1220 (2021)
5. Ayoobi, N., Sharifrazi, D., Alizadehsani, R., Shoeibi, A., Gorriz, J.M., Moosaei, H., Mosavi, A.: Time series forecasting of new cases and new deaths rate for COVID-19 using deep learning methods. Results Phys. **27**, 104495 (2021)
6. Weizman, O., Duceau, B., Trimaille, A., Pommier, T., Cellier, J., Geneste, L., Bonnet, G.: Machine learning-based scoring system to predict in-hospital outcomes in patients hospitalized with COVID-19. Arch. Cardiovasc. Dis. **115**(12), 617–626 (2022)
7. Althobaity, Y., Wu, J., Tildesley, M.J.: Non-pharmaceutical interventions and their relevance in the covid-19 vaccine rollout in Saudi Arabia and Arab Gulf countries. Infect. Dis. Modell. **7**(3), 545–560 (2022)
8. Hethcote, H.W.: The mathematics of infectious diseases. SIAM Rev. **42**(4), 599–653 (2000)
9. Kucharski, A.J., Russell, T.W., Diamond, C., Liu, Y., Edmunds, J., Funk, S., Flasche, S.: Early dynamics of transmission and control of COVID-19: a mathematical modelling study. Lancet Infect. Dis. **20**(5), 553–558 (2020)
10. Peng, L., Yang, W., Zhang, D., Zhuge, C., Hong, L. Epidemic analysis of COVID-19 in China by dynamical modeling (2020). Preprint arXiv:2002.06563
11. Iboi, E.A., Ngonghala, C.N., Gumel, A.B.: Will an imperfect vaccine curtail the COVID-19 pandemic in the US? Infect. Dis. Modell. **5**, 510–524 (2020)
12. Shen, M., Zu, J., Fairley, C.K., Pagán, J.A., An, L., Du, Z., Zhang, L.: Projected COVID-19 epidemic in the United States in the context of the effectiveness of a potential vaccine and implications for social distancing and face mask use. Vaccine **39**(16), 2295–2302 (2021)
13. Delamater, P.L., Street, E.J., Leslie, T.F., Yang, Y.T., Jacobsen, K.H.: Complexity of the basic reproduction number (R0). Emerg. Infect. Dis. **25**(1), 1 (2019)
14. Hamra, G., MacLehose, R., Richardson, D.: Markov chain Monte Carlo: an introduction for epidemiologists. Int. J. Epidemiol. **42**(2), 627–634 (2013)
15. Betancourt, M.: A conceptual introduction to Hamiltonian Monte Carlo (2017). Preprint arXiv:1701.02434
16. Acuña-Zegarra, M.A., Díaz-Infante, S., Baca-Carrasco, D., Olmos-Liceaga, D.: COVID-19 optimal vaccination policies: a modeling study on efficacy, natural and vaccine-induced immunity responses. Math. Biosci. **337**, 108614 (2021)
17. Iyaniwura, S.A., Falcão, R.C., Ringa, N., Adu, P.A., Spencer, M., Taylor, M., Otterstatter, M.: Mathematical modeling of COVID-19 in British Columbia: an age-structured model with time-dependent contact rates. Epidemics **39**, 100559 (2022)
18. Acuña-Zegarra, M.A., Santana-Cibrian, M., Velasco-Hernandez, J.X.: Modeling behavioral change and COVID-19 containment in Mexico: a trade-off between lockdown and compliance. Math. Biosci. **325**, 108370 (2020)
19. Andrade, J., Duggan, J.: An evaluation of Hamiltonian Monte Carlo performance to calibrate age-structured compartmental SEIR models to incidence data. Epidemics **33**, 100415 (2020)
20. CSSEGISandData: COVID-19 Data Repository by the Center for Systems Science and Engineering (CSSE) at Johns Hopkins University (2023). https://github.com/CSSEGISandData/COVID-19

21. Li, Q., Guan, X., Wu, P., Wang, X., Zhou, L., Tong, Y., et al., Feng, Z.: Early transmission dynamics in Wuhan, China, of novel coronavirus–infected pneumonia. New England J. Med. **382**, 1199–1207 (2020)
22. Mizumoto, K., Kagaya, K., Zarebski, A., Chowell, G.: Estimating the asymptomatic proportion of coronavirus disease 2019 (COVID-19) cases on board the Diamond Princess cruise ship, Yokohama, Japan, 2020. Eurosurveillance **25**(10), 2000180 (2020)
23. Tang, B., Wang, X., Li, Q., Bragazzi, N.L., Tang, S., Xiao, Y., Wu, J.: Estimation of the transmission risk of the 2019-nCoV and its implication for public health interventions. J. Clin. Med. **9**(2), 462 (2020)
24. Morocco Population (2023) - Worldometer. https://www.worldometers.info/world-population/morocco-population/
25. Zou, L., Ruan, F., Huang, M., Liang, L., Huang, H., Hong, Z., Wu, J.: SARS-CoV-2 viral load in upper respiratory specimens of infected patients. New England J. Med. **382**(12), 1177–1179 (2020)
26. Lye, A., Cicirello, A., Patelli, E.: Sampling methods for solving Bayesian model updating problems: a tutorial. Mechan. Syst. Signal Process. **159**, 107760 (2021)
27. Hoffman, M.D., Gelman, A.: The No-U-Turn sampler: adaptively setting path lengths in Hamiltonian Monte Carlo. J. Mach. Learn. Res. **15**(1), 1593–1623 (2014)
28. Stan Development Team: Stan Modeling Language User's Guide and Reference Manual, Version 2.17. 0 (2017)
29. Kim, J.H., Marks, F., Clemens, J.D.: Looking beyond COVID-19 vaccine phase 3 trials. Nature Med. **27**(2), 205–211 (2021)

Predicting the Infection Level of COVID-19 Virus Using Normal Distribution-Based Approximation Model and PSO

Samar Wazir, Gautam Siddharth Kashyap, Karan Malik, and Alexander E. I. Brownlee

1 Introduction

Many harmful diseases can now be treated because of advances in technology and medicine, but there are still several unique infectious diseases that spread quickly and kill millions of people before a vaccine is developed. The resulting pandemics put the global economy in jeopardy in addition to endangering human life. In 1918, the Spanish Flu claimed the lives of 50–100 million individuals [1], and on January 21, 2023, new coronavirus (COVID-19) had infected more than 672,965,004 people, of whom 6,742,859 had died [2]. It is impossible to anticipate how long it will take to produce a pandemic vaccine, but during this time, the infection rate, human mortality, and economic damage can all be decreased by taking preventive measures. The amount and accessibility of medical supplies and medication is the key issue faced in the fight against the pandemic. Following an illness, each patient experiences different health issues. Because some people have robust immune systems, the infection rate is in check. These individuals merely require medicine and appropriate isolation (in the case of COVID-19). However, if the IL is high, the patient will require intensive care, a ventilator, or other equipment [3]. To make the best use of resources in the instance of COVID-19, the key elements should be kept in mind:

S. Wazir · G. S. Kashyap (✉)
Department of Computer Science and Engineering, SEST, Jamia Hamdard, New Delhi, India

K. Malik
Arizona State University, Tempe, AZ, USA

A. E. I. Brownlee
Division of Computing Science & Mathematics, University of Stirling, Stirling, UK
e-mail: sbr@cs.stir.ac.uk

1. Calculating the expected future demand for ventilators.
2. Predicting if a patient simply needed isolation or quarantine rather than hospitalisation based on symptoms and illness infection patterns.
3. How many days must pass before antibodies are produced and the patient can recuperate on their own?
4. Calculate the degree of infection in the human body on a specific day following the onset of symptoms by taking into factors like age, smoking, BMI, chronic illness, and gender.

For the above-discussed factors, an algorithm must first be developed before a mathematical model can be used to estimate the IL. The model should then be tested on a sizable volume and a diverse range of datasets to approximate the findings. This chapter takes an innovative method to figuring out the human body's IL after a specified number of days is put forth. This technique takes advantage of the well-known Gaussian distribution, which turns out to be a very accurate predictor of IL. Later, a method for determining Total Infection (TI) in the human body is established by taking into account several significant risk factors connected to COVID-19. Using IL, an algorithm known as the Infection Level Predictor (ILP) was created and put to use on the dataset made available by [4]. The ILP can approximate the IL by observing the infection trends of both a single nation and all countries taken collectively. This work also introduces the PSO algorithm, which is used with the same datasets. Finally, the PSO and ILP are compared.

This chapter is as follows: In the next section, we will see the related works of the approaches that had been used for determining COVID-19. The background of the bell curve is covered in Sect. 3. Section 4 provides examples to help explain the IL algorithm. The TI algorithm is detailed in Sect. 5. The ILP algorithm is presented in Sect. 6. The IL method is tested on a few examples as provided in Sect. 7. The background of PSO is explained in Sect. 8. The experimental findings of PSO are explained in Sect. 9. ILP and PSO outcomes are compared in Sect. 10, and this is concluded with some conclusions and recommendations for further research in Sect. 11.

2 Related Works

The COVID-19 pandemic makes its debut in Wuhan City, China, in December 2019 [5], and from there it quickly erupted across the entire nation. Because of this unidentified threat to human life, the majority of China's cities were put on lockdown. The situation deteriorated from February to April 2020, when this infectious disease spread to the majority of the world's nations and more than 4 million infection cases, including 0.3 million deaths, were reported. The battle to create a vaccine and treatments for this virus begins. To reduce the risk to property and human life, several combined mathematical and computer science approach for Severe Acute Respiratory Syndrome (SARS) and COVID-19. These approaches'

solutions are based on infection rates so that an estimate of the number of patients after a few days can be made. The SARS outbreak was anticipated using an ordinary differential equation by concentrating on the point of infection rate prediction [6]. When this data is reviewed and compared, the model's forecast accurately reflects the characteristics of real-world data, such as the SARS outbreak in Singapore. By employing Markov switching models to find sluggish pandemics, H.M. Lu [7] extends the challenge of identifying outbreak patterns. In another instance, a streamlined Susceptible-Infectious-Removed (SIR) model is used to estimate the pandemic's infection rate. This forecast indicates the incidence rate and the point at which mortality cases begin to decline [8]. The usage of a Polynomial Neural Network with Corrective Feedback (PNN+cf) [9] was suggested as another method for the frequency of COVID-19 illness. Similarly, in [10], a novel mathematical model for COVID-19 was employed to assess the transmission of the disease from Wuhan to other cities utilising datasets of cases both inside and outside of Wuhan. Controlling COVID-19 outbreaks also benefits from using the model for case isolation and contact tracing [11]. The COVID-19 epidemic in India is anticipated to start on January 30, 2020, and a mathematical model [12] employing Iterative Laplace Transform Method (ILTM) has been created to predict future cases, control, and prevention. The incubation period is crucial to a virus's ability to spread. If precautions have been followed during this time, the chance of spreading can be significantly reduced. Numerous evolutionary algorithms have also been employed for this purpose, such as the PSO with Support Vector Machine (SVM) approach utilised in [13] by Sheela and Arun for COVID-19 screening and quantification. PSO using fuzzy series was used by Kumar and Susan [14] to estimate the COVID-19 infection. Likewise, [15–19], have been applied to prevent or optimise COVID-19 infections.

The bell curve, one of the most common notions used in various mathematical models to distribute and forecast the success and failure of events in people's lives, along with the Gaussian and normal distributions, has proven to be particularly useful. Similar to this, PSO-based techniques are particularly practical because they are simple to use and put into practice. The aforementioned techniques provide an overview of the issues with medical science. A prediction model can provide a rough answer that can be crucial for resource management, treatment planning, and diagnosis. In the case of COVID-19, it is exceedingly risky to interact with the patient; therefore, it will be very beneficial to become aware of IL in advance for the better treatment of medical professionals, employees, and equipment management.

3   Background

The COVID-19 infection pattern can be associated with the bell curve. We use the COVID19_open_line_list dataset for our research [4]. Take a look at Table 1, which displays an example of this data. Each entry in this dataset describes an event, between the beginning of symptoms and the patient's death or discharge. These

Table 1 Dataset for age group 28–30

ID	Age	S	K_1	K_2	K_3	S_1	S_2	S_3
671	28	1/20/2020	1/22/2020	1/23/2020	1/28/2020	2	3	8
6136	28	1/29/2020	2/3/2020	2/3/2020	2/22/2020	5	5	24
164	29	1/23/2020	1/23/2020	1/24/2020	1/28/2020	0	1	5
649	30	1/3/2020	1/10/2020	1/15/2020	1/15/2020	7	12	12
646	30	1/23/2020	1/24/2020	1/24/2020	2/12/2020	1	1	20

Where, S = Date_Onset_Symptoms, K_1 = Date_Admission_Hospital, K_2 = Date_Confirmation, K_3 = Date_Death_Or_Discharge, S_1 = Admission-Onset, S_2 = Confirmation-Onset, S_3 = Death/Dis-Onset
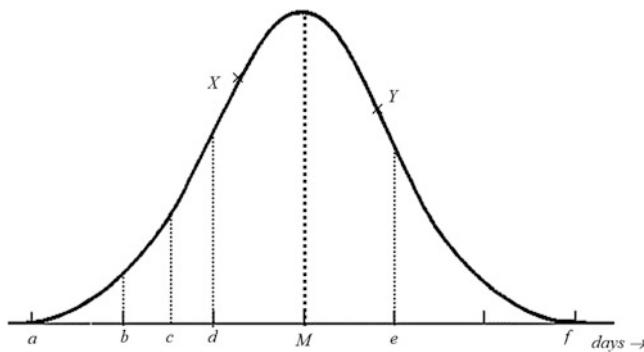
Fig. 1 Bell curve of COVID-19 infection pattern

occurrences appear to follow a pattern that corresponds to the rise and fall of IL in the human body. The bell curve shown in Fig. 1 can be used to correlate the data in Table 1 with it. On this curve, the various manifestations of COVID-19 infection in the human body can be plotted as follows:

- At point a infection starts.
- It will take 3–13 days for the onset of symptoms (incubation period) [20]. In this case, 13 days are considered and presented by point b.
- At point c, the patient was admitted to the hospital.
- At point d, patient test results have been confirmed.
- At point M (median, 22 days), the IL is maximum and it is assumed that on this day human body has developed antibodies and started fighting the virus by itself.
- At point e, the patient has been discharged or died.
- If it is discharged and recovered even when the virus stays in the body for 14 days [20] and can still spread infection to others. This is represented by point f.
- X and Y are the points where IL can be predicted.

In this discussion, several highly significant factors that have the potential to alter the bell curve's slope are referred to as COVID-19 risk factors [4, 20–25]. These are as follows: (1) Age (A), (2) Gender (G), (3) Chronic Disease (D), (4) Smoking (Sm), and (5) BMI (B). Because infection patterns vary depending on age group, it

is crucial to utilise a separate bell curve for each age group. For example, infections in the elderly are more severe due to their weakened immune systems than in the young. The normal distribution formula can be used to create the bell curve as shown below:

$$X = \frac{1}{\sigma\sqrt{2\pi}} e^{\frac{-(i-\mu)^2}{2\sigma^2}} \tag{1}$$

Here, μ is the average value of the sample, σ is the standard deviation, and X is the value given in Fig. 1 or the probability at a particular point.

4 Problem Statement 1: How to Calculate Infection Level (IL) by Coronavırus in the Human Body

In this case, the IL can be estimated using the normal distribution and risk factors. The age and number of days after infection can be utilised to predict the COVID-19 infection pattern using the IL formula.

4.1 *Proposed Solution*

In this step, a database of COVID-19 patient records is considered as D with parameters: (1) $N =$ The number of rows in the database, (2) $ID =$ Id of the admitted patient, (3) $A =$ Age of the patient, (4) $S =$ Date of onset symptoms, and (5) $K_i =$ Date of activities of patient, for example, date of admission to the hospital, date of confirmation of infection, and date of death/discharge. Where $i = 1, 2, 3, \ldots, n$ is the number of activities.

Definition 4.1 Calculation of the actual number of days.

Let $S_i =$ amount of days spent on certain activities of the patient. Therefore, it can be said that

$$S_i = K_i - S \tag{2}$$

$X_i =$ An actual amount of days spent on certain activities of the patient after infection. It is considered here that the incubation period is 13 days [10]. Therefore,

$$X_i = S_i + 13 \quad \text{OR} \quad X_i = (K_i - S) + 13 \tag{3}$$

Definition 4.2 Selection of constant C_s and C_E.

Constant C_s can be defined as the start day of infection when the patient got infected by the virus. It is before the incubation period. Therefore, it is considered on the first day or $C_s = 0$. Constant C_E can be defined as the end day of infection. It includes 14 days after the day when the symptom ends. It is considered here that the virus stays in the human body for 17 days (as per the guidelines [20]). Hence, C_E can be calculated as follows:

$$
\begin{array}{ccccc}
C_E & = & 13+17 & +14 & = 44 \\
\downarrow & & \downarrow & \downarrow & \downarrow \\
\text{Incubation} & & \text{Virus Active} & \text{Ending} C_E & \text{Time Period}
\end{array}
\tag{4}
$$

Definition 4.3 Calculation of sample average

Let μ be the sample average of the population which can be calculated as:

$$
\mu = \frac{\sum_{i=1...n,\ j=1...N} X_{ij} + C_S + C_E}{n \times N + 2}
\tag{5}
$$

Definition 4.4 Calculation of Standard Deviation

Let σ be the standard deviation, therefore σ can be calculated as:

$$
\sigma = \sqrt{\frac{\sum_{i=1...n,\ j=1...N} \left(X_{ij} - \mu\right)^2 + (C_S - \mu)^2 + (C_E - \mu)^2}{n \times N + 2}}
\tag{6}
$$

Definition 4.5 Calculation of IL

The Cumulative Distribution Function of normal distribution can be used to determine the infection in the human body after x days for IL such as:

$$
IL(x) = \begin{cases}
\sum_{i=1}^{x} \frac{1}{\sigma \sqrt{2\pi}} e^{\frac{-(i-\mu)^2}{2\sigma^2}} & for\ x \leq 22 \\
1 - \sum_{i=1}^{x} \frac{1}{\sigma \sqrt{2\pi}} e^{\frac{-(i-\mu)^2}{2\sigma^2}} & for\ x > 22
\end{cases}
\tag{7}
$$

4.2 Example

Consider the Table 1 dataset which has been extracted from the COVID19_open_line _list dataset [4], for the age group of 28–30. The description of Table 1 columns are as follows: (1) ID: Patient ID, (2) Age: Patient age, (3) Data_onset_symptoms: date of first symptoms occur, (4) Date_admission_hospital: date of the patient admitted to hospital, (5) Date_confirmation: date of confirmation of infection,

and (6) Date_death_or_discharge: date of death or discharge of patient. Note: In our proposed method, the above three are considered as different activities of the patient infection life cycle (K_i): (1) Admission-onset: The amount of days from the beginning of symptoms to admission, (2) Confirmation-onset: The amount of days between the beginning of symptoms and confirmation of infection, and (3) Death/dis-onset: Amount of days between the beginning of symptoms and death or discharge of patient. The IL can be calculated in Table 2 and its infection pattern is given in Fig. 2.

Table 2 Calculation of mean, standard deviation, and Infection Level (IL)

S_i	X_i with C_S and C_E (x)	μ	σ	$IL(x)$
NA	0	21.06	9.980951	0.01742834
0	13	21.06	9.980951	0.20967821
1	14	21.06	9.980951	0.2396753
1	14	21.06	9.980951	0.2396753
1	14	21.06	9.980951	0.2396753
2	15	21.06	9.980951	0.2718735
3	16	21.06	9.980951	0.30608944
5	18	21.06	9.980951	0.37958001
5	18	21.06	9.980951	0.37958001
5	18	21.06	9.980951	0.37958001
7	20	21.06	9.980951	0.45771092
8	21	21.06	9.980951	0.49760179
12	25	21.06	9.980951	0.34651297
12	25	21.06	9.980951	0.34651297
20	33	21.06	9.980951	0.11579389
24	37	21.06	9.980951	0.05512815
NA	44	21.06	9.980951	0.01077014

Where, S_i = The pattern of activities days

Fig. 2 Infection pattern for age group 28–30
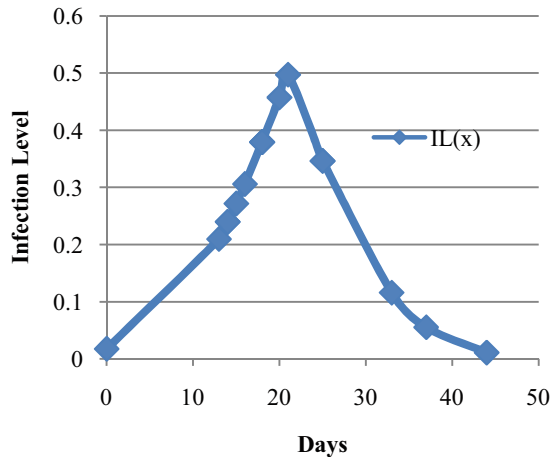
Now consider the following:

Scenario 1 A person of age 29 has been infected by COVID-19. If the person has been feeling the symptoms for the past 17 days. Then calculate the IL in the patient.
In this case, $Age = 29 \in Age\ group\ 28 - 30$

$$x = 17 + 13 = 30$$

Therefore, from Table 2

$$\mu = 21.06,\ and\ \sigma = 9.980951$$

Hence, IL can be calculated from Eq. (7) as follows:

$$IL(x) = \frac{1}{\sigma\sqrt{2\pi}} e^{\frac{-(x-\mu)^2}{2\sigma^2}}$$

$$IL(x) = 1 - \sum_{i=1}^{x} \frac{1}{\sigma\sqrt{2\pi}} e^{\frac{-(i-\mu)^2}{2\sigma^2}} \quad for\ x > 22$$

$$IL(30) = 0.1852$$

If the patient's IL is around 18.52% after 17 days and based on the bell curve for this group (Fig. 2), this patient does not require medication. For this patient, just quarantine is needed. At this point, the antibodies are more powerful than the virus.

5   Problem Statement 2: How to Calculate Total Infection (TI) by Coronavırus in the Human Body by Considering Risk Factors

The important risk factors that can affect infection of the virus can be as follows:

1. *Age* (*A*): It has been observed [26] that the chances of infection are higher in people having old age (maybe more than 60 years) or in children (maybe less than 5 years) due to weak immunity. In the proposed research, IL is calculated based on age groups.
2. *Gender* (*G*): It has been detected that male is more infected compared to females. Therefore, TI is calculated by considering the percentage of males or females in the database of a particular country or region.

3. *Chronic disease* (*D*): People having diseases like diabetes, cancer, lung infection, and others are at increased COVID-19 pose a high risk of serious disease.
4. *Smoking* (*Sm*): Smoking negatively impacts lung health and the COVID-19 virus attacks the lungs as well. Therefore, after the infection, conditions can be very bad for a smoker or chain smoker.
5. *BMI* (*B*): The BMI is also an important risk factor and if BMI is not in under normal range then the chances of infection become very high. As per the guideline [4, 20–25], the normal range of BMI is from 18.5 to 30.0. Persons having BMI below 18.5 or above 30.0 are highly vulnerable to COVID-19 illness. Hence, the value of B can be calculated as follows:

$$B = \begin{cases} 0 & if\ BMI \geq 18.5\ and\ BMI \leq 30.0 \\ \frac{BMI}{100} & if\ BMI < 18.5 \\ \frac{18.5 - BMI + 30.0}{100} & if\ BMI > 30.0 \end{cases} \tag{8}$$

5.1 Total Infection (TI)

TI can be calculated by the average of the risk factors (*rf*). So TI can be represented as follows:

$$TI = \frac{rf}{t} \tag{9}$$

Here, *rf* is the sum of risk factors value and *t* is the number of risk factors. In our case, five risk factors have been considered. Therefore, TI can be denoted as follows:

$$TI = \frac{IL + G + D + Sm + B}{5} \tag{10}$$

Now consider the following:

Scenario 2 An individual who is 29 years old has a COVID-19 infection in India. If the individual has experienced the symptoms over the last 17 days, then figure out the patient's IL. If the infected individual is a diabetic man with a blood sugar level of 210 mg/dL and a BMI of 32.5, determine the TI if the subject has COVID-19 infection. (The maximum blood sugar level allowed is 300 mg/dL, and the normal range is 140 mg/dL; there are 100,000 infected people in India, of which 78,000 are men [27]).

In this case,
IL can be calculated as given in Scenario 1.

So,

$$IL = 0.1852,$$

$$G = \frac{78,000}{100,000} = 0.78,$$

$$D = \frac{210 - 140}{300 - 140} = \frac{70}{160} = 0.4375,$$

$$Sm = 0,$$

$$BMI = \frac{18.5 - 32.5 + 30}{100} = 0.16$$

Total infection can be calculated from Eq. (10) as follows:

$$TI = \frac{0.1852 + 0.78 + 0.4375 + 0 + 0.16}{5} = 0.3125 \approx 32\%$$

6 Infection Level Predictor (*ILP*) Algorithm

Based on the patient's age as well as the amount of days since the beginnings of symptoms, the ILP algorithm is used to forecast the likelihood of IL. The level of prediction is determined by studying a database of people in the same age group. ILP algorithm is as follows:

ILP (Age A, Days x, Database DB)

1. *arr[N×n],arr[0]=0, arr[N×n -1]*
2. *LB = A - (A % 10), UB = LB+10*
3. *If (A > LB &&A ≤ UB)*
4.   *for i = 1 to arr.size-1*
5. *S = DB.on_set_symptoms*
6.   *for k = 1 to n*
7. *arr[i] = DB.activity(k) − S +13*
8.   *end for*
9.   *end for*
10. *end if*
11. *μ = mean. arr[i]*

12. $\sigma = stddev.\ arr[i]$

13. $IL(x) = \begin{cases} \sum_{i=1}^{x} \frac{1}{\sigma\sqrt{2\pi}} e^{\frac{-(i-\mu)^2}{2\sigma^2}} & for\ x \le 22 \\ 1 - \sum_{i=1}^{x} \frac{1}{\sigma\sqrt{2\pi}} e^{\frac{-(i-\mu)^2}{2\sigma^2}} & for\ x > 22 \end{cases}$

In the given ILP algorithm, the input is the age of the patient, the number of days after that IL is predicted and the database in the given format as in Table 1. First, an array *arr* of size $N \times n$ is declared followed by the calculation of the age group from *Lower Bound (LB)* to *Upper Bound (UB)*. Second, from lines 3 to 10, the pattern of the count of days is recorded in *arr* for that particular age group. Finally, the mean and standard deviation is predicted for deciding the IL.

7 Model Validation

The prediction of IL is primarily based on the pattern of infection whose speed may be different in diverse climates or regions. Therefore, IL can be predicted for a particular region based on the database of that specific region. In this case, the COVID19_open_line_list dataset [4] from Wuhan, China, is used. This dataset has a record of 13,479 patients from 0.08 to 96 years of age. As discussed earlier, the total survival time of the virus has been taken as 44 days so 22 days can be assumed as the peak time of infection. The database is divided into different age groups and 80% of the data of each age group is used for training purposes, that is, for drawing the bell curve, the other data is used for testing purposes, that is, for predicting the IL and comparing it with training data prediction level. The precise division of data in different age groups and RMSE value is shown in Table 3.

Table 3 Age groups of COVID19_open_line_list dataset

Age group	Total records	Records in training	Records in testing	RMSE
0–10	21	17	4	0.009712
11–20	22	18	4	0.009165
21–30	160	144	16	0.029310
31–40	264	245	19	0.011038
41–50	256	240	18	0.033060
51–60	195	181	16	0.009427
61–70	138	124	16	0.018123
71–80	61	51	12	0.012309

8   Background of PSO

Eberhart and Kennedy [28] developed PSO, a population-based stochastic optimisation approach. The social behaviour of fish schooling and bird grouping encourages it. PSO is a technique that uses a swarm of moving particles, each of which is treated as a possible solution to the optimisation problem under consideration. These particles can move in a variety of multi-dimensional spaces. Assume that the position and velocity of particle x at time step y are represented by vectors $p_x(y)$ and $v_x(y)$, respectively. Each particle's position is modified based on its own and the swarm's collective experience. The particle, to be more accurate, moves away from its current position $p_x(y)$ to the next position $p_x(y+1)$ as follows:

$$p_x(y+1) = p_x(y) + v_x(y+1) \tag{11}$$

The velocity of particle x can be updated as follows:

$$v_x(y+1) = v_x(y) + c_1 r_1 \left[p_{best} - p_x(y) \right] + c_2 r_2 \left[p_{current} - p_x(y) \right] \tag{12}$$

where, p_{best} = the particle best position; $p_{current}$ = the particle current position; c_1 and c_1 = constants; r_1 and r_1 = random values in the range $[0, 1]$; $p_{best} - p_x(y)$ = cognitive components of particle x; $p_{current} - p_x(y)$ = social components of particle x.

The cognitive component is derived from the optimisation experience and data of individual particles. The social component, on the other hand, is based on data exchange among all particles. The particle search method was combined in both components.

9   Experimental Results of PSO

The fundamental concept is to reduce the error between the model's predictions and the actual data by using PSO to optimise the model's parameters, such as transmission rates and recovery rates. This can be achieved by utilising the PSO algorithm to iteratively alter the model's parameters until the difference between predictions and observed data is reduced. It would be possible to create more precise forecasts of the COVID-19 viral IL by modifying the ILP model's parameters using PSO. Following is the proposed pseudocode:

1. Prepare the data for modelling by importing the dataset.
2. Choose a mathematical model to describe the viral spread, such as the ILP model.
3. In addition to the original data model's predictions and the data observed is the objective function that needs to be optimised.
4. Set each particle's initial position and speed in the swarm.

Table 4 Age groups of COVID19_open_line_list dataset using PSO

Age group	Total records	Records in training	Records in testing	RMSE
0–10	21	17	4	0.009648
11–20	22	18	4	0.009781
21–30	160	144	16	0.024802
31–40	264	245	19	0.016089
41–50	256	240	18	0.02359
51–60	195	181	16	0.013433
61–70	138	124	16	0.014453
71–80	61	51	12	0.016945

5. Use the chosen mathematical model and the collected data to assess the fitness, or objective function, of each particle.
6. Update the best-known position of each particle according to its current fitness.
7. According to the best-known position of all particles, and determine the global-known position of the swarm.
8. Update each particle's velocity in relation to its best-known position, global-known position, and current position.
9. Depending on each particle's new velocity, adjust each one's position.
10. For a predetermined optimal solution or until a stopping criterion is satisfied, repeat steps 5 through 9.
11. Make forecasts about future infection levels using the PSO algorithm's optimal position.

The proposed algorithm has been implemented on Google Colab on a PC with AMD E1-6010 APU 1.35 GHz-4GB RAM. The proposed algorithm has been run on the same parameters as the ILP algorithm mentioned in Sect. 7 and the results were obtained after 30 sample runs. The precise division of data in different age groups and RMSE value is shown in Table 4 using PSO.

10   Comparisons of ILP and PSO

The ILP is a numerical model that approximates viral proliferation using a normal distribution, while PSO is a method of optimisation that is employed in order to improve the characteristics of the model to best fit the data. Both ILP and PSO provide information about the performance of the model for different age groups, including the total amount of records used, the records used for testing and training, and the RMSE of the model's predictions. One of the main differences between ILP and PSO is the method used to train and test the model. Another difference between the ILP and PSO is the performance of the model, as measured by the RMSE values as shown in Fig. 3. The RMSE values in PSO are generally very small, ranging from 0.009648 to 0.016945. This suggests that the model's predictions for
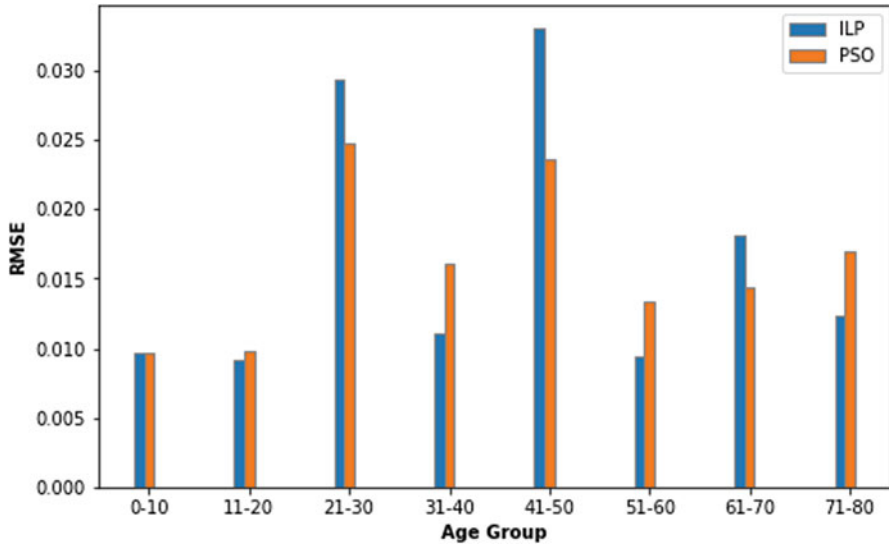
Fig. 3 Difference between ILP versus PSO

the different age groups are very accurate. On the other hand, the RMSE values in ILP are generally higher, ranging from 0.009427 to 0.033060. This suggests that the predictions for the different age groups may not be as accurate when using ILP.

It is worth mentioning that perhaps the RMSE is a result of the variation between anticipated and actual values, and that a lower RMSE is better value represents a better performance of the model. Therefore, based on the RMSE values, it seems that the PSO has a better performance than the ILP. The results of ILP and PSO also show that the performance of the model varies for different age groups. For example, in PSO, the RMSE values for the age groups 0–10 and 11–20 are particularly low, at 0.009648 and 0.009781, respectively, indicating that the model's predictions for these age groups are very accurate. On the other hand, the RMSE values for the age group 21–30 are higher, at 0.024802, indicating that the model's predictions for this age group may not be as accurate. Similarly, in ILP, the RMSE values for the age group 61–70 and 71–80 are higher compared to the other age groups, indicating that the model's predictions for these age groups may not be as accurate.

It is also worth noting that the sample size for each age group also varies, and that may affect the accuracy of the predictions. For instance, age groups 0–10 and 11–20 have fewer records, which may make the predictions more uncertain. On the other hand, age groups 21–30 and 31–40 have more records and thus the predictions may be more accurate. Another point to consider is that the model's predictions are only as good as the data and information used to train and test it. Therefore, it is important to make sure that the data used is relevant and reliable, and that the model is trained and tested using appropriate techniques. In conclusion, ILP and PSO present the results of a model that was used to predict the IL of COVID-19.

11   Conclusion and Future Directions

The authors have demonstrated that it is possible to estimate the COVID-19 viral IL using a normal distribution-based approximation model and PSO. In this chapter, a mathematical model that simulates the transmission of the virus using a normal distribution is used, and PSO is then employed to optimise the model's parameters to best match the data. Three algorithms have been used in this work to predict COVID-19 infections. The IL algorithm has been implemented in the first section of this chapter along with a few examples to validate the suggested algorithm. To forecast the overall IL of COVID-19, an ILP method has also been constructed in addition to the IL algorithm. The output of the ILP method is founded on the pattern of viral infection in a particular area or nation, and it is effective at predicting the IL in a patient after a certain number of days. The speed at which a virus spreads might vary depending on the weather; for example, in dry weather, the speed is slower than in cold weather. In such a circumstance, the spread pattern changed, and IL changed as a result. To compare the outcomes of the ILP method on the same datasets with the same settings, a PSO algorithm is also employed. According to experimental findings, PSO performs better than the ILP algorithm. Any forecasts produced using this or any other method, though, must be regarded with caution because COVID-19 is a complicated and continuously evolving issue. Additionally, it is crucial to take into account every aspect that could influence the COVID-19 outbreak, including population density, travel, and public health initiatives.

In future research, more variables can be taken into account and added to the IL or TI forecast, such as the fact that different nations have varied childhood vaccination programmes, which might change their inhabitants' immunity and, as a result, alter the infection pattern. Using more sophisticated optimisation methods, like genetic algorithms or other metaheuristic optimisation algorithms, to optimise the model's parameters is another topic of future research.

References

1. Walsh, B.: Covid-19: the history of pandemics. BBC Future. https://www.bbc.com/future/article/20200325-covid-19-the-history-of-pandemics. Last accessed 19 Dec 2021
2. Dennison Himmelfarb, C.R., Baptiste, D.: Coronavirus disease (COVID-19). J. Cardiovasc. Nurs. **35**, 318–321 (2020). https://doi.org/10.1097/jcn.0000000000000710
3. Mertz, L.: Quick thinking turns out low-cost ventilators. IEEE Pulse. **11**, 31–34 (2020). https://doi.org/10.1109/MPULS.2020.2995436
4. SRK: Novel Corona Virus 2019 Dataset. Kaggle. https://www.kaggle.com/sudalairajkumar/novel-corona-virus-2019-dataset. Last accessed 19 Dec 2021
5. Zhu, H., Wei, L., Niu, P.: The novel coronavirus outbreak in Wuhan, China. Glob. Health Res. Policy. **5**, 1–3 (2020). https://doi.org/10.1186/s41256-020-00135-6
6. Ang, K.C.: A simple model for a SARS epidemic. Teach. Math. Appl. **23**, 181–188 (2004). https://doi.org/10.1093/teamat/23.4.181
7. Lu, H.M., Zeng, D., Chen, H.: Prospective infectious disease outbreak detection using Markov switching models. IEEE Trans. Knowl. Data Eng. **22**, 565–577 (2010). https://doi.org/10.1109/TKDE.2009.115

8. Zhong, L., Mu, L., Li, J., Wang, J., Yin, Z., Liu, D.: Early prediction of the 2019 novel coronavirus outbreak in the mainland China based on simple mathematical model. IEEE Access. **8**, 51761–51769 (2020). https://doi.org/10.1109/ACCESS.2020.2979599

9. Fong, S.J., Li, G., Dey, N., Gonzalez-Crespo, R., Herrera-Viedma, E.: Finding an accurate early forecasting model from small dataset: a case of 2019-nCoV novel coronavirus outbreak. Int. J. Interact. Multimed. Artif. Intell. **6**, 132 (2020). https://doi.org/10.9781/ijimai.2020.02.002

10. Kucharski, A.J., Russell, T.W., Diamond, C., Liu, Y., Edmunds, J., Funk, S., Eggo, R.M., Sun, F., Jit, M., Munday, J.D., Davies, N., Gimma, A., van Zandvoort, K., Gibbs, H., Hellewell, J., Jarvis, C.I., Clifford, S., Quilty, B.J., Bosse, N.I., Abbott, S., Klepac, P., Flasche, S.: Early dynamics of transmission and control of COVID-19: a mathematical modelling study. Lancet Infect. Dis. **20**, 553–558 (2020). https://doi.org/10.1016/S1473-3099(20)30144-4

11. Hellewell, J., Abbott, S., Gimma, A., Bosse, N.I., Jarvis, C.I., Russell, T.W., Munday, J.D., Kucharski, A.J., Edmunds, W.J., Sun, F., Flasche, S., Quilty, B.J., Davies, N., Liu, Y., Clifford, S., Klepac, P., Jit, M., Diamond, C., Gibbs, H., van Zandvoort, K., Funk, S., Eggo, R.M.: Feasibility of controlling COVID-19 outbreaks by isolation of cases and contacts. Lancet Glob. Health. **8**, e488–e496 (2020). https://doi.org/10.1016/S2214-109X(20)30074-7

12. Shaikh, A.S., Shaikh, I.N., Nisar, K.S.: A mathematical model of COVID-19 using fractional derivative: outbreak in India with dynamics of transmission and control. Adv. Differ. Equ. **2020**, 1–19 (2020). https://doi.org/10.1186/s13662-020-02834-3

13. Sheela, M.S., Arun, C.A.: Hybrid PSO–SVM algorithm for Covid-19 screening and quantification. Int. J. Inf. Technol. **14**, 2049–2056 (2022). https://doi.org/10.1007/s41870-021-00856-y

14. Kumar, N., Susan, S.: Particle swarm optimization of partitions and fuzzy order for fuzzy time series forecasting of COVID-19. Appl. Soft Comput. **110**, 107611 (2021). https://doi.org/10.1016/j.asoc.2021.107611

15. Ding, C., Chen, Y., Liu, Z., Liu, T.: Prediction on transmission trajectory of COVID-19 based on particle swarm algorithm. Pattern Recogn. Lett. **152**, 70–78 (2021). https://doi.org/10.1016/j.patrec.2021.09.003

16. Haouari, M., Mhiri, M.: A particle swarm optimization approach for predicting the number of COVID-19 deaths. Sci. Rep. **11**, 1–13 (2021). https://doi.org/10.1038/s41598-021-96057-5

17. Martínez-Álvarez, F., Asencio-Cortés, G., Torres, J.F., Gutiérrez-Avilés, D., Melgar-García, L., Pérez-Chacón, R., Rubio-Escudero, C., Riquelme, J.C., Troncoso, A.: Coronavirus optimization algorithm: a bioinspired metaheuristic based on the COVID-19 propagation model. Big Data. **8**, 308–322 (2020). https://doi.org/10.1089/big.2020.0051

18. Sahafizadeh, E., Khajeian, M.: Modeling COVID-19 in Iran using Particle Swarm Optimization algorithm. medRxiv. 2021.04.10.21255244 (2021). https://doi.org/10.1101/2021.04.10.21255244

19. Shen, C., Zhang, K., Tang, J.: A COVID-19 detection algorithm using deep features and discrete social learning particle swarm optimization for edge computing devices. ACM Trans. Internet Technol. **22**, 1–17 (2022). https://doi.org/10.1145/3453170

20. WHO: Coronavirus disease 2019 (COVID-19). Situation report-72. Highlights (2020). https://www.who.int/docs/default-source/coronaviruse/situation-reports/20200401-sitrep-72-covid-19.pdf

21. Petrilli, C.M., Jones, S.A., Yang, J., Rajagopalan, H., O'Donnell, L., Chernyak, Y., Tobin, K.A., Cerfolio, R.J., Francois, F., Horwitz, L.I.: Factors associated with hospital admission and critical illness among 5279 people with coronavirus disease 2019 in New York City: prospective cohort study. BMJ. **369**, m1966 (2020). https://doi.org/10.1136/bmj.m1966

22. Herrnstein, R., Murray, C.: The Bell Curve: Intelligence and Class Structure in American Life. Free Press Paperbacks (1996) https://books.google.co.in/books?hl=en&lr=&id=s4CKqxi6yWIC&oi=fnd&pg=PR11&dq=Herrnstein,+Richard+J.,+and+Charles+Murray.+The+bell+curve:+Intelligence+and+class+structure+   in+American+life.+Simon+and+Schuster,+2010.&ots=gcz-b-qkG7&sig=U1cbI0cWZCrImjpjLtRAgX. Last accessed 19 Dec 2021

23. Bracey, G.W.: Final Exam: A Study of the Perpetual Scrutiny of American Education. Historical Perspectives on Assessment, Standards, Outcomes, and Criticism of U.S. Public Schools, 248p. Agency for Instructional Technology (1995)

24. Fendler, L., Muzaffar, I.: The history of the bell curve: sorting and the idea of normal. Educ. Theory. **58**, 63–82 (2008). https://doi.org/10.1111/j.1741-5446.2007.0276.x
25. Jordan, R.E., Adab, P., Cheng, K.K.: Covid-19: risk factors for severe disease and death (2020). https://www.bmj.com/content/368/bmj.m1198, https://doi.org/10.1136/bmj.m1198
26. Kluge, D.H.H.P.: Statement – Older People are at Highest Risk from COVID-19, But All Must Act to Prevent Community Spread, pp. 7–10. World Health Organization (2020)
27. Huizen, J.: Blood sugar chart: target levels, management, risks, and more. https://www.medicalnewstoday.com/articles/317536#monitoring-levels. Last accessed 20 Dec 2021
28. Kennedy, J., Eberhart, R.: Particle swarm optimization. Proc. ICNN'95 – Int. Conf. Neural Networks. **4**, 1942–1948. https://doi.org/10.1109/ICNN.1995.488968

An Optimal Vaccination Scenario for COVID-19 Transmission Between Children and Adults

Derya Avcı and Mine Yurtoğlu

1 Introduction

The WHO declared pneumonia cases with unknown causes in Wuhan, in 2019. Then, the WHO announced this threat as a new coronavirus outbreak that has not been seen before in humans. In a short time, the epidemic turned into a pandemic named by COVID-19 and affected the whole world [1]. Coronaviruses are single-stranded RNA viruses. These viruses primarily occur in wild animals and spread from there to humans. Since they are viruses with high mutation ability, they are defined as pathogens with a high epidemic rate.

Typical symptoms of COVID-19 are high fever, the loss of taste and smell, and persistent dry cough. In particular, people with chronic diseases such as diabetes, cardiac insufficiency, pneumonia, and hypertension are in the risk group. Also, especially children and teenagers are at high risk of infection because they are in close contact with their infected parents [2]. The well-known way of spreading the virus is through droplets and direct contact. Unfortunately, these are very common in social life due to close contact. For this reason, it can be said that the most difficult to implement among the COVID-19 measures is social distance. Vaccination can be considered one of the most effective methods due to its feasibility and sustainability as experienced in many epidemics.

The COVID-19 pandemic, which brought many negative changes in our social and individual lives, has been the focus of attention of many branches of science. One of them is the analysis of the system properties of the mathematical models developed for the COVID-19 pandemic. Thus, it is possible to predict the course of the disease more efficiently and economically. The epidemiological model proposed

D. Avcı (✉) · M. Yurtoğlu
Department of Mathematics, Balıkesir University, Balıkesir, Turkey
e-mail: dkaradeniz@balikesir.edu.tr

by Kermack and McKendrick was accepted as the basis of mathematical epidemiology in the literature [3]. Today, the increase in epidemics and their interactions with each other has led to a more complex structure in mathematical models [4–6]. In this sense, many studies have been carried out to develop new COVID-19 models. In the reference [7], the authors have introduced a novel model that discusses quarantined and hospitalized individuals with real data for the COVID-19 outbreak in Portugal. In [8], the effect of mask use was investigated in a generalized SEIR model that considers asymptomatic infectious individuals. Recently, Nainggolan et al. [9] have studied the system analysis and optimal control of a COVID-19 model regarding symptomatic and asymptomatic infected individuals in Indonesia. Similarly, Saha et al. [10] have proposed a new COVID-19 model for Hong Kong and performed stability and bifurcation analyzes of the model by fitting the real data and also determined the optimal vaccination strategy. Rois et al. [11] have introduced a novel model for Indonesia in the case of comorbidity and have also analyzed the effect of training and treatment optimal control parameters on the model. Ojo et al. [12] have also examined the optimal control measures for a model that represents the interaction of tuberculosis and COVID-19 diseases. In [13], masking and hygiene have been examined as optimal control parameters for a model developed using real data from the USA, Italy, South Africa, and Nigeria. Also, different types of mathematical models and corresponding optimal control formulations have been constructed for Peru [14], India [15], Bangladesh [16], and so on.

On the other hand, although integer-order derivatives are often used to model epidemics, fractional-order derivatives also have advantages such as hereditary and memory properties while modeling the disease transmissions. Some of the COVID-19 studies addressed with fractional derivatives can be mentioned as follows: Baleanu et al. [17] have proposed a COVID-19 model with Caputo–Fabrizio fractional derivative. Azroul and Hammouch [18] have introduced an SIQR model with Mittag–Leffler kernel and have studied on the existence of the solutions, stability analysis, and numerical solutions. Al-Husban et al. [19] have proposed the existence and uniqueness of the solutions and also the global stability of a fractional incommensurate order COVID-19 model. From a different perspective, Abbes et al. [20] have presented a discrete-time fractional-order model by adapting real data. Joshi et al. [21] have modeled the transmission of COVID-19 with fractional derivative for a double-vaccinated population. Moualkia [22] has presented a variable-order model for the Omicron variant of the COVID-19 pandemic with a stochastic viewpoint. Özköse et al. [23] have proposed a COVID-19 model with fractional derivative by taking real data from Congo and by considering comorbidity.

Controlling the spread of a disease is as significant as modeling it to secure the social and economic interests of society. For this purpose, preventive measures considered as control strategies should be carefully determined by using the available resources in the most effective and least costly way. Such problems are among the research topics of optimal control theory [24–28]. With the emergence of COVID-19, the optimal control problems (OCPs) of epidemics have come to the fore again, and the interest in them has increased [29–33]. In the literature, different optimal prevention and treatment strategies for COVID-19 have been researched

so far, such as vaccination, medication, social distancing, hygiene, and non-drug interventions. Among them, Zamir et al. [34] have researched the OCP with non-pharmaceutical intervention for a new model of COVID-19. Gatyeni et al. [35] have proposed a COVID-19 model by fitting the data from South Africa and formulated the OCP with the control parameters: mask usage, social distance, testing, and continuous screening. Butt et al. [36] have constructed a COVID-19 model for determining the optimal quarantine rates for different compartments.

Recently, fractional disease models have also been frequently studied in optimal control theory. If the system and/or cost function contains fractional derivative, it is named by fractional optimal control problem (FOCP). Among the studies on FOC of COVID-19, Sweilam et al. [37] have presented the optimal control of COVID-19 applying a hybrid method consisting of nonstandard finite difference and the Grünwald–Letnikov numerical methods. Zamir et al. [38] have studied the influence of non-pharmaceutical controls for a COVID-19 model governed by fractional derivative. Bonyah et al. [39] have investigated global stability, existence and uniqueness of solutions, and optimal measures for a COVID-19 spreading model equipped with Mittag–Leffler kernel. Eroğlu and Yapışkan [40] have discussed an optimal control strategy combining the plasma transfusion and vaccination for a fractional COVID-19 model. By an unusual technique, Vellappandi and Govindaraj [41] have obtained the optimality conditions for an FOCP constructed on a COVID-19 model using the Gateaux derivative. Baba et al. [42] have suggested a fractional COVID-19 model by fitting real data from Thailand and have adapted vaccination control to the model.

In this chapter, vaccination control for the adults is adapted to the model representing the COVID-19 transmission between adults and children. The optimality system is solved by the joint implementation of the fourth-order Runge–Kutta (RK4) method and the forward–backward sweep algorithm. Numerical simulations are performed in MATLAB software. It is concluded that although only adults are vaccinated in the proposed optimal control strategy, a remarkable reduction of infected children is also observed. This shows how important vaccination is, even if it is applied to a bounded group. Section 2 presents the controlled model with its parameters. The OCP is formulated in Sect. 3. The numerical results for controlled and uncontrolled cases are graphically illustrated and interpreted comparatively in Sect. 4.

2   Model Description

The rates of transmission and recovery of COVID-19 disease differ in children and adults. This chapter presents the OCP for an age-based COVID-19 model that takes this important distinction into account. The discussed model has been first proposed by Lazebnik and Bunimovich-Mendrazitsky [43] in sense of system analysis. The model consists of S_c (susceptible children), S_a (susceptible adults), I_c (infected children), I_a (infected adults), R_c (recovered children), and R_a (recovered adults). Also, death individual compartments are added to the model so that D_c and D_a

represent death children and deceased adults, respectively. The total children and adult populations are, respectively, represented by N_c and N_a. Hence, the total population is $N = N_c + N_a$.

The basis model is as follows:

$$
\left.
\begin{aligned}
\frac{dS_c(t)}{dt} &= -S_c(t)\frac{\beta_{cc}I_c(t)+\beta_{ca}I_a(t)}{N_c(t)} - \alpha S_c(t), \\[2mm]
\frac{dS_a(t)}{dt} &= \alpha S_c(t) - S_a(t)\frac{\beta_{ac}I_c(t)+\beta_{aa}I_a(t)}{N_a(t)}, \\[2mm]
\frac{dI_c(t)}{dt} &= S_c(t)\frac{\beta_{cc}I_c(t)+\beta_{ca}I_a(t)}{N_c(t)} - \alpha I_c(t) - \gamma_c I_c(t), \\[2mm]
\frac{dI_a(t)}{dt} &= S_a(t)\frac{\beta_{ac}I_c(t)+\beta_{aa}I_a(t)}{N_a(t)} + \alpha I_c(t) - \gamma_a I_a(t), \\[2mm]
\frac{dR_c(t)}{dt} &= \gamma_c \rho_c I_c(t) - \alpha R_c(t), \\[2mm]
\frac{dR_a(t)}{dt} &= \alpha R_c(t) + \gamma_a \rho_a I_a(t), \\[2mm]
\frac{dD_c(t)}{dt} &= \gamma_c \psi_c I_c(t), \\[2mm]
\frac{dD_a(t)}{dt} &= \gamma_a \psi_a I_a(t).
\end{aligned}
\right\}
\tag{1}
$$

The parameters of the model can be detailed as follows:

A : the COVID-19 threshold age for children, which is considered to be an average of 13 years in days

$\alpha = \frac{1}{A}$: the transition rate from children to adults per day

β_{ac} : the infection rate of a susceptible adult because of an infected child per day

β_{ca} : the infection rate of a susceptible child because of an infected adult per day

β_{cc} : the infection rate of a susceptible child because of an infected child per day

β_{aa} : the infection rate of a susceptible adult because of an infected adult per day

γ_c : mean recovery time of infected children

γ_a : mean recovery time of infected adults

ρ_c : the recovery rate of children

ρ_a : the recovery rate of adults

ψ_c : the rate of a child not recovering

ψ_a : the rate of an adult not recovering

In this chapter, vaccination policy is applied only to susceptible individuals in accordance with the reality. Vaccinated adults leave the susceptible compartment and transition to the recovered compartment. In the cost functional, the control function $u(t)$ denotes the cost of vaccination. Also, t_f represents the length of vaccination period.

The set of admissible control functions is defined as

$$
U_{ad} = \left\{ u(t) \mid 0 \le u(t) \le 1, 0 \le t \le t_f \right\}.
\tag{2}
$$

Thus, the model to which the control is adapted is as follows:

$$
\left.\begin{aligned}
\frac{dS_c(t)}{dt} &= -S_c(t)\frac{\beta_{cc}I_c(t)+\beta_{ca}I_a(t)}{N_c(t)} - \alpha S_c(t), \\[2mm]
\frac{dS_a(t)}{dt} &= \alpha S_c(t) - S_a(t)\frac{\beta_{ac}I_c(t)+\beta_{aa}I_a(t)}{N_a(t)} - u(t)S_a(t), \\[2mm]
\frac{dI_c(t)}{dt} &= S_c(t)\frac{\beta_{cc}I_c(t)+\beta_{ca}I_a(t)}{N_c(t)} - \gamma_c I_c(t) - \alpha I_c(t), \\[2mm]
\frac{dI_a(t)}{dt} &= S_a(t)\frac{\beta_{ac}I_c(t)+\beta_{aa}I_a(t)}{N_a(t)} - \gamma_a I_a(t) + \alpha I_c(t), \\[2mm]
\frac{dR_c(t)}{dt} &= \gamma_c \rho_c I_c(t) - \alpha R_c(t), \\[2mm]
\frac{dR_a(t)}{dt} &= \gamma_a \rho_a I_a(t) + \alpha R_c(t) + u(t)S_a(t), \\[2mm]
\frac{dD_c(t)}{dt} &= \gamma_c \psi_c I_c(t), \\[2mm]
\frac{dD_a(t)}{dt} &= \gamma_a \psi_a I_a(t)
\end{aligned}\right\}
\tag{3}
$$

with the initial conditions in [43].

It is clear that all parameters in the model satisfy the non-negativity condition.

3 Problem Formulation with Vaccination Control

As mentioned in the earlier, WHO-approved vaccines are available for COVID-19. The optimum effectiveness of vaccination programs depends on their feasibility. In this process, the length of time period and the cost of vaccination are quite important. For any underdeveloped and developing country, a continuous vaccination program may not be a socially and economically rational strategy. People in these countries need low-cost production to access the vaccine. Hence, in this study, considering all these realities, a control $u(t)$ representing the vaccination is adapted to the system. It is aimed to maximize vaccinated adults in a limited time period with minimum cost.

3.1 Description of Cost Function

For introducing the OCP, the costs to be optimized should be determined to describe the functional meaning the main objective. Since the purpose can change in the problems of optimal control of diseases, the cost function naturally differs depending on the main aim. In the present OCP, the cost of disease burden proportional to infected adults is represented by

$$\int_0^{t_f} I_a(t)dt,$$

and the cost of disease burden proportional to infected children is defined by

$$\int_0^{t_f} I_c(t)dt.$$

Similarly, the total cost of the vaccination program is as follows:

$$\int_0^{t_f} \frac{w}{2}u^2(t)dt.$$

The cost function in the problem is in a quadratic form according to the control variable. In some OCPs, it can also be defined in a quadratic form according to the effect level of the control. w is an important positive weighting coefficient that offsets the cost of vaccination.

Thus, the cost function to be minimized is defined as

$$J[u] = \int_0^{t_f} \left[I_a(t) + I_c(t) + \frac{w}{2}u^2(t) \right] dt. \tag{4}$$

As a result, the Lagrangian necessary to determine the optimal system is as follows: $\mathcal{L} = I_c(t) + I_a(t) + \frac{w}{2}u^2(t)$.

3.2 Existence of Optimal Control

After describing the total cost, the main question that comes to mind is: does the objective functional called J really reach its minimum value? The following theorem [44] ensures this:

Theorem 1 *There is at least one optimal control function in the set of admissible controls to minimize the cost function*

$$\min J[u] = \int_0^{t_f} \left[I_a(t) + I_c(t) + \frac{w}{2}u^2(t) \right] dt$$

if the following conditions are provided:

(1) *U_{ad} and the set of state solutions are not empty.*
(2) *U_{ad} is bounded and convex.*
(3) *The right side of the system* (3) *is continuous. Also, state and control equations are bounded.*
(4) *The Lagrangian $\mathcal{L}$ is convex on U_{ad} and is bounded.*
(5) *The Lagrangian $\mathcal{L}$ satisfies the following inequalities: $c_1, c_2 > 0$, and $\eta > 1$*

$$I_a(t) + I_c(t) + \frac{w}{2}u^2(t) \geq c_1 \left(|u|^2\right)^{\frac{\eta}{2}} - c_2.$$

The proof of this theorem can be seen simply by the steps detailed in [44, 45].

3.3 Characterization of Optimal Control

Pontrayagin's Maximum Principle is applied to find the optimality conditions. Thus, the optimal control function is achieved. For this, the Hamiltonian function $\mathcal{H}$ is described by

$$\mathcal{H} = \mathcal{L} + \sum_{i=1}^{8} \lambda_i f_i,$$

$$= I_a + I_c + \frac{w}{2}u^2$$

$$+\lambda_1(t)\left[-S_c(t)\frac{\beta_{cc}I_c(t)+\beta_{ca}I_a(t)}{N_c(t)} - \alpha S_c(t)\right]$$

$$+\lambda_2(t)\left[\alpha S_c(t) - S_a(t)\frac{\beta_{ac}I_c(t)+\beta_{aa}I_a(t)}{N_a(t)} - u(t)S(t)\right]$$

$$+\lambda_3(t)\left[S_c(t)\frac{\beta_{cc}I_c(t)+\beta_{ca}I_a(t)}{N_c(t)} - \alpha I_c(t) - \gamma_c I_c(t)\right] \tag{5}$$

$$+\lambda_4(t)\left[S_a(t)\frac{\beta_{ac}I_c(t)+\beta_{aa}I_a(t)}{N_a(t)} + \alpha I_c(t) - \gamma_a I_a(t)\right]$$

$$+\lambda_5(t)\left[\gamma_c\rho_c I_c(t) - \alpha R_c(t)\right] + \lambda_6(t)\left[\gamma_a\rho_a I_a(t) + \alpha R_c(t) + u(t)S(t)\right]$$

$$+\gamma_c\psi_c\lambda_7(t)I_c(t) + \gamma_a\psi_a\lambda_8(t)I_a(t).$$

Here, $\lambda_i(t)$, $i = 1, ...8$, denotes the adjoint variables and f_i represents the right side of the system (3).

Theorem 2 *Suppose u^* is the optimal control function and $\left(S_c^*, I_c^*, R_c^*, D_c^*, S_a^* I_a^*, R_a^*, D_a^*\right)$ is the optimal solution set that minimize the cost function* (4). *Hence, there are $\lambda_i(t)$ ($i = 1, ..., 8$) adjoint functions that provide the following system:*

$$\frac{d\lambda_1}{dt} = \lambda_1(t) \left\{ \frac{\left[\beta_{cc} I_c^*(t) + \beta_{ca} I_a^*(t)\right]\left[I_c^*(t) + R_c^*(t) + D_c^*(t)\right]}{\left(N_c^*(t)\right)^2} + \alpha \right\} - \lambda_2(t)\, \alpha$$

$$- \lambda_3(t) \left\{ \frac{\left[\beta_{cc} I_c^*(t) + \beta_{ca} I_a^*(t)\right]\left(I_c^*(t) + R_c^*(t) + D_c^*(t)\right)}{\left(N_c^*(t)\right)^2} \right\},$$

$$\frac{d\lambda_2}{dt} = \lambda_2(t) \left\{ \frac{\left[\beta_{ac} I_c^*(t) + \beta_{aa} I_a^*(t)\right]\left[I_a^*(t) + R_a^*(t) + D_a^*(t)\right]}{\left(N_a^*(t)\right)^2} + u^*(t) \right\}$$

$$- \lambda_4(t) \left\{ \frac{\left[\beta_{ac} I_c^*(t) + \beta_{aa} I_a^*(t)\right]\left[I_a^*(t) + R_a^*(t) + D_a^*(t)\right]}{\left(N_a^*(t)\right)^2} \right\} - \lambda_6(t)\, u^*(t),$$

$$\frac{d\lambda_3}{dt} = -1 + \lambda_1(t) \left\{ \frac{S_c^*(t)\left[\beta_{cc}\left(S_c^*(t) + R_c^*(t) + D_c^*(t)\right) - \beta_{ca} I_a^*(t)\right]}{\left(N_c^*(t)\right)^2} \right\} + \lambda_2(t)\, \frac{S_a^*(t)\, \beta_{ac}}{N_a^*(t)}$$

$$- \lambda_3(t) \left\{ \frac{S_c^*(t)\left[\beta_{cc}\left(S_c^*(t) + R_c^*(t) + D_c^*(t)\right) - \beta_{ca} I_a^*(t)\right]}{\left(N_c^*(t)\right)^2} - \gamma_c - \alpha \right\}$$

$$- \lambda_4(t) \left(\frac{S_a^*(t)\, \beta_{ac}}{N_a^*(t)} + \alpha \right) - \lambda_5(t)\, \gamma_c \rho_c - \lambda_7(t)\, \gamma_c \psi_c,$$

$$\frac{d\lambda_4}{dt} = -1 + \lambda_1(t)\, \frac{S_c^*(t)\, \beta_{ca}}{N_c^*(t)} + \lambda_2(t) \left\{ \frac{S_a^*(t)\left[\beta_{aa}\left(D_a^*(t) + S_a^*(t) + R_a^*(t)\right)\right]}{\left(N_a^*(t)\right)^2} \right\}$$

$$- \lambda_2(t)\, \frac{\beta_{ac} I_c^*(t) S_a^*(t)}{\left(N_a^*(t)\right)^2} - \lambda_3(t)\, \frac{S_c^*(t)\, \beta_{ca}}{N_c^*(t)}$$

$$- \lambda_4(t) \left\{ \frac{S_a^*(t)\left[\beta_{aa}\left(S_a^*(t) + R_a^*(t) + D_a^*(t)\right) - \beta_{ac} I_c^*\right]}{\left(N_a^*(t)\right)^2} - \gamma_a \right\}$$

$$- \lambda_6(t)\, \gamma_a \rho_a - \lambda_8(t)\, \gamma_a \psi_a,$$

$$\frac{d\lambda_5}{dt} = -\lambda_1(t)\, \frac{\left[\beta_{cc} I_c^*(t) + \beta_{ca} I_a^*(t)\right] S_c^*(t)}{\left(N_c^*(t)\right)^2} + \lambda_3(t) \left\{ \frac{\left[\beta_{cc} I_c^*(t) + \beta_{ca} I_a^*(t)\right] S_c^*(t)}{\left(N_c^*(t)\right)^2} \right\}$$

$$+ \lambda_5(t)\, \alpha - \lambda_6(t)\, \alpha,$$

$$\frac{d\lambda_6}{dt} = -\lambda_2(t)\, \frac{\left[\beta_{aa} I_a^*(t) + \beta_{ac} I_c^*(t)\right] S_a^*(t)}{\left(N_a^*(t)\right)^2} + \lambda_4(t)\, \frac{\left[\beta_{aa} I_a^*(t) + \beta_{ac} I_c^*(t)\right] S_a^*(t)}{\left(N_a^*(t)\right)^2},$$

$$\frac{d\lambda_7}{dt} = -\lambda_1(t)\, \frac{\left[\beta_{cc} I_c^*(t) + \beta_{ca} I_a^*(t)\right] S_c^*(t)}{\left(N_c^*(t)\right)^2} + \lambda_3(t)\, \frac{\left[\beta_{cc} I_c^*(t) + \beta_{ca} I_a^*(t)\right] S_c^*(t)}{\left(N_c^*(t)\right)^2},$$

$$\frac{d\lambda_8}{dt} = -\lambda_2(t)\, \frac{\left[\beta_{ac} I_c*(t) + \beta_{aa} I_a^*(t)\right] S_a^*(t)}{\left(N_a^*(t)\right)^2} + \lambda_4(t)\, \frac{\left[\beta_{ac} I_c^*(t) + \beta_{aa} I_a(t)\right] S_a^*(t)}{\left(N_a^*(t)\right)^2}.$$

such that the transversality conditions are as follows:

$$\lambda_i(t_f) = 0, \ (i = 1, ..., 8).$$

As a result, the corresponding optimal control function is

$$u^* = \min\left\{\max\left\{\frac{(\lambda_2 - \lambda_6)\, S_a^*(t)}{w}, 0\right\}, 1\right\}. \tag{6}$$

Proof The optimality conditions that consist of the state, adjoint, and control systems are, respectively, given by

State system:

$$\frac{dS_c(t)}{dt} = \frac{\partial \mathcal{H}}{\partial \lambda_1}, \ \frac{dS_a(t)}{dt} = \frac{\partial \mathcal{H}}{\partial \lambda_2}, \ \frac{dI_c(t)}{dt} = \frac{\partial H}{\partial \lambda_3}, \ \frac{dI_a(t)}{dt} = \frac{\partial \mathcal{H}}{\partial \lambda_4},$$

$$\frac{dR_c(t)}{dt} = \frac{\partial \mathcal{H}}{\partial \lambda_5}, \ \frac{dR_a(t)}{dt} = \frac{\partial H}{\partial \lambda_6}, \ \frac{dD_c(t)}{dt} = \frac{\partial \mathcal{H}}{\partial \lambda_7}, \ \frac{dD_a(t)}{dt} = \frac{\partial \mathcal{H}}{\partial \lambda_8}.$$

Adjoint system :

$$\frac{d\lambda_1}{dt} = -\frac{\partial H}{\partial S_c}, \ \frac{d\lambda_2}{dt} = -\frac{\partial H}{\partial S_a}, \ \frac{d\lambda_3}{dt} = -\frac{\partial \mathcal{H}}{\partial I_c}, \ \frac{d\lambda_4}{dt} = -\frac{\partial \mathcal{H}}{\partial I_a}, \tag{7}$$

$$\frac{d\lambda_5}{dt} = -\frac{\partial \mathcal{H}}{\partial R_c}, \ \frac{d\lambda_6}{dt} = -\frac{\partial \mathcal{H}}{\partial R_a}, \ \frac{d\lambda_7}{dt} = -\frac{\partial \mathcal{H}}{\partial D_c}, \ \frac{d\lambda_8}{dt} = -\frac{\partial \mathcal{H}}{\partial D_a}.$$

Control system:

$$\frac{\partial \mathcal{H}}{\partial u} = 0.$$

It is obviously seen that the original system represents the state system in optimality conditions. We acquire the adjoint system from (7) in the following:

$$\frac{d\lambda_1}{dt} = -\frac{\partial H}{\partial S_c^*}$$

$$= \lambda_1(t)\left\{\frac{\left[\beta_{cc} I_c^*(t) + \beta_{ca} I_a^*(t)\right]\left[I_c^*(t) + R_c^*(t) + D_c^*(t)\right]}{N_c^2(t)} + \alpha\right\} - \lambda_2(t)\,\alpha$$

$$-\lambda_3(t)\left\{\frac{\left[\beta_{cc} I_c^*(t) + \beta_{ca} I_a^*(t)\right]\left[I_c^*(t) + R_c^*(t) + D_c^*(t)\right]}{\left(N_c^*(t)\right)^2}\right\},$$

$$\frac{d\lambda_2}{dt} = -\frac{\partial \mathcal{H}}{\partial S_a^*}$$

$$= \lambda_2\,(t) \left\{ \frac{\left[\beta_{ac} I_c^*(t) + \beta_{aa} I_a^*(t)\right]\left[I_a^*(t) + R_a^*(t) + D_a^*(t)\right]}{N_a^2\,(t)} + u^*\,(t) \right\}$$

$$-\lambda_4\,(t) \left\{ \frac{\left[\beta_{ac} I_c^*(t) + \beta_{aa} I_a^*(t)\right]\left[I_a^*(t) + R_a^*(t) + D_a^*(t)\right]}{\left(N_a^*(t)\right)^2} \right\}$$

$$-\lambda_6\,(t)\,u^*\,(t)\,,$$

$$\frac{d\lambda_3}{dt} = -\frac{\partial \mathcal{H}}{\partial I_c^*} = -1 + \lambda_1\,(t) \left\{ \frac{S_c^*(t)\left[\beta_{cc}\left(S_c^*(t) + R_c^*(t) + D_c^*(t)\right) - \beta_{ca} I_a^*(t)\right]}{\left(N_c^*(t)\right)^2} \right\}$$

$$+\lambda_2\,(t)\,\frac{S_a^*(t)\,\beta_{ac}}{N_a^*(t)}$$

$$-\lambda_3\,(t) \left\{ \frac{S_c^*(t)\left[\beta_{cc}\left(S_c^*(t) + R_c^*(t) + D_c^*(t)\right) - \beta_{ca} I_a^*(t)\right]}{\left(N_c^*(t)\right)^2} - \gamma_c - \alpha \right\}$$

$$-\lambda_4\,(t) \left(\frac{S_a^*(t)\,\beta_{ac}}{N_a^*(t)} + \alpha \right) - \lambda_5\,(t)\,\gamma_c \rho_c - \lambda_7\,(t)\,\gamma_c \psi_c,$$

$$\frac{d\lambda_4}{dt} = -\frac{\partial \mathcal{H}}{\partial I_a^*} = -1 + \lambda_1\,(t)\,\frac{S_c^*(t)\,\beta_{ca}}{N_c^*(t)}$$

$$+\lambda_2\,(t) \left\{ \frac{S_a^*(t)\left[\beta_{aa}\left(S_a^*(t) + R_a^*(t) + D_a^*(t)\right)\right]}{\left(N_a^*(t)\right)^2} \right\}$$

$$-\lambda_2\,(t)\,\frac{\beta_{ac} I_c^*(t) S_a\,(t)}{\left(N_a^*(t)\right)^2} - \lambda_3\,(t)\,\frac{S_c^*(t)\,\beta_{ca}}{N_c^*(t)}$$

$$-\lambda_4\,(t) \left\{ \frac{S_a^*(t)\left(\beta_{aa}\left[S_a^*(t) + R_a^*(t) + D_a^*(t)\right] - \beta_{ac} I_c^*\right)}{\left(N_a^*(t)\right)^2} - \gamma_a \right\}$$

$$-\lambda_6\,(t)\,\gamma_a \rho_a$$

$$-\lambda_8\,(t)\,\gamma_a \psi_a,$$

$$\frac{d\lambda_5}{dt} = -\frac{\partial \mathcal{H}}{\partial R_c^*} = -\lambda_1(t) \frac{\left[\beta_{cc} I_c^*(t) + \beta_{ca} I_a^*(t)\right] S_c^*(t)}{\left(N_c^*(t)\right)^2}$$

$$+\lambda_3(t) \frac{\left[\beta_{cc} I_c^*(t) + \beta_{ca} I_a^*(t)\right] S_c^*(t)}{\left(N_c^*(t)\right)^2} + \lambda_5(t)\alpha - \lambda_6(t)\alpha,$$

$$\frac{d\lambda_6}{dt} = -\frac{\partial \mathcal{H}}{\partial R_a^*} = -\lambda_2(t) \frac{\left[\beta_{ac} I_c^*(t) + \beta_{aa} I_a^*(t)\right] S_a^*(t)}{\left(N_a^*(t)\right)^2}$$

$$+\lambda_4(t) \frac{\left[\beta_{ac} I_c^*(t) + \beta_{aa} I_a(t)\right] S_a^*(t)}{\left(N_a^*(t)\right)^2},$$

$$\frac{d\lambda_7}{dt} = -\frac{\partial \mathcal{H}}{\partial D_c^*} = -\lambda_1(t) \left\{ \frac{\left[\beta_{cc} I_c^*(t) + \beta_{ca} I_a^*(t)\right] S_c^*(t)}{\left(N_c^*(t)\right)^2} \right\}$$

$$+\lambda_3(t) \left\{ \frac{\left[\beta_{cc} I_c^*(t) + \beta_{ca} I_a^*(t)\right] S_c^*(t)}{\left(N_c^*(t)\right)^2} \right\},$$

$$\frac{d\lambda_8}{dt} = -\frac{\partial \mathcal{H}}{\partial D_a^*} = -\lambda_2(t) \frac{\left[\beta_{ac} I_c^*(t) + \beta_{aa} I_a^*(t)\right] S_a^*(t)}{\left(N_a^*(t)\right)^2}$$

$$+\lambda_4(t) \frac{\left[\beta_{ac} I_c^*(t) + \beta_{aa} I_a^*(t)\right] S_a*(t)}{\left(N_a^*(t)\right)^2}$$

subject to the transversality conditions $\lambda_i(t_f) = 0$
($i = 1, ..., 8$). In addition, the optimal control function satisfies

$$\left. \frac{\partial \mathcal{H}}{\partial u} \right|_{u=u^*} = wu^* \left(\lambda_6(t) - \lambda_2(t)\right) S_a^*(t) = 0 \tag{8}$$

such that

$$u^* = \frac{(\lambda_2 - \lambda_6) S_a^*(t)}{w}. \tag{9}$$

4   Numerical Simulations and Discussion

In this part, we will analyze the behavior of the model with or without the vaccination effect. In the graphs, the system is considered as with and without control effect. In addition, the effect of the weight coefficient, which is an important parameter for the cost function, will be interpreted with graphics.

All numerical calculations are made by performing MATLAB software. The RK4 method is applied to find the numerical solutions of optimal system. In this iterative method, first, the state system given by Eq. (3) is solved by the forward RK4 method with the predictive control, and then the adjoint system obtained by Theorem 2 is solved by the backward RK4 method. The algorithm continues to run until the difference between the consecutive values of the iteration is less than the specified tolerance value. Problem parameters used for the simulations are $A = 4745$ (13 years), $\alpha = 0.00021$ [46], $\gamma_c = 0.5$ $\gamma_a = 0.0714$, $\beta_{ca} = 0.266$, $\beta_{ac} = 0.0001$, $\beta_{cc} = 0.308$, $\beta_{aa} = 0.308$, $\rho_a = 0.942$, $\rho_c = 0.99$, $\psi_a = 0.05$, $\psi_c = 0.0001$ [43]. The initial conditions are: $S_c(0) = 0.280$, $S_a(0) = 0.719$, $I_c(0) = 0$, $I_a(0) = 0.001$, $R_c(0) = 0$, $R_a(0) = 0$, $D_c(0) = 0$, $D_a(0) = 0$. As can be clearly seen from the figures, the numerical results are illustrated by normalizing the real values of $N = 1000$, $N_a = 720$, and $N_c = 280$. In addition, the time period of vaccination is accepted as $t_f = 30$days.

From Fig. 1, a significant reducing effect is also observed in the number of infected children, even though only adults are vaccinated. In addition, the number of recovered adults is increased considerably, and the number of dead adults is almost zero during the vaccination period. As a natural result of this graph, the serious decrease in the number of infected children has also led to a decrease in the number
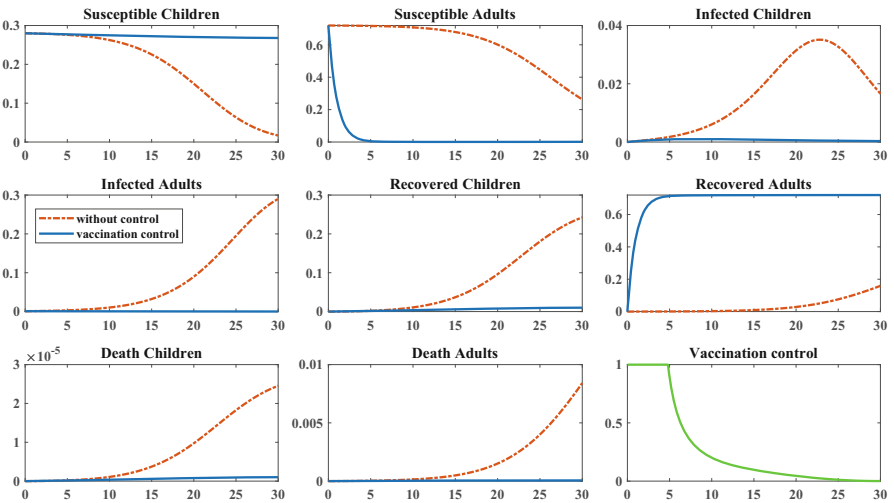
Fig. 1 The impact of adult vaccination on model
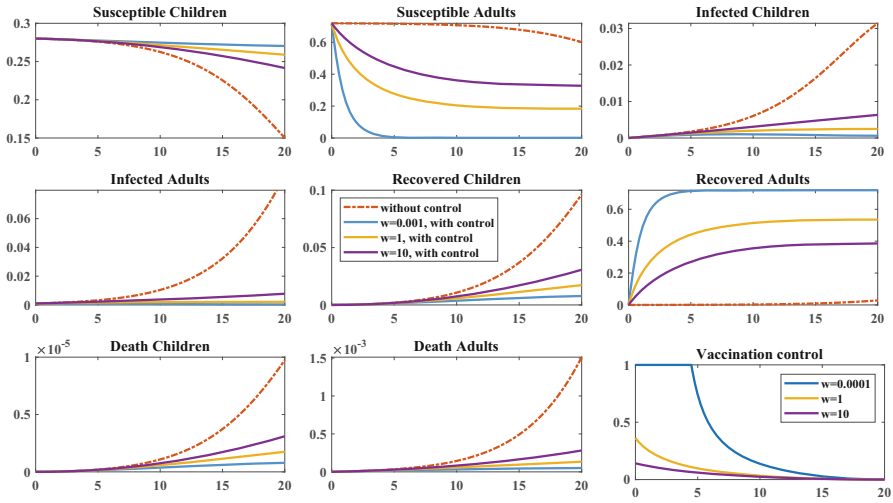
Fig. 2 The effect of weight coefficient w

of recovered children. The reduction of infected children is especially important for the continuity of education life. This is an important result for children. For adults, the continuity of their working life is also very important.

The weight parameter, which determines the efficiency level of the optimal control, is worth examining [47, 48]. In Fig. 2, we examine the behavior of controlled and uncontrolled systems with different weighting coefficients. Here, $t_f = 20$ *days* and all the remaining parameters and initial conditions are the same as in Fig. 1. Graphs are obtained by changing the weight coefficient w, which represents the cost of the adult vaccination control. By choosing three values of $w : w = 0.0001$, $w = 1$, and $w = 10$, respectively, we investigated the effect of control on the system dynamics, consisting of child and adult populations. Vaccination is of course a good precaution. However, governments also care about cost analysis in their vaccination policy. Unfortunately, when costs increase, there is a decrease in the vaccination rate. In Fig. 2, when the value of the weight coefficient increases, the control effect, i.e., vaccination rate, naturally decreases. This means that as the cost of vaccination increases, the number of vaccinated individuals will decrease, and the number of infected individuals will increase. This is also a predictable result of the problem. In conclusion, the contribution of the present OCP to the literature is to show the lower the cost of vaccination, the more people are vaccinated.

5   Concluding Remarks

This chapter proposes an optimal vaccination scenario for a COVID-19 spreading model represented the transmission between children and adults. The aim of the suggested OCP is reducing the number infected people with the minimum cost of vaccination. In the proposed scenario, only the vaccination of adults is considered. The optimality conditions have been calculated by Hamilton's principle. The RK4 method is applied with the forward–backward sweep algorithm to get the numerical results. Although only adults have been vaccinated, the rate of infection in both adults and children decreased significantly. This clearly shows how effective vaccination is. As it is already remembered, the development of different vaccines has been an important threshold in stopping the spread of COVID-19 because the most effective way in such viral epidemics is to improve herd immunity. Although this is not the ultimate goal of this chapter, strategies such as hygiene, masking, training, and treatment can also be evaluated as control parameters in addition to the vaccination. For the future studies, the present model can be discussed with combined control strategies. The effect of fractional operators on the model can also be researched comparatively. In addition, the effect of various incidence and treatment rates on the model is among the subjects worth investigating.

References

1. WHO: Coronavirus disease 2019 (COVID-19): Situation Report, 51 (2020)
2. WHO: Q&As on COVID-19 and related health topics (2021). https://www.who.int/emergencies/diseases/novel-coronavirus-2019/question-and-answers-hub
3. Kermack, W.O., McKendrick, A.G.: A contribution to the mathematical theory of epidemics. Proc. R. Soc. Lond. Ser. A Math. Phys. Eng. Sci. **115**(772), 700–721 (1927)
4. Li, G., Jin, Z.: Global stability of a SEIR epidemic model with infectious force in latent, infected and immune period. Chaos Solit. Fractals **25**(5), 1177–1184 (2005)
5. Granich, R.M., Gilks, C.F., Dye, C., De Cock, K.M., Williams, B.G.: Universal voluntary HIV testing with immediate antiretroviral therapy as a strategy for elimination of HIV transmission: a mathematical model. Lancet **373**(9657), 48–57 (2009)
6. Berge, T., Ouemba Tassé, A.J., Tenkam, H.M., Lubuma, J.: Mathematical modeling of contact tracing as a control strategy of Ebola virus disease. Int. J. Biomath. **11**(07), 1850093 (2018)
7. Lemos-Paião, A.P., Silva, C.J., Torres, D.F.: A new compartmental epidemiological model for COVID-19 with a case study of Portugal. Ecol. Complex. **44**, 100885 (2020)
8. Eikenberry, S.E., Mancuso, M., Iboi, E., Phan, T., Eikenberry, K., Kuang, Y., Gumel, A.B.: To mask or not to mask: modeling the potential for face mask use by the general public to curtail the COVID-19 pandemic. Infect. Dis. Model. **5**, 293–308 (2020)
9. Nainggolan, J., Harianto, J., Tasman, H.: An optimal control of prevention and treatment of COVID-19 spread in Indonesia. Commun. Math. Biol. Neurosci. **2023**(3), 1–22 (2023)
10. Saha, P., Biswas, S.K., Biswas, M.H.A., Ghosh, U.: An SEQAIHR model to study COVID-19 transmission and optimal control strategies in Hong Kong. Nonlinear Dyn. **111**, 1–21 (2023). https://doi.org/10.1007/s11071-022-08181-0
11. Rois, M.A., Alfiniyah, C., Chukwu, C.W.: Dynamic analysis and optimal control of COVID-19 with comorbidity: a modeling study of Indonesia. Front. Appl. Math. Stat. **8**, 1096141 (2023)

12. Ojo, M.M., Peter, O.J., Goufo, E.F.D., Nisar, K.S.: A mathematical model for the co-dynamics of COVID-19 and tuberculosis. Math. Comput. Simul. **207**, 499–520 (2023)
13. Oke, S.I., Ekum, M.I., Akintande, O.J., Adeniyi, M.O., Adekiya, T.A., Achadu, O.J., Salawu, S.O.: Optimal control of the coronavirus pandemic with both pharmaceutical and non-pharmaceutical interventions. Int. J. Dyn. Control, 1–25 (2023). https://doi.org/10.1007/s40435-022-01112-2
14. Kouidere, A., Balatif, O., Rachik, M.: Cost-effectiveness of a mathematical modeling with optimal control approach of spread of COVID-19 pandemic: a case study in Peru. Chaos Solit. Fractals **10**, 100090 (2023). https://doi.org/10.1016/j.csfx.2022.100090
15. Rao, M.A., Venkatesh, A.: SEAIQHRDP mathematical model analysis for the transmission dynamics of COVID-19 in India. J. Comput. Anal. Appl. **31**(1), 96–116 (2023)
16. Hye, M.A., Biswas, M.H.A., Uddin, M.F., Saifuddin, M.: Mathematical modeling of Covid-19 and Dengue co-infection dynamics in Bangladesh: optimal control and data-driven analysis. Comput. Math. Model. **33**, 173–192 (2022). https://doi.org/10.1007/s10598-023-09564-7
17. Baleanu, D., Mohammadi, H., Rezapour, S.: A fractional differential equation model for the COVID-19 transmission by using the Caputo-Fabrizio derivative. Adv. Differ. Equ. **2020**(1), 1–27 (2020)
18. Hamou, A.A., Rasul, R.R., Hammouch, Z., Özdemir, N.: Analysis and dynamics of a mathematical model to predict unreported cases of COVID-19 epidemic in Morocco. Comput. Appl. Math. **41**(6), 289 (2022)
19. Al-Husban, A., Djenina, N., Saadeh, R., Ouannas, A., Grassi, G.: A new incommensurate fractional-order COVID 19: modelling and dynamical analysis. Mathematics **11**(3), 555 (2023). https://doi.org/10.3390/math11030555
20. Abbes, A., Ouannas, A., Shawagfeh, N., Jahanshahi, H.: The fractional-order discrete COVID-19 pandemic model: stability and chaos. Nonlinear Dyn. **111**(1), 965–983 (2023)
21. Joshi, H., Jha, B. K., Yavuz, M.: Modelling and analysis of fractional-order vaccination model for control of COVID-19 outbreak using real data. Math. Biosci. Eng. **20**(1), 213–240 (2023)
22. Moualkia, S.: Mathematical analysis of new variant Omicron model driven by Lévy noise and with variable-order fractional derivatives. Chaos Solit. Fractals **167**, 113030 (2023)
23. Özköse, F., Habbireeh, R., Şenel, M.T.: A novel fractional order model of SARS-CoV-2 and Cholera disease with real data. J. Comput. Appl. Math. **423**, 114969 (2023)
24. Lenhart, S., Workman, J.T.: Optimal Control Applied to Biological Models. Chapman & Hall/CRC, Boca Raton (2007)
25. Gaff, H., Schaefer, E.: Optimal control applied to vaccination and treatment strategies for various epidemiological models. Math. Biosci. Eng. **6**(3), 469 (2009)
26. Bonyah, E., Okosun, K.O.: Mathematical modeling of Zika virus. Asian Pac. J. Trop. Dis. **6**(9), 673–679 (2016)
27. Lemos-Paião, A.P., Silva, C.J., Torres, D.F.: An epidemic model for cholera with optimal control treatment. J. Comput. Appl. Math. **318**, 168–180 (2017)
28. Kheiri, H., Jafari, M.: Optimal control of a fractional-order model for the HIV/AIDS epidemic. Int. J. Biomath. **11**(07), 1850086 (2018)
29. Ameen, I., Baleanu, D., Ali, H.M.: An efficient algorithm for solving the fractional optimal control of SIRV epidemic model with a combination of vaccination and treatment. Chaos Solit. Fractals **137**, 109892 (2020)
30. Naik, P.A., Zu, J., Owolabi, K.M.: Global dynamics of a fractional order model for the transmission of HIV epidemic with optimal control. Chaos Solit. Fractals **138**, 109826 (2020)
31. Avcı, D., Soytürk, F.: A comparative study on optimal control of a computer virus spread. In Conf. Proc. Sci. Technol. **5**(1), 192–202 (2022)
32. Avcı, D., Soytürk, F: Optimal control strategies for a computer network under virus threat. J. Comput. Appl. **419**, 114740 (2023)
33. Eroğlu, B.B. İ., Yapışkan, D.: Comparative analysis on fractional optimal control of an SLBS model. J. Comput. Appl. **421**, 114840 (2023)

34. Zamir, M., Shah, Z., Nadeem, F., Memood, A., Alrabaiah, H., Kumam, P.: Non-pharmaceutical interventions for optimal control of COVID-19. Comput. Methods Progr. Biomed. **196**, 105642 (2020)
35. Gatyeni, S.P., Chukwu, C.W., Chirove, F., Nyabadza, F.: Application of optimal control to the dynamics of COVID-19 disease in South Africa. Sci. Afr. **16**, e01268 (2022)
36. Butt, A.I.K., Imran, M., Batool, S., Nuwairan, M.A.: Theoretical analysis of a COVID-19 CF-fractional model to optimally control the spread of pandemic. Symmetry **15**(2), 380 (2023)
37. Sweilam, N.H., Al-Mekhlafi, S.M., Baleanu, D.: A hybrid fractional optimal control for a novel Coronavirus (2019-nCov) mathematical model. J. Adv. Res. **32**, 149–160 (2021)
38. Zamir, M., Nadeem, F., Abdeljawad, T., Hammouch, Z.: Threshold condition and non-pharmaceutical interventions's control strategies for elimination of COVID-19. Results Phys. **20**, 103698 (2021)
39. Bonyah, E., Sagoe, A.K., Kumar, D., Deniz, S.: Fractional optimal control dynamics of coronavirus model with Mittag-Leffler law. Ecol. Complex. **45**, 100880 (2021)
40. Eroğlu, B.B. İ., Yapışkan, D.: An optimal control strategy to prevent the spread of COVID-19. Conf. Proc. Sci. Technol. **5**(1), 182–186 (2022)
41. Vellappandi, M., Govindaraj, V.: Operator theoretic approach to optimal control problems characterized by the Caputo fractional differential equations. RICO **10**, 100194 (2023)
42. Baba, I.A., Humphries, U.W., Rihan, F.A.: Role of vaccines in controlling the spread of COVID-19: a fractional-order model. Vaccines **11**(1), 145 (2023)
43. Lazebnik, T., Bunimovich-Mendrazitsky, S.: The signature features of COVID-19 pandemic in a hybrid mathematical model-implications for optimal work-school lockdown strategy. Adv. Theory Simul. **4**(5), 2000298 (2021)
44. Fleming, W.H., Rishel, R.W.: Deterministic and Stochastic Optimal Control. Springer, New York (1975)
45. Lukes, D.L.: Differential Equations: Classical to Controlled, Mathematics in Science and Engineering. Academic, New York (1982)
46. Dong, Y., Mo, X., Hu, Y., Qi, X., Jiang, F., Jiang, Z., Tong, S.: Epidemiology of COVID-19 among children in China. Pediatrics **145**(6), e20200702 (2020)
47. Okosun, K.O., Makinde, O.D.: Optimal control analysis of malaria in the presence of non-linear incidence rate. Appl. Comput. Math. **12**(1), 20–32 (2013)
48. Ali, H.M., Ameen, I.G.: Save the pine forests of wilt disease using a fractional optimal control strategy. Chaos Solit. Fractals **132**, 109554 (2020)

Part II
Intelligent Control Techniques
and Covid-19 Pandemic

The Role of Artificial Intelligence and Machine Learning for the Fight Against COVID-19

Andrés Iglesias, Akemi Gálvez, and Patricia Suárez

1 How COVID-19 Pandemic Affected Our Lives and It Is Still Doing So

The COVID-19 (sometimes also written Covid) pandemic is a global health crisis caused by the novel coronavirus SARS-CoV-2 [1, 2]. The first outbreak was identified in Wuhan, China in December 2019 and has since spread rapidly, being declared a worldwide pandemic by the World Health Organization [3]. The COVID-19 pandemic has had a significant impact on the world in almost all aspects of our daily life in many different ways. Some areas of major impact of the disease are:

– *Physical health:* The COVID-19 has infected hundreds of millions of people globally, causing significant morbidity and mortality. Although the figures may differ strongly depending on the source and procedures followed for data record, storage, and analysis, it is generally acknowledged that at the time this work is written, the number of coronavirus cases has exceeded the seven hundred millions, with more than seven million of deceased, and probably millions of people affected by long-term effects, called post-COVID-19 syndrome, and also for post-acute sequelae of Covid infection (PASC). On the positive side, vaccines

A. Iglesias (✉) · A. Gálvez
Computer Graphics & Artificial Intelligence Group, Department of Applied Mathematics & Computational Sciences, University of Cantabria, Santander, Spain

Faculty of Pharmaceutical Sciences, Toho University, Funabashi, Japan
e-mail: iglesias@unican.es; galveza@unican.es

P. Suárez
Computer Graphics & Artificial Intelligence Group, Department of Applied Mathematics & Computational Sciences, University of Cantabria, Santander, Spain
e-mail: suarezp@unican.es

for COVID-19 have been developed to limit the spread of the disease, and they have shown to be effective [4]. However, as the coronavirus mutates, new variants are appearing worldwide, putting an additional stress on the development of new vaccines to cope with the new variants more effectively.

– *Mental health and social issues:* The pandemic has significantly impacted our mental health [5]. Many parts of the world have endured harsh lockdowns, forcing their population into long periods of social isolation, with many people experiencing increased stress, anxiety, and depression. The pandemic has highlighted the need for greater investment in mental health resources and support services and has disrupted social interactions, leading to increased feelings of loneliness and isolation for many people. It has also highlighted the importance of community support and the role of social connections in promoting health and well-being [6].

– *Healthcare systems:* The pandemic has put a tremendous strain on healthcare systems around the world, with many hospitals and healthcare workers overwhelmed by the surge in cases. Additionally, the pandemic has highlighted the importance of public health measures such as hand hygiene, mask wearing, not hand shaking, or vaccination, among others. New procedures have been raised to curb the spread of the disease, ranging from new healthcare protocols to social distancing [7].

– *Economy and job market:* The COVID-19 has caused widespread economic disruption. The pandemic's economic impact has been extremely severe, causing job losses and a significant decline in economic growth worldwide, as reported by the International Monetary Fund [8]. Due to strict lockdowns, reduced mobility, and other factors, many businesses have been forced to close, with many people losing their jobs as a result [9]. Governments around the world have implemented a range of economic stimulus measures to try to mitigate the impact of the pandemic, but the economic effects will still be felt for years to come. On the other hand, COVID-19 has forced many people to work from home, which has highlighted the importance of remote work and flexible working arrangements. It has also led to a shift in how businesses operate and communicate, with many companies embracing digital tools and online collaboration.

– *Travel industry and tourism:* The pandemic has severely impacted the travel industry, with many countries imposing travel restrictions and border closures [10]. This has led to a significant reduction in international travel and has had a major impact on the tourism industry.

– *Education:* The pandemic has led to widespread school closures and disruptions to education, with many students forced to learn remotely. This has highlighted the importance of access to technology and Internet connectivity, as well as the need for innovative approaches to education [11].

– *Technology:* The pandemic has sped up the adoption of digital technologies in many areas, from telemedicine to online shopping [12]. It has also highlighted the importance of access to technology, particularly for vulnerable populations who may not have reliable Internet access or the necessary digital skills.

– *Environment:* In the environment, while the reduction in travel and economic activity has led to lower greenhouse gas emissions and improved air quality in some areas, it has also led to an increase in plastic waste and a decline in recycling rates [13].
– *Politics and governance:* The pandemic has had a significant impact on politics and governance, with many countries implementing emergency measures to manage the public health crisis. This has raised questions about civil liberties and the role of government in responding to pandemics.
– *Others:* The pandemic has highlighted the need for global cooperation and collaboration, particularly in the areas of public health and scientific research. It has also exposed the vulnerabilities of global supply chains and the importance of preparedness for future pandemics. And finally the pandemic has highlighted the critical role of scientific research in understanding and responding to public health crises. It has also exposed the challenges and limitations of scientific communication and the importance of clear and accurate public messaging.

As shown in this section, the COVID-19 pandemic has impacted dramatically on various aspects of life, including health, education, the economy, and the environment. The development of effective vaccines for COVID-19 has shown promise in controlling the disease. However, the pandemic's long-term impact on society and the economy remains uncertain so far, as the world is still coping with the pandemic.

2 Artificial Intelligence and Machine Learning Against COVID-19

The coronavirus pandemic has spawned an unprecedented public health crisis that has impacted societies worldwide. Healthcare providers and public health systems have had to rapidly adapt to new and evolving challenges in order to contain the expansion of the virus. Artificial intelligence (AI) and machine learning (ML) have played a significant role in the pandemic response, offering innovative and efficient solutions to the challenges posed by the virus.

The ability of AI to quickly process and analyze vast amounts of data has proven essential for the fight against the virus. Here are some examples of how AI has been applied to address the covid pandemic [14–17]:

– *Medical diagnosis:* One potential benefit of using AI and machine learning in COVID-19 diagnosis is the ability to process huge amounts of data quickly and accurately. This could help to identify patterns or markers that might not be detectable with more traditional methods. On the other hand, advanced AI algorithms have been developed to help diagnose COVID-19 based on medical imaging, e.g., computer tomography (CT) scans or X-ray images. These algorithms can quickly and accurately detect COVID-19 pneumonia, which can

help with early diagnosis and treatment. For example, the paper in [18] developed an AI algorithm to detect COVID-19 from chest CT scans. The method achieved a total accuracy of 89.5% in its internal validation, with 0.87 of sensitivity and 0.88 of specificity. Regarding the external testing dataset, it showed a 79.3% of total accuracy, with 0.67 of sensitivity and 0.83 of specificity. In addition, the results of the first two nucleic acid tests were negative for a set of 54 images, while 46 images were predicted by the algorithm as positive in COVID-19, yielding an accuracy of 85.2%. Another potential benefit is the ability to reduce the risk of transmission by allowing for contactless screening and diagnosis. This could be especially useful in settings like airports, hospitals, and other high-traffic areas. Despite the potential benefits, there are also some concerns about the use of AI and machine learning in coronavirus diagnosis. For example, there is a risk that algorithms could be biased or produce inaccurate results, especially if they are trained on incomplete or biased datasets.

– *Drug discovery:* AI has been used to help accelerate drug discovery for COVID-19. The researchers have also used Machine Learning (ML) algorithms to screen thousands of potential drug candidates and identify those that are most likely to be effective against the virus [19]. For example, the startup Insilico Medicine used AI to identify a potential drug candidate for Covid in a very short time. On February 23, 2023, it has been announced in newspapers and other media that the world's first generative AI-designed COVID drug will soon begin clinical trials [20].

– *Contact tracing and tracking:* At the dawn of the pandemic, some experts suggested that AI and machine learning could be applied to help track the virus spreading in real time, potentially allowing for earlier identification of outbreaks and more targeted interventions. Following these remarks, AI has been used to help with contact tracing, which involves identifying individuals who may have been exposed to the virus [21]. Contact tracing apps use AI to identify potential transmission chains and notify individuals with potential close contact with someone tested positive. For example, the authors were required to install and activate the COCOA (Contact-Confirming Application) app in their personal smartphones for COVID-19 tracking during their stays in Japan in 2021 and 2022. A study published in [22] found that digital contact tracing could be effective in controlling the Covid propagation when combined with other public health measures.

– *Vaccine development:* AI and ML have played a significant role in the development of vaccines for Covid, by aiding in the identification of potential vaccine targets and in the optimization of vaccine production processes. This has enabled the development of vaccines in record time, paving the way for global vaccination efforts.

– *Predictive modeling:* AI has been used to develop predictive models to forecast the spread of COVID-19 and to guide public health interventions. These models take into account factors such as infection rates, population demographics, and mobility patterns to predict how the virus is likely to spread. For example, the University of California Los Angeles developed an AI model capable of

predicting the Covid spreading up to three weeks in advance with an accuracy of 94%. A remarkable advantage of that model is its accuracy. The primary reason to explain it is that the model does not rely only on confirmed COVID-19 cases and fatalities, but it also infers additional data fields (i.e., the number of untested and unreported cases) by data analysis of the model. Such inferences are then used to predict how quickly the disease will spread [23]. As a result, this model is claimed to be more accurate than most other alternatives currently available. After that work, other epidemic models that take into account the multiple factors affecting the rate of disease spread have been generated worldwide. In the work in [24], prediction algorithms were developed and validated for estimating the risk of mortality related to the COVID-19 as well as the rate of hospital admission for adults in UK after they received one or two doses of COVID-19 vaccination.

– *Public health management:* AI and ML are used to develop prediction models for Covid dissemination, enabling public health officials to make informed decisions regarding resource allocation and disease containment efforts. Many health management-related decision-making plans have been set up based on such epidemic models. For instance, AI and ML can be applied to help predict which patients are most likely to require hospitalization or intensive care, allowing for more efficient allocation of resources [25, 26].

– *Robotics:* AI-powered robots have been used in hospitals and other medical institutions to perform tasks such as delivering medications or cleaning patient rooms. These robots can help minimize the risk of infection for healthcare workers, patients, and their relatives. For example, the Danish company UVD Robots developed a robot that uses UV light to disinfect hospital rooms [27]. The robot uses ultraviolet light for disinfection and killing of several viruses, bacteria, and other types of harmful microorganisms by breaking down their DNA structure. The robot is said to be effective at a ratio of 99,99% of the bacteria and viruses.

As a summary of this section, the use of AI and ML has been instrumental to fight against the coronavirus. The ability of AI and ML to analyze huge amounts of data, identify patterns, and make predictions has helped the researchers and healthcare professionals in the development of vaccines, tracking the evolution of the virus, and predicting potential outbreaks. Moreover, AI and ML have enabled the automation of some tasks that are crucial in the fight against the pandemic, reducing the workload on healthcare professionals and allowing for quicker response times and more efficient and better informed measures.

3   AI and ML for COVID-19 Diagnosis

The Covid pandemic has brought unprecedented challenges to healthcare systems and the global economy. As the figures of confirmed cases worldwide continue to rise, the need for innovative solutions to manage and mitigate the spread of the virus

has become critical. The use of AI and ML in COVID-19 diagnosis has been an area of intensive research since the outbreak of the pandemic. AI and ML have shown promising results in the early detection, diagnosis, and management of COVID-19 [21, 22, 28].

One potential use of AI and ML in this area is the analysis of medical imaging, mainly chest X-rays, and CT scans. By analyzing these images, deep learning algorithms and other AI methods can identify patterns and markers that are indicative of COVID-19 and can help clinicians to make a more accurate diagnosis. In [29], the network Mobile Net, a state-of-the-art deep learning architecture based on the popular convolutional neural networks (CNNs), was trained from scratch and applied to investigate the relevance of different extracted features for a classification task. A large dataset of images associated with 6 different diseases and comprised of 3,905 X-ray images was used to train the network MobileNet v2. The results showed that this strategy of training the convolutional networks from scratch leads to superior results with respect to other transfer learning techniques, not only in distinguishing the X-ray images among the seven classes but also between the COVID-19 and non-COVID-19 scenarios. In particular, they achieved an accuracy of 87.66% for the classification task among the seven classes. In addition, an accuracy of 99.18% is achieved for the detection of COVID-19, with a sensitivity of 97.36%, and a specificity of 99.42%. These results are a clear indication that performing training from scratch on CNNs may reveal vital biomarkers. Furthermore, such biomarkers can be related to the COVID-19 disease but are not necessarily limited to that case. On the other hand, the high accuracy achieved for classification seems to suggest that further examination is required to harness the full potential of X-ray imaging for this task.

In a study conducted in China, the researchers developed an AI method for diagnosis of COVID-19 from chest CT scans with 96% of accuracy [21]. The AI algorithm was trained using a deep learning method referred to as COVNet based on a CNN, which can analyze and classify image features. The CNN architecture used in the study was a 3D version of the popular ResNet-50 model, consisting of multiple layers that can learn and extract features from the input images. The input of this deep learning model is a set of CT images corresponding to a sequence of slices, while the output is a set of generated features for the slices, which are subsequently combined by using a max-pooling operation. The resulting feature map is inputted to a fully connected layer using softmax (i.e., the normalized exponential function) as the activation function. This generates a probability score for each category from the three classes: COVID-19, CAP (community-acquired pneumonia), and other lung conditions. The dataset used in this work was comprised of 4,352 chest CT scans from 3,322 patients. The per-scan sensitivity for COVID-19 detection in the independent test set was 90% (with 95% confidence interval [CI]: 83%, 94%; a total of 114 out of 127 scans), while the specificity was 96% (95% CI: 93%, 98%; a total of 294 out of 307 scans). The results of this work indicate that AI and ML can be valuable tools for the timely and accurate diagnosis of the COVID-19 disease.

In a work published in [30], a deep learning AI algorithm for Covid detection from frontal chest radiographs called DeepCOVID-XR was trained and tested on a large clinical data set, where the coronavirus tests are conducted through the reverse-transcription polymerase chain reaction (RT-PCR). Essentially, DeepCOVID-XR is an ensemble of CNNs carefully tailored for coronavirus detection. The network was trained and validated on 14,788 images (4,253 positive for the disease) and then tested on 2,214 images (1,192 positive). The performance of the algorithm was compared with the assessments of five experienced thoracic radiologists on 300 random test images. The data sets included a total of 5,853 patients (mean age, 58 years $\pm$ 19; 3101 women). For the whole data set, the accuracy of the method was 83%, with an AUC (area under the characteristic curve) of 0.90. These results show that the performance of DeepCOVID-XR for coronavirus detection compares well with that of experienced thoracic radiologists, a solid evidence of the ability of this network to detect the disease.

In [31], the authors developed a deep learning model for detection of patients affected by COVID-19 from CT images. The model, called Details Relation Extraction neural network (DRENet), was based on the pretrained ResNet50 neural network, enriched with Feature Pyramid Network (FPN) for feature extraction of the top-K details of each image. Under such architecture, the deep learning algorithm has proved to be effective in capturing subtle differences in medical images. The model was trained with images of chest CT scans of patients from hospitals in two provinces in China. The training data set consisted of 777 CT images from 88 patients with Covid, 505 images from 100 patients with bacterial pneumonia, and 708 images from 86 healthy people. The authors concluded that the model can perform accurate discrimination of the COVID-19 patients with respect to the group of patients with bacteria pneumonia. From their experiments, they obtained an AUC of 0.95 and values of 0.96 and 0.79 for the sensitivity and the precision, respectively.

Another potential use of AI and ML in Covid diagnosis is in the analysis of patient data, such as vital signs, laboratory test results, and medical histories. By analyzing these data, AI algorithms can assist in the prediction of which patients are at highest risk of developing severe disease. The systematic review published in [26] evaluated the accuracy of prediction models for diagnosis and prognosis of the disease. The authors found that several ML-based models showed high performance. They can be used, for instance, to track the evolution of the disease by analyzing data recording the movements and interactions of infected individuals [32]. For example, the South Korean government used AI to trace the movements of infected individuals and identify potential contacts. AI and ML are also helpful to develop prediction models to assist in the identification of those patients most likely to require hospitalization or simply those who mostly benefit from certain treatments. This can help allocate healthcare resources more efficiently and ensure that patients receive the most appropriate care for their clinical condition.

Recently, some researchers have developed an AI system that can identify individuals who may have been exposed to Covid using as input the sound of their coughs [33], one of the most visible and persistent manifestations of the COVID-19 disease. The model incorporated four deep learning algorithms, embodied as

two multilayer perceptrons, a convolutional neural network, and an ensemble called *MSCCov19Net* combining all features from the other three models. This architecture was trained using supervised learning with public datasets, which allowed it to learn to differentiate between cough sounds from coronavirus positive and negative individuals. The model then underwent testing to assess its accuracy in identifying COVID-19 positive cases. The results show a system accuracy of 61.5 and 90.4% for two different datasets. Other initiatives in this line of research have been described in the literature, ranging from the COUGHVID data set in [34] to the works in [35, 36] and [37] for computational architectures designed for preliminary screening and diagnosis of Covid from cough sounds. Other AI-based approaches for Covid diagnosis from cough recordings can also be found in [38, 39]. These works reveal that deep learning methods have a strong potential as low-cost non-invasive scalable tools for identifying potential Covid cases in large populations from a very simple and economic input. However, they also noted that further research and validation are needed before it can be implemented as a diagnostic tool in clinical settings.

Another interesting AI-based approach is the use of AI-powered wearable devices that can track and monitor individuals' movements, allowing for more efficient contact tracing [40]. One example of such a device is TraceTogether, a wearable token developed by the Singaporean government. The device uses Bluetooth signals to communicate with other devices in close proximity, recording the duration and distance of the interaction. If a user is tested positive for coronavirus, his/her device's data could be used to quickly identify and contact those who were in close proximity to the infected individual, allowing for more targeted and efficient contact tracing. In other cases, wearables have been used to detect early signs of the disease through different physiological signals, like the heartbeat rate [41] or the temperature of the body [42]. Other illustrative examples of this approach are given in [43–47]. Interested readers are kindly referred to [48] and [49] for two comprehensive reviews about wearable devices and sensors for health monitoring systems and with regard to the COVID-19 monitoring, respectively.

4   AI and ML for COVID-19 Drug Discovery and Repurposing

AI and ML can also be used to accelerate drug discovery by predicting which compounds are most likely to be effective against COVID-19 [50]. Traditional drug discovery methods can be time-consuming and expensive, and many potential drug candidates are often missed due to limitations in data analysis. AI-based methods can rapidly scan large datasets and identify patterns and relationships that would be difficult for humans to discern [51].

In [52], different ML approaches for prediction of repurposed drugs are considered and analyzed. The pool of methods include support vector machine (SVM), random forest (RF), K-Nearest Neighbor (K-NN), artificial neural networks, and

deep learning. All these models were applied to the prediction of promising repurposed drug candidates to fight against Covid, selected from pre-scanning using the DrugBank [53, 54].

The review in [55] introduced guidelines on the use of AI techniques for accelerating drugs repurposing or repositioning for the COVID-19 disease. The paper in [56] discusses how AI methods are changing the current landscape with regard to drug discovery and repurposing. Deep learning applications to these purposes are also discussed in [57]. A hybridization of convolutional neural networks and random forests is used in [58] for learning drug functions from chemical structures. Drug target prediction using deep neural networks and ML is discussed, for instance, in [59–65].

The researchers have used AI and ML tools to identify potential treatments and repurpose existing drugs for Covid patients. These algorithms are used to analyze the molecular structure of existing drugs and identify several drugs that could be repurposed for efficient treatment of COVID-19. Some drugs identified by these algorithms are currently being tested in clinical trials. In January 2020, scientists at AI platform BenevolentAI used AI to identify the rheumatoid arthritis drug baricitinib as a potential candidate for COVID-19 treatment [66]. This drug has since been approved for emergency use in the USA, in particular, for the treatment of hospitalized COVID-19 adult patients requiring mechanical ventilation, supplemental oxygen, or ECMO (extracorporeal membrane oxygenation).

The research approach of BenevolentAI platform involves the use of AI to analyze large datasets and identify potential drug candidates. The company has developed its own proprietary AI platform, which combines natural language processing, machine learning, and knowledge graphs to extract information from various sources such as scientific literature, clinical trial data, and electronic health records. In the case of COVID-19, BenevolentAI's AI platform has analyzed various types of data, including genomic and proteomic data, to identify potential targets for drug development. The platform can identify protein–protein interactions, predict the effects of small molecules on protein activity, and suggest potential drug candidates for repurposing, which involves finding new uses for existing drugs based on their similarity or their ability to target specific molecular pathways. This approach can significantly shorten the time it takes to develop a new drug, as the safety and pharmacokinetics of the drug are already established. However, the drug must still be rigorously tested in clinical trials to establish its safety and efficacy for the new uses and indications. In addition to drug discovery, BenevolentAI is also using its AI platform to identify biomarkers for COVID-19 diagnosis and prognosis. By analyzing patient data, the platform can identify patterns that may be indicative of disease severity or progression, which could help clinicians make more informed treatment decisions.

A research team from the University of California, San Francisco, used AI to screen over 1 billion small molecules and identify 23 that were predicted to be effective against the virus. The researchers used a computational tool called MoleculeNet, which is a deep learning platform for drug discovery that uses multiple AI algorithms to analyze large datasets of chemical compounds [67]. The

tool uses virtual screening to predict the properties of small molecules and how they interact with biological targets. To screen the large library of small molecules, the researchers used the computational resources of the OpenPandemics—COVID-19 project, which is a collaboration between the researchers at UCSF and the University of Washington, as well as volunteers from around the world who donate their computer processing power. The team trained MoleculeNet on a large dataset of small molecules and their biological activities to predict which compounds would be most effective against the virus. Then, they validated the predictions using laboratory experiments and found that several of the small molecules were effective at inhibiting the replication of the virus in cell cultures.

5 AI and ML for COVID-19 Forecasting

Another way AI and ML have been utilized against Covid is in the forecasting of the pandemic. AI and ML models have been developed to predict the evolution and expansion of the virus, the number of cases, and the potential impact of different interventions. These models use a range of data, including epidemiological, clinical, and social data, to generate forecasts. In [68], the authors developed an app named PMCP, for mortality prediction of COVID-19 patients at the time of admission at a hospital. In a study conducted in Iran and the UK with 797 patients diagnosed with COVID-19, the researchers applied an AI model to predict the risk of mortality and the severity of the disease for patients at intensive care units (ICUs) to determine and optimize their treatment strategies [69]. From a set of 66 documented parameters, they identified 15 factors proved to have the highest predictive value. They include general factors such gender and age, clinical parameters such as blood urea nitrogen, albumin, creatinine, white blood cell count, international normalized ratio (INR), mean corpuscular volume (MCV), lymphocyte count, segmented neutrophil count, mean cell hemoglobin (MCH), and red cell distribution width (RDW), in addition to the history of neurological, cardiovascular, and respiratory disorders. The model had a sensitivity of 70% and a specificity of 75% and was able to identify the areas most in need of resources and interventions.

The researchers in [70] used a machine learning model using the UK Biobank (UKBB) data for risk forecasting of the chances to develop severe or fatal infections, while also uncovering major factors of risk involved. In their approach, they used hospitalization as an indicator for the severity of the disease and a group of 97 clinical variables as predictors. Such variables were collected before COVID-19 outbreak and included demographic factors, blood measurements, comorbidities, anthropometric measures, and some other risk factors such as heavy drinking or smoking. The prediction models were created using XGboost with gradient-boosted trees. State-of-the-art techniques such as MissForest (a random forest-based ML algorithm for data imputation) and multiple imputation by chained equation (MICE) were used for missing data imputation of datasets. From their experimental results, they concluded that XGboost ML models exhibit a good predictive power,

particularly noticeable for mortality. In fact, their models worked notably better for mortality prediction than for the severity of disease, with an AUC of 81–83% for the former. Overall, the researchers found that their machine learning model had a good prediction rate. They also found that their model could be used to identify countries that were likely to be particularly hard hit by the pandemic, which could help the policymakers prepare and allocate resources more effectively.

The work in [71] proposes an ML forecasting model to predict the number of Covid cases in India. They suggests that accurate forecasting of COVID-19 cases can help public health officials in resource allocation and policymaking. The authors applied linear regression, vector autoregression, and multilayer perceptrons on the Kaggle dataset with 80 instances to forecast the number and trend of infected cases in India.

The work in [72] aimed to investigate whether Google Trends data might be used as predictors of the number of COVID-19 infections in the United States. The authors utilized ML models to analyze the relationships between Google Trends data and COVID-19 cases. To this purpose, the authors collected the daily cumulative counts of confirmed infections, along with the number of deceases, obtained from a public repository of Johns Hopkins University. Although the data contained 422 symptoms with potential relationship with the disease, they limited their experiments to nine symptoms: hypoxemia, hypoxia, ageusia, dysgeusia, pneumonia, fever, chills, anosmia, and shortness of breath. Then, they used LSTM (long short-term memory) networks to create predictive models for four forecasting tasks related to the COVID-19. This work suggests that Google search trends data can be a useful tool to predict the spread of the disease and that they can arguably improve the performance of ML-based forecasting models. However, the authors note that further research is needed to validate these findings and to develop more accurate models.

The work in [73] developed a hidden pattern detection-enabled ML model on reported COVID-19 cases to forecast potential infections. First, a dimensionality reduction was carried out to identify the key parameters allowing to uncover hidden patterns. Then, a forecasting analysis was conducted through an unbiased hierarchical Bayesian estimator to ascertain past infections from current deceases. As a result, they were able to predict the number of undetected infections in USA and Canada. A different machine learning forecasting model used to predict ICU admission, length of stay, and mortality of COVID-19 patients at admission-time at hospitals is reported in [74].

The paper in [75] applied a combination of genetic algorithms with an improved SEIR model for epidemic trend forecasting in China. The paper in [76] applied genetic operators to optimize convolutional networks for COVID-19 detection from X-ray images of the chest. In [77], a computational architecture comprised of three main components, an unsupervised feature extractor based on a convolutional autoencoder, a feature selector based on a multi-objective genetic algorithms, and a binary classifier based on a set of support vector machines, was applied for the automatic identification of undetected COVID-19 cases from medical images. In [78], a new algorithm called GABFCov 19 was introduced for identification of

positive cases of the disease. The work in [79] combined genetic evolution and an ML classifier for COVID-19 diagnosis from blood samples. The paper in [80] applies a genetic-based image reconstruction algorithm for COVID-19 detection from X-ray images via digital holography.

The COVID-19 pandemic has posed significant challenges for hospitals and healthcare providers worldwide, leading to the development of new tools and technologies to help manage the influx of patients. The authors in [81] developed a CDSS (clinical decision support system) for COVID-19 patients classification at hospital admission based on the severity of the disease. The work used a multicenter cohort of COVID-19 patients from hospitals in China, Italy, Spain and Belgium. The data collected from these patients included demographic information, clinical characteristics, laboratory values, and treatment outcomes. The study utilized a range of statistical and ML techniques to develop and validate the CDSS. The CDSS is based on an ML model that uses clinical features to predict the severity of COVID-19 in patients at hospital admission and to triage patients into one of the three severity risk groups (low, intermediate, or high). This system provides a valuable tool for healthcare providers to triage COVID-19 patients at hospital admission, based on their severity risk score. Other recent related works can be found in [82, 83].

6   Conclusion

The pandemic of COVID-19 has created an unprecedented need for innovative solutions to manage and mitigate the spread of the virus. During this painful process, AI and ML have been revealed as valuable tools for the fight against the disease. The researchers and experts have turned to artificial intelligence and machine learning to develop models and tools that can help with the diagnosis, forecasting, and management of COVID-19 [84]. These tools have been used to diagnose the virus, forecast its spread, and identify potential treatments, and they have shown promising results in identifying COVID-19 biomarkers from medical images, accurately diagnosing the virus using X-ray and CT scan images, and predicting hospitalization and mortality rates. AI-enabled analysis of worldwide data has also been used to predict the potential of drug repurposing for COVID-19. As the pandemic continues to evolve and new variants are being reported over the time, AI and ML will continue to play a critical role in the global effort to manage and control the evolution of the coronavirus and its variants.

One of the lessons learned after three years of COVID-19 pandemic is that AI and ML have played a major role in the fight against the disease, offering innovative and efficient solutions to the challenges posed by the pandemic [85]. Overall, the pandemic of COVID-19 has demonstrated the potential of AI and ML in healthcare and has provided an opportunity for us to improve our understanding of how these technologies can be used to address global health challenges [86]. The pandemic has also highlighted the relevance of technology in addressing global health challenges,

and the role that AI and ML can play in advancing healthcare. As such, it is likely that we will continue to see increased adoption of these technologies in healthcare, not just in the fight against pandemics but also in everyday healthcare settings. As we move forward, there is a need for continued research and development in the field, in order to fully realize the potential of these powerful tools in healthcare and public health. By harnessing the power of AI and ML, we can continue to fight COVID-19 and mitigate its effects.

It is important to note however that the use of AI and ML in healthcare is not without its challenges. There are ethical concerns around their use in healthcare more broadly, including questions around data privacy and security, bias, data ownership, and the potential for algorithmic decision-making to exacerbate existing social inequalities and other social problems [87, 88]. Also, there are critical voices and many open questions about the lack of proper regulation to tackle these issues. As with any new technology, it will be important to continue to evaluate and refine the use of AI and ML for COVID-19 and other pandemics, in terms of both its accuracy and effectiveness and its broader social and ethical implications [89, 90].

References

1. Centers for Disease Control and Prevention: Symptoms of COVID-19. Retrieved from https://www.cdc.gov/coronavirus/2019-ncov/symptoms-testing/symptoms.html (2022). Last Accessed 1 March 2023
2. Centers for Disease Control and Prevention: Transmission. Retrieved from https://www.cdc.gov/coronavirus/2019-ncov/transmission/index.html (2021). Last Accessed 1 March 2023
3. World Health Organization. Coronavirus disease (COVID-19) pandemic. Retrieved from https://www.who.int/emergencies/diseases/novel-coronavirus-2019. Last Accessed 1 March 2023
4. Centers for Disease Control and Prevention: Vaccines for COVID-19. Retrieved from https://www.cdc.gov/coronavirus/2019-ncov/vaccines/index.html (2021). Last Accessed 1 March 2023
5. World Health Organization: Mental health and COVID-19. Retrieved from https://www.who.int/teams/mental-health-and-substance-use/mental-health-and-covid-19 (2020). Last Accessed 1 March 2023
6. Centers for Disease Control and Prevention: Coping with stress. Retrieved from https://www.cdc.gov/mentalhealth/stress-coping/cope-with-stress/managing-stress-anxiety.html (2021). Last Accessed 1 March 2023
7. Ugail, H., Aggarwal, R., Iglesias, A., Howard, N., Campuzano, A., Suárez, P., Maqsood, M., Aadil, F., Mehmood, I., Gleghorn, S., Taif, K., Kadry, S., Muhammad, K.: Social distancing enhanced automated optimal design of physical spaces in the wake of the COVID-19 pandemic. Sustain. Cities Soc. **68**, Paper 102791 (2021)
8. International Monetary Fund: World Economic Outlook, April 2020: The Great Lockdown. Retrieved from https://www.imf.org/en/Publications/WEO/Issues/2020/04/14/weo-april-2020 (2020). Last Accessed 1 March 2023

9. International Labour Organization: COVID-19 and the world of work. Retrieved from https://www.ilo.org/global/topics/coronavirus/lang--en/index.htm (2021). Last Accessed 1 March 2023

10. United Nations World Tourism Organization: Impact assessment of the COVID-19 outbreak on international tourism. Retrieved from https://www.unwto.org/impact-assessment-of-the-covid-19-outbreak-on-international-tourism (2023). Last Accessed 1 March 2023

11. UNESCO: Education: from school closure to recovery. Retrieved from https://en.unesco.org/covid19/educationresponse (2021). Last Accessed 1 March 2023

12. Ting, D., Carin, L., Dzau, V., Wong, T.: Digital technology and COVID-19. Nat Med. **26**(4), 459–461 (2020)

13. Mofijur, M., Fattah, I.M.R., Alam, M.A., Islam, A.B.M.S., Ong, H.C., Rahman, S.M.A., Najafi, G., Ahmed, S.F., Uddin, M.A., Mahlia, T.M.I.: Impact of COVID-19 on the social, economic, environmental and energy domains: lessons learnt from a global pandemic. Sustain Prod Consum. **26**, 343–359 (2021)

14. Alimadadi, A., Aryal, S., Manandhar, I., Munroe, P.B., Joe, B.: Artificial intelligence and machine learning to fight COVID-19. Physiol. Genom. **52**(4), 200–202 (2020)

15. Swayamsiddha, S., Prashant, K., Shaw, D., Mohanty, C.: The prospective of Artificial Intelligence in COVID-19 Pandemic. Health Technol. (Berl). **11**(6), 1311–1320 (2021)

16. Rahman, M.M., Khatun, F., Uzzaman, A., Sami, S.I., Bhuiyan, M.A., Kiong, T.S.: A comprehensive study of artificial intelligence and machine learning approaches in confronting the coronavirus (COVID-19) pandemic. Int. J. Soc. Determ. Health Health Serv. **51**(4), 446–461 (2021)

17. Chang, Z., Zhan, Z., Zhao, Z., You, Z., Liu, Y., Yan, Z., Fu, Y., Liang, W., Zhao, L.: Application of artificial intelligence in COVID-19 medical area: a systematic review. J. Thoracic Dis. **13**(12), 7034–7053 (2021)

18. Wang, S., Kang, B., Ma, J., Zeng, X., Xiao, M., Guo, J., Cai, M., Yang, J., Li, Y., Meng, X., Xu, B.: A deep learning algorithm using CT images to screen for Corona virus disease (COVID-19). Eur Radiol. **31**(8), 6096–6104 (2021)

19. Mak, K., Pichika, M.: Artificial intelligence in drug development: present status and future prospects. Drug. Discovery Today. **24**(3), 773–780 (2019)

20. Toronto Star: World's first generative AI-designed COVID drug to start clinical trials. Retrieved from: https://www.thestar.com/news/canada/2023/02/23/its-perfect-worlds-first-generative-ai-designed-covid-drug-to-start-clinical-trials.html. Last Accessed 1 March 2023

21. Li, L., Qin, L., Xu, Z., Yin, Y., Wang, X., Kong, B., Bai, J., Lu, Y., Fang, Z., Song, Q., Cao, K., Liu, D., Wang, G., Xu, Q., Fang, X., Zhang, S., Xia, J., Xia, J.: Using Artificial Intelligence to Detect COVID-19 and community-acquired pneumonia based on pulmonary CT: evaluation of the diagnostic accuracy. Radiology. **296**(2), E65–E71 (2020)

22. Ferretti, L., Wymant, C., Kendall, M., Zhao, L., Nurtay, A., Abeler-Dörner, L., Parker, M., Bonsall, D., Fraser, C.: Quantifying SARS-CoV-2 transmission suggests epidemic control with digital contact tracing. Science **368**(6491), eabb6936 (2020)

23. UCLA Newsroom: UCLA machine-learning model is helping CDC predict spread of COVID-19. Retrieved from https://newsroom.ucla.edu/releases/machine-learning-model-cdc-covid19 . Last Accessed 1 March 2023

24. Hippisley-Cox, J., Coupland, C.A., Mehta, N., Keogh, R.H., Diaz-Ordaz, K., Khunti, K., Lyons, R.A., Kee, F., Sheikh, A., Rahman, S., Valabhji, J., Harrison, E.M., Sellen, P., Haq, N., Semple, M.G., Johnson, P.W.M., Hayward, A., Nguyen-Van-Tam, J.S.: Risk prediction of COVID-19 related death and hospital admission in adults after covid-19 vaccination: national prospective cohort study. British Med. J. **374**, n2244 (2021). Erratum in: British Med. J. **374**, n2300 (2021)

25. Vaishya, R., Javaid, M., Khan, I.H., Haleem, A.: Artificial intelligence (AI) applications for COVID-19 pandemic. Diabetes Metab Syndr. **14**(4), 337–339 (2020)

26. Wynants, L., Van Calster, B., Collins, G.S., Riley, R.D., Heinze, G., Schuit, E., Bonten, M.M.J., Dahly, D.L., Damen, J.A.A., Debray, T.P.A., de Jong, V.M.T., De Vos, M., Dhiman, P.,

Haller, M.C., Harhay, M.O., Henckaerts, L., Heus, P., Kammer, M., Kreuzberger, N., Lohmann, A., Luijken, K., Ma, J., Martin, G.P., McLernon, D.J., Andaur Navarro, C.L., Reitsma, J.B., Sergeant, J.C., Shi, C., Skoetz, N., Smits, L.J.M., Snell, K.I.E., Sperrin, M., Spijker, R., Steyerberg, E.W., Takada, T., Tzoulaki, I., van Kuijk, S.M.J., van Bussel, B., van der Horst, I.C.C., van Royen, F.S., Verbakel, J.Y., Wallisch, C., Wilkinson, J., Wolff, R., Hooft, L., Moons, K.G.M., van Smeden, M. Prediction models for diagnosis and prognosis of covid-19: systematic review and critical appraisal. British Med. J. **369**, m1328 (2020). Update in: British Med. J. **372**, n236 (2021). Erratum in: British Med. J. **369**, m2204 (2020)

27. European Commisssion: Danish disinfection robots save lives in the fight against the Corona virus. Retrieved from: https://digital-strategy.ec.europa.eu/en/news/danish-disinfection-robots-save-lives-fight-against-corona-virus. Last Accessed 1 March 2023

28. Pawar, M.V., Pawar, A.M., Bhapkar, H., Anuradha, J., Bachate, R., Sharma, A., Bhoyar, S., Shardoor, N.: Artificial intelligence-based solutions for COVID-19. In: Data Science for COVID-19, pp. 167–89. Academic, Cambridge (2022)

29. Apostolopoulos, I.D., Aznaouridis, S.I., Tzani, M.A.: Extracting possibly representative COVID-19 biomarkers from X-ray images with deep learning approach and image data related to pulmonary diseases. J. Med. Biol. Eng. **40**(4), 462–469 (2020). https://doi.org/10.1007/s40846-020-00514-6

30. Wehbe, R.M., Sheng, J., Dutta, S., Chai, S., Dravid, A., Barutcu, S., Wu, Y., Cantrell, D.R., Xiao, N., Allen, B.D., MacNealy, G.A., Savas, H., Agrawal, R., Parekh, N., Katsaggelos, A.K.: DeepCOVID-XR: an artificial intelligence algorithm to detect COVID-19 on chest radiographs trained and tested on a large U.S. clinical data set. Radiology. **299**(1), E167–E176 (2021)

31. Song, Y., Zheng, S., Li, L., Zhang, X., Zhang, X., Huang, Z., Chen, J., Wang, R., Zhao, H., Chong, Y., Shen, J., Zha, Y., Yang, Y.: Deep learning enables accurate diagnosis of novel coronavirus (COVID-19) with CT images. IEEE/ACM Trans. Comput. Biol. Bioinform. **18**(6), 2775–2780 (2021)

32. Majeed, A., Zhang, X.: On the adoption of modern technologies to fight the COVID-19 pandemic: a technical synthesis of latest developments. COVID **3**, 90–123 (2023)

33. Ulukaya, S., Sarıca, A.A., Erdem, O., Karaali, A.: MSCCov19Net: multi-branch deep learning model for COVID-19 detection from cough sounds. Med. Biol. Eng. Comput. **24**, 1–11 (2023)

34. Orlandic, L., Teijeiro, T., Atienza, D.: The COUGHVID crowdsourcing dataset, a corpus for the study of large-scale cough analysis algorithms. Sci. Data **8**, 156 (2021)

35. Mohammed, E.A., Keyhani, M., Sanati-Nezhad, A., Hezaji, S.H., Far, B.H.: An ensemble learning approach to digital corona virus preliminary screening from cough sounds. Sci. Rep. **11**, 15404 (2021)

36. Imran, A., Posokhova, I., Qureshi, H.N., Masood, U., Riaz, M.S., Ali, K., John, C.N., Hussain, M.I., Nabeel, M.: AI4COVID-19: AI enabled preliminary diagnosis for COVID-19 from cough samples via an app. Inform. Med. Unlocked. **20**, 100378 (2020)

37. Laguarta, J., Hueto, F., Subirana, B.: COVID-19 artificial intelligence diagnosis using only cough recordings. IEEE Open J. Eng. Med. Biol. **1**, 275–281 (2020)

38. Soltanian, M., Borna, K.: COVID-19 recognition from cough sounds using lightweight separable-quadratic convolutional network. Biomed. Sig. Process. Control **72**, 103333 (2022)

39. Coppock, H., Gaskell, A., Tzirakis, P., Baird, A., Jones, L., Schuller, B.: End-to-end convolutional neural network enables COVID-19 detection from breath and cough audio: a pilot study. BMJ Innov. **7**(2), 356–362 (2021)

40. Hijazi, H., Abu Talib, M., Hasasneh, A., Bou Nassif, A., Ahmed, N., Nasir, Q.: Wearable devices, smartphones, and interpretable artificial intelligence in combating COVID-19. Sensors **21**, 8424 (2021)

41. Hasty, F., Garc'a, G., Dávila, C.H., Wittels, S.H., Hendricks, S., Chong, S.: Heart rate variability as a possible predictive marker for acute inflammatory response in COVID-19 patients. Mil. Med. **186**, e34–e38 (2020)

42. Chung, Y.T., Yeh, C.Y., Shu, Y.C., Chuang, K.T., Chen, C.C., Kao, H.Y., Ko, W.-C., Chen, P.-L., Ko, N.Y.: Continuous temperature monitoring by a wearable device for early detection of febrile events in the SARS-CoV-2 outbreak in Taiwan, 2020. J. Microbiol. Immunol. Infect. **53**, 503 (2020)

43. Hirten, R.P., Danieletto, M., Tomalin, L., Choi, K.H., Zweig, M., Golden, E., Kaur, S., Helmus, D., Biello, A., Pyzik, R., et al.: Use of physiological data from a wearable device to identify SARS-CoV-2 infection and symptoms and predict COVID-19 diagnosis: observational study. J. Med. Int. Res. **23**, e26107 (2021)

44. Zhu, G., Li, J., Meng, Z., Yu, Y., Li, Y., Tang, X., Dong, Y., Sun, G., Zhou, R., Wang, H., et al.: Learning from large-scale wearable device data for predicting the epidemic trend of COVID-19. Discrete Dyn. Nat. Soc. **2020**, 6152041 (2020)

45. Quer, G., Radin, J.M., Gadaleta, M., Baca-Motes, K., Ariniello, L., Ramos, E., Kheterpal, V., Topol, E.J., Steinhubl, S.R.: Wearable sensor data and self-reported symptoms for COVID-19 detection. Nat. Med. **27**, 73–77 (2020)

46. Lonini, L., Shawen, N., Botonis, O., Fanton, M., Jayaraman, C., Mummidisetty, C.K., Shin, S.Y., Rushin, C., Jenz, S., Xu, S., et al.: Rapid screening of physiological changes associated with COVID-19 using soft-wearables and structured activities: a pilot study. IEEE J. Transl. Eng. Health Med. **9**, 1–11 (2021)

47. Al Bassam, N., Hussain, S.A., Al Qaraghuli, A., Khan, J., Sumesh, E., Lavanya, V.: IoT based wearable device to monitor the signs of quarantine remote patients of COVID-19. Informat. Med. Unlocked **24**, 100588 (2021)

48. Banaee, H., Ahmed, M.U., Loutfi, A.: Data mining for wearable sensors in health monitoring systems: a review of recent trends and challenges. Sensors **13**, 17472–17500 (2013)

49. Channa, A., Popescu, N., Skibinska, J., Burget, R.: The rise of wearable devices during the COVID-19 pandemic: a systematic review. Sensors **21**, 5787 (2021)

50. Pharmaphorum: How AI is fighting COVID-19: the companies using intelligent tech to find new drugs. Retrieved from: https://pharmaphorum.com/views-analysis-digital/how-ai-is-fighting-covid-19-the-companies-using-intelligent-tech-to-find-new-drugs (2020). Last Accessed 1 March 2023

51. Mohanty, S., Rashid, M.H.A., Mridul M., Mohanty C., Swayamsiddha S.: Application of artificial intelligence in COVID-19 drug repurposing. Diabetes Metab. Syndr. **14**(5), 1027–1031 (2020)

52. Rajput, A., Thakur, A., Mukhopadhyay, A., Kamboj, S., Rastogi, A., Gautam, S., Jassal, H., Kumar, M.: Prediction of repurposed drugs for coronaviruses using artificial intelligence and machine learning. Comput. Struct. Biotechnol. J. **19**, 3133–3148 (2021)

53. DrugBank database. Retrieved from: https://www.drugbank.com. Last Accessed 1 March 2023

54. Wishart, D.S., Feunang, Y.D., Guo, A.C., Lo, E.J., Marcu, A., Grant, J.R., Sajed, T., Johnson, D., Li, C., Sayeeda, Z., Assempour, N., Iynkkaran, I., Liu, Y., Maciejewski, A., Gale, N., Wilson, A., Chin, L., Cummings, R., Le, D., Pon, A., Knox, C., Wilson, M.: DrugBank 5.0: a major update to the DrugBank database for 2018. Nucleic Acids Res. **46**(D1), D1074–1082 (2018)

55. Zhou, Y., Wang, F., Tang, J., Nussinov, R., Cheng, F.: Artificial intelligence in COVID-19 drug repurposing. Lancet Digit Health. **2**(12), e667–e676 (2020)

56. Fleming, N.: How artificial intelligence is changing drug discovery. Nature **557**, S55–57 (2018)

57. Aliper, A., Plis, S., Artemov, A., Ulloa, A., Mamoshina, P., Zhavoronkov, A.: Deep learning applications for predicting pharmacological properties of drugs and drug repurposing using transcriptomic data. Mol. Pharm. **13**, 2524–30 (2016)

58. Meyer, J.G., Liu, S., Miller, I.J., Coon, J.J., Gitter, A.: Learning drug functions from chemical structures with convolutional neural networks and random forests. J. Chem. Inf. Model. **59**, 4438–49 (2019)

59. Gao, K.Y., Fokoue, A., Luo, H., Iyengar, A., Dey, S., Zhang, P.: Interpretable drug target prediction using deep neural representation. In: Proceedings of the Twenty-Seventh International Joint Conference on Artificial Intelligence, pp. 3371–3377 (2018)

60. Wen, M., Zhang, Z., Niu, S., Sha, H., Yang, R., Yun, Y., Lu, H.: Deep-learning-based drug-target interaction prediction. J. Proteome Res. **16**(4), 1401–1409 (2017)

61. Zhou, Y., Hou, Y., Shen, J., Mehra, R., Kallianpur, A., Culver, D.A.: A network medicine approach to investigation and population-based validation of disease manifestations and drug repurposing for COVID-19. PLoS Biol. **18**(11), Paper 3000970 (2020)

62. Nguyen, T., Le, H., Quinn, T.P., Nguyen, T., Le, T.D., Venkatesh, S.: GraphDTA: predicting drug-target binding affinity with graph neural networks. Bioinformatics. **37**(8), 1140–1147 (2021)

63. D'Souza, S., Prema, K.V., Balaji, S.: Machine learning models for drug-target interactions: current knowledge and future directions. Drug Discovery Today. **25**(4), 748–756 (2020)

64. Zhang, T., Leng, J., Liu, Y.: Deep learning for drug-drug interaction extraction from the literature: a review. Briefings Bioinformat. **21**(5), 1609–1627 (2020)

65. Vamathevan, J., Clark, D., Czodrowski, P., Dunham, I., Ferran, E., Lee, G., Li, B., Madabhushi, A., Shah, P., Spitzer, M., Zhao, S.: Applications of machine learning in drug discovery and development. Nat. Rev. Drug Discovery **18**(6), 463–477 (2019)

66. BenevolentAI: FDA converts emergency approval of baricitinib – first identified as a COVID treatment by BenevolentAI – to a full approval. Retrieved from: covid-19 https://www.benevolent.com/news/fda-converts-emergency-approval-of-baricitinib-first-identified-as-a-covid-treatment-by-benevolentai-to-a-full-approval

67. Wu, Z., Ramsundar, B., Feinberg, E.N., Gomes, J., Geniesse, C., Pappu, A.S., Leswing, K., Pande, V.: MoleculeNet: a benchmark for molecular machine learning. Chem Sci. **9**(2), 513–530 (2017)

68. Lin, J.K., Chien, T.W., Wang, L.Y., Chou, W.: An artificial neural network model to predict the mortality of COVID-19 patients using routine blood samples at the time of hospital admission: development and validation study. Med. (Baltimore). **100**(28), e26532 (2021)

69. Jamshidi, E., Asgary, A., Tavakoli, N., Zali, A., Setareh, S., Esmaily, H., Jamaldini, S.H., Daaee, A., Babajani, A., Sendani Kashi, M.A., Jamshidi, M., Jamal, Rahi S., Mansouri, N.: Using machine learning to predict mortality for COVID-19 patients on day 0 in the ICU. Front Digit. Health. **13**(3), 681608 (2022)

70. Wong, K.C., Xiang, Y., Yin, L., So, H.C.: Uncovering clinical risk factors and predicting severe COVID-19 cases using UK biobank data: machine learning approach. JMIR Public Health Surveill. **7**(9), e29544 (2021)

71. Sujath, R., Chatterjee, J.M., Hassanien, A.E.: A machine learning forecasting model for COVID-19 pandemic in India. Stochast. Environ. Res. Risk Assess. **34**, 959–972 (2020)

72. Alruily, M., Ezz, M., Mostafa, A.M., Yanes, N., Abbas, M., El-Manzalawy, Y.: Prediction of COVID-19 transmission in the United States using google search trends. Computers, Mat. Continua **71**(1), 1751–1768 (2022)

73. Vaid, S., Cakan, C., Bhandari, M.: Using machine learning to estimate unobserved COVID-19 infections in North America. J. Bone Joint. Surg. Am. **102**(13), e70 (2020)

74. Saadatmand, S., Salimifard, K., Mohammadi, R., Kuiper, A., Marzban, M., Farhadi, A.: Using machine learning in prediction of ICU admission, mortality, and length of stay in the early stage of admission of COVID-19 patients. Ann. Oper. Res. **29**, 1–29 (2022)

75. Qiu, Z., Sun, Y., He, X. et al.: Application of genetic algorithm combined with improved SEIR model in predicting the epidemic trend of COVID-19, China. Sci. Rep. **12**, Paper 8910 (2022)

76. Mahendra, M.I., Kurniawan, I.: Optimizing convolutional neural network by using genetic algorithm for COVID-19 detection in chest X-ray image. In: Proceedings of the 2021 International Conference on Data Science and Its Applications, ICoDSA 2021, Bandung, Indonesia, pp. 135–140 (2021)

77. Bansal, S., Singh, M., Dubey, R.K., Panigrahi, B.K.: Multi-objective genetic algorithm based deep learning model for automated COVID-19 detection using medical image data. J. Med. Biol. Eng. **41**, 678–689 (2021)

78. Sharma, S., Jain, A.: An algorithm to identify the positive COVID-19 cases using genetic algorithm (GABFCov 19). J. Interdiscip. Math. **24**(1), 109–124 (2021)

79. Doewes, R.I., Nair, R., Sharma, T.: Diagnosis of COVID-19 through blood sample using ensemble genetic algorithms and machine learning classifier. World J. Eng. **19**(2), 175–182 (2021)

80. Kaya, G.U., Onur, Ozge, T.: Genetic algorithm based image reconstruction applying the digital holography process with the discrete orthonormal stockwell transform technique for diagnosis of COVID-19. Comput. Biol. Med. **148**, Paper 105934 (2022)
81. Wu, G., Yang, P., Xie, Y,, Woodruff, H.C., Rao, X., Guiot, J., Frix, A.N., Louis, R., Moutschen, M., Li, J., Li, J., Yan, C., Du, D., Zhao, S., Ding, Y., Liu, B., Sun, W., Albarello, F., D'Abramo, A., Schinina, V., Nicastri, E., Occhipinti, M., Barisione, G., Barisione, E., Halilaj, I., Lovinfosse, P., Wang, X., Wu, J., Lambin, P.: Development of a clinical decision support system for severity risk prediction and triage of COVID-19 patients at hospital admission: an international multicentre study. Eur. Respirat. J. **56**(2), Paper 2001104 (2020)
82. Wendland, P., Schmitt, V., Zimmermann, J., Häger, L., Göpel, S., Schenkel-Häger, C., Kschischo, M.: Machine learning models for predicting severe COVID-19 outcomes in hospitals. Inform. Med. Unlocked. **37**, Paper 101188 (2023)
83. Taheriyan, M., Ayyoubzadeh, S.M., Ebrahimi, M., Niakan Kalhori, S., Abooei, A.H., Gholamzadeh, M., Ayyoubzadeh, S.M.: Prediction of COVID-19 patients' survival by deep learning approaches. Med. J. Islamic Repub. Iran. **29**(36), 144 (2022)
84. Khanna, V.V., Chadaga, K., Sampathila, N., Prabhu, S., Chadaga, R., Umakanth, S.: Diagnosing COVID-19 using artificial intelligence: a comprehensive review. Netw. Model. Anal. Health Inform. Bioinforma. **11**, 25 (2022)
85. Lalmuanawma, S., Hussain, J., Chhakchhuak, L.: Applications of machine learning and artificial intelligence for Covid-19 (SARS-CoV-2) pandemic: a review. Chaos Solitons Fractals. **139**, 110059 (2020)
86. Vinod, D.N., Prabaharan, S.R.S.: COVID-19-the role of artificial intelligence, machine learning, and deep learning: a newfangled. Arch. Comput. Methods Eng. **30**, 2667–2682 (2023)
87. Anshari, M., Hamdan, M., Ahmad, N., Ali, E., Haidi, H.: COVID-19, artificial intelligence, ethical challenges and policy implications. AI Soc. **19**, 1–14 (2022)
88. Kritikos, M.: Artificial intelligence (AI) in a time of pandemics: Developing options for the ethical governance of COVID-19 AI applications. In: Ethics, Integrity and Policymaking: The Value of the Case Study, Chapter 13. Springer, Cham (2022).
89. World Health Organization (WHO): Guidance for managing ethical issues in infectious disease outbreaks. Retrieved from: https://apps.who.int/iris/handle/10665/250580 (2016). Last Accessed 1 March 2023
90. Hao, K.: Coronavirus is forcing a trade-off between privacy and public health. MIT Technology Review. Retrieved from: https://www.technologyreview.com/s/615396/coronavirus-is-forcing-a-trade-off-between-privacy-and-public-health/ (2020). Last Accessed 1 March 2023

Coronavirus Lung Image Classification with Uncertainty Estimation Using Bayesian Convolutional Neural Networks

Mfundo Monchwe, Ibidun C. Obagbuwa, and Alfred Mwanza

1 Introduction

A component of artificial intelligence (AI), computer vision, enables computers to perceive and comprehend the visual environment [2, 11, 29]. One key aspect of this field is deep learning. This method mimics the human brain's ability to process information and carry out actions such as object detection and tracking, speech recognition, natural language processing, and decision-making [2, 9, 11, 29]. Deep learning models identify and classify objects from video feeds and cameras and react to these identifications or classifications in a specified way. Computer vision and neural networks are the basis for deep learning [2, 9, 26]. Deep learning combines various types of computer vision techniques and is the foundation for many advanced applications in the field. These techniques include image segmentation [2, 9, 26], image classification [16], object detection [14], and object tracking [19]. Image segmentation involves dividing an image into smaller sections for further analysis, while object detection involves identifying specific objects within an image for identification.

The coronavirus outbreak has profoundly impacted individuals and communities, generating dread and death. The virus primarily affects the lungs and respiratory system, making lung imaging a crucial tool for detecting its presence. In the diagnostic process, lung images are analyzed to identify the presence of coronavirus within the lungs. With the advancement of technology, scientists are utilizing computer vision and deep learning techniques to aid in the identification of COVID-19 in individuals. The likelihood of false positive and false negative errors in

M. Monchwe · I. C. Obagbuwa (✉) · A. Mwanza
Department of Computer Science and Information Technology, School of Natural & Applied Sciences, Sol Plaatje University, Kimberley, South Africa
e-mail: ibidun.obagbuwa@spu.ac.za; alfred.mwanza@spu.ac.za

the identification and diagnosis of disease is reduced by the application of deep learning to the processing of COVID-19 radiography pictures [12, 29]. This method offers a unique opportunity to give patients quick, affordable, and secure diagnostic services. Given the importance of public health security and pandemic management, COVID-19 early detection is crucial. Testing is critical, as the virus may not present symptoms for 7–14 days (incubation period) [17].

Early diagnosis of COVID-19 using the reverse transcript polymerase chain reaction (RT-PCR) test is difficult based on an individual's symptoms [17, 29]. In the aftermath of the worldwide health disaster, the healthcare industry is looking for new technology and strategies to identify and control the coronavirus epidemic. Several studies have been conducted to use deep learning to address the shortcomings of COVID-19 diagnostic tests using radiological lung image datasets [4, 5, 12]. Many studies have used radiological image dataset and focused on using the global glass detection method to detect coronavirus with different accuracies. Previous studies in this area have primarily utilized nonprobabilistic machine learning methods, with popular algorithms including decision trees (DT) and others that fall under supervised machine learning. However, one of the limitations of nonprobabilistic machine learning approaches does not provide opportunities for making decisions under uncertainty and building models using both data and domain knowledge [21]. There is a growing need for an approach or a system for classifying images and measuring the degree of uncertainty or confidence in the predictions made by the neural networks.

A probabilistic framework for representing and managing uncertainty in models and predictions was presented in [13]. Within this framework, Bayesian convolutional neural networks (BCNNs) are a type of probabilistic machine learning technique. The study [7] developed the "Bayes-SAR Net," a Bayesian CNN capable of robustly classifying SAR image classification while evaluating the degree of uncertainty or confidence of the CNN's decision-making process. In this chapter, Bayesian CNNs were utilized for the classification of coronavirus lung images, as it has been established as the most efficient method for decision-making that incorporates uncertainty quantification [7, 10, 13, 21].

1.1 Problem Statement

The coronavirus pandemic continues to pose a significant threat, resulting in numerous deaths and infections worldwide. One question that arises is how we can aid healthcare professionals in detecting and predicting the virus. Given that previous research has shown that RT-PCR tests can take an amount of duration to yield results and often have low sensitivity, alternative approaches are needed. Another area for improvement is that the models examined in the literature on COVID-19 need quantification of uncertainty, making it challenging to gauge confidence in their predictions. Nonprobabilistic machine learning methods can identify whether a patient has the virus or not, but they do not incorporate

domain knowledge or provide quantification of uncertainty in their predictions. The probabilistic machine learning approach will help create a probabilistic machine learning solution for measuring uncertainty and convergence [7, 10, 13, 21]. A coronavirus prediction model employing lung imaging datasets with inevitability is the goal of this work, which sets out to construct this model using probabilistic machine learning techniques.

2   Related Work

Numerous articles discuss the current coronavirus problem and look into using deep learning and machine learning approaches to help predict and track the disease's spread and how it affects our daily life [18, 19, 27]. Covid-19 was identified in December 2019. Symptoms of Covid-19 include coughing, fever, chills, shortness of breath, painful muscles, sore throat, and loss of taste or smell. The Middle East respiratory syndrome, also known as severe acute respiratory syndrome, may result from the virus' high contagiousness and capacity to transmit from person to person [18].

The RT-PCR test is a widely used method for identifying the presence of coronavirus in individuals [5]. The procedure involves collecting a sample from the nose or throat of a patient using a swab and then analyzing it in a machine that detects the virus [17]. The RT-PCR test requires samples to be transported to a testing facility where the machines for analysis are located. This process can be time-consuming, and there is a possibility of the virus being inactive by the time the results are obtained. RT-PCR can produce negative results in an infected person. RT-PCR was shown to have a significant probability of producing false negatives and many false positives [17]. The sensitivity of the RT-PCR test could be higher, which raises concerns about the level of confidence (frequentist) or how credible (Bayesian) is in the results it produces. This uncertainty is further reinforced by the test's lower chance of detecting the virus in the early stages of infection.

Using deep convolutional neural network (CNN) model, Jain et al. demonstrated how COVID-19 can be detected from X-ray images. The model's efficiency was evaluated using a collection of X-ray images of people with viral pneumonitis, lung opacity, and COVID-19 [16]. Jain et al. revealed that a deep learning model based on convolutional neural networks (CNNs) was used to successfully identify COVID-19 X-ray images and that the model had a high accuracy rate in classifying X-ray images that are either COVID-19 or not. Furthermore, the model's capacity to distinguish between COVID-19, lung opacity, and viral pneumonia emphasizes its potential for real-world applications. However, the study indicates certain limitations associated with the use of X-ray images for COVID-19 identification, such as the low sensitivity of X-rays in identifying early-stage COVID-19 and the limited availability of X-ray images of COVID-19 patients [16]. Jain et al. concluded by providing useful insights into deep learning for detecting COVID-19 in X-ray pictures, and their findings indicate that this methodology has the potential

to build a viable method for COVID-19 identification. However, further research is necessary to address the limitations of using X-ray images for the identification of COVID-19 [16].

Gozes et al. developed a rapid AI development process for detecting and monitoring COVID-19 using CT image analysis and deep learning [14]. They introduced a 3-D deep learning architecture that uses both 2-D and 3-D global representative characteristics to improve the precision of COVID-19 identification. To preprocess the 3-D CT scan, Unet-17-based extraction of the lung region's region of interest using segmentation was utilized. After pre-processing, the image is sent to COVNet for prediction. Gozes et al. generate feature vectors for each slice, which are then used for COVID-19 detection. They report that the proposed technique obtained good classification accuracy, recall, and precision in COVID-19 detection and that the majority of coronavirus opacities were discovered around the lungs' margins [14]. The quantification of uncertainty was not introduced; therefore, the researcher is uncertain about how confident the model is in prediction.

Using CT images, Xu et al. [28] published a deep learning system that screens for novel coronavirus disease pneumonia. XU et al. proposed utilizing a deep convolutional neural network (DCNN) model to analyze CT scans to reduce the number of false negative cases [24, 28, 30].The study utilized a set of CT scans from COVID-19 patients, achieving a high accuracy rate of 97.5% in detecting the virus and a low false positive rate of 94.4%. According to Xu et al. [28], the suggested deep learning system has the potential to be employed as a COVID-19 screening tool in clinical settings [28].

Li et al. [19] examined and analyzed the utility of AI to detect COVID-19 and community-acquired pneumonia (CAP) using lung CT images. Li et al. utilized a deep learning system that was trained on a set of CT images from COVID-19 patients, CAP patients, and patients with other respiratory disorders. The AI system has a good diagnosis accuracy for COVID-19, according to the study, with an area under the receiver operating characteristic curve (AUC) of 0.97. With an AUC of 0.95, the algorithm also demonstrated a high diagnostic accuracy for CAP. Furthermore, the algorithm could distinguish between COVID-19 and CAP with an AUC of 0.98. The AI algorithm was able to perform better compared to radiologists' interpretation of the CT images. Li et al. suggested that using AI to detect COVID-19 and CAP in lung CT scans can improve diagnostic accuracy and reduce the workload for radiologists [19]. Overall, the results of this study were awe-impressive. However, the sample size of this study is relatively small, and further research with a larger scale and different dataset is required to confirm these findings.

The study by Ghaderzadeh and Asadi [12] was a comprehensive evaluation of the utilization of deep learning algorithms in identifying and diagnosing COVID-19 utilizing radiological modalities. Ghaderzadeh and Asadi reviewed various studies that have utilized CT and X-ray images along with deep learning to identify COVID-19, analyzed the performance of the models used in these studies, and discussed the advantages and limitations of utilizing deep learning for the identification of COVID-19. In addition, they emphasized the significance of data annotation in

influencing the effectiveness of deep learning models. Overall, in-depth information about the state of deep learning technology is provided in this chapter for COVID-19 detection using radiology modalities [12].

Agrawal and Choudhary [1] suggested "FocusCOVID," a deep learning algorithm, to detect COVID-19 using chest X-ray images [1]. Agrawal and Choudhary developed a deep learning model employing a CNN architecture on a collection of chest X-ray pictures. The CNN was created using a dataset of chest X-ray pictures from COVID-19 positive and negative patients, and it was tested on a second dataset. The suggested model accurately predicted COVID-19 from chest X-ray pictures, according to the study [1]. This study has a significant advantage in that it uses deep learning to detect COVID-19 from chest X-ray pictures, a reasonably inexpensive and widely available imaging modality. This can be a valuable tool for more advanced imaging modalities in areas with limited resources. A limitation of this study is that it is based on a small dataset of chest X-ray images. As a result, the model's performance may not generalize to larger, more diverse datasets. Additionally, the study did not evaluate the model's performance in a multi-ethnic population, which may affect the model's performance in different populations.

Alazab et al. [5] recommended utilizing deep learning approaches to identify and forecast COVID-19 using X-ray images. Alazab et al. suggested a deep learning model that categorizes X-ray pictures as positive or negative for COVID-19 using a combination of convolutional neural networks (CNNs) and long short-term memory (LSTM) networks. To train and assess the model, they employed a dataset of X-ray images from COVID-19 patients and healthy persons, and they found that their model obtained an overall accuracy of 96.7% in detecting COVID-19 [5]. One potential advantage of this approach is that it can be faster and more accurate in detecting COVID-19 than traditional methods. However, a limitation of this study is that the dataset used needs to be bigger, which may affect the generalizability of the findings. Additionally, Alazab et al. [5] needed to provide information on the performance of their model on unseen data, which limits the interpretability of their results.

Paluru et al. [22] presented a deep learning model called "AnamNet," which is intended for segmentation of anomalies in COVID-19 chest CT images. Paluru et al. claimed that the model is lightweight, which allows it to be deployed in resource-constrained environments such as mobile devices [22]. The model was constructed and analyzed utilizing a dataset of patients' COVID-19 chest CT images, and its performance was contrasted to that of other cutting-edge approaches, and the results showed that AnamNet achieved high accuracy and outperformed other models in terms of computational efficiency. The results showed that AnamNet achieved high accuracy and outperformed other models in terms of computational efficiency. The anamNet method can be a diagnostic aid in identifying COVID-19 patients and can be useful in resource-constrained environments. However, one limitation of this study is that it is based on a relatively small dataset of chest CT images, and future research can investigate the performance of the model on more extensive and more diverse datasets [22].

Al-Waisy et al. [3] describe Covid-DeepNet, a deep learning system aiming to improve the identification of COVID-19 pneumonia in chest X-ray images. To boost detection accuracy, the system employs a hybrid multimodal deep learning technique that integrates various deep learning models. According to the study, the system performed well in detecting COVID-19 instances, with an overall accuracy of 97.17% [3]. The implementation of a hybrid multimodal deep learning approach in this chapter has the potential to improve detection accuracy [3]. One potential disadvantage is that the study only examined the system's performance on chest X-ray pictures, which may not be generalizable to other imaging modalities [3].

Burdick et al. [6] described a machine learning model that uses electronic health record data to predict respiratory decompensation in COVID-19 patients. The study was conducted using data from the "Rapid Emergency Department Sepsis Trial" (READY), a multicenter observational study of patients with COVID-19 [6]. Modified Early Warning Score (MEWs) is superior to the diagnostic ratio produced by the suggested model. Out of all these accomplishments and more, the suggested model is more sensitive (0.90) and more specific($p < 0.05$) than the MEWS model. Burdick et al. discovered that the machine learning model could accurately predict respiratory decompensation in COVID-19 patients. One advantage of this approach is that it can identify patients at high risk of respiratory failure early, allowing for timely intervention and improving patient outcomes [6]. However, one limitation is that the study is based on a limited dataset and does not quantify the uncertainty in prediction and may also not generalizable to other populations.

Hu et al. provided a methodology for training and fine-tuning the model using weak annotation (image-level labels) [15]. The study examined the suggested framework's performance on a large dataset of CT scans, and the results revealed that the proposed method had achieved good accuracy and sensitivity in detecting COVID-19 infections. This method can be a valuable tool for early diagnosis and triage of COVID-19 patients, which can help to enhance COVID-19 pandemic management [15]. One advantage of this approach is a promising approach for improving the diagnostic accuracy of COVID-19. It could help promptly diagnose the disease, which is vital for preventing its spread [15]. However, the study does not provide information about the real-world performance of the model and its generalizability across different institutions and imaging modalities.

The increasing demand for principled machine learning approaches by non-specialists in various fields led to the increased support of probabilistic modeling [20, 25]. This is due to the need for transparent models with quantification of uncertainty, specifically models that can be very knowledgeable when they do not know [20, 25]. This will be mainly useful in determining the level of certainty of the prediction made and understanding why a certain prediction was made. However, probabilistic machine learning is concerned with problems of decision-making [13].

Based on a thorough review of current literature, deep learning models have been effectively utilized in classifying COVID-19 patients using radiographical lung images. However, it is worth noting that there need to be more studies that adopt a probabilistic machine learning approach, specifically Bayesian CNNs, in the prediction of COVID-19 using radiographical lung images. As a result, this chapter

aims to bridge that gap by utilizing a Bayesian CNNs approach in the classification of lung images in COVID-19 patients, offering a unique perspective and potential advancements in the field.

2.1 Nonprobabilistic and Probabilistic Classification

Duerr et al. explained that traditional deep learning models, such as feedforward neural networks, are typically trained with a nonprobabilistic approach, meaning they output a single-point estimate of the class or value of interest [8]. This can be very problematic because it needs to consider the prediction's uncertainty, which can lead to overconfidence in the model's results. Duerr et al. discussed how this lack of uncertainty can be addressed through probabilistic models, such as Bayesian neural network. These models can output probability distributions over the class or value of interest, which can provide a more nuanced understanding of the model's predictions [20, 21].

Additionally, Duerr et al. also mention that probabilistic deep learning models can be used to regularize traditional deep learning models. This can be done by introducing a probability distribution over the model weights, which can help prevent overfitting and improve the model's generalizability [8]. One of the main advantages of probabilistic classification is that it allows for modeling uncertainty. For example, it can consider the possibility of misclassification and provide more accurate predictions when the decision boundary is uncertain. Additionally, probabilistic classification can generate probabilistic models for other machine learning tasks, such as clustering and density estimation. However, probabilistic classification also has its limitations. For example, it can be computationally expensive, particularly with large datasets. Furthermore, probabilistic classification can be sensitive to the choice of model and prior distributions, making it difficult to interpret the results. In summary, Duerr et al. in the book "Probabilistic Deep Learning" argue that nonprobabilistic deep learning models can lead to overconfidence in predictions and can be improved by incorporating probabilistic models such as Bayesian neural networks [8]. These models can provide a more nuanced understanding of the model's predictions and can also be used to regularize traditional deep learning models [8, 20, 21].

2.2 Bayesian Neural Networks

Bayesian neural networks (BNNs) probabilistic machine learning models combine strengths of neural networks and Bayesian method [21]. In traditional neural networks, the model's parameters are fixed, meaning the model's predictions are deterministic [20, 21]. However, BNNs model the uncertainty in the parameters, which allows them to make probabilistic predictions. One of the key advantages

of BNNs is that they can quantify the uncertainty in their predictions [20, 21]. This is particularly useful in applications where accurate uncertainty estimates are crucial, such as medical diagnosis. Capturing the generated uncertainty in the posterior prediction distribution is frequently beneficial. This may be accomplished by calculating and marginalizing the parameters given the Eq. (1) below:

$$p(a|s, D) = \int p(a|s, \theta) p(\theta|D) d\theta. \tag{1}$$

One way to interpret Bayesian neural networks is a collection of various neural networks that differ in their weights [21]. By averaging out the uncertainty in the parameters, it becomes much more possible to circumvent the issue of overfitting [21].

2.3 Bayesian Learning

Murphy explored the use of Bayesian methods in neural networks [21]. Integrating epistemic uncertainty, which accounts for the model's parameters, is an essential feature of Bayesian neural networks. This contrasts aleatoric uncertainty, which accounts for uncertainty in the data. By marginalizing the parameters, Bayesian neural networks can avoid overfitting and provide a more robust approach to machine learning. Furthermore, Bayesian neural networks can be seen as an ensemble of differently weighted neural networks, further enhancing their performance. Overall, the incorporation of Bayesian methods in neural networks provides a powerful tool for probabilistic machine learning [21].

2.4 Variational Inference

The goal of variational inference is to use a simpler distribution to approximate the posterior distribution, in a similar process to the Laplace method but in a more elaborate way [21]. We can compute this simpler distribution by solving an optimization problem of finding the closest possible distribution to the posterior using quantifying closeness. A common way of measuring closeness between distributions is using the Kullback–Leibler (KL) divergence. A useful metric for comparing the similarity of two probability distributions is the Kullback–Leibler. A useful metric for comparing the similarity of two probability distributions is the Kullback–Leibler [21]. Given a training dataset $\mathcal{D}$, the KL divergence can be employed in the context of neural networks to estimate the actual posterior distribution of the network's weights, denoted by $\mathbf{w}$. Unfortunately, it is impossible to analytically solve the posterior distribution $p(\mathbf{w}|\mathcal{D})$. As a result an approximation is made using variational distribution $q(\mathbf{w}|\boldsymbol{\theta})$ of a given functional form, with

parameters denoted by $\boldsymbol{\theta}$. In order to minimize the KL divergence between the variational distribution and the true posterior, the parameters should be estimated [21].

$$\mathcal{F}(\mathcal{D}, \boldsymbol{\theta}) = \mathrm{KL}(q(\mathbf{w}|\boldsymbol{\theta}) \parallel p(\mathbf{w})) - \mathbb{E}_{q(\mathbf{w}|\boldsymbol{\theta})} \log p(\mathcal{D}|\mathbf{w}). \tag{2}$$

The optimization goal, often known as the cost function, is formally expressed by Eq. (2). The KL divergence $\mathrm{KL}(q(\mathbf{w}|\boldsymbol{\theta}) \parallel p(\mathbf{w}))$ is a measure of the dissimilarity between two probability distribution. The second term of the cost function $\mathbb{E}_{q(\mathbf{w}|\boldsymbol{\theta})} \log p(\mathcal{D}|\mathbf{w})$ is also known as the variational energy [21]. Minimizing this cost function, we may identify the ideal of the parameters values $\boldsymbol{\theta}$ that minimize the dissimilarity between the variational distribution and true posterior [21].

3 Research Methodology

Ghahramani [13] presented the Bayesian approach as a framework for understanding and making inferences in machine learning and artificial intelligence [13]. The usage of Bayes' theorem, which states that the posterior probability of a hypothesis given certain data is proportional to the product of the likelihood of the data given the hypothesis and the prior probability of the hypothesis, is the core premise of this technique [13]. Mathematically, this is expressed as

$$p(\theta|D) = \frac{p(D|\theta) p(\theta)}{p(D)}. \tag{3}$$

In Eq. (3), θ represents the model parameters, D represents the data, $p(\theta|D)$ represents the posterior probability of the parameters given the data, $p(D|\theta)$ represents the likelihood of the data given the parameters, $p(\theta)$ represents the prior probability of the parameters, and $p(D)$ represents the marginal likelihood of the data [13]. Given the data, we may use this equation to infer model parameters based on our prior knowledge and ideas about the parameters. Equation (3) can also be verbalized as Eq. (4) such as

$$posterior = \frac{likelihood * prior}{marginal likelihood}. \tag{4}$$

3.1 Probabilistic Framework

The Bayesian approach provides a natural framework for incorporating uncertainty and incorporating prior knowledge into machine learning models [13]. It also provides a way to perform model selection and to evaluate the relative plausibility

of different models, given the data. The Bayesian approach is particularly useful in the context of deep learning, where the high dimensionality of the model makes it difficult to obtain a point estimate of the parameters [13, 20, 21]. Instead, the Bayesian approach allows us to represent the uncertainty in the parameters using probability distributions [13].

3.1.1 Why Probabilistic Framework

– Probabilistic models make predictions that take into account the inherent uncertainty in the data and make more informed decisions.
– Offers a common framework across different fields [13, 21].

3.2 Dataset Description

The COVID radiography dataset is comprised of X-ray images separated into four distinct categories: COVID, lung opacity, normal, and viral pneumonia. This chapter aimed to utilize the dataset to classify and predict the coronavirus presence in the lungs using standard CNNs and Bayesian convolutional neural network. The Bayesian neural network will provide probabilities for each class, will sum up to one. Click on this link to access dataset Dataset link.

Let us have a preview of dataset in Fig. 1.

3.3 Research Design

The Bayesian approach is a widely utilized method for determining the parameters of a probabilistic model and estimating the uncertainty associated with these parameters [8]. The Bayesian modeling approach incorporates a novel form of uncertainty known as epistemic uncertainty. This results in improved prediction accuracy and more accurate quantification of the uncertainty in the predicted outcome distribution [8].

This chapter will implement data pre-processing techniques after collecting the COVID-19 radiography data, which includes cleaning and normalizing the images in the dataset. The implementation of TensorFlow library will be used in the model, and it will consist of two layers, namely the *convolutional2DReparameterization* layer, which takes into consideration the aleatoric uncertainty caused by the quality of the data, and the *DenseReparameterization* layer, which takes into consideration the epistemic uncertainty arising from the model itself [8]. Finally, the Bayesian CNN model will be employed to classify and predict COVID-19 in the radiographical lung image dataset.

(a) COVID-image

(b) Lung-Opacity-image

(c) Normal-image

(d) Viral-Pneumonia-image
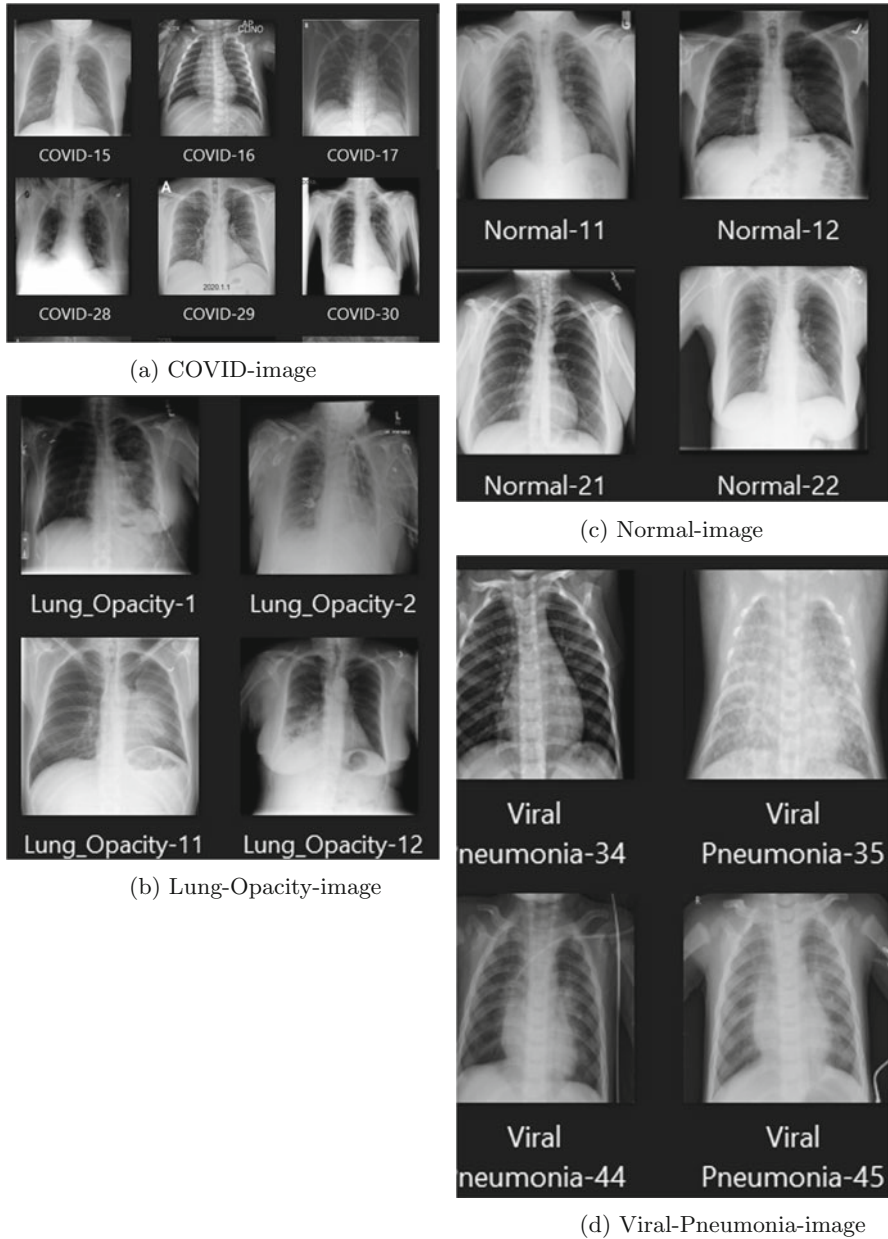
Fig. 1 In the dataset, the total number of images is 21,165 lung images, where by (**a**) has 3,616 images, (**b**) has 6,012 images, (**c**) has 10,192 images, and lastly (**d**) has 1,345 images

3.4 Modeling Process

Below are the steps:

1. Loading the COVID radiography image dataset
2. Creating Standard CNN model
3. Creating Bayesian model

The COVID-radiography dataset was utilized, which can be freely accessed on Kaggle (refer to Sect. 3.2 for further details). The dataset is described in more detail in Sect. 3.2. One needs to download the zip file and extract it to a location of choice to obtain the dataset. Then, you can proceed to the coding stage.

3.4.1 Loading the COVID-Radiography Image Dataset

Upon opening the dataset, it will become apparent that it does not come pre-divided into training and test data files. However, we will manually perform this division. To start, the following necessary libraries will be imported:

Listing 1 Sample code for python libraries

```python
import tensorflow as tf
import tensorflow_probability as tfp
from tensorflow.keras.models import Sequential
from tensorflow.keras.layers import Dense, Flatten,
    Conv2D, MaxPooling2D
from tensorflow.keras.losses import SparseCategorical
    Crossentropy
import numpy as np
import os
import matplotlib.pyplot as plt
import pandas as pd
import splitfolders
tfd = tfp.distributions
tfpl = tfp.layers
```

The *split-folders* library is used to split the COVID-radiography dataset into training and test folders. The process is simple and efficient. In the code implementation, the input path and folder name of the dataset to be split are specified, followed by the path and folder name of the output folders. The code implementation is shown below:

Listing 2 Sample code for splitting the dataset

```python
import splitfolders
input_dir = os.path.join('C:/../dataset/')
output_dir = os.path.join('C:/./dataset_splitted/')
```

```
s p l i t f o l d e r s . r a t i o ( input_dir ,  output=output_dir ,
    s e e d = 1337 ,  r a t i o = ( . 8 , . 2 ) )
```

The splitting of the folder into training and test sets is performed using the *split-folders* library, as shown in Listing 2. The process of splitting is simple and easy to follow. The first step is to specify the path and name of the folder to be split. Then, specify the path and name of the output folder. The following code demonstrates the implementation of the splitting process using the library. The ratio of the split is set to 80% for training and 20% for validation. The output of the code is a new folder named "COVID-19 Radiography Dataset splitted," which contains separate folders for training and validation. The next step is to define the training and test datasets from these new folders.

Listing 3 Sample code for test and train
```
t r a i n _ d i r  =  o s . p a t h . j o i n ( ’ C : / . . . / d a t a s e t / t r a i n / ’ )
t e s t _ d i r  = o s . p a t h . j o i n ( ’ C : / . . . / d a t a s e t / v a l / )
```

The following code implements the use of an image generator from TensorFlow to generate and label both the training and test data:

Given the function in Fig. 2, it is called to generate training and test sets by passing the variables *train-dir* and *test-dir*:

From Fig. 3, it is discovered that about 16,930 images belong to 4 classes for train generator and about 4,235 images belong to 4 classes for test generator. The figures shown in the dataset are loaded, and the next step is coronavirus classification model. The purpose of this chapter is to show comparison between standard CNN and Bayesian CNNs.

```
from tensorflow.keras.preprocessing.image import ImageDataGenerator

def image_generator(train_par_dir, test_par_dir):
    train_datagen = ImageDataGenerator(rescale= 1/255)
    test_datagen = ImageDataGenerator(rescale=1/255)

    train_generator= train_datagen.flow_from_directory(train_par_dir,
                                            target_size = (75,75),
                                            batch_size = 256,
                                            class_mode = 'categorical',
                                            subset = 'training')
    test_generator = test_datagen.flow_from_directory(test_par_dir,
                                            target_size = (75,75),
                                            batch_size = 256,
                                            class_mode = 'categorical')

    return train_generator, test_generator
```

Fig. 2 Image generator

```
train_generator,test_generator = image_generator(train_dir,test_dir)

Found 16930 images belonging to 4 classes.
Found 4235 images belonging to 4 classes.
```

Fig. 3 Calling out functions
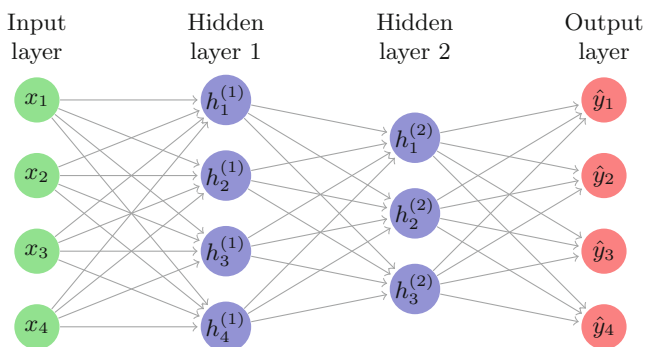
Fig. 4 Simple representation of CNN

3.4.2 Creating Standard CNN Model

Note that standard CNN model is referred as nonprobabilistic model that is already discussed in Sect. 2.1 about the specifics and the behavior of it:

Figure 4 depicts the architecture for a standard CNN model, while Fig. 5 shows the model sequential, and the model in total has 197,548 parameters with 6152 parameters at the beginning and 2052 at the end. Figure 6 presents the implementation code for creating the CNN. We later compared these parameters with Bayesian model. In the next step, the model was compiled using Adam optimizer. Since the problem is a classification problem, categorical cross-entropy as the loss function was used. In Fig. 7, the model is compiled using Adam optimizer for the model and categorical cross-entropy as the loss function and metrics accuracy used. While, in Fig. 8, the model is trained in total of 100 epochs, since 100 epochs is enough for the loss function to converge.

Finally, make predictions based on images in the test set with the trained model. First create a function to preprocess the image that we want to predict and assign the model to make a prediction based on the image in Fig. 9.

3.4.3 Creating Bayesian CNN Model

To build a Bayesian CNN, first import necessary libraries which is already. This chapter used TensorFlow probability library to create first and last layers for the neural networks model.

```
Model: "sequential"

_____
Layer (type)                 Output Shape              Param #
=================================================================
conv2d (Conv2D)              (None, 60, 60, 8)         6152

max_pooling2d (MaxPooling2D) (None, 30, 30, 8)         0

conv2d_1 (Conv2D)            (None, 28, 28, 32)        2336

max_pooling2d_1 (MaxPooling2 (None, 14, 14, 32)        0

conv2d_2 (Conv2D)            (None, 12, 12, 64)        18496

max_pooling2d_2 (MaxPooling2 (None, 6, 6, 64)          0

conv2d_3 (Conv2D)            (None, 4, 4, 64)          36928

max_pooling2d_3 (MaxPooling2 (None, 2, 2, 64)          0

flatten (Flatten)            (None, 256)               0

dense (Dense)                (None, 512)               131584

dropout (Dropout)            (None, 512)               0

dense_1 (Dense)              (None, 4)                 2052
=================================================================
Total params: 197,548
Trainable params: 197,548
Non-trainable params: 0
_____
```

Fig. 5 Output CNN

This time is building the CNN model with a Bayesian perspective. The architecture will be the same as the standard CNN model that was built before refer to Sect. 3.4.1. The model has 4 convolutional layers before flattening it and using dense layer at a very end.

Now let us halt for moment, you might be wondering if thee CNN architecture will be the same, then what is the difference between the standard CNN model and the Bayesian CNN model. The differences are the first convolutional layer and last layer of the model.

Convolutional2DReparameterization Layer

Previous studies that detected COVID-19 using x-ray images, those studies [6, 15, 23, 28] deviate from the conventional *Conv2D* layer in the first layer of their model and adopt the **Convolutional2DReparameterization** layer. This layer is designed

```
from tensorflow.keras.layers import Dropout

model = Sequential([
    Conv2D(input_shape=(75,75,3), filters=8, kernel_size=16, activation ='relu'),
    MaxPooling2D(2,2),
    Conv2D(32,(3,3), activation='relu'),
    MaxPooling2D(2,2),
    Conv2D(64,(3,3), activation= 'relu'),
    MaxPooling2D(2,2),
    Conv2D(64,(3,3), activation ='relu'),
    MaxPooling2D(2,2),
    Flatten(),
    Dense(512, activation = 'relu'),
    Dropout(0.2),
    Dense(units=4, activation='softmax')
])

model.summary()
```

Fig. 6 Standard CNN

```
M  model.compile(optimizer='adam', loss='categorical_crossentropy',metrics=['accuracy'])
```

Fig. 7 Compile part

```
history = model.fit(
    train_generator,
    steps_per_epoch=10,
    epochs=100,
    verbose =1)
```

Fig. 8 Train cell

to incorporate aleatoric uncertainty, which arises from the inherent variability in the data. Unlike the standard CNN model that outputs a deterministic value, this layer outputs a value drawn from a distribution, adding an additional layer of uncertainty in the analysis. This layer creates an output from a distribution, and then the researcher needs to define several notes as the argument:

– **Prior for kernel and bias parameters**—This is the prior assumption about how the distribution appears before the data are considered. The research creates the prior for both the kernel and bias parameters using TensorFlow's default normal distribution function. This normal distribution has non-trainable parameters, which is consistent with our prior.

```
def import_and_predict(image_data, label):

    img = cv2.imread(image_data)
    img = cv2.cvtColor(img, cv2.COLOR_RGB2BGR)

    plt.imshow(img)
    plt.axis('off')

    img_resize = (cv2.resize(img, dsize =(75,75), interpolation=cv2.INTER_CUBIC))/255.

    img_reshape = img_resize[np.newaxis,...]

    prediction = model.predict(img_reshape)
    print(prediction)

    label_prediction = label[np.argmax(prediction)]

    return label_prediction
```

Fig. 9 Predicting function

- **Posterior for kernel and bias parameters**—This is the posterior belief about how the distribution appears after looking at the data. Because this is a belief formed after viewing the data, we must specify the posterior with trainable parameters. As a result, the researcher employed TensorFlow's default function for normal distribution.
- **Kullback–Leibler divergence**—This is the approach for determining how different one distribution is from the reference distribution. This approach is employed in this situation to measure the divergence of our prior and posterior. The lower the value, or when it is zero, the two distributions are derived from the same distribution. To define the KL divergence, the research uses the available function from TensorFlow. The researcher makes sure to scale KL divergence such that it is only applied once per epoch. A rule of thumb to scale this KL divergence is by dividing it by the total number of the training images. The stack of layers after this layer is the same as the previous standard CNN Fig. 6. Instead of using a normal dense layer, the researcher uses *DenseReparameterization* layer.

DenseReparameterization

If the *convolutional2DReparameterization* section "Convolutional2DReparameterization Layer" is to take aleatoric uncertainty into account, then this *DenseReparameterization* layer is applied to take epistemic uncertainty into account. Epistemic uncertainty is the uncertainty that arises from the model itself. To apply this layer, the research passes the same arguments as in Conv2dReparameterization, the kernel prior and posterior, the bias prior and posterior, as well as the divergence function for KL divergence. As an output, the researcher passes his dense layer to a final one-hot categorical layer of 4 units Fig. 1 as the researcher has 4 classes in the COVID-19 lung image classification. Below is the entire implementation to build the Bayesian CNN model:

Bayesian CNN model, from Fig. 11. We can tell there's much difference compared to the output from Fig. 5, but this research will discuss in detail in Sect. 4.

4 Analysis and Results

4.1 Introduction

In this chapter, the comparison of the standard CNN model Fig. 6 and Bayesian CNN model Fig. 10 shall be done. The research also exposes the outputs and how they are different from each other in terms of prediction.

4.2 Comparisons of Two Models Output

As shown in Fig. 11, the model summary that the chapter generated from the Bayesian CNN model, it is shown that at the first convolutional layer and last denser layer, the number of parameters is twice as many as the parameter in standard CNN model in Fig. 5.

This is simply due to change of weight parameters from a single deterministic value into a value that is drawn from a distribution. Since the research used a normal

```
divergence_fn = lambda q,p,_:tfd.kl_divergence(q,p)/16930

model_bayes = Sequential([

    tfpl.Convolution2DReparameterization(input_shape=(75,75,3), filters=8, kernel_size=16, activation='relu',
                                        kernel_prior_fn = tfpl.default_multivariate_normal_fn,
                                        kernel_posterior_fn=tfpl.default_mean_field_normal_fn(is_singular=False),
                                        kernel_divergence_fn = divergence_fn,
                                        bias_prior_fn = tfpl.default_multivariate_normal_fn,
                                        bias_posterior_fn=tfpl.default_mean_field_normal_fn(is_singular=False),
                                        bias_divergence_fn = divergence_fn),
    MaxPooling2D(2,2),
    Conv2D(32, (3,3), activation='relu'),
    MaxPooling2D(2,2),
    Conv2D(64, (3,3), activation='relu'),
    MaxPooling2D(2,2),
    Conv2D(64, (3,3), activation='relu'),
    MaxPooling2D(2,2),
    Flatten(),
    Dense(512, activation='relu'),
    Dropout(0.2),
    tfpl.DenseReparameterization(units=tfpl.OneHotCategorical.params_size(4), activation=None,
                                kernel_prior_fn = tfpl.default_multivariate_normal_fn,
                                kernel_posterior_fn=tfpl.default_mean_field_normal_fn(is_singular=False),
                                kernel_divergence_fn = divergence_fn,
                                bias_prior_fn = tfpl.default_multivariate_normal_fn,
                                bias_posterior_fn=tfpl.default_mean_field_normal_fn(is_singular=False),
                                bias_divergence_fn = divergence_fn
                                ),
    tfpl.OneHotCategorical(4)

])
model_bayes.summary()
```
```
C:\Users\Mfund\anaconda3\lib\site-packages\tensorflow\python\keras\engine\base_layer.py:2191: UserWarning: `layer.add_variab
le` is deprecated and will be removed in a future version. Please use `layer.add_weight` method instead.
  warnings.warn('`layer.add_variable` is deprecated and '
```

Fig. 10 BCNN code

```
Model: "sequential_1"
_____
 Layer (type)                 Output Shape              Param #
=================================================================
 conv2d_reparameterization (C (None, 60, 60, 8)         12304
_____
 max_pooling2d_4 (MaxPooling2 (None, 30, 30, 8)         0
_____
 conv2d_4 (Conv2D)            (None, 28, 28, 32)        2336
_____
 max_pooling2d_5 (MaxPooling2 (None, 14, 14, 32)        0
_____
 conv2d_5 (Conv2D)            (None, 12, 12, 64)        18496
_____
 max_pooling2d_6 (MaxPooling2 (None, 6, 6, 64)          0
_____
 conv2d_6 (Conv2D)            (None, 4, 4, 64)          36928
_____
 max_pooling2d_7 (MaxPooling2 (None, 2, 2, 64)          0
_____
 flatten_1 (Flatten)          (None, 256)               0
_____
 dense_2 (Dense)              (None, 512)               131584
_____
 dropout_1 (Dropout)          (None, 512)               0
_____
 dense_reparameterization (De (None, 4)                 4104
_____
 one_hot_categorical (OneHotC multiple                  0
=================================================================
Total params: 205,752
Trainable params: 205,752
Non-trainable params: 0
_____
```

Fig. 11 BCNN architecture

distribution, then it has two parameters instead of just one: the mean and standard deviation. Let us begin with prediction using the standard CNN model from the test set:

As shown in Fig. 12, the standard CNN model predicts with 0.956 probability that the image belongs to COVID class. This means that the model is very certain that the image is COVID. Again let us pick another image from the test set, to see if the model can predict the image of viral pneumonia correctly.

The standard CNN model predicts with 0.996 probability that the image belongs to viral pneumonia class. This means that the model is very certain that the image is COVID. The model looks great in the sense it managed to predict two of the images from the test correctly. However, the research does not know how certain is the model in assigning that 0.956 in Fig. 12 and 0.996 in Fig. 13 probability on each of the images above. Is the model really that confident to assign high-probability

```
image3_dir = os.path.join(test_dir+'COVID/COVID-2.png')
prediction_1 =import_and_predict(image3_dir, label)
```

```
[[0.95666546 0.01134403 0.02780131 0.00418921]]
```



```
prediction_1
```

```
'COVID'
```

Fig. 12 Output for COVID prediction using standard CNN

```
image6_dir = os.path.join(test_dir +'Viral Pneumonia/Viral Pneumonia-1.png')
prediction_4 = import_and_predict(image6_dir,label)
```

```
[[5.9221038e-06 1.0599486e-04 3.8753327e-03 9.9601269e-01]]
```



```
prediction_4
```

```
'Viral Pneumonia'
```

Fig. 13 Output for viral pneumonia prediction using standard CNN

values to the images? The chapter does not know if the model knows what it does not know. Hence, the research took the Bayesian approach to cover such uncertainty.

4.3   Predicting Images from Test Data

Even though the research created a probabilistic model, this research will not obtain the same probability value while predicting an image. As a result, the research will assign the model to estimate our image several times rather than just once. In this research, the model will be asked to predict a single image 400 times rather than simply once as shown in Fig. 14.

Next step, based on that 400 predictions, this research creates 95% prediction interval for probabilities. Figure 14 depicts the function implementation:

Function takes two arguments with a for loop that ranges for 400 predictions for 95% prediction interval for probabilities and setting green as true label.

Now this research moves to predicting images from the test set and sees how the model predicts the image. For the predictions, the research in the code predicted for all classes but for the purpose of report will show two images just like the same way for standard CNN above: the COVID and viral pneumonia

```python
def import_and_predict_bayes(image, true_label):

    #read image
    img = cv2.imread(image)
    img = cv2.cvtColor(img, cv2.COLOR_BGR2RGB)

    #show the image
    plt.imshow(img)
    plt.axis('off')

    img_resize = (cv2.resize(img, dsize=(75, 75), interpolation=cv2.INTER_CUBIC))/255.

    predicted_probabilities = np.empty(shape=(400, 4))

    for i in range(400):

        predicted_probabilities[i] = model_bayes(img_resize[np.newaxis,...]).mean().numpy()[0]

    pct_2p5 = np.array([np.percentile(predicted_probabilities[:, i], 2.5) for i in range(4)])
    pct_97p5 = np.array([np.percentile(predicted_probabilities[:, i], 97.5) for i in range(4)])

    fig, ax = plt.subplots(figsize=(12,6))
    bar = ax.bar(np.arange(4), pct_97p5, color='red')
    bar[true_label].set_color('green')
    bar = ax.bar(np.arange(4), pct_2p5-0.02, color='white')
    Labels = ['COVID', ' Lung Opacity', 'Normal','Viral Pneumonia']
    ax.set_xticks(range(0,4))
    ax.set_xticklabels(Labels)
    #ax.set_xticklabels([' '] + [x for x in label])
    ax.set_ylim([0, 1])
    ax.set_ylabel('Probability')
    plt.show()
```

Fig. 14 Predict function for BCNN

The model correctly predicts the image with a probability of 0.76. Which is great? However, when you observe the results from the Bayesian CNN model, the aleatoric and epistemic uncertainties exist when predicting COVID image.

Now let us predict for the second image, which is viral pneumonia:

– The aleatoric uncertainty is shown as the model assigns a little bit of high probability to lung opacity class that is close to the COVID class as shown in Fig. 15.
– The epistemic uncertainty is shown as the model is not certain how to assign probability values to each of the classes.

With our prior standard CNN, the model accurately predicts that the picture is viral pneumonia with a probability value of 0.988. However, when looking at the Bayesian CNN model findings depicted in the Fig. 16, the aleatoric and epistemic exist while predicting the viral pneumonia picture.
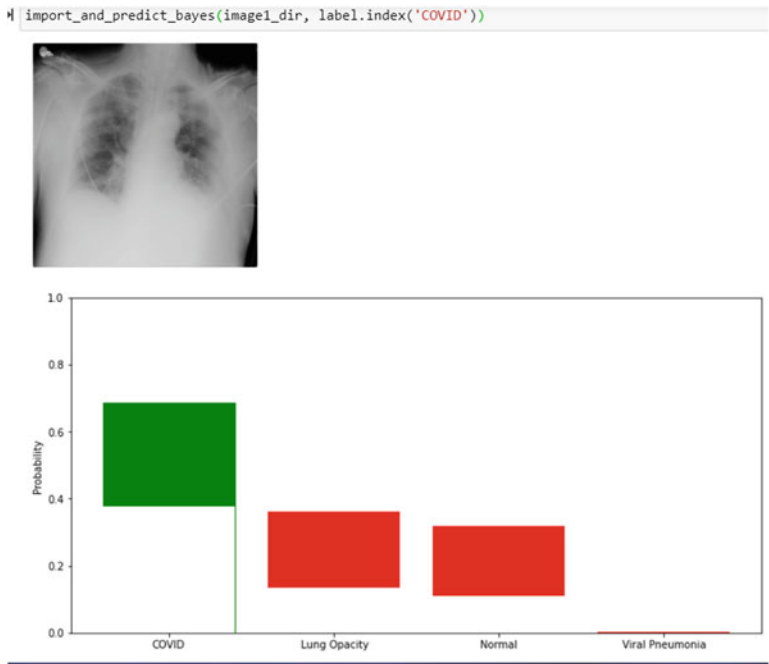
Fig. 15 Output for COVID using BCNN

```
import_and_predict_bayes(image8_dir,label.index('Viral Pneumonia'))
```
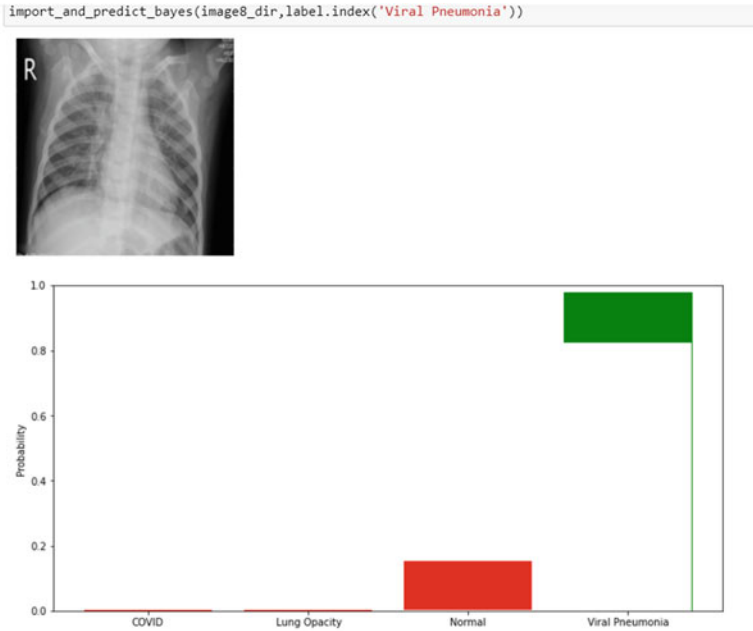

Fig. 16 Output for viral pneumonia using BCNN

5 Conclusion

In this chapter, a probabilistic machine learning approach, Bayesian convolutional neural network (BCNN), was developed to classify COVID-19 images. The BCNN model is equipped with the ability to assess uncertainty and produce more reliable predictions in diagnosing COVID-19. The model was applied to predict COVID images 400 times, and the results demonstrate that the BCNN model can provide varying probabilities in each run, enabling it to identify complex cases. The chapter's findings suggest the potential of BCNNs in medical imaging and disease diagnosis, and the results serve as a starting point for further exploration and development in this area.

In terms of accuracy, the study does not compare the BCNN model with other methods, so it needs to be clarified how it stacks up in terms of performance. Potential avenues for future work in this area include enhancing the accuracy of the BCNN model by fine-tuning its parameters and incorporating a more extensive image dataset. Additionally, the model can be evaluated on other imaging data types, such as X-rays and CT scans, to determine its potential for diagnosing other illnesses.

However, the chapter has certain limitations, including the limited sample size of the images utilized for training the model, which may have impacted the predictions' accuracy. In the future, a more extensive and varied image dataset should be used for model training. Another challenge is the computational cost associated with Bayesian convolutional neural networks, which may pose difficulties in real-world implementation.

Despite these limitations, the findings of this chapter suggest the potential of BCNNs in the field of medical imaging and disease diagnosis. They are a starting point for further exploration and development in this area.

References

1. Agrawal, T., Choudhary, P.: FocusCovid: automated COVID-19 detection using deep learning with chest X-ray images. Evolving Syst. **2021**, 1–15 (2021)
2. Agarwal, P., Swami, S., Malhotra, S.K.: Artificial intelligence adoption in the post COVID-19 new-normal and role of smart technologies in transforming business: a review. J. Sci. Technol. Policy Manag. **2022**, (2022)
3. Al-Waisy, A.S., Mohammed, M.A., Al-Fahdawi, S., Maashi, M.S., Garcia-Zapirain, B., Abdulkareem, K.H., Mostafa, S.A., Kumar, N.M., Le, D.-N.: Covid-DeepNet: hybrid multimodal deep learning system for improving COVID-19 pneumonia detection in chest X-ray images. Comput. Mater. Continua **67**(2), 2409–2429 (2021)
4. Alafif, T., Tehame, A.M., Bajaba, S., Barnawi, A., Zia, S.: Machine and deep learning towards COVID-19 diagnosis and treatment: survey, challenges, and future directions. Int. J. Environ. Res. Public Health **18**(3), 1117 (2021)
5. Alazab, M., Awajan, A., Mesleh, A., Abraham, A., Jatana, V., Alhyari, S.: Covid-19 prediction and detection using deep learning. Int. J. Comput. Informat. Syst. Ind. Manag. Appl. **12**, 168–181 (2020)
6. Burdick, H., Lam, C., Mataraso, S., Siefkas, A., Braden, G., Dellinger, R., McCoy, A., Vincent, J., Green-Saxen, A., Barners, G., Hoffman, J., Calvert, J., Pellegrini, E., Das, R.: Prediction of respiratory decompensation in COVID-19 patients using machine learning: the READY trial. Comput. Biol. Med. **124**, 103949 (2020)
7. Dera, D., Rasool, G., Bouaynaya, N.C., Eichen, A., Shanko, S., Cammerata, J., Arnold, S.: Bayes-SAR Net: Robust SAR image classification with uncertainty estimation using Bayesian convolutional neural network. In: 2020 IEEE International Radar Conference (RADAR), pp. 362–367 (2020)
8. Duerr, O., Sick, B., Murina, E.: Probabilistic Deep Learning: With Python, Keras and TensorFlow Probability. Manning Publications, Shelter Island (2020)
9. Fares, O.H., Butt, I., Lee, S.H.M.: Utilization of artificial intelligence in the banking sector: a systematic literature review. J. Financ. Serv. Mark., **2022**, 1–18 (2022)
10. Gal, Y., Islam, R., Ghahramani, Z.: Deep Bayesian active learning with image data. In: Precup, D., Teh, Y.W. (eds.), Proceedings of the 34th International Conference on Machine Learning. Proceedings of Machine Learning Research, vol. 70, pp. 1183–1192. PMLR (2017)
11. Georgevici, A.I., Terblanche, M.: Neural networks and deep learning: a brief introduction. Intensive Care Med. **45**(5), 712–714 (2019)
12. Ghaderzadeh, M., Asadi, F.: Deep learning in the detection and diagnosis of COVID-19 using radiology modalities: a systematic review, J. Healthcare Eng. **2021**, 6677314, p. 10, (2021). https://doi.org/10.1155/2021/6677314
13. Ghahramani, Z.: Probabilistic machine learning and artificial intelligence. Nature **521**(7553), 452–459 (2015)

14. Gozes, O., Frid-Adar, M., Greenspan, H., Browning, P.D., Zhang, H., Ji, W., Bernheim, A., Siegel, E.: Rapid AI development cycle for the coronavirus (COVID-19) pandemic: Initial results for automated detection & patient monitoring using deep learning CT image analysis (2020). Preprint arXiv:2003.05037

15. Hu, S., Gao, Y., Niu, Z., Jiang, Y., Li, L., Xiao, X., Wang, M., Fang, E.F., Menpes-Smith, W., Xia, J., Ye, H., Yang, G.: Weakly supervised deep learning for covid-19 infection detection and classification from CT images. IEEE Access **8**, 118869–118883 (2020)

16. Jain, G., Mittal, D., Thakur, D., Mittal, M.K.: A deep learning approach to detect Covid-19 coronavirus with X-ray images. Biocybern. Biomed. Eng. **40**(4), 1391–1405 (2020)

17. Kathuria, A.: Fighting coronavirus with AI: Improving testing with deep learning and computer vision. https://bit.ly/3GxIdZP/ (2020). KDnuggets, Accessed 12 March 2020

18. Lauren, M.: What is coronavirus? https://bit.ly/3ydeJgX (2021). Johns Hopkins Medicine, Accessed 14 March 2021

19. Li, L., Qin, L., Xu, Z., Yin, Y., Wang, X., Kong, B., Bai, J., Lu, Y., Fang, Z., Song, Q., et al.: Using artificial intelligence to detect COVID-19 and community-acquired pneumonia based on pulmonary CT: evaluation of the diagnostic accuracy. Radiology **296**(2), E65–E71 (2020)

20. Murphy, K.P.: Machine Learning: A Probabilistic Perspective. MIT Press, Cambridge (2012)

21. Murphy, K.P.: Probabilistic Machine Learning: An Introduction. MIT Press, Cambridge (2022)

22. Paluru, N., Dayal, A., Jenssen, H.B., Sakinis, T., Cenkeramaddi, L.R., Prakash, J., Yalavarthy, P.K.: Anam-Net: Anamorphic depth embedding-based lightweight CNN for segmentation of anomalies in COVID-19 chest CT images. IEEE Trans. Neural Netw. Learn. Syst. **32**(3), 932–946 (2021)

23. Rahman, T., Khandakar, A., Qiblawey, Y., Tahir, A., Kiranyaz, S., Kashem, S. B.A., Islam, M.T., Al Maadeed, S., Zughaier, S.M., Khan, M.S., et al.: Exploring the effect of image enhancement techniques on COVID-19 detection using chest X-ray images. Comput. Biol. Med. **132**, 104319 (2021)

24. Tan, W., Liu, P., Li, X., Liu, Y., Zhou, Q., Chen, C., Gong, Z., Yin, X., Zhang, Y.: Classification of COVID-19 pneumonia from chest CT images based on reconstructed super-resolution images and VGG neural network. Health Informat. Sci. Syst. **9**(1), 1–12 (2021)

25. Thomas, A. Model transparency and explainability. https://bit.ly/3DBCsbr (2020). Ople.ai. Accessed 4 July 2020

26. Voulodimos, A., Doulamis, N., Doulamis, A., Protopapadakis, E.: Deep learning for computer vision: a brief review. Comput. Intell. Neurosci. **2018** (2018)

27. Webmd: Coronavirus and COVID-19: What you should know. https://www.webmd.com/lung/coronavirus/ (2021). Webmd, Accessed 09 Dec 2021

28. Xu, X., Jiang, X., Ma, C., Du, P., Li, X., Lv, S., Yu, L., Ni, Q., Chen, Y., Su, J., Lang, G., Li, Y., Zhao, H., Liu, J., Xu, K., Ruan, L., Sheng, J., Qiu, Y., Wu, W., Liang, T., Li, L.: A deep learning system to screen novel coronavirus disease 2019 pneumonia. Engineering **6**(10), 1122–1129 (2020)

29. Zafar, N., Ahamed, J.: Emerging technologies for the management of COVID19: a review. Sustain. Oper. Comput. **3**, 249–257 (2022)

30. Zoabi, Y., Deri-Rozov, S., Shomron, N.: Machine learning-based prediction of COVID-19 diagnosis based on symptoms. npj Digital Med. **4**(1), 1–5 (2021)

Identify Unfavorable COVID Medicine Reactions from the Three-Dimensional Structure by Employing Convolutional Neural Network

Pranab Das and Dilwar Hussain Mazumder

1 Introduction

The unfavorable COVID medicine reactions are the adverse reactions of medicine in the patient's body [1]. Knowing the toxic reactions or adverse responses of the medicines in COVID therapy will be vital for medicine development. Nowadays, COVID medicine development is an essential task in modern medicine discovery [2]. The world currently faces a complex situation in developing an effective medicine for coronavirus disease to treat patients by the scientific community. Most researchers are investigating developing an adequate medicine to treat this disease.

Medicine development is the time needed, expensive, and the success rate of medicine is poor [3, 4]. One of the reasons for the unsuccess of medicine is unfavorable reactions, which can waste chemical compounds, time, and capital. Therefore, the computational approach is needed to learn about a newly developed medicine. Several computational approaches are employed in medicine development [5, 6]. One of the most popular and effective computational approaches is CNN [7]. The reason behind choosing CNN classifier over the traditional machine learning classifier is that CNN performs well on image data compared to the other machine learning approaches. Because of unfavorable medicine reactions, most medicines fail during discovery, development, and design. Due to some medicine unfavorable reactions, patients may die [8]. So, an efficient approach is needed to analyze the unfavorable reactions of newly developed medicines. Studies of hazardous medicine reactions enhance the efficacy of medicine development and the safety of patient health. Correctly identifying hazardous medicine reactions

P. Das and D. H. Mazumder (✉)
Department of Computer Science and Engineering, National Institute of Technology Nagaland, Dimapur, India

enhances medicine safety and minimizes the time, chemical wastage, and cost of medicine discovery.

The preliminary contribution of this chapter is to present a CNN framework to predict COVID medicine reactions from the three-dimensional structure that have not been previously used to predict unfavorable reactions of COVID medicine.

Following the introduction section, literature review works have been provided, followed by the proposed framework to identify unfavorable COVID medicine reactions, which includes a description of the medicine structure and their hazardous response and an explanation for the stated problem solution. Further, the performance measure method and experiment parameter settings with the results have been presented in the section on experiment performance evaluation. Finally, the experiment outcome has been summarized.

2   Related Work

This section summarizes various strategies and medicine descriptors employed to identify medicine's unfavorable reactions.

In their work, Das et al. [9] identify unfavorable medicine reactions from drug functions. They applied random forest, decision tree, k-nearest neighbor, extra tree classifiers, and multi-layer perceptron neural network to identify unfavorable medicine reactions. They found that the extra tree classifier acquired 99.95% accuracy. In a different work, Das et al. [10] analyzed unfavorable medicine reactions from the integrated medicine properties (drug function, one-dimensional structure of medicine, and 17 molecules properties). The authors employed a deep neural network on the combination drug descriptors. They reported the highest ROC score of 99.99% achieved on the combination of drug function and the one-dimensional structure of medicine. Ietswaart et al. [11] associated harmful reactions with medicine by employing a random forest classifier. The authors utilized a pharmacovigilance assay as an input feature to associate harmful reactions with medicine. There presented methodology achieved the lowest hamming—loss of 9%. An artificial neural network model is presented by Shankar et al. [12] to identify medicine pair unfavorable reactions from the one-dimensional structure of medicine and gene expression. Their artificial neural network classifier reported an accuracy score of 82%. Antidepression unfavorable medicine reactions are predicted by Gunes et al. [13] from biological properties (medicine target, enzyme, and transporter) and the one-dimensional structure of medicine. The authors applied k-nearest neighbors, multi-layer perceptron, and support vector machine to integrate medicine properties. They found that the multi-layer perceptron classifier performed and got the highest AUC value of 69.50%. Hatmal et al. [14] identify COVID vaccine unfavorable reactions from demographic data by online survey. They employed multi-layer perceptron, XGBoost, K-star, and random forest and obtained that the random forest model acquired an accuracy value of 80%. In their work, Swathi et al. [15] analyze unfavorable medicine reactions from medical health forms. Random

forest, support vector machine, decision tree, naive Bayes, and logistic regression classifier are utilized to predict unfavorable medicine reactions. The author noticed that the random forest reported the best accuracy value of 62.40%. Wang et al. [16] provided a deep neural network to detect unfavorable medicine reactions from biological properties, 17 molecule properties, and biomedical literature information. They compared their model with a linear support vector machine, Gaussian naive Bayes, and probability matrix factorizer. The authors found that the presented deep neural network achieved the best AUC value of 84.40%. Jamal et al. [17] predict unfavorable cardiovascular medicine reactions from the one-dimensional structure of medicine, phenotypic, and biological properties. The authors applied random forest and sequential minimization optimization approach. Further, they found that the random forest classifier and sequential minimization optimization approach reached the best accuracy value of 93.83% on the phenotypic and biological drug descriptors. In a different work [18], Jamal et al. predict unfavorable neurological medicine reactions from the one-dimensional structure of medicine, phenotypic, and biological properties. They applied a support vector machine on the distinct combination of drug properties. They achieved the highest accuracy score of 94.18% on combining the one-dimensional structure of medicine, phenotypic, and biological properties. Pouliot et al. [19] predict unfavorable medicine reactions from body organ class by employing logistic regression and report the best AUC value of 92%. Liu et al. [20] detected unfavorable medicine reactions from medical reports with the help of a support vector machine and obtained an AUC value of 85%. Jahid et al. [21] presented an ensemble approach to predict unfavorable medicine reactions by applying a one-dimensional structure of medicine. Their ensemble approach achieved the highest AUC value of 62%. Jiang et al. [22] detected unfavorable medicine reactions from the tweet using naive Bayes, support vector machine, and maximum entropy. They found that the ME approach reported the highest F1 value of 84%. Potential unfavorable medicine reactions are identified from integrated drug properties (protein–protein interaction, medicine target, and one-dimensional structure of medicine) by Huang et al. [23]. For the prediction task, a support vector machine has been employed and reported a 70% AUC score. Labute et al. [24] identified unfavorable medicine reactions by employing a logistic regression model from protein targets. Their logistic regression model achieved an AUC value of 74%. Zhang et al. [25] provided a feature-selection-based multi-label nearest-neighbor method to predict unfavorable medicine reactions from medicine targets and chemical information. Their proposed approach acquired the best AUPR value of 48.02%. Niu et al. [26] identified unfavorable medicine reactions from the one-dimensional structure of medicine from medicine targets, chemical descriptors, and chemical substructure. The authors employed a support vector machine, sparse canonical correlation analysis, k-nearest neighbor, and neural network to identify unfavorable medicine reactions. Their neural network model achieved the highest AUC value of 89.59% on medicine target properties.

There are various computational approaches (k-nearest neighbor, sparse canonical correlation analysis, decision tree, maximum entropy, artificial neural network, random forest, future-selection-based k-nearest neighbor, deep neural network,

extra tree classifiers, probability matrix factorization, naive Bayes, logistic regression, sequential minimization optimization, XGBoost, and support vector machine) available for identifying unfavorable medicine reactions. From the above literature survey, it can be noticed that drug function, one-dimensional structure of medicine, 17 molecule drug-like properties, pharmacovigilance assay, gene expression, medicine target, enzyme, transporter, demographic data, online electronic health form, protein–protein interaction, gene ontology, biomedical literature, phenotypic descriptors, system organ class, patient medical report, and Twitter post have been employed to identify unfavorable medicine reactions. However, the three-dimensional structure of medicine still needs to be employed to identify unfavorable reactions.

3   The Proposed Procedure and Dataset

The problem of identifying unfavorable COVID medicine reactions from the three-dimensional structure has been defined in this section. The dataset and proposed procedure for addressing the stated problem have also been demonstrated.

3.1   Dataset

The procedure of preparing the COVID Unfavorable Medicine Reactions Dataset (CUMRD) for executing the proposed framework is illustrated diagrammatically in Fig. 1 and will be discussed further below.
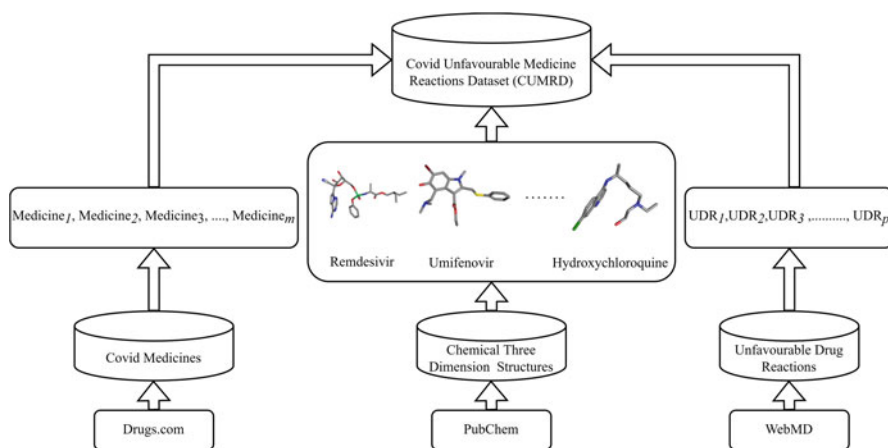

Fig. 1 Preparation process of the COVID drug side effects dataset

3.1.1 Medicine

Several medicines are available to treat coronavirus disease in Drugs.com [27]. Among them, only 18 medicine with three-dimensional structures are available in PubChem, including Remdesivir, Colchicine, Dexamethasone, Hydroxychloroquine, Protein kinase inhibitors 1, Methylprednisolone, Peginterferon Lambda, Umifenovir, Hydroxychloroquine sulfate, Ritonavir, PF-07321332, Bemcentinib, Zyesami, Chloroquine phosphate, Fluvoxamine, MK-4482, Favipiravir, and Baricitinib.

3.1.2 Three-Dimensional Structure of Medicine

To build the CNN classifier, first, three-dimensional structures of medicine were collected from PubChem [28]. The three-dimensional structure of medicine is an image data type showing the organization of atoms and bonds in a molecule. This structure is collected from PubChem with the help of the "urllib.request" python package. Each structure is collected by giving the Compound IDentifier (CID) number of each medicine, which are collected from Drugs.com [27].

3.1.3 Unfavorable COVID Medicine Reactions

A medicine can have unfavorable reactions, which may harm the patient. Unfavorable COVID medicine reactions are harmful, adverse, and unwanted reactions. The unwanted medicine reactions are obtained from the WebMD [29], which consists of 29 unfavorable COVID medicine reactions (Muscle Pain, Headache, Swelling, Changes in Taste, Abdominal Cramps, Weakness, Liver Function Test Abnormal, Rash, Irregular Heartbeat, Abdominal Pain, Seizures, Blood Pressure Increased, Nausea, Fever, Decreased Appetite, Trouble Breathing, Drowsiness, Asthma Attack, Sore Mouth, Stomach Upset, Heartburn, Diarrhea, Vomiting, Chills, Sweating, Trouble Sleeping, Constipation, Tired and Heavy, and Dizziness) on human health, corresponding to 18 medicine. Therefore, unfavorable medicine reaction identification is an essential task in medicine discovery.

3.2 Problem Statement

This section defines the problem statement. Let medicine = $\{Medicine_1,$ $Medicine_2, Medicine_3, ..., Medicine_k, ..., Medicine_m\}$ be the set of Medicine, IF = $\{IF_1, IF_2, IF_3, ..., IF_l, ..., IF_r\}$ be the set of image features (IF) of medicine, and UMR = $\{UMR_1, UMR_2, UMR_3, ..., UMR_o, ..., UMR_p\}$ be the set of Unfavorable Medicine Reactions (UMR) where each UMRo represents the Unfavorable Medicine Reactions for a $Medicine_k$ with image features IF.
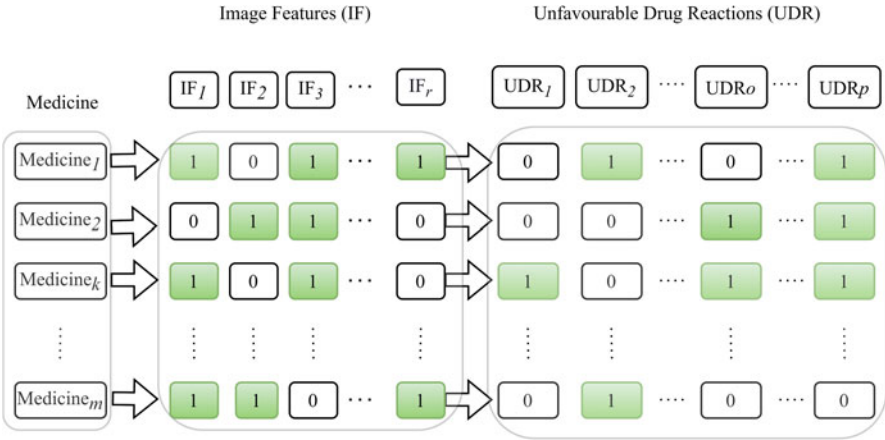
Fig. 2 Problem statement for identifying unfavorable COVID medicine reactions from the three-dimensional structure

Table 1 Example of multiple unfavorable COVID medicine reactions

Medicine	Rash	Irregular heartbeat	Stomach upset	Nausea	Trouble breathing	......	Vomiting
Remdesivir	1	1	0	1	1	......	1

A $medicine_k$ can have multiple unfavorable medicine reactions. Therefore, identifying unfavorable medicine reactions is a multi-label identification issue [25, 30]. Figure 2 illustrates the multi-label unfavorable medicine reactions corresponding to their three-dimensional structure. Here, unfavorable medicine reactions are denoted by a binary number, where zero signifies the absence and one implies the existence of unfavorable medicine reactions. Table 1 shows the multi-label unfavorable medicine reactions for Remdesivir medicine, whose some of the unfavorable reactions are Rash, Irregular Heartbeat, Vomiting, Nausea, and Trouble Breathing, etc.

3.3   The Proposed Architecture

Figure 3 depicts the proposed methodology of working architecture. It takes the three-dimensional structure of medicine corresponding to different medicine as input to identify unfavorable medicine reactions. The main focus of this chapter is to present an efficient CNN classifier model to identify unfavorable medicine reactions. This work employs a multi-label CNN classifier to investigate the unfavorable medicine reactions from the three-dimensional structure of medicine. Based on the problem statement, a multi-label CNN classifier is developed to identify potential hazardous reactions of COVID medicine.
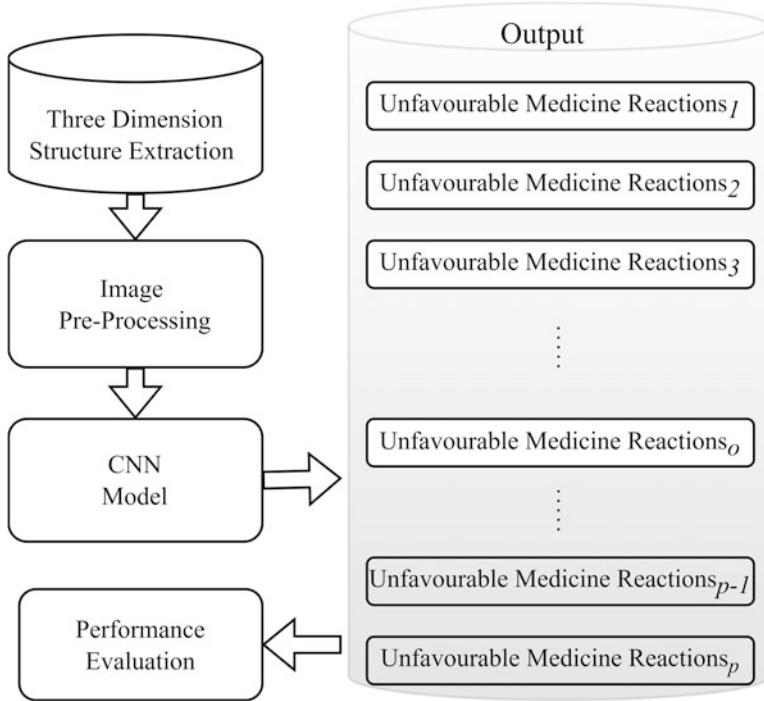
Fig. 3 Working process of the presented architecture

4 Setup and Results of the Experiment

4.1 Performance Measure Definition

For evaluating the performance, the example-based (EB) method is used with the CNN classification algorithm and pre-trained models, and the following metrics have been used: Accuracy (A), Hamming Loss (H-L), Precision (P), Recall (R), F1, and ROC–AUC score [31]. Consider $D_k = \{(d_i, Y_i) | i = 1, 2, ..., N\}$ is a collection of multi-label (ML) data, where Y_i is the actual set of the class labels for data sample d_i unseen by the classifier model $F_{ML}: d_i \rightarrow 2^{|Y|}$ and $Z_i = F_{ML} : (d_i)$ is the predicted set of the label by the classifier, and N represents the overall number of samples:

– **Accuracy (A):** For each sample, accuracy is defined as the proportion of accurately predicted labels to all labels for that sample, and the final accuracy is the average among all samples.

$$Accuracy_{EB}(F_{ML}, D_k) = \frac{1}{N} \sum_{i=1}^{N} \frac{|Y_i \cap Z_i|}{|Y_i \cup Z_i|}. \tag{1}$$

– **Precision (P):** For each sample, the proportion of accurately predicted labels to all actual labels is known as precision, and the overall precision is the average among all samples.

$$Precision_{EB}(F_{ML}, D_k) = \frac{1}{N} \sum_{i=1}^{N} \frac{|Y_i \cap Z_i|}{|Z_i|}. \tag{2}$$

– **Recall (R):** For each instance, recall is the proportion of a certain label that the classifier has predicted as belonging to that label. The overall recall is the average among all samples.

$$Recall_{EB}(F_{ML}, D_k) = \frac{1}{N} \sum_{i=1}^{N} \frac{|Y_i \cap Z_i|}{|Y_i|}. \tag{3}$$

– **F1 Measure:** F1 measure is determined by the harmonic mean of both recall and precision. The F1 measure indicates a balanced precision and recall score.

$$F1_{EB}(F_{ML}, D_k) = \frac{1}{N} \sum_{i=1}^{N} \frac{2|Y_i \cap Z_i|}{|Y_i| + |Z_i|}. \tag{4}$$

– **Hamming Loss (H-L):** It is the portion of the wrongly predicted labels to the overall number of labels. Here Δ is the symmetric difference of the actual and predicted sets, and Q represents the number of possible class labels.

$$Hamming - Loss_{EB}(F_{ML}, D_k) = \frac{1}{N} \sum_{i=1}^{N} \frac{1}{Q} |Y_i \Delta Z_i|. \tag{5}$$

– **ROC-AUC:** ROC-AUC is generally used for multi-label binary classification problems, which shows how the recall versus precision correlation interchange for each cut-off. ROC-AUC indicates how well the classification model separates the positive and negative classes.

4.2 Setup of the Experiment

The parameters of the CNN and pre-trained model classifiers are provided in this section. The three-dimensional structures are used as an input feature of the CNN classifier to execute the experiment. The CNN model and pre-trained models are implemented using TensorFlow in Google Colab. The leave-one-out cross-validation approach is utilized to split the training and testing medicine structure to identify harmful reactions. Each three-dimensional chemical structure is used to

test the model, and the remaining chemical three-dimensional structure is used to train the model. RGB channel is used, and the structures are resized to 100*100 pixels with the 15 epochs in the CNN and pre-trained classifiers. For the loss function, binar_crossentropy is set, and learning_rate is set to 0.0001 with the Adam optimizer. For the convolutional layer and output layer, the ReLU and sigmoid activation functions are set, respectively. Dropout is used to overcome the issue of classifier overfitting problem and set to 0.2 dropouts after each layer. The quantity of units inside the CNN classifier output layer is set to the equal number of labels in the COVID Unfavorable Medicine Reactions Dataset (CUMRD). The threshold of the CNN classifier is set to 0.5 for the outcome; if the value predicted by the model is equal to or higher than 0.5, then it assumes that the unfavorable reactions of medicine belong to that specific label, otherwise, not. The convolutional layer and the number of units in each layer affect the CNN classifier performance. So different convolutional layers are tested for the experiment. The model was also tested with the distinct convolutional unit, and it is found that the first layer with 16 units, the second layer with 32 units, the third layer with 64, and the fourth layer with 128 units performed best. The CNN classifier with one convolutional layer performs better than the other layer. Similarly, all the pre-trained models have also been tested with different parameters and obtained that DenseNet201, Inceptionv3, MobileNetv2, ResNet50, and VGG19, with a dropout rate of 0.2, and setting GlobalAveragePooling2D achieved good results. All other parameters are the same as mentioned for the CNN model.

4.3 Results and Discussions

The performance of the CNN classifier on the three-dimensional structure to identify unfavorable COVID medicine reactions is shown in Table 2. In one convolutional layer, the CNN classifier achieved the highest accuracy (A) value of 87.16%, the lowest Hamming (L-H) loss of 12.83%, and the highest precision score of 77.88%, recall value of 70.76%, the highest F1 measure of 72.07%, and highest ROC-AUC value of 80.97%. The CNN model outperformed the performance

Table 2 Performance of CNN and pre-trained classifiers on the three-dimensional structure to identify unfavorable COVID medicine reactions

# Model	A	H-L	P	R	F1	ROC–AUC
CNN	87.16%	12.83%	77.88%	70.76%	72.07%	80.97%
DenseNet201	85.44%	14.55%	77.47%	66.36%	68.42%	78.36%
InceptionV3	86.78%	13.21%	77.40 %	69.91%	71.16%	80.23%
MobileNetV2	85.63%	14.36%	76.87%	70.98%	71.48%	79.44%
ResNet50	80.07%	19.92%	67.63%	51.20%	55.97%	68.96%
VGG19	78.58%	22.41%	61.57%	37.72%	43.87%	63.42%

of pre-trained models (DenseNet201, InceptionV3, MobileNetV2, ResNet50, and VGG19). Among the pre-trained models, InceptionV3 performs well compared to DenseNet201, MobileNetV2, ResNet50, and VGG19 models. It achieved an accuracy score of 86.78%, a recall score of 69.91%, a hamming loss of 13.21%, a precision value of 77.40%, an F1 measure value of 71.16%, and an ROC-AUC value of 80.23%. On the other hand, the DenseNet201 model achieved 85.44% accuracy, 14.55% hamming loss, 77.47% precision, 66.36% recall, 68.42% F1 score, and 78.36% ROC-AUC score. The MobileNetV2 transfer learning model achieved an accuracy score of 85.63%, a hamming loss of 14.36%, a precision score of 76.87%, a recall score of 70.98%, a F1 measure value of 71.48%, and an ROC-AUC of 79.44%. The ResNet50 classifier achieved an accuracy value of 80.07%, a hamming loss of 19.92%, a precision score of 67.63%, a recall value of 51.20%, an F1 measure of 55.97%%, and an ROC-AUC value of 68.96%. VGG19 model achieved an accuracy score of 78.58%, a recall score of 37.72%, a hamming loss of 22.41%, a precision value of 61.57%, an F1 measure value of 43.87%, and an ROC-AUC value of 63.42%.

The presented multi-label convolutional neural network model performance suggests that the three-dimensional structures of medicine are adequate for identifying unfavorable COVID medicine reactions. It also outperformed the performance of pre-trained transfer learning models (DenseNet201, MobileNetV2, ResNet50, VGG19, InceptionV3 models) and achieved the highest accuracy score of 87.16%. The suggested CNN model can also be utilized to identify unfavorable COVID medicine reactions during medicine discovery, design, and development.

4.4 ROC-AUC Curve

The ROC-AUC curve of the CNN classifier and pre-trained models on three-dimensional structures have been discussed in this section. The convolutional neural network classifier ROC-AUC value varies with respect to distinct convolutional layers. The convolutional neural network classifier with one convolutional layer achieved the best receiver operator characteristic curves among all convolutional layers on the three-dimensional structure. It reports the best ROC-AUC value of 80.97%. On the other hand, it can be observed from Fig. 4b the InceptionV3 model performed best and acquired an ROC-AUC value of 80.23%% compared to other pre-trained models (MobileNetV2, DenseNet201, ResNet50, and VGG19 models). The MobileNetV2 model achieved an ROC-AUC value of 79.44%, which can be seen from Fig. 4c. DenseNet201, ResNet50, and VGG19 models achieved ROC-AUC scores of 78.36%, 68.96%, and 63.42%, respectively, which can be observed from Figs. 4d–f.
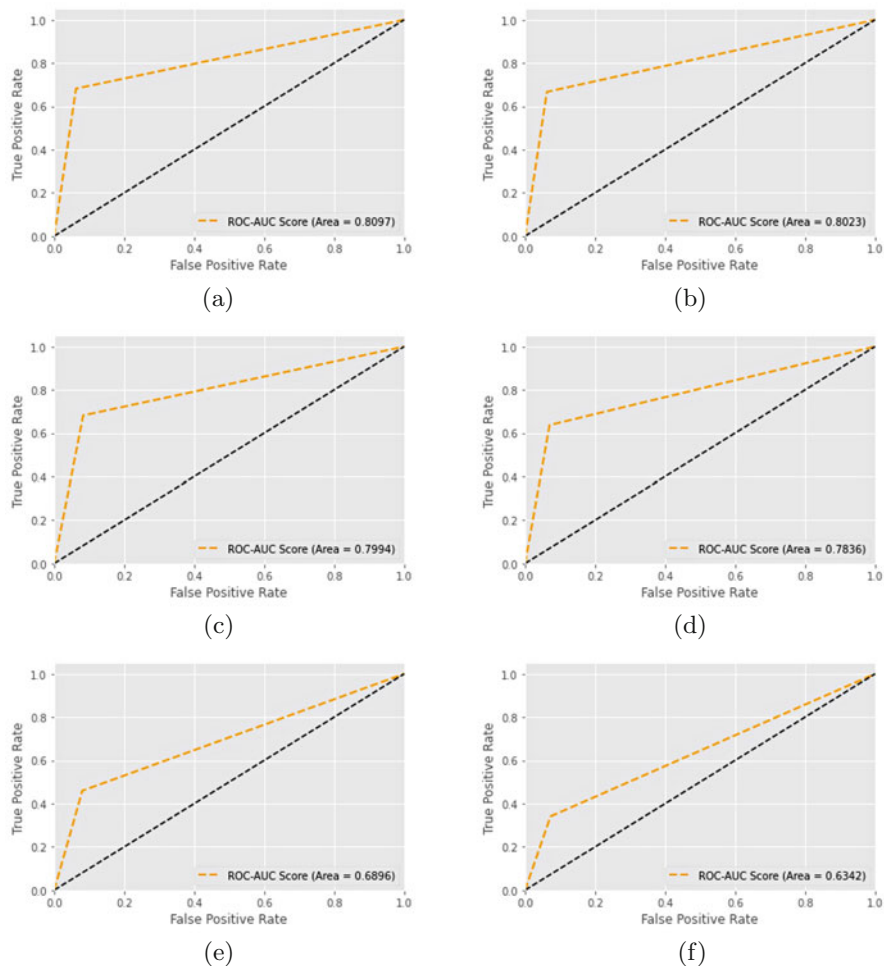
Fig. 4 ROC-AUC curve of CNN and pre-trained models. (**a**) ROC-AUC curve of CNN. (**b**) ROC-AUC curve of InceptionV3. (**c**) ROC-AUC curve of MobileNetV2. (**d**) ROC-AUC curve of DenseNet201. (**e**) ROC-AUC curve of ResNet50. (**f**) ROC-AUC curve of VGG19

5   Conclusion

Identifying COVID unfavorable medicine reactions of the novel medicine is an attractive approach to speed up the medicine development process. This chapter provided a CNN classifier for identifying unfavorable COVID medicine reactions from the three-dimensional structure of medicine. The three-dimensional chemical structure is obtained from PubChem, and unfavorable medicine reactions are collected from WebMD to perform the experiment, which is illustrated in Fig. 1. The identification power of the three-dimensional structure of medicine shows that

COVID unfavorable medicine reactions can be identified effectively. A medicine can have more than one unfavorable reaction, as shown in Fig. 2. Therefore, a multi-label CNN framework has been presented in the current work, shown in Fig. 3. The presented CNN model outperformed the pre-trained model's performance (DenseNet201, MobileNetV2, ResNet50, VGG19, InceptionV3 models). Its high performance on the three-dimensional structure of medicine justifies its prominence in adequacy and dependability in modern medicine discovery, development, and design. Based on the ROC-AUC score wise, the models can be ranked as CNN > InceptionV3 > MobileNetV2 > DenseNet201 > ResNet50 > VGG19, which scores are presented in Fig. 4. The presented CNN classifier achieved an accuracy score of 87.16%, and the model can effectively identify adverse medicine responses. Employing a more advanced CNN classifier can give more effective results in the three-dimensional structure of medicine. Further, it can be integrated with other medical information such as amino acid sequence, MEDLINE literature information, gene ontology, protein information, and chemical interaction to identify unfavorable reactions. Therefore, there is still scope for more research into building effective computational models by combining different medicine properties.

References

1. Karch, F.E., Lasagna, L.: Adverse drug reactions: a critical review. JAMA **234**(12), 1236–1241 (1975)
2. Calvo, E., Canadillas, D., Carbajo, U.: AI against COVID-19.
3. Das, P.: Multi-label long short-term memory-based framework to analyse drug functions from biological properties. IJISRT (2022)
4. Das, P., Mazumder, D.H.: Predicting drug functions from adverse drug reactions by multi-label deep neural network. In: Multimodal AI in Healthcare: A Paradigm Shift in Health Intelligence, pp. 215–226. Springer (2022)
5. Das, P., et al.: BRMCF: Binary relevance and MLSMOTE based computational framework to predict drug functions from chemical and biological properties of drugs. In: IEEE/ACM Transactions on Computational Biology and Bioinformatics (2022)
6. Das, P., Mazumder, D.H.: An extensive survey on the use of supervised machine learning techniques in the past two decades for prediction of drug side effects. Artif. Intell. Rev. 1–28 (2023)
7. Li, J., et al.: Drug discovery approaches using quantum machine learning. In: 2021 58th ACM/IEEE Design Automation Conference (DAC), pp. 1356–1359. IEEE (2021)
8. Chung, W.-H., Wang, C.-W., Dao, R.-L.: Severe cutaneous adverse drug reactions. J. Dermatology **43**(7), 758–766 (2016)
9. Das, P., Sangma, J.W., Pal, V.: Predicting adverse drug reactions from drug functions by binary relevance multi-label classification and MLSMOTE. In: Practical Applications of Computational Biology & Bioinformatics, 15th International Conference (PACBB 2021), pp. 165–173. Springer (2022)
10. Das, P., Yogita, Pal, V.: Integrative analysis of chemical properties and functions of drugs for adverse drug reaction prediction based on multi-label deep neural network. J. Integr. Bioinform. **19**(3), 20220007 (2022)
11. Ietswaart, R., et al.: Machine learning guided association of adverse drug reactions with in vitro target-based pharmacology. EBioMedicine **57**, 102837 (2020)

12. Shankar, S., et al.: Predicting adverse drug reactions of two-drug combinations using structural and transcriptomic drug representations to train an artificial neural network. Chem. Biol. Drug Des. **97**(3), 665–673 (2021)
13. Güüneş, S.S., et al.: Primum non nocere: In silico prediction of adverse drug reactions of antidepressant drugs. Comput. Toxicol. **18**, 100165 (2021)
14. Hatmal, M.M., et al.: Side effects and perceptions following COVID-19 vaccination in Jordan: a randomized, cross-sectional study implementing machine learning for predicting severity of side effects. Vaccines **9**(6), 556 (2021)
15. Swathi, D.N., et al.: Predicting drug side-effects from open source health forums using supervised classifier approach. In: 2020 5th International Conference on Communication and Electronics Systems (ICCES), pp. 796–800. IEEE (2020)
16. Wang, C.-S., et al.: Detecting potential adverse drug reactions using a deep neural network model. J. Med. Internet Res. **21**(2), e11016 (2019)
17. Jamal, S., et al.: Computational models for the prediction of adverse cardiovascular drug reactions. J. Transl. Med. **17**(1), 1–13 (2019)
18. Jamal, S., et al.: Predicting neurological adverse drug reactions based on biological, chemical and phenotypic properties of drugs using machine learning models. Sci. Rep. **7**(1), 1–12 (2017)
19. Pouliot, Y., Chiang, A.P., Butte, A.J.: Predicting adverse drug reactions using publicly available PubChem BioAssay data. Clin. Pharmacol. Ther. **90**(1), 90–99 (2011)
20. Liu, Y., et al.: Using temporal patterns in medical records to discern adverse drug events from indications. In: AMIA Summits on Translational Science Proceedings, 2012 (2012), p. 47
21. Jamiul Jahid, M., Ruan, J.: An ensemble approach for drug side effect prediction. In: 2013 IEEE International Conference on Bioinformatics and Biomedicine, pp. 440–445. IEEE (2013)
22. Jiang, K., Zheng, Y.: Mining Twitter data for potential drug effects. In: Proceedings of the Advanced Data Mining and Applications: 9th International Conference, ADMA 2013, Hangzhou, China, December 14–16, 2013, Part I 9, pp. 434–443. Springer (2013)
23. Huang, L.-C., Wu, X., Chen, J.Y.: Predicting adverse drug reaction profiles by integrating protein interaction networks with drug structures. Proteomics **13**(2), 313–324 (2013)
24. LaBute, M.X., et al.: Adverse drug reaction prediction using scores produced by large-scale drug-protein target docking on high-performance computing machines. PloS One **9**(9), e106298 (2014)
25. Zhang, W., et al.: Predicting drug side effects by multi-label learning and ensemble learning. BMC Bioinform. **16**(1), 1–11 (2015)
26. Niu, S.-Y., et al.: DSEP: a tool implementing novel method to predict side effects of drugs. J. Comput. Biol. **22**(12), 1108–1117 (2015)
27. Plumb, A.L.: Drugs.com: drug information online 2004. Ref. Rev. **18**(6), 41–41 (2004)
28. Kim, S., et al.: PubChem substance and compound databases. Nucl. Acids Res. **44**(D1), D1202–D1213 (2016)
29. BRANCHED-CHAIN AMINO ACIDS.: Uses, Side Effects, Interactions and Warnings–WebMD (2017). Webmd.com. Retrieved 8 October 2017
30. Afdhal, D., Ananta, K.W., Hartono, W.S.: Adverse drug reactions prediction using multi-label linear discriminant analysis and multi-label learning. In: 2020 International Conference on Advanced Computer Science and Information Systems (ICACSIS), pp. 69–76. IEEE (2020)
31. Das, P., Mazumder, D.H.: Predicting anatomical therapeutic chemical drug classes from 17 molecules' properties of drugs by multi-label binary relevance approach with MLSMOTE. In: 2021 5th International Conference on Computational Biology and Bioinformatics, pp. 1–7 (2021)

Using Reinforcement Learning for Optimizing COVID-19 Vaccine Distribution Strategies

Robertas Damaševičius, Rytis Maskeliūnas, and Sanjay Misra

1 Introduction

The COVID-19 pandemic is a global health crisis caused by the novel coronavirus SARS-CoV-2. It first emerged in Wuhan, China, in late 2019 and rapidly spread across the world, leading to the World Health Organization declaring it a global pandemic in March 2020. As of February 2023, the pandemic has affected over 200 million people globally and caused over 4 million deaths. The COVID-19 pandemic has had a profound impact on virtually all aspects of society, including healthcare systems [1], the global economy [2], researcher collaboration [3], and day-to-day life [4]. In response to the pandemic, governments and health organizations around the world have implemented a range of measures, including lockdowns, travel restrictions, and widespread testing and vaccination programs. The COVID-19 pandemic clearly indicates that economic and social well-being are strongly linked to population health [5].

Vaccination has emerged as a key tool in the fight against the pandemic, with several vaccines having been developed and authorized for emergency use [6]. The successful deployment of these vaccines is critical to controlling the spread of the virus and reducing the number of COVID-19 cases and deaths. One of the

R. Damaševičius (✉)
Department of Applied Informatics, Vytautas Magnus University, Kaunas, Lithuania
e-mail: robertas.damasevicius@vdu.lt

R. Maskeliūnas
Department of Multimedia Engineering, Kaunas University of Technology, Kaunas, Lithuania
e-mail: rytis.maskeliunas@ktu.lt

S. Misra
Department of Applied Data Science, Institute for Energy Technology, Halden, Norway
e-mail: sanjay.misra@ife.no

169

key challenges in responding to the pandemic has been the efficient and effective distribution of vaccines to curb the spread of the virus [7, 8]. The complex and rapidly changing nature of the pandemic has made it challenging for traditional methods of vaccine allocation and delivery to keep up and has highlighted the need for innovative approaches to address this problem [9]. Traditional methods of vaccine allocation and delivery involve a combination of centralized planning and on-the-ground implementation [10]. Centralized planning typically involves forecasting demand for vaccines, determining which populations should receive priority, and allocating vaccine supplies based on these factors. This process can be informed by data on the number of confirmed COVID-19 cases, the number of hospitalizations, and the age and health status of individuals in the population [11]. Once vaccines are allocated, the process of delivering them to individuals can be complex and multi-faceted. In many cases, vaccines are delivered through healthcare providers, such as hospitals, clinics, and pharmacies. In some instances, mobile teams may be deployed to provide vaccinations in communities that are remote or have limited access to healthcare facilities. Delivery of vaccines can also be influenced by a range of logistical and operational challenges, such as limited storage and transportation capabilities, the need for cold chain management, and the availability of personnel to administer the vaccines [12]. Forecasting demand for vaccines can be difficult, particularly in the context of a rapidly evolving pandemic. This can result in over-allocation or under-allocation of vaccine supplies, which can have significant implications for public health outcomes [13]. Traditional approaches are often based on predetermined allocation plans and delivery schedules, which can be slow to respond to changes in demand or supply. This lack of flexibility can limit the ability to quickly respond to emerging needs, such as changes in the number of confirmed COVID-19 cases or the emergence of new variants of the virus. Traditional methods of vaccine delivery may not be well-suited to reach all individuals in a population, particularly those who are marginalized or have limited access to healthcare services. This can result in unequal distribution of vaccines, which can impact public health outcomes and exacerbate existing health disparities [14]. The process of delivering vaccines can be complex and resource-intensive and is subject to a range of logistical and operational challenges, such as limited storage and transportation capabilities, the need for cold chain management, and the availability of personnel to administer the vaccines [15]. Public resistance or hesitancy to receive COVID-19 vaccines can also impact the effectiveness of traditional approaches [16]. This can include concerns about vaccine safety, efficacy, or the speed at which vaccines have been developed and approved [17]. Addressing these challenges and overcoming vaccine hesitancy will be critical to ensuring the success of traditional approaches to vaccine allocation and delivery. These challenges can have a significant impact on the speed and efficiency of vaccine delivery and may limit the number of individuals who can be vaccinated in a given time frame.

Artificial intelligence (AI) has been utilized in several ways to help address the COVID-19 pandemic, including: predictive modeling [18–20], contact tracing, image analysis, drug discovery, and virus protein analysis [21]. AI has been useful in

assisting healthcare workers, researchers, and policymakers in their response to the pandemic and finding solutions to its related problems. Reinforcement learning (RL) is a type of AI that has emerged as a promising approach for optimizing complex systems in real time [22]. RL algorithms use trial-and-error learning to identify the best actions to take in a given situation, based on their expected outcomes. RL has been applied to a wide range of domains, including healthcare [23, 24], economics and finance [25], transportation [26], education [27], and robotics [28], among others. In the context of vaccine distribution, RL has the potential to provide real-time optimization of vaccine allocation and delivery strategies, taking into account a range of factors such as vaccine storage and transport requirements, population demographics, and regulatory restrictions, among others [29]. This can help to ensure that vaccines are distributed in a way that maximizes public health outcomes, taking into account the complex and rapidly changing nature of the pandemic [30]. The use of RL for optimizing COVID-19 vaccine distribution strategies is an area of growing interest and research [31–34]. However, there are also significant challenges and limitations associated with using RL in this context, such as limited data availability, complex system dynamics, and ethical and social implications. Additionally, the field is still in its infancy, and there is a need for further research and development to better understand the impact of RL on vaccine distribution outcomes and to develop more effective and efficient RL algorithms for this domain [35].

This survey aims to provide a comprehensive overview of the use of RL for optimizing COVID-19 vaccine distribution strategies and its potential impact on public health outcomes. The authors will review the state of the art in RL applied to vaccine distribution, discuss the challenges and limitations of using RL in this context, and suggest future directions for research and development in this field. The chapter is dedicated to researchers, practitioners, and policymakers working in the areas of AI, public health, and vaccine distribution.

The aims of this chapter are as follows:

– To provide a comprehensive overview of RL and its applications to vaccine distribution
– To review the current state of the art in RL for optimizing COVID-19 vaccine distribution strategies and to analyze the potential benefits and limitations of using RL in this context
– To identify the challenges and limitations of using RL for COVID-19 vaccine distribution and to suggest directions for future research and development in this field
– To discuss the ethical and social implications of using RL for COVID-19 vaccine distribution and to provide recommendations for addressing these implications
– To provide insights and recommendations for researchers, practitioners, and policymakers working in the areas of AI, public health, and vaccine distribution

We formulate the following research questions and objectives of this chapter:

– How has RL been applied to vaccine distribution?

– What are the potential benefits and limitations of using RL for vaccine distribution?
– What is the methodology for using RL for optimizing COVID-19 vaccine distribution strategies, and what are the key steps and components involved in this process?

The remaining parts of this chapter are structured as follows. Section 2 provides a detailed description of the methodology for using RL for optimizing COVID-19 vaccine distribution strategies, including the problem formulation, data collection and preparation, model development, model validation and evaluation, and deployment and real-time monitoring. The section also provides a review of the existing literature on RL and vaccine distribution and highlights the gaps and opportunities for further research. Section 3 as an illustrative example describes the generic architecture of the RL-based system for vaccine allocation and distribution. Section 4 evaluates the benefits and challenges of RL for vaccine distribution task. Section 5 presents the answers to research questions of this study. The section also provides an analysis of the benefits and limitations of using RL for vaccine distribution and provides recommendations for future research and development. Section 6 discusses future directions for research and development based on using RL for vaccine distribution. Section 7 provides a conclusion to the study, summarizing the main findings and contributions of the study, and highlighting the potential of RL for optimizing COVID-19 vaccine distribution strategies. The section also provides recommendations for future research and development in this area.

2 Reinforcement Learning (RL)

2.1 Definition and Key Concepts

This chapter uses several key concepts and definitions that are important to understand in order to fully grasp the scope and objectives of the research. In this section, we will define and provide explanations of the most important terms used in the study.

RL is a type of machine learning that focuses on learning how to make decisions in an environment by observing the consequences of those decisions. The goal of RL is to learn a policy, or a mapping from states to actions, that maximizes some notion of cumulative reward over time. Formally, let S be the set of states, A be the set of actions, $R(s, a)$ the reward function that maps states and actions to rewards, and $\pi(a|s)$ the policy that maps states to actions. The objective of RL is to find the policy $\pi^*(a|s)$ that maximizes the expected cumulative reward, defined as

$$J(\pi) = \mathbb{E}\pi \left[\sum_{t=0}^{\infty} \gamma^t R(s_t, a_t) \right],$$

where $s_0, s_1, ..., s_t$ are the states visited according to the policy π, $a_0, a_1, ..., a_t$ are the actions taken according to the policy π, and $\gamma \in [0, 1)$ is a discount factor that determines the importance of future rewards.

2.2   Main Concepts and Methods in Reinforcement Learning Domain

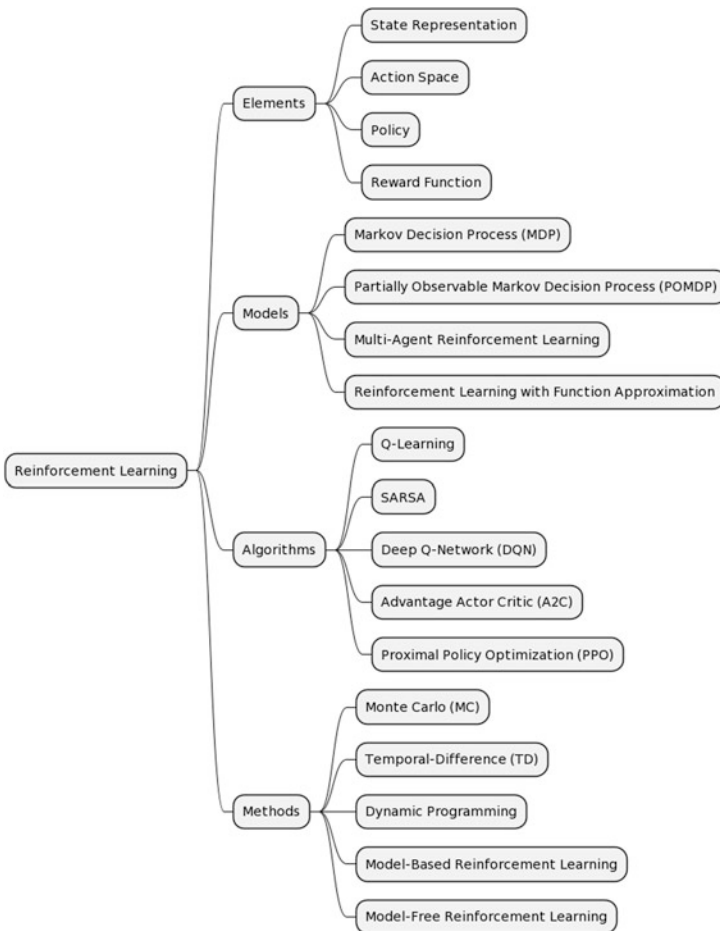A mind map of concepts in the RL domain is presented in Fig. 1.

Fig. 1 Mind map of reinforcement learning concepts

The mind map represents the various concepts and sub-topics in the field of RL. State representation is the description of the current situation or environment in a form that can be processed by the RL algorithm. Action space is the set of possible actions that can be taken in the environment. Policy is the mapping of states to actions, representing the strategy or behavior of the agent. Reward function is the function that defines the reward signal for the agent, used to measure its performance. Models describe the interaction between the agent and the environment in RL. Markov decision process (MDP) is a mathematical model that defines the relationship between the state, action, and reward. Partially observable MDP (POMDP) is an extension of MDP for situations where the state is not fully observable [36]. In multi-agent RL, multiple agents interact with each other and the environment. In RL with function approximation, the policy is represented as a function approximation rather than a table. Q-Learning is an off-policy RL algorithm that uses the Q-function to learn the optimal policy. SARSA is an on-policy RL algorithm that uses the action-value function to learn the optimal policy. Deep Q-Network (DQN) is a variant of Q-learning that uses deep neural networks to represent the Q-function. Advantage actor critic (A2C) is an algorithm that uses both an actor and a critic to learn the optimal policy [37]. Proximal policy optimization (PPO) is an algorithm that uses gradient ascent to update the policy in a stable manner [38]. Methods are different approaches used to solve RL problems. Monte Carlo (MC) method that uses sample-based estimates to evaluate the expected return. Temporal-difference (TD) method that uses the prediction error to update the estimate of the return [39]. Dynamic programming method that uses value iteration or policy iteration to solve the RL problem. In model-based RL, the model of the environment is used to plan the optimal policy. In model-free RL, the policy is learned directly from experience without a model of the environment.

These definitions and concepts provide the foundation for the research questions and objectives of this study and are central to understanding the methodology, results, and conclusions of the study.

2.3 Applications of RL

RL has a wide range of potential applications in various fields, including robotics, gaming, autonomous systems, and more recently, healthcare. Some of the most notable applications of RL include:

- Robotics: RL has been used to train robots to perform various tasks, such as grasping objects, walking, and flying. In these applications, the robot learns to take actions in its environment to achieve a desired goal, such as picking up an object or reaching a target location [28].
- Gaming: RL has been applied to game AI, allowing game agents to learn to play games such as chess, Go, and even video games, by trial and error. The game agent learns to make decisions based on the outcome of its actions, such as winning or losing the game [27].

– Autonomous systems: RL has been used to control autonomous systems such as self-driving cars, drones, and robots. In these applications, the RL algorithm learns to make decisions based on sensory information, such as camera inputs or GPS data, in order to achieve a desired goal, such as avoiding obstacles or reaching a target location [26].
– Healthcare: RL has recently been applied to healthcare, including COVID-19 vaccine distribution. In these applications, the RL algorithm learns to make decisions based on various factors, such as vaccine supply and demand, population demographics, and public health policies, in order to optimize the distribution of the vaccine [40, 41].

These are just a few examples of the potential applications of RL. With the increasing popularity of machine learning and AI, the potential applications of RL are likely to continue to grow and expand in the coming years.

2.4 Overview of RL Approaches to Vaccine Distribution

Over the past few years, there has been growing interest in using RL to optimize COVID-19 vaccine distribution strategies [42, 43]. This is due to the complex and rapidly changing nature of the pandemic, which requires dynamic and adaptable solutions that can respond to changing conditions in real time. RL provides a powerful and flexible framework for addressing these types of problems, as it allows the agent to learn from experience and make decisions based on the outcomes of its actions. COVID-19 vaccine distribution refers to the process of transporting and administering the COVID-19 vaccine to eligible individuals [33, 44]. The vaccine distribution process is a complex and dynamic system that is influenced by factors such as vaccine supply and demand, population demographics, and public health policies.

Optimization refers to the process of finding the best solution to a problem, given certain constraints and objectives. In the context of this study, optimization refers to finding the best strategy for COVID-19 vaccine distribution that meets the objectives of efficiently distributing the vaccine to eligible individuals, while also considering factors such as vaccine supply and demand, population demographics, and public health policies. RL has been applied to optimize COVID-19 vaccine distribution strategies, as a way to address the complex and rapidly changing nature of the pandemic. The goal of these applications is to determine the most effective way to allocate limited vaccine supplies to various populations, taking into account factors such as vaccine efficacy, demand, and distribution costs.

One approach to using RL for vaccine distribution is to model the problem as a MDP, where the state of the system is defined by the distribution of the vaccine and the actions of the agent are decisions about how to allocate the vaccine. The reward function is designed to capture the desired behavior of the agent, such as maximizing the number of people vaccinated or minimizing the spread of the virus.

The agent learns to make decisions based on the outcomes of its actions, in order to maximize the reward over time.

Another approach is to use multi-agent RL (MARL), where multiple agents represent different entities in the vaccine distribution system, such as hospitals, clinics, and government agencies [45]. The agents learn to coordinate their actions to achieve a common goal, such as maximizing the number of people vaccinated. In this approach, the agents need to take into account not only the state of their own environment, but also the state of other agents and the impact of their actions on the overall system.

There has also been a significant amount of research on the development of reward functions for vaccine distribution [31, 46]. The reward function is a critical component of the RL algorithm, as it determines the behavior of the agent. Researchers have explored the use of various reward functions, including those that prioritize the number of people vaccinated, the speed of the vaccine rollout, and the minimization of the spread of the virus. These studies have demonstrated the importance of carefully considering the design of the reward function, as it can have a significant impact on the behavior of the agent. RL-based approaches to vaccine distribution have been shown to be effective in simulation studies, where they can be tested under different scenarios and conditions [33]. For example, simulations have been used to compare the performance of RL-based approaches to traditional optimization methods, such as linear programming, and to evaluate the impact of different reward functions on the behavior of the agent [47].

Despite the promising results of these studies, there are still several challenges and limitations that need to be addressed in order to apply RL to vaccine distribution in real-world settings. For example, there may be limited data available to train the RL algorithms, or there may be constraints on the actions of the agent, such as legal or ethical considerations. Additionally, the rapidly changing nature of the pandemic means that the environment is constantly evolving, and the agent must be able to adapt to these changes in real time.

Summarizing, the state of the art in RL for vaccine distribution is still in its early stages, but there is a growing body of research that demonstrates its potential as a powerful tool for optimizing vaccine distribution strategies. With ongoing research and development, RL is likely to become an increasingly important tool for improving public health outcomes and addressing the challenges posed by COVID-19.

3   Illustrative Example of a RL-Based System for Vaccine Allocation and Distribution

As an illustrative example demonstrating the use of RL for vaccine allocation and distribution, we present a description of a hypothetical RL-based vaccine allocation and distribution system.

3.1   Generic Architecture

A generic architecture of a RL-based system for vaccine allocation and distribution can have the following components:

– Environment: The environment in this case would be the vaccine distribution network, including storage and transportation systems, healthcare facilities, and population demographics.
– State representation: The state representation would consist of the current inventory levels of the vaccine at different storage and healthcare facilities, the number of vaccines administered, and the number of people in different demographics who are eligible for the vaccine.
– Action Space: The action space would consist of different decisions that the system can make, such as the allocation of vaccines to different healthcare facilities, the transportation of vaccines from one facility to another, and the administration of vaccines to eligible individuals.
– Reward Function: The reward function would measure the success of the system's decisions and provide feedback on how to improve future decisions. For example, the reward function might prioritize higher vaccination coverage, faster vaccine administration, or a more equitable distribution of vaccines to different demographics [48].
– Policy: The policy would be the algorithm that the RL system uses to make decisions. This could be a deep neural network, a decision tree, or another type of machine learning model that is trained on the environment and the reward function to optimize vaccine distribution outcomes.
– Model: The model would be the internal representation of the environment that the policy uses to make decisions. This could be a simplified or abstract representation of the vaccine distribution network that is updated over time as the system interacts with the environment.
– Simulation: The system would be tested and trained through simulations, allowing for the exploration and optimization of different policies and models. The simulation results would provide insight into the effectiveness of different approaches and inform the development of a final implementation strategy.

This generic architecture outlines the key components of an RL-based system for vaccine allocation and distribution. However, the specifics of each component will vary depending on the specific challenges and requirements of the vaccine distribution network. Future research could focus on refining and optimizing these components to improve the overall efficiency and effectiveness of the RL-based vaccine distribution system.

The generic architecture of an RL-based system for vaccine allocation and distribution is given in Fig. 2.

In this architecture, the "Environment" component represents the dynamic and changing vaccine stock and demand information. The "Agent" component represents the decision-making process, including the policy, RL algorithm, and value function. The "Evaluation" component represents the metrics and perfor-
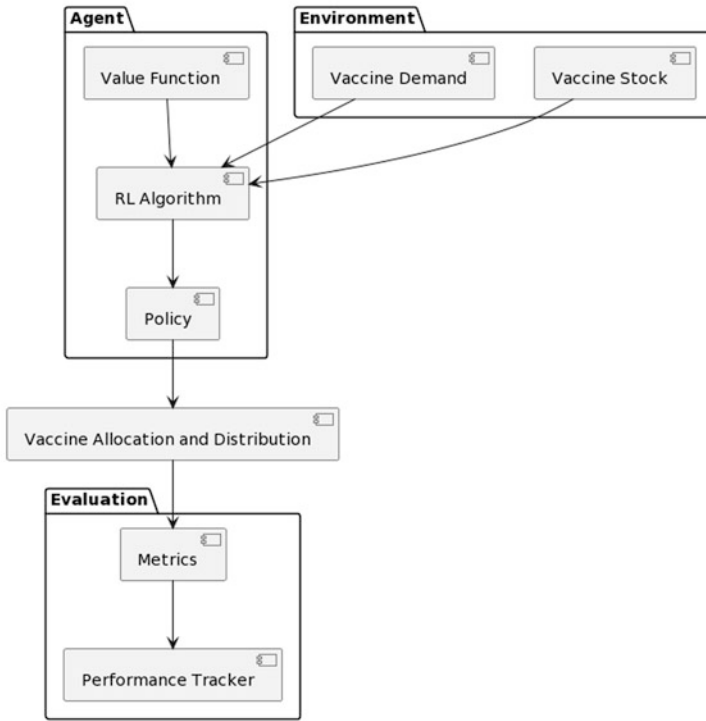
Fig. 2 Generic architecture of RL-based vax allocation and distribution system

Fig. 3 Class diagram of RL-based vax allocation and distribution system

mance tracker used to evaluate the effectiveness of the vaccine allocation and distribution strategy. The arrows represent the flow of information and decision-making processes in the system.

3.2 Classes of the System

We assume that the system is designed using the principles of object-oriented design. The class diagram of the system is given in Fig. 3.

This class diagram defines the classes VaccineAllocationSystem, State, Action, Reward, Location, Population, VaccineSupply, VaccinationRate, Amount, Effi-

ciency, and Equity. The VaccineAllocationSystem class is the main class that performs the vaccine allocation and distribution using RL. It has methods for learning from the past decisions and rewards, choosing the best action based on the current state, and allocating the vaccine based on the selected action. The State class represents the current state of the system and includes information about the location, population, vaccine supply, and vaccination rate. The Action class represents the action that can be taken by the system and includes information about the amount of vaccine to allocate and the destination. The Reward class represents the reward received after taking the action and includes information about the efficiency and equity of the allocation. The other classes represent additional information and data used by the system, such as location, population, vaccine supply, vaccination rate, amount, efficiency, and equity.

3.3 Components of the System

The component diagram of the system is given in Fig. 4.

"Vaccine Stock" component keeps track of the available quantity of vaccines at different locations. "Vaccine Allocation" component decides the distribution
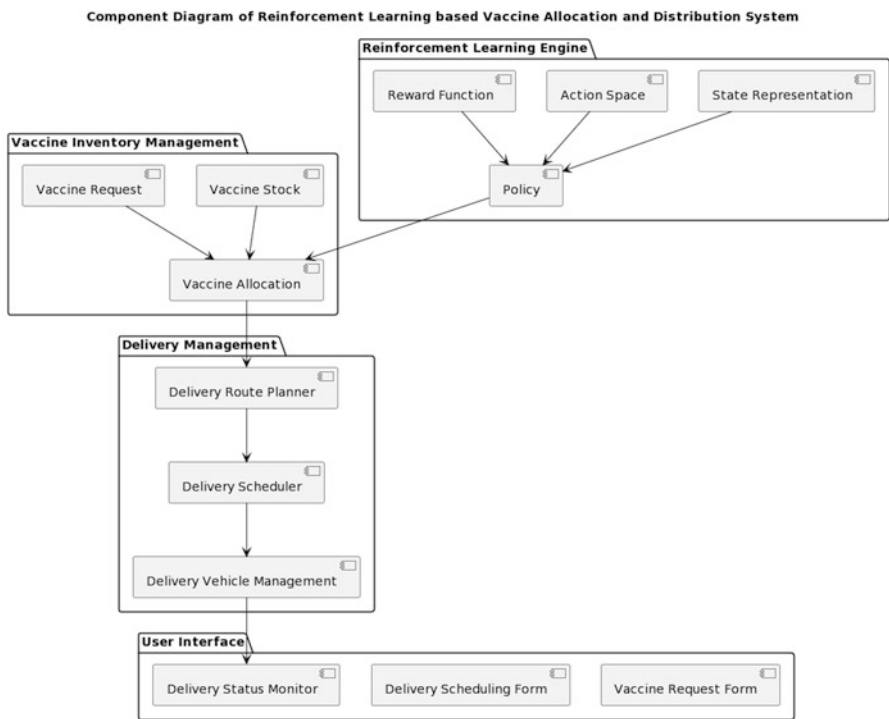

Fig. 4 Component diagram of RL-based vax allocation and distribution system

of vaccines among different regions based on factors such as population density, healthcare infrastructure, and priority groups. "Vaccine Request" component receives requests for vaccines from healthcare facilities and other entities. "Delivery Route Planner" component plans the most efficient delivery route for vaccines to reach the destination. "Delivery Scheduler" component schedules the delivery of vaccines based on the availability of delivery vehicles, delivery personnel, and other resources. "Delivery Vehicle Management" component manages the delivery vehicles, such as assigning vehicles to delivery routes and monitoring the status of vehicles during delivery. "Delivery Status Monitor" component monitors the delivery status of vaccines, such as whether they have been delivered, are in transit, or have encountered any issues. "State Representation" component represents the current state of the vaccine distribution system, which includes information about the vaccine stock, delivery status, and other relevant factors. "Policy" component represents the decision-making mechanism in the RL-based system, which maps states to actions. "Action Space" component defines the possible actions that the RL-based system can take in a given state. "Reward Function" component defines the reward signal used by the RL-based system to learn the optimal policy, which maps states and actions to a scalar reward value.

3.4 Typical Operations of the System

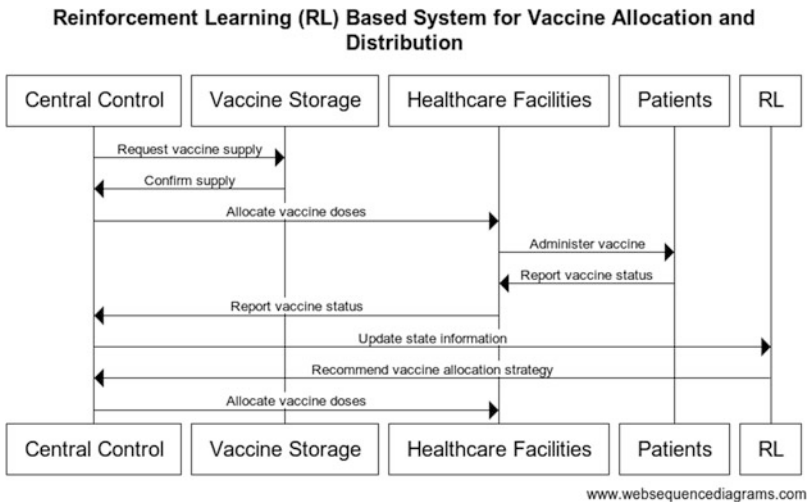The typical operations of the system are described in Fig. 5.

Fig. 5 Typical operations of RL-based vax allocation and distribution system

In this diagram, the central control (C) acts as the decision-maker for the vaccine allocation and distribution system. It communicates with the vaccine storage (V) to request and confirm the supply of vaccines. The healthcare facilities (H) receive allocated vaccine doses and administer them to patients (P). Patients report the status of their vaccines back to the healthcare facilities, which then report the information back to the central control. The central control uses this information to update the state of the system and communicates with the reinforcement learning component (RL) to get recommendations on vaccine allocation strategies. The central control then implements the recommended strategy and allocates vaccine doses to the healthcare facilities.

3.5   Deployment

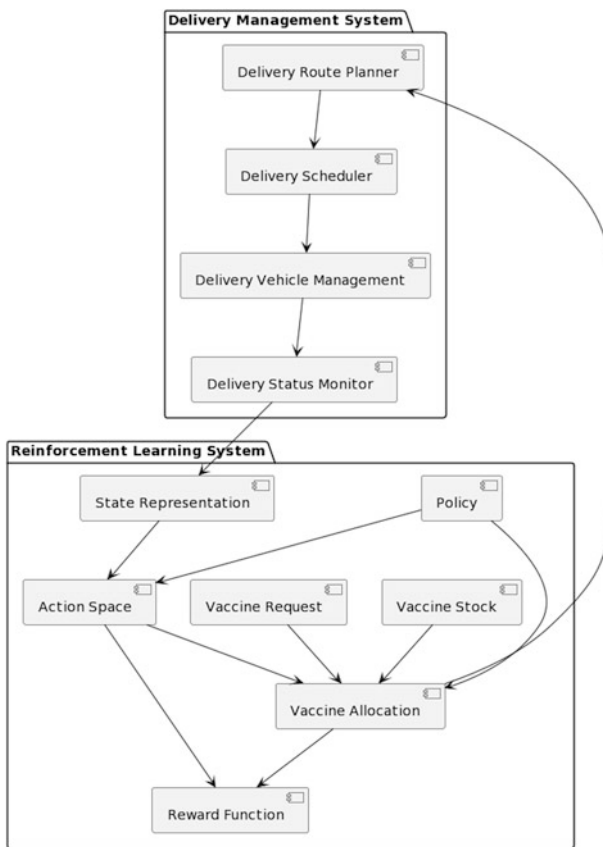The deployment diagram of the system is given in Fig. 6.

Fig. 6 Deployment diagram of RL-based vax allocation and distribution system

The deployment diagram represents the flow of information between components in the RL-based system for vaccine allocation and distribution and shows the physical deployment of these components. The diagram shows two packages, the reinforcement learning system and the delivery management system. The components within the reinforcement learning system include [Vaccine Stock], [Vaccine Allocation], [Vaccine Request], [State Representation], [Policy], [Action Space], and [Reward Function]. The components within the delivery management system include [Delivery Route Planner], [Delivery Scheduler], [Delivery Vehicle Management], and [Delivery Status Monitor]. The diagram represents the flow of data and information between these components. [Vaccine Stock] provides information to [Vaccine Allocation], and [Vaccine Request] is also input into [Vaccine Allocation]. The output of [Vaccine Allocation] is used by the [Delivery Route Planner], which provides input to the [Delivery Scheduler]. The [Delivery Scheduler] provides input to the [Delivery Vehicle Management], which in turn provides information to the [Delivery Status Monitor]. The [Delivery Status Monitor] provides input to the [State Representation], which is used by the [Action Space]. The [Policy] and [Action Space] both provide input to the [Reward Function], and [Vaccine Allocation] is also an input to the [Reward Function]. The output of the [Reward Function] is used by [Policy] and [Action Space] to adjust the [Vaccine Allocation].

3.6 Incorporating Domain-Specific Knowledge and Constraints

RL is a powerful tool for optimizing COVID-19 vaccine distribution strategies, but its effectiveness is dependent on the ability to incorporate domain-specific knowledge and constraints [49]. Domain-specific knowledge refers to information about the particular problem or environment being addressed, such as the logistics of vaccine distribution, the behavior of individuals and communities in response to the pandemic, and the regulations and policies in place [50]. Constraints refer to limitations on the actions that can be taken by the RL agent, such as ethical considerations, legal requirements, and resource limitations.

One of the key challenges in incorporating domain-specific knowledge and constraints into RL is defining the reward function. The reward function is used to guide the RL agent toward making decisions that achieve the desired objectives, such as minimizing the spread of the virus or maximizing the number of people vaccinated. However, defining the reward function in a way that accurately reflects the domain-specific knowledge and constraints can be a complex task. One approach to addressing this challenge is to incorporate domain experts into the design and implementation of the RL algorithm. This can involve consulting with public health experts, epidemiologists, and other specialists to ensure that the reward function accurately reflects the goals and constraints of the vaccine distribution process. Additionally, the use of expert-generated heuristics, which are rules of thumb based

on experience and knowledge of the domain, can help to improve the accuracy of the reward function and the performance of the RL algorithm.

Another approach is to use techniques such as transfer learning, which allows the RL algorithm to leverage experience from related problems to improve its performance in the current environment [34, 46]. This can be particularly useful in situations where data are limited, as it allows the agent to leverage knowledge from similar problems to make better decisions. Incorporating constraints into the RL algorithm can also be a challenge. For example, there may be legal requirements or ethical considerations that restrict the actions of the agent. To address this, the RL algorithm can be designed to include these constraints as part of the reward function, or they can be implemented as constraints on the action space. Additionally, it is important to carefully consider the potential consequences of the decisions made by the agent, as the actions taken by the agent may have unintended consequences that impact public health outcomes.

Incorporating domain-specific knowledge and constraints into RL is crucial for optimizing COVID-19 vaccine distribution strategies. This requires careful consideration of the reward function and the constraints on the agent's actions and can be achieved through collaboration with domain experts and the use of transfer learning and constraint-based techniques. By taking these steps, the RL algorithm can be designed to accurately reflect the goals and constraints of the vaccine distribution process and to make decisions that are aligned with the overall goals of improving public health outcomes.

4 Evaluation of RL for Vaccine Distribution

4.1 Benefits of RL for Vaccine Distribution

RL has the potential to significantly impact COVID-19 vaccine distribution by providing optimized strategies for allocating vaccines, resources, and personnel. Some of the key benefits of using RL for vaccine distribution include:

– Optimization: RL algorithms can continuously learn from the outcomes of their actions and adjust their strategies over time to achieve better results. This makes RL well-suited for addressing complex problems such as vaccine distribution, where multiple objectives and constraints must be considered [30, 35, 42, 51–53].
– Flexibility: RL algorithms can adapt to changing circumstances, such as changes in the distribution of the virus or in the availability of vaccines, making them well-suited for addressing dynamic and unpredictable environments. The agent can be programmed to consider a variety of different factors, such as the number of people vaccinated, the speed of the vaccine rollout, and the minimization of the spread of the virus. This allows the agent to find the optimal trade-

off between different objectives, which is important in a complex and rapidly evolving situation like the COVID-19 pandemic [43].

– Improved accuracy: By incorporating domain-specific knowledge and constraints into the reward function, RL algorithms can make more accurate decisions that align with the overall goals of improving public health outcomes.
– Enhanced decision-making: RL algorithms can provide decision-makers with insights and recommendations for optimizing vaccine distribution, taking into account a wide range of variables such as vaccine supply, population demographics, and local regulations [35, 51, 53].
– Increased efficiency: RL algorithms can help to minimize waste and optimize resource allocation, leading to more efficient use of vaccines, personnel, and resources [32, 35].
– Improved transparency: By using a data-driven approach, RL algorithms can provide a transparent and easily understandable explanation of the decision-making process, helping to increase public trust in the vaccine distribution process.
– Improved scalability: RL algorithms can be easily scaled to address vaccine distribution on a national or even global scale, allowing for more efficient and effective coordination of resources and personnel [51].
– Learnability: The agent can continuously improve its behavior based on the outcomes of its actions, which is particularly important in a rapidly changing environment like the COVID-19 pandemic. Additionally, RL allows the agent to make decisions in real time, which is critical in a situation where time is of the essence and quick action is needed to minimize the spread of the virus.

The use of RL for vaccine distribution has the potential to significantly improve public health outcomes by providing optimized strategies for allocating vaccines, resources, and personnel. RL has several strengths that make it an attractive approach for optimizing COVID-19 vaccine distribution strategies. By leveraging the strengths of RL, decision-makers can make more informed and accurate decisions that align with the overall goals of improving public health.

4.2 Challenges and Limitations of RL

Despite its many potential applications and successes, RL also faces several challenges and limitations that need to be addressed. Some of the most significant challenges and limitations of RL include:

– Credit assignment problem: One of the main challenges in RL is determining which actions of the agent are responsible for the outcomes that it experiences. This is known as the credit assignment problem and can lead to slow and suboptimal learning [54].
– Exploration–exploitation trade-off: Another challenge in RL is balancing the need for exploration and exploitation. The agent needs to explore its environment

to gather information about its possible outcomes, but also needs to exploit that information to make the best decisions. Balancing this trade-off is a key challenge in RL [55].

– Scalability: RL algorithms can be computationally expensive, especially as the size of the state and action spaces increase. This can make RL difficult to scale to large and complex environments [56].

– Model uncertainty: In many RL algorithms, the agent must model its environment in order to make decisions. Model uncertainty, or the lack of certainty in the model, can lead to suboptimal decisions and slow learning [51].

– Reward design: The choice of reward function can have a significant impact on the behavior of the agent. Designing an appropriate reward function that effectively captures the desired behavior of the agent can be challenging.

– Availability of data: In order for the RL algorithm to learn, it needs to have access to large amounts of data about the vaccine distribution process. However, in many cases, there may be limited data available, which can make it difficult to train the agent effectively.

– Complexity: RL algorithms can be computationally intensive, which can make it challenging to implement them in real-world scenarios, particularly in resource-constrained environments such as healthcare systems. Additionally, there may be ethical or legal constraints on the actions of the agent, which can make it difficult to implement RL in a way that is consistent with these constraints [35, 42].

These are just a few of the challenges and limitations of RL that need to be considered, particularly in terms of the availability of data, the complexity of the algorithms, and the rapidly changing nature of the pandemic. Addressing these challenges and limitations is a key area of research in RL, and the development of new algorithms and techniques to overcome these challenges is ongoing. Despite these challenges, RL is a promising tool for improving public health outcomes and addressing the challenges posed by COVID-19, and ongoing research and development is likely to lead to significant advances in this field.

4.3   Limitations and Risks of RL for Vaccine Distribution

While RL has the potential to significantly impact COVID-19 vaccine distribution, it is important to acknowledge the limitations and risks associated with its use. Some of the key challenges and limitations include:

– Data quality and availability: RL algorithms require high-quality and reliable data to learn from, and decisions made by these algorithms are only as good as the data they are trained on. This can be a challenge in the context of vaccine distribution, where data may be incomplete, biased, or unavailable in real time.

– Model complexity: RL algorithms can be complex and difficult to interpret, making it challenging for decision-makers to understand how the algorithms are making decisions [35, 42].

– Model bias: RL algorithms can be biased if the data used to train them are biased, which can result in suboptimal or unethical decisions.
– Lack of transparency: Some RL algorithms may be seen as black boxes, making it difficult for decision-makers to understand the logic behind the recommendations made by the algorithms.
– Technical limitations: RL algorithms can be computationally intensive and require significant computational resources to run, which can be a challenge for organizations with limited computational capacity.
– Ethical considerations: The use of RL for vaccine distribution raises important ethical considerations, such as fairness and equity in vaccine allocation [42], privacy, and the impact on vulnerable populations.
– Model robustness: RL algorithms may not perform well in the face of new or unexpected situations, such as changes in the distribution of the virus or in the availability of vaccines, which can result in suboptimal or incorrect decisions [51].
– Rigidity: The rapidly changing nature of the COVID-19 pandemic means that the environment is constantly evolving, which can make it difficult for the RL algorithm to keep up with these changes. This requires the agent to be highly adaptable and able to quickly respond to new information and changing conditions, which can be a significant challenge.

Therefore, while RL has the potential to significantly impact COVID-19 vaccine distribution, it is important to be aware of the limitations and risks associated with its use. Careful consideration of these challenges is necessary to ensure that the use of RL for vaccine distribution is safe, effective, and ethical.

4.4 Ethical and Social Implications of RL for Vaccine Distribution

The use of RL for COVID-19 vaccine distribution raises important ethical and social implications that must be carefully considered. Some of the key ethical and social implications include:

– Fairness and equity: RL algorithms may make decisions that are not fair or equitable, such as favoring certain populations over others. This can result in unequal access to vaccines, which can perpetuate existing social and health disparities [42].
– Privacy: RL algorithms may collect, store, and use sensitive personal information, such as health information, which can raise concerns about privacy and data security.
– Bias: RL algorithms can perpetuate existing biases and discrimination if the data used to train them are biased. This can result in unfair or unequal treatment of certain populations.

– Impact on vulnerable populations: RL algorithms may have unintended consequences for vulnerable populations, such as those who are marginalized, elderly, or have underlying health conditions [57].
– Public trust: The use of RL algorithms for vaccine distribution may be perceived as opaque and lacking in transparency, which can undermine public trust in the distribution process [58].
– Responsibility and accountability: The use of RL algorithms for vaccine distribution raises questions about who is responsible and accountable for the decisions made by the algorithms [59].
– Societal and cultural factors: The use of RL algorithms for vaccine distribution must take into account cultural and societal factors, such as cultural attitudes toward vaccines, trust in healthcare systems, and public attitudes toward technology [60].

The use of RL for COVID-19 vaccine distribution raises important ethical and social implications that must be carefully considered. The potential benefits of RL must be balanced against the potential risks and negative consequences, and appropriate measures must be taken to ensure that the use of RL is safe, ethical, and equitable.

5   Answers to Research Questions

5.1   Research Question 1: How Has RL Been Applied to Vaccine Distribution?

RL has been applied to vaccine distribution in several ways, including optimization of vaccine allocation and delivery strategies, real-time monitoring of vaccine supply chains, and dynamic adjustment of vaccine distribution strategies in response to changing conditions on the ground [61–63]. Some examples of RL applied to vaccine distribution include:

– Optimizing vaccine allocation: RL algorithms can be used to optimize the allocation of vaccines to different regions or populations, taking into account factors such as vaccine storage and transport requirements, population demographics, and regulatory restrictions, among others [30, 52, 64, 65].
– Real-time monitoring of vaccine supply chains: RL algorithms can be used to monitor the movement of vaccines through the supply chain in real time, providing insights into bottlenecks, delays, and other issues that may affect vaccine distribution outcomes [66].
– Dynamic adjustment of vaccine distribution strategies: RL algorithms can be used to dynamically adjust vaccine distribution strategies in response to changing conditions on the ground, such as changes in the number of cases or the emergence of new variants of the virus [32].

5.2 Research Question 2: What Are the Potential Benefits and Limitations of Using RL for Vaccine Distribution?

The key benefits of using RL for COVID-19 vaccine distribution include:

– Real-time optimization: RL algorithms can provide real-time optimization of vaccine distribution strategies, allowing for dynamic and effective allocation of vaccines in response to changing conditions on the ground [67].
– Improved efficiency: RL algorithms can help to optimize the efficiency of vaccine distribution, reducing waste, increasing vaccine uptake, and reducing the impact of vaccine hesitancy [68].
– Increased transparency: RL algorithms can provide increased transparency into vaccine distribution outcomes, helping to identify areas for improvement and to ensure that decisions are being made in an ethical and socially responsible manner [69].

Despite the potential benefits of using RL for vaccine distribution, there are also significant challenges and limitations associated with using RL for COVID-19 vaccine distribution:

– Limited data availability: The use of RL for vaccine distribution requires high-quality data on population demographics, vaccine supply chains, and other relevant factors. However, data availability is often limited, particularly in low- and middle-income countries, which can make it difficult to develop accurate RL algorithms [70].
– Complex system dynamics: The vaccine distribution system is complex and rapidly changing, making it challenging to develop accurate RL algorithms that can adapt to changing conditions in real time [56].
– Ethical and social implications: The use of RL for vaccine distribution has significant ethical and social implications, such as potential biases in vaccine allocation and the impact of RL algorithms on vulnerable populations.
– Lack of transparency: Some RL algorithms are highly complex and lack transparency, which can make it difficult to understand how decisions are being made and to ensure that decisions are being made in an ethical and socially responsible manner [69].

The state of the art in RL for optimizing COVID-19 vaccine distribution strategies has the potential to provide real-time optimization and increased efficiency of vaccine distribution. However, further research and development is needed to address the limitations and challenges associated with using RL for this purpose, including limited data availability, complex system dynamics, ethical and social implications, and lack of transparency.

5.3 Research Question 3: What Is the Methodology for Using RL for Optimizing COVID-19 Vaccine Distribution Strategies, and What Are the Key Steps and Components Involved in This Process?

The methodology for using RL for optimizing COVID-19 vaccine distribution strategies involves several key steps and components, including:

– Problem formulation: The first step in using RL for vaccine distribution is to formulate the problem in terms of the decision-making process, the state space, the action space, and the reward function. This involves defining the objectives of the vaccine distribution process, the available information and constraints, and the criteria for success.
– Data collection and preparation: The second step is to collect and prepare high-quality data on population demographics, vaccine supply chains, and other relevant factors. These data are used to train and validate the RL algorithms and to evaluate the performance of the vaccine distribution strategy.
– Model development: The third step is to develop an RL model that can learn from the collected data and optimize vaccine distribution strategies in real time. This involves selecting an appropriate RL algorithm, such as deep reinforcement learning or multi-agent reinforcement learning, and defining the architecture and parameters of the model.
– Model validation and evaluation: The fourth step is to validate and evaluate the RL model using the collected data. This involves testing the model with simulated scenarios and evaluating its performance in terms of vaccine coverage, vaccine waste, and other relevant metrics.
– Deployment and real-time monitoring: The final step is to deploy the RL model in real-world settings and to monitor its performance in real time. This involves integrating the RL model into the vaccine distribution system and using real-time data to dynamically adjust the vaccine distribution strategy in response to changing conditions on the ground.

The methodology for using RL for optimizing COVID-19 vaccine distribution strategies involves several key steps and components, including problem formulation, data collection and preparation, model development, model validation and evaluation, and deployment and real-time monitoring. Effective implementation of this methodology requires a strong interdisciplinary collaboration between computer scientists, epidemiologists, and public health experts and a deep understanding of the complexities of the vaccine distribution system.

6   Future Directions for Research and Development

Future research directions on advancing RL approaches for vaccine distribution can be stated as follows:

– Developing explainable RL: RL algorithms can be complex and difficult to interpret, making it challenging for stakeholders to understand their decisions and the underlying logic. There is a need to develop explainable RL algorithms that can provide clear, interpretable explanations of the decisions being made. This will help ensure that the decisions made by the algorithms are trustworthy and that stakeholders can understand how and why decisions are being made [71].
– Enhancing fairness and equity: RL algorithms must be designed to ensure fairness and equity and to minimize bias and discrimination. This can be achieved by using unbiased data, designing algorithms that incorporate fairness constraints, and using counterfactual reasoning to assess the potential impact of decisions on different populations [72].
– Improving privacy and security: RL algorithms must be designed to protect sensitive information, such as health information, and to ensure the privacy and security of data. This can be achieved by using privacy-preserving methods, such as differential privacy, and by incorporating security measures into the algorithms [73].
– Evaluating real-world impact: RL algorithms must be evaluated in real-world settings to assess their effectiveness and impact. This will help determine the extent to which RL can help optimize vaccine distribution and improve public health outcomes [74].
– Incorporating real-world data: By using real-world data to train and evaluate RL algorithms, future research can improve the accuracy and effectiveness of the algorithms and ensure that the results are generalizable to real-world settings. For example, RL algorithms can be enhanced by incorporating patient-specific information, such as age, health status, and prior vaccine history, to make more informed decisions about vaccine distribution [75].
– Enhancing scalability and robustness: RL algorithms must be designed to be scalable and robust, so that they can handle large and complex real-world problems. This will help ensure that the algorithms can be effectively used in real-world settings to improve public health outcomes.
– Improving decision-making under uncertainty: RL algorithms must be designed to make decisions under uncertainty, such as predicting future disease spread, and to adapt to changing circumstances. This will help ensure that the algorithms are effective in unpredictable and rapidly changing situations, such as pandemics [76].
– Incorporating population health metrics: RL algorithms must be designed to incorporate population health metrics, such as the overall health of the population, to make informed decisions about vaccine distribution [77].

- Improving data quality: RL algorithms are heavily dependent on the quality of the data used to train and evaluate them. Future research can focus on improving the quality of the data used in RL to ensure that the algorithms make accurate and effective decisions [78].
- Addressing ethical and social considerations: RL algorithms must be designed to address ethical and social considerations, such as fairness and equity, to ensure that the decisions made by the algorithms are safe, ethical, and equitable [79].
- Enhancing robustness: RL algorithms must be designed to be robust, so that they can handle large and complex real-world problems. Future research can focus on enhancing the robustness of RL algorithms to ensure that the algorithms are effective in real-world settings [80].

7 Conclusion

In this chapter, we have explored the potential of reinforcement learning (RL) for optimizing COVID-19 vaccine distribution strategies, which has not been done before. We reviewed the state of the art in RL for vaccine distribution, including the strengths and limitations of RL approaches, the ethical and social implications of using RL for vaccine distribution, and the challenges and limitations of RL. Our research has shown that RL can be an effective approach for optimizing vaccine distribution strategies by taking into account a wide range of factors, including the available resources, vaccine demand, and the spread of the virus. However, RL algorithms must be designed to address ethical and social considerations, such as fairness and equity, and to be robust, interpretable, and adaptable to changing circumstances. To improve the public health outcomes through RL, future research must focus on incorporating domain-specific knowledge, improving data quality, enhancing interpretability, and addressing ethical and social considerations. Additionally, future research must focus on improving the decision-making ability of RL algorithms under uncertainty, to ensure that the algorithms are effective in unpredictable and rapidly changing situations.

RL has the potential to be a valuable tool for optimizing COVID-19 vaccine distribution strategies and improving public health outcomes. However, the limitations and challenges of RL must be addressed to ensure that the algorithms are used safely, effectively, and in a manner that considers ethical and social considerations. One of the key limitations of this study is the current state of data availability and quality. Although significant efforts are being made to collect and analyze data on the COVID-19 pandemic and the vaccine distribution process, there is still a need for high-quality data that can be used to train and validate RL algorithms. Additionally, the complexity of the vaccine distribution system, including the interplay between vaccine supply and demand, population demographics, and public health policies, poses a significant challenge for the development and deployment of effective RL models. Another limitation of this study is the limited understanding of the underlying mechanisms of RL and the lack of consensus on the best practices for

using RL in real-world settings. This requires ongoing research and development to refine the methodology and to address the limitations of this approach.

Future research can address or mitigate these limitations and challenges of RL and ensure that RL is used safely, effectively, and in a manner that considers ethical and social considerations. Despite these limitations, the potential of RL for optimizing COVID-19 vaccine distribution strategies is significant, and the results of this study can serve as a foundation for further research and development in this area. The study provides valuable insights into the benefits and limitations of using RL for vaccine distribution and can inform the development of more effective and efficient vaccine distribution strategies that can help to mitigate the impact of the COVID-19 pandemic. Still, there is a need for further research to advance RL approaches for COVID-19 vaccine distribution. This will help ensure that the use of RL is safe, ethical, and effective and that the potential benefits of RL are realized in practice.

References

1. Lohela-Karlsson, M., Mellgren, E.C.: Health consequences of the COVID-19 pandemic among health-care workers: a comparison between groups involved and not involved in COVID-19 care. Healthcare **10**(12), 2540 (2022)
2. Kumar, N.M., Mohammed, M.A., Abdulkareem, K.H., Damasevicius, R., Mostafa, S.A., Maashi, M.S., Chopra, S.S.: Artificial intelligence-based solution for sorting covid related medical waste streams and supporting data-driven decisions for smart circular economy practice. Process Saf. Environ. Prot. **152**, 482–494 (2021)
3. Damaševičius, R., Zailskaitė-Jakštė, L.: Impact of covid-19 pandemic on researcher collaboration in business and economics areas on national level: a scientometric analysis. J. Doc. **79**(1), 183–202 (2023)
4. Girdhar, A., Kapur, H., Kumar, V., Kaur, M., Singh, D., Damasevicius, R.: Effect of covid-19 outbreak on urban health and environment. Air Qual. Atmos. Health **14**(3), 389–397 (2021)
5. Malleret, T., Schwab, K.: Great Narrative (The Great Reset Book 2) (2021)
6. Machado, B.A.S., Hodel, K.V.S., dos Santos Fonseca, L.M., Pires, V.C., Mascarenhas, L.A.B., da Silva Andrade, L.P.C., Moret, M.A., Badaró, R.: The importance of vaccination in the context of the COVID-19 pandemic: a brief update regarding the use of vaccines. Vaccines **10**(4), 591 (2022)
7. Santini, S.: Optimal covid-19 vaccination strategies with limited vaccine and delivery capabilities. ACM Trans. Comput. Healthcare **2**(4), 1–16 (2021)
8. Trad, F., El Falou, S.: Testing different covid-19 vaccination strategies using an agent-based modeling approach. SN Comput. Sci. **3**(4), 307 (2022)
9. MacIntyre, C.R., Costantino, V., Trent, M.: Modelling of covid-19 vaccination strategies and herd immunity, in scenarios of limited and full vaccine supply in NSW, Australia. Vaccine **40**(17), 2506–2513 (2022)
10. Wilder-Smith, A., Longini, I., Zuber, P.L., Bärnighausen, T., Edmunds, W.J., Dean, N., Masserey Spicher, V., Benissa, M.R., Gessner, B.D.: The public health value of vaccines beyond efficacy: methods, measures and outcomes. BMC Med. **15**(1), 138 (2017)
11. Kohli, M., Maschio, M., Becker, D., Weinstein, M.C.: The potential public health and economic value of a hypothetical COVID-19 vaccine in the United States: Use of cost-effectiveness modeling to inform vaccination prioritization. Vaccine **39**(7), 1157–1164 (2021)

12. Fahrni, M.L., An-Nisaa' Ismail, I., Refi, D.M., Almeman, A., Yaakob, N.C., Saman, K.Md., Mansor, N.F., Noordin, N., Babar, Z.-U.-D.: Management of COVID-19 vaccines cold chain logistics: a scoping review. J. Pharm. Policy Pract. **15**(1), 16 (2022)

13. Monrad, J.T., Quaade, S., Powell-Jackson, T.: Supply, then demand? health expenditure, political leanings, cost obstacles to care, and vaccine hesitancy predict state-level COVID-19 vaccination rates. Vaccine **40**(45), 6528–6548 (2022)

14. Wouters, O.J., Shadlen, K.C., Salcher-Konrad, M., Pollard, A.J., Larson, H.J., Teerawattananon, Y., Jit, M.: Challenges in ensuring global access to COVID-19 vaccines: production, affordability, allocation, and deployment. Lancet **397**(10278), 1023–1034 (2021)

15. Comes, T., Sandvik, K.B., Van de Walle, B.: Cold chains, interrupted. J. Humanit. Logist. Supply Chain Manag. **8**(1), 49–69 (2018)

16. Lin, C., Tu, P., Beitsch, L.M.: Confidence and receptivity for covid-19 vaccines: a rapid systematic review. Vaccines **9**(1), 1–32 (2021)

17. Yafooz, W.M.S., Emara, A.M., Lahby, M.: Detecting Fake News on COVID-19 Vaccine from YouTube Videos Using Advanced Machine Learning Approaches, volume 1001 of Studies in Computational Intelligence (2022)

18. Awotunde, J.B., Ogundokun, R.O., Misra, S.: Cloud and IoMT-based big data analytics system during COVID-19 pandemic. In: Internet Things (2021)

19. Awotunde, J.B., Ogundokun, R.O., Adeniyi, E.A., Misra, S.: Visual Exploratory Data Analysis Technique for Epidemiological Outbreak of COVID-19 Pandemic. EAI/Springer Innovations in Communication and Computing (2022)

20. Olaleye, T., Abayomi-Alli, A., Adesemowo, K., Arogundade, O.T., Misra, S., Kose, U.: SCLAVOEM: hyper parameter optimization approach to predictive modelling of Covid-19 infodemic tweets using smote and classifier vote ensemble. Soft Comput. **27**(6), 3531–3550 (2022)

21. Kumar, V., Singh, D., Kaur, M., Damaševičius, R.: Overview of current state of research on the application of artificial intelligence techniques for Covid-19. PeerJ Comput. Sci. **7**, 1–34 (2021)

22. Ladosz, P., Weng, L., Kim, M., Oh, H.: Exploration in deep reinforcement learning: a survey. Inf. Fusion **85**, 1–22 (2022)

23. Capizzi, G., Sciuto, G.L., Napoli, C., Polap, D., Wozniak M.: Small lung nodules detection based on fuzzy-logic and probabilistic neural network with bioinspired reinforcement learning. IEEE Trans. Fuzzy Syst. **28**(6), 1178–1189 (2020)

24. Allioui, H., Mohammed, M.A., Benameur, N., Al-Khateeb, B., Abdulkareem, K.H., Garcia-Zapirain, B., Damaševičius, R., Maskeliūnas, R.: A multi-agent deep reinforcement learning approach for enhancement of covid-19 CT image segmentation. J. Pers. Med. **12**(2), 309 (2022)

25. Charpentier, A., Élie, R., Remlinger, C.: Reinforcement learning in economics and finance. Comput. Econ. (2021). https://doi.org/10.48550/arXiv.2003.10014

26. Zhang, R., Yu, R., Xia, W.: Constraint-aware policy optimization to solve the vehicle routing problem with time windows. Inf. Technol. Control **51**(1), 126–138 (2022)

27. Maskeliunas, R., Damasevicius, R., Paulauskas, A., Ceravolo, M.G., Charalambous, M., Kambanaros, M., Pampoulou, E., Barbabella, F., Poli, A., Carvalho, C.V.: Deep reinforcement learning-based iTrain serious game for caregivers dealing with post-stroke patients. Information **13**(12), 564 (2022)

28. Mehmood, A., Shaikh, I.U.H., Ali, A.: Application of deep reinforcement learning tracking control of 3WD omnidirectional mobile robot. Inf. Technol. Control **50**(3), 507–521 (2021)

29. Osama, T., Razai, M.S., Majeed, A.: Covid-19 vaccine allocation: addressing the United Kingdom's colour-blind strategy. J. R. Soc. Med. **114**(5), 240–243 (2021)

30. Rey, D., Hammad, A.W., Saberi, M.: Vaccine allocation policy optimization and budget sharing mechanism using reinforcement learning. Omega (United Kingdom) **115**, (2023). https://doi.org/10.1016/j.omega.2022.102783

31. Tan, P.: Covid-19 vaccine distribution policy design with reinforcement learning. In: ACM Int. Conf. Proceeding Series, pp. 103–108 (2021)

32. Beigi, A., Yousefpour, A., Yasami, A., Gómez-Aguilar, J.F., Bekiros, S., Jahanshahi, H.: Application of reinforcement learning for effective vaccination strategies of coronavirus disease 2019 (covid-19). Eur. Phys. J. Plus **136**(5), 609 (2021)

33. Awasthi, R., Guliani, K.K., Khan, S.A., Vashishtha, A., Gill, M.S., Bhatt, A., Nagori, A., Gupta, A., Kumaraguru, P., Sethi, T.: Vacsim: learning effective strategies for covid-19 vaccine distribution using reinforcement learning. Intell. Based Med. **6**, (2022). https://doi.org/10.1016/j.ibmed.2022.100060

34. Trad, F., El Falou, S.: Towards using deep reinforcement learning for better covid-19 vaccine distribution strategies. In: 2022 7th Int. Conf. on Data Science and Machine Learning Applications, CDMA 2022, pp. 7–12 (2022)

35. Hao, Q., Huang, W., Xu, F., Tang, K., Li, Y.: Reinforcement learning enhances the experts: large-scale covid-19 vaccine allocation with multi-factor contact network. In: ACM SIGKDD Int. Conf. on Knowledge Discovery and Data Mining, pp. 4684–4694 (2022)

36. Zhou, Z., Lai, L., Dong, Y.: Quantification of value of information associated with optimal observation actions within partially observable Markov decision processes. KSCE J. Civil Eng. **26**(12), 5173–5186 (2022)

37. Babaeizadeh, M., Frosio, I., Tyree, S., Clemons, J., Kautz, J.: Reinforcement learning through asynchronous advantage actor-critic on a GPU. In: 5th Int Conf on Learning Representations, ICLR 2017 - Conference Track Proceedings (2017)

38. Sun, Y., Yuan, X., Liu, W., Sun, C.: Model-based reinforcement learning via proximal policy optimization. In: 2019 Chinese Automation Congress, CAC 2019, pp. 4736–4740 (2019)

39. Devraj, A.M., Kontoyiannis, I., Meyn, S.P.: Differential temporal difference learning. IEEE Trans. Autom. Control **66**(10), 4652–4667 (2021)

40. Coronato, A., Naeem, M., De Pietro, G., Paragliola, G.: Reinforcement learning for intelligent healthcare applications: a survey. Artif. Intell. Med. **109**, (2020). https://doi.org/10.1016/j.artmed.2020.101964

41. Yu, C., Liu, J., Nemati, S., Yin, G.: Reinforcement learning in healthcare: a survey. ACM Comput. Surv. **55**(1), 1–36 (2021)

42. Munguía-López, A.C., Ponce-Ortega, J.M.: Fair allocation of potential covid-19 vaccines using an optimization-based strategy. Process Integr. Optim. Sustain. **5**(1), 3–12 (2021)

43. Valizadeh, J., Boloukifar, S., Soltani, S., Jabalbarezi Hookerd, E., Fouladi, F., Andreevna Rushchtc, A., Du, B., Shen, J.: Designing an optimization model for the vaccine supply chain during the covid-19 pandemic. Expert Syst. Appl. **214**, (2023). https://doi.org/10.1016/j.eswa.2022.119009

44. Gedikli, T., Cayir Ervural, B.: Identification of Optimum COVID-19 Vaccine Distribution Strategy Under Integrated Pythagorean Fuzzy Environment. In: Lecture Notes in Mechanical Engineering (2022)

45. Zong, K., Luo, C.: Reinforcement learning based framework for COVID-19 resource allocation. Comput. Ind. Eng. **167**, 107960 (2022)

46. Faris, J.G., Orbidan, D., Wells, C., Petersen, B.K., Sprenger, K.G.: Moving the needle: Employing deep reinforcement learning to push the boundaries of coarse-grained vaccine models. Front. Immunol. **13**, (2022). https://doi.org/10.3389/fimmu.2022.1029167

47. Nguyen, Q.D., Prokopenko, M.: A general framework for optimising cost-effectiveness of pandemic response under partial intervention measures. Sci. Rep. **12**(1), 19482 (2022)

48. Bubar, K.M., Reinholt, K., Kissler, S.M., Lipsitch, M., Cobey, S., Grad, Y.H., Larremore, D.B.: Model-informed covid-19 vaccine prioritization strategies by age and serostatus. Science **371**(6532), 916–921 (2021)

49. Khandker, S.S., Godman, B., Jawad, M.I., Meghla, B.A., Tisha, T.A., Khondoker, M.U., Haq, M.A., Charan, J., Talukder, A.A., Azmuda, N., Sharmin, S., Jamiruddin, M.R., Haque, M., Adnan, N.: A systematic review on covid-19 vaccine strategies, their effectiveness, and issues. Vaccines **9**(12), 1387 (2021)

50. Ibrahim, D., Kis, Z., Tak, K., Papathanasiou, M.M., Kontoravdi, C., Chachuat, B., Shah, N.: Model-based planning and delivery of mass vaccination campaigns against infectious disease: application to the COVID-19 pandemic in the UK. Vaccines **9**(12), 1460 (2021)

51. Thul, L., Powell, W.: Stochastic optimization for vaccine and testing kit allocation for the covid-19 pandemic. Eur. J. Oper. Res. **304**(1), 325–338 (2023)
52. Kumar, A., Kumar, G., Ramane, T.V., Singh, G.: Optimal covid-19 vaccine stations location and allocation strategies. Benchmarking (2022). https://doi.org/10.1101/2020.12.31.20249099
53. Libotte, G.B., Lobato, F.S., Platt, G.M., Silva Neto, A.J.: Determination of an optimal control strategy for vaccine administration in covid-19 pandemic treatment. Comput. Methods Programs Biomed. **196**, (2020). https://doi.org/10.1016/j.cmpb.2020.105664
54. Feng, L., Xie, Y., Liu, B., Wang, S.: Multi-level credit assignment for cooperative multi-agent reinforcement learning. Appl. Sci. **12**(14), 6938 (2022)
55. Bastani, H., Drakopoulos, K., Gupta, V., Vlachogiannis, I., Hadjichristodoulou, C., Lagiou, P., Magiorkinis, G., Paraskevis, D., Tsiodras, S.: Efficient and targeted COVID-19 border testing via reinforcement learning. Nature **599**(7883), 108–113 (2021)
56. Chen, J., Chou, S.-Y., Yu, T.H.-K., Rizqi, Z.U., Hang, D.T.: System dynamics analysis on the effectiveness of vaccination and social mobilization policies for COVID-19 in the United States. PLOS ONE **17**(8), e0268443 (2022)
57. Belenguer, L.: AI bias: exploring discriminatory algorithmic decision-making models and the application of possible machine-centric solutions adapted from the pharmaceutical industry. AI Ethics **2**(4), 771–787 (2022)
58. Hardt, K., Schmidt-Ott, R., Glismann, S., Adegbola, R., Meurice, F.: Sustaining vaccine confidence in the 21st century. Vaccines **1**(3), 204–224 (2013)
59. Martin, K., Waldman, A.: Are algorithmic decisions legitimate? the effect of process and outcomes on perceptions of legitimacy of AI decisions. J. Bus. Ethics (2022)
60. Ilogu, L.C., Lugovska, O., Vojtek, I., Prugnola, A., Callegaro, A., Mazzilli, S., Van Damme, P.: The intent of students to vaccinate is influenced by cultural factors, peer network, and knowledge about vaccines. Hum. Vaccin. Immunother. **18**(1), 1938492 (2021)
61. Volpp, K.G., Loewenstein, G., Buttenheim, A.M.: Behaviorally informed strategies for a national covid-19 vaccine promotion program. J. Am. Med. Assoc. (JAMA) **325**(2), 125–126 (2021)
62. Foy, B.H., Wahl, B., Mehta, K., Shet, A., Menon, G.I., Britto, C.: Comparing covid-19 vaccine allocation strategies in India: a mathematical modelling study. Int. J. Infect. Dis. **103**, 431–438 (2021)
63. Tuite, A.R., Zhu, L., Fisman, D.N., Salomon, J.A.: Alternative dose allocation strategies to increase benefits from constrained covid-19 vaccine supply. Ann. Intern. Med. **174**(4), 570–572 (2021)
64. Ferranna, M., Cadarette, D., Bloom, D.E.: Covid-19 vaccine allocation: modeling health outcomes and equity implications of alternative strategies. Engineering **7**(7), 924–935 (2021)
65. Lemaitre, J.C., Pasetto, D., Zanon, M., Bertuzzo, E., Mari, L., Miccoli, S., Casagrandi, R., Gatto, M., Rinaldo, A.: Optimal control of the spatial allocation of covid-19 vaccines: Italy as a case study. PLoS Comput. Biol. **18**(7), (2022). https://doi.org/10.1371/journal.pcbi.1010237
66. Rolf, B., Jackson, I., Müller, M., Lang, S., Reggelin, T., Ivanov, D.: A review on reinforcement learning algorithms and applications in supply chain management. Int. J. Prod. Res., 1–29, (2022). https://doi.org/10.1080/00207543.2022.2140221
67. Scroggins, S., Goodson, J., Afroze, T., Shacham, E.: Spatial optimization to improve COVID-19 vaccine allocation. Vaccines **11**(1), 64 (2022)
68. Sallam, M.: COVID-19 vaccine hesitancy worldwide: a concise systematic review of vaccine acceptance rates. Vaccines **9**(2), 160 (2021)
69. Bernal, J., Mazo, C.: Transparency of artificial intelligence in healthcare: insights from professionals in computing and healthcare worldwide. Appl. Sci. **12**(20), 10228 (2022)
70. Hu, H., Xu, J., Liu, M., Lim, M.K.: Vaccine supply chain management: an intelligent system utilizing blockchain, IoT and machine learning. J. Bus. Res. **156**, 113480 (2023)
71. Heuillet, A., Couthouis, F., Díaz-Rodríguez, N.: Explainability in deep reinforcement learning. Knowl. Based Syst. **214**, 106685 (2021)

72. Sikstrom, L., Maslej, M.M., Hui, K., Findlay, Z., Buchman, D.Z., Hill, S.L.: Conceptualising fairness: three pillars for medical algorithms and health equity. BMJ Health Care Inform. **29**(1), e100459 (2022)
73. Wu, C., Qiao, T., Qiu, H., Shi, B., Bao, Q.: Individualism or collectivism: a reinforcement learning mechanism for vaccination decisions. Information **12**(2), 66 (2021)
74. Kwak, G.H., Ling, L., Hui, P.: Deep reinforcement learning approaches for global public health strategies for COVID-19 pandemic. PLOS ONE **16**(5), e0251550 (2021)
75. Moos, J., Hansel, K., Abdulsamad, H., Stark, S., Clever, D., Peters, J.: Robust reinforcement learning: a review of foundations and recent advances. Mach. Learn. Knowl. Extract. **4**(1), 276–315 (2022)
76. Demertzis, K., Taketzis, D., Tsiotas, D., Magafas, L., Iliadis, L., Kikiras, P.: Pandemic analytics by advanced machine learning for improved decision making of COVID-19 crisis. Processes **9**(8), 1267 (2021)
77. Liu, Y., Sandmann, F.G., Barnard, R.C., Pearson, C.A.B., Pastore, R., Pebody, R., Flasche, S., Jit, M.: Optimising health and economic impacts of COVID-19 vaccine prioritisation strategies in the WHO European region: a mathematical modelling study. Lancet Reg. Health Europe **12**, 100267 (2022)
78. Singh, V., Chen, S.-S., Singhania, M., Nanavati, B., Kar, A.K., Gupta, A.: How are reinforcement learning and deep learning algorithms used for big data based decision making in financial industries—a review and research agenda. Int. J. Inf. Manag. Data Insights **2**(2), 100094 (2022)
79. Lepri, B., Oliver, N., Pentland, A.: Ethical machines: the human-centric use of artificial intelligence. iScience **24**(3), 102249 (2021)
80. Swazinna, P., Udluft, S., Runkler, T.: Overcoming model bias for robust offline deep reinforcement learning. Eng. Appl. Artif. Intell. **104**, 104366 (2021)

Incorporating Contextual Information and Feature Fuzzification for Effective Personalized Healthcare Recommender System

Mohammed Wasid and Khalid Anwar

1 Introduction

Today, the advancements in information and communication technologies have paved the way for innovations and developments in several fields. In this context, recommender systems (RSs) are one of the efficient tools used for decision-making and information filtering in many real-world problems. In today's technology-aided world, RSs extract information from users' reviews and ratings to know their choices and sentiments and accordingly generate recommendations for them [1]. Recommender systems recommend everything from movies, news, books [2], songs, and websites to more personalized recommendations for matrimonial matches, job opportunities, healthcare service, etc. A typical recommender system is shown in Fig. 1.

Generally, recommender systems are categorized into three types depending on how recommendations are made [3]. Accordingly, content-based filtering (CB), collaborative filtering (CF), and hybrid filtering are recognized as the major filtering techniques of recommender systems. The CB technique utilizes items description and users' past preferences to recommend products. In contrast, the CF technique is based on the notion of the neighborhood and generates recommendations to the users by using the ratings of similar users who are known as neighbors. The CF technique is the most extensively used technique for designing the RSs, but it has certain issues like cold start and data sparsity. Similarly, the CB technique has issues like long tail, new user, and overspecialization. It means each recommendation

M. Wasid

Interdisciplinary Centre for Artificial Intelligence, Aligarh Muslim University, Aligarh, India

K. Anwar (✉)

Department of Computer Science, Aligarh Muslim University, Aligarh, India
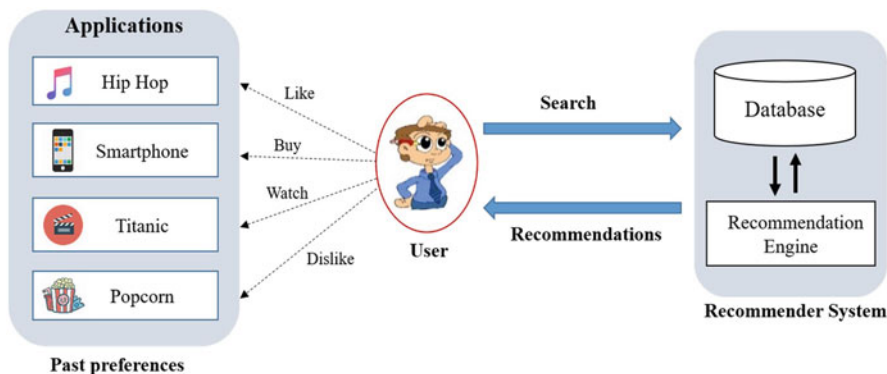
Fig. 1   A typical representation of a recommender system

technique has certain benefits and downsides. Therefore, to overcome the limitations of CB and CF techniques, hybrid filtering techniques are developed by combining different filtering techniques [4]. A typical recommender system uses any one or combination of techniques for making effective recommendations for the users [5].

In real-life scenarios, people are searching for pertinent health information about which they are worried. The Internet is a rich source of this information, but we must exercise caution if we do not want to obtain hazardous details. Health recommender systems (HRSs) are becoming a new trend for relevant health information as these systems recommend the most pertinent data based on the needs of the patient [6]. The primary objectives of HRS are to obtain reliable health information from the Internet, to analyze which is suited for the patient profile, to adapt their selection methods to the knowledge domain, and to learn from the best recommendations. Health recommendation systems are a viable alternative when it comes to offering tools to aid physicians with disease diagnosis, particularly during pandemics. During COVID-19, doctors were mainly concerned with the symptoms of the disease, as in some cases, the mild cold cough symptoms caused confusion about COVID-19. Therefore, if the symptoms of a disease can be identified correctly, then treatment can be given accordingly. Moreover, in any healthcare recommender system, it is necessary to identify the context associated with the disease, for example, whether the people are suffering from a disease in a particular season spring, summer, autumn, or winter. Similarly, weather conditions also play an important role, for example, sunny, rainy, stormy, snowy, or cloudy. Some diseases generally spread in rainy weather conditions.

RSs have a vital role in the health sector in terms of supporting individual health-related decision-making. The proposed approach is intended to build a recommendation framework for helping patients in the decision-making processes in healthcare services using a collaborative filtering technique. Health recommendation systems enhance the utility of technologies and decrease information overload.

2   Literature Review

Literature suggests that many recommender systems are designed in the healthcare domain for various purposes. Different applications of HRS are drug recommendation, food recommendation, healthcare service recommendation, and doctor recommendation by analyzing the health condition of an individual. In the past, drug recommender systems were developed to reduce the human error involved in medicine prescriptions to patients. The drug RS helps doctors identify and recommend more accurate medicine by analyzing the historical records of the patients [7]. Many researchers have developed the drug RS for specific diseases. For example, authors in [8] applied a multi-criteria decision-making approach to patient oncology and developed an anti-diabetic drug recommendation approach. On the other hand, [9] used ontologies to describe information regarding patient characteristics and anti-diabetes drugs. In addition to combining ontologies with rule-based decision-making, this system imposes constraints on treatment goals and dosage prescriptions. The established rules recommend medications for each patient according to their characteristics.

Authors in [10] developed a RS that enables physicians to search for pharmacological information and recommends medications to patients depending on their condition, allergies, and previous drug interactions. This RS stores drug-related rules and interactions using ontologies and ICD codes. These rules are the inputs that the RS uses to develop the best appropriate medications for patients. Similarly, authors in [11] developed a semantic framework known as PANACEA to aid physicians in prescribing pharmaceuticals based on the indications of the drugs' active substances. PANACEA makes drug recommendations based on standardized medical terminologies and criteria controlling drug-drug and drug-disease interactions. In another study, authors in [12] developed a drug recommender system that would assist physicians in recommending more appropriate and precise prescriptions for migraine-disease patients. In this RS, the information about patients is stored in a graph database. Nodes and edges structure the database. Nodes represent information about patients, allergies, diseases, and medications, whereas the relationships between these nodes are shown using edges.

Moreover, a collaborative filtering technique was used to develop a RS that predicts the risk factors for a patient with chronic disease [13]. In contrast, authors in [14] developed a hybrid recommender system by combining CB and CF techniques for recommending workout sessions based on historical behaviors, preferences, and physical condition of individuals. Similarly, authors in [15] developed iDoctor, which is a personalized RS for recommending doctors to an individual based on their sentiments. The RS analyzes the ratings and reviews of the users to explore their feelings and sentiments, and preferences. The RS consists of three modules: topic modeling, sentiment analysis, and hybrid matrix factorization. The sentiment analysis module computes the emotional offset of user testimonials. The topic modeling module collects user preferences and doctor characteristics based on user ratings (e.g., prescribing behavior, specialty, and fee range). The collected data is

utilized by the module for hybrid matrix factorization in order to compute doctors' ratings and recommend the doctor accordingly.

In another study, authors in [16] designed a HRS framework for monitoring and self-assessment during the isolation of COVID-19. The HRS also recommends medicine and self-care measures during the isolation period based on the symptoms of the patient. The HRS was trained by taking the data of people who suffered from COVID in the past. The HRS was based on the CF technique and used Pearson correlation for computing the similarities. Similarly, authors in [17] developed a HRS that computes the similarities between COVID-19 patients based on the X-ray images of their chests. The HRS recommends health resources like doctors and medicine to patients who are infected with COVID-19 by analyzing the medical history of similar patients. While authors in [18] developed a drug recommender system for patients suffering from infectious diseases, the RS takes different symptoms of the patients as input, find similar patients from the database, and accordingly recommends the drugs to the patients. The HRS is highly efficient and effective in recommending drugs to patients suffering from infectious diseases by ensuring the safety of other patients and health workers.

By going through the above-discussed studies, we analyze that healthcare systems are being developed using various intelligent techniques. However, most of these studies do not consider similar patients based on their historical health records, and also situational or contextual cases have not been explored to the best of our knowledge.

3   Proposed Recommendation Framework

The prime motive of a framework is to stimulate the process of completing the assigned task successfully and establish a better understanding of the main components or phases of the recommendation process. There are following three phases in our recommendation framework, as shown in Fig. 2.

- *Phase 1* – Patient Profile Formation
- *Phase 2* – Similarity Computation and Neighborhood Set Formation
- *Phase 3* – Prediction and Recommendations

3.1   *Phase 1 – Patient Profile Formation*

The patient profile is basically a collection of the patient's personal information, which may be referred to as a simplified model of the patient. A patient may be modeled based on the type and amount of patient-specific information stored in the patient profile. The majority of prior work on patient profile modeling relied solely on overall ratings [19]. These methods fail while dealing with diverse
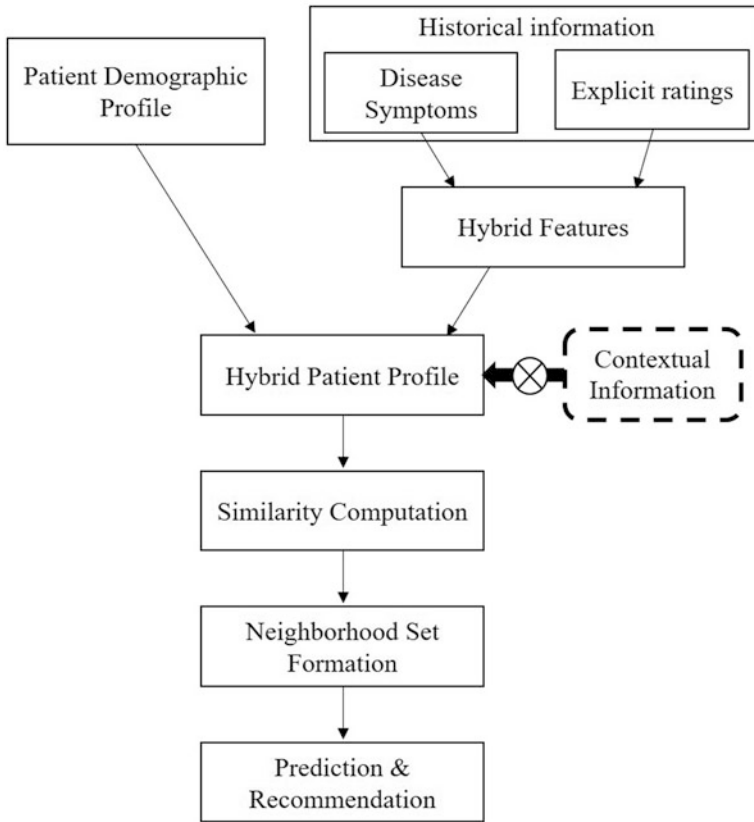
Fig. 2 Block diagram of the proposed recommendation framework

Table 1 Typical profile of a patient

Rating	Age	Gender	Occupation	Symptoms presence	Contextual factor			
4	30	Male/0	Teacher/19	00110000000010010	*Crc1*	*Crc2*	*Crc3*	*Crc4*

information, such as demographic data and situation-related information. Therefore, this phase ensures that all information should be considered for building a patient profile, which is used for computing similarity. A representative patient profile would properly reflect the patient's history, preferences, and records in every aspect. Table 1 depicts a patient profile having demographic features of the patient, and the total number of symptoms shown in the patient is represented by "1s."

For better understanding, we consider Table 2 of only three patients who have suffered from multiple diseases based on four symptoms. In columns S_i, $i = 1, 2, 3, 4$, one (1) indicates the symptom present in the patient, and 0 otherwise. Also, a non-zero value in the patient rating columns specifies the level (1 – low, 5 – very

Table 2 Example dataset for patient-disease ratings

Disease	Corresponding symptoms				Patient ratings		
	S_1	S_2	S_3	S_4	Patient 1	Patient 2	Patient 3
1	1	0	1	0	1	3	0
2	0	0	1	0	5	2	4
3	1	1	0	1	0	1	3
4	0	1	0	1	4	0	3
5	1	0	1	0	0	0	4
6	0	0	1	1	2	5	0
7	1	1	1	0	0	0	2
8	1	0	0	1	0	3	3
9	0	1	1	0	1	5	3
10	0	1	0	0	0	3	3

high) by which the patient has suffered from that disease, and zero indicates that the patient has not suffered from that disease.

In order to identify the seriousness of a disease in a patient, we need to identify those symptoms which are the most affecting the health of a patient. Based on the genre interestingness measure [20], we created a disease seriousness measure (DSM) which considers various symptoms s of the patient p on multiple diseases.

$$DSM(p, s) = \frac{2 \times nf \times RDR(p, s) \times MRDC(p, s)}{RDR(p, s) + MRDC(p, s)}, \tag{1}$$

where MRDC denotes the modified relative disease count of symptoms s for patient p and considers only those diseases which have rating values 3, 4, and 5. The MRDC can be computed using the following equation:

$$MRDC(p, s) = \frac{\sum_{d \in D_j \subset C_i} \Omega_3\left(r_{p,d}\right) + 2 \times \Omega_4\left(r_{p,d}\right) + 3 \times \Omega_5\left(r_{p,d}\right)}{3 \times TC(p)}, \tag{2}$$

While the Relative Disease Rating (RDR) only considers diseases with ratings of 2 or higher and the total number of ratings (TR) provided by the patient.

$$RDR(p, s) = \frac{\sum_{d \in D_j \subset C_i \geq 3} r_{p,d}}{TR(p)}, \tag{3}$$

In Eq. (1), nf is used for normalizing purpose. In this work, the maximum rating in the system is selected as the value of nf, and it can also be selected as the global average rating ($TR(p)/TC(p)$), where total count (TC) refers to the total number of diseases the patient has diagnosed with.

Moreover, age and DSM have been identified as fuzzy features in order to address the uncertainty associated with them. Old, middle-aged, and young are the three

fuzzy sets derived from the "age" attribute after fuzzification [21]. The membership functions of these fuzzy sets are as follows.

$$Young\ (z) = \begin{cases} 1, & z \le 20, \\ (35 - z)\,/15, & 20 < z \le 35, \\ 0, & z > 35, \end{cases} \tag{4a}$$

$$Middle\ (z) = \begin{cases} 0, & z \le 20,\ z > 60, \\ (z - 20)\,/15, & 20 < z \le 35, \\ 1, & 35 < z \le 45, \\ (60 - z)\,/15, & 45 < z \le 60, \end{cases} \tag{4b}$$

$$Old\ (z) = \begin{cases} 0, & z \le 45, \\ (z - 45)\,/15, & 45 < z \le 60, \\ 1, & z > 60, \end{cases} \tag{4c}$$

On the basis of the severity of the disease, the DSM can also be classified into six fuzzy sets, namely, very bad (VB), bad (B), average (A), good (G), very good (V), and excellent (E). Equation (5) shows their corresponding membership functions [20].

$$VB(z) = \begin{cases} 1 - z, & z \le 1, \\ 0, & z > 1, \end{cases} \tag{5a}$$

$$T_{(y)}(z) = \begin{cases} 0, & z \le y - 2,\ z > y, \\ z - y + 2, & y - 2 < z \le y - 1, \\ y - z, & y - 1 < z \le y, \end{cases} \tag{5b}$$

where $T_{(y)}$ depicts the bad, average, good, and very good for each $y = 2, 3, 4$, and 5, respectively.

$$E(z) = \begin{cases} 0, & z \le 4, \\ z - 4, & 4 < z \le 5, \end{cases} \tag{5c}$$

After applying DSM and fuzzy operations to the attributes in Table 1, Table 3 displays the patient profile. Let us assume DSM is 2.80 for the sake of conceptual understanding.

Table 3 Patient profile after applying DSM and fuzzification

	Age			Disease seriousness measure					
Quantifier	Young	Middle	Old	Very bad	Bad	Average	Good	Very good	Excellent
Membership value	0.733	0.267	0	0	0	0.2	0.8	0	0

Now, we identified four different contextual variables to be incorporated into the patient profile to make situational health recommendations. A concise context variable can be written as $Cv\{at_1, at_2, at_3, \ldots, at_m\}$, where m is the number of attributes the context variable C_v is associated with. For example, SEASON {Spring, Summer, Autumn, Winter} has four different attributes. Now, we apply the following contextual rating count $CRC(x,y)$ method to find the normalized count for the attribute y of context x.

$$CRC\,(x,\,y) = \frac{\sum_{d \in m}^{|D|} r_{d,y}}{|\,D\,|},$$ (6)

where $r_{n,\,y}$ shows the historical rating count of attribute y for the disease d, and D is the number of diseases a patient is infected with.

In the same way, profiles of all patients can be created, which are then used in the similarity computation and neighborhood set (similar patients) formation phase.

3.2   Phase 2 – Similarity Computation and Neighborhood Set Formation

Having built a patient profile, RSs match the active patient to the available database according to a suitable similarity measure. According to the computed similarity values, the relationship between the active patient and with remaining patients is established, which enables RSs to form a neighborhood set for the active patient. The selection of a similarity measure is application-dependent and actually based on the nature of the patient profile features [22]. Some modifiers to the similarity function have also been introduced to refine or enhance the ability of the recommender system to find close neighbors [23].

Once patient profiles are generated, the RS computes the similarity among the patient profiles to form the neighborhood sets using the modified Euclidean global fuzzy distance formula.

$$Gfd\,(P,\,Q) = \sqrt{\sum_{k=1}^{z} Lfd(p_k, q_k)^2 + \sum_{l=1}^{c} dis\,(p_l, q_l)},$$ (7)

where P and Q are the profile vector of length z, and c is the number of contextual variables. Lfd is the local fuzzy distance and is computed as

$$Lfd\,(p_k, q_k) = dis\,(p_k, q_k) \times d\,(p_k, q_k),$$ (8)

where $d(p_k, q_k)$ represents the difference between vectors p and q. The size of the vectors is m, and $dis(p_k, q_k)$ is the Euclidean distance which can be calculated using the following equation:

$$dis\,(p_k, q_k) = \sqrt{\sum_{e=1}^{m} \left(p_{k,e} - q_{k,e}\right)^2}, \tag{9}$$

where $p_{k,e}$ denotes the membership value of the kth feature in the eth fuzzy set.

After computing, the similarity between the active patient and other patients in the system, the neighbors of the active patient can be identified. The top-N patients or the patients whose similarity is greater than a certain threshold could be chosen to fix the neighborhood set's size [24].

3.3   Phase 3 – Prediction and Recommendations

In the phase above, after obtaining the neighborhood set, the RS predicts the rating of the unseen patient p based on the average ratings of the patients who are present in the neighborhood set. The active patient's medication is collectively prescribed by the patients in the neighborhood set. The following formula is used to calculate the patient's predicted rating, $Pre_{p,d}$ for disease d.

$$pre_{p,d} = \bar{r}_p + N_f \sum_{q \in N} Gfd\,(P, Q) \times \left(r_{q,d} - \bar{r}_q\right), \tag{10}$$

$Gfd(P,Q)$ is the similarity/distance between active patient p and neighborhood patient q. $\bar{r}_p$ is the average of the ratings made by patient p to all diseases. The multiplier N_f is a normalizing factor and is usually defined as

$$N_f = \frac{1}{\sum_{q \in N} |\,Gfd\,(P, Q)\,|} \tag{11}$$

The weighted sum (Eq. 10), which is also called Resnick's prediction formula [25], is an extensively used prediction function. Because patients usually vary in their use of rating scales, Resnick's prediction formula compensates for rating scale variations. This will keep predicted ratings for a given patient to fall around the mean rating of a given active patient.

4   Experiments and Results

We chose to run our tests on the LDOS-CoMoDa dataset because it is well known in the recommendation field even though, as far as we are aware, there is no data available regarding patients' historical ratings of the disease with contextual variables.

4.1 Experimental Settings

The experiments were performed on the LDOS-CoMoDa dataset. The dataset was pre-processed and only those patients were extracted who have recorded at least 5 ratings. The refined dataset thus left with 48 patients and 1144 diseases with 1964 ratings. From the pre-processed dataset, we have generated ten random experiment sets. For each random experiment set, 5 patients were chosen randomly as active patients and the remaining 43 patients as training. Such a random separation was intended to perform extensive experiments, where all the experiments are repeated ten times, once with each experiment set. These experiment sets are referred to as experiment set-1, experiment set-2, . . . , and experiment set-10. The entire ratings were randomly divided into training (66%) and testing (34%) sets. The training set was used to find a set of neighbors for each patient, while the test set was used to test the performance of the RS. The top 20 most similar neighbors were selected as a neighborhood set. Overall, many experiments were conducted to compare the performance of the following approaches.

- *Pearson Recommender System (PRS)* – uses Pearson correlation measure for identifying similar patients.
- *Fuzzy Recommender System (FRS)* – uses a modified fuzzy distance method for identifying similar patients.
- *Context-Aware Fuzzy RS (CFRS)* – incorporates contextual features {Season, Location, Weather, Mood} in FRS using a contextual rating count approach.

4.2 Experimental Results and Discussion

The MAE, RMSE, and coverage for all ten experiment sets for the examined methods are presented and discussed in this section. Results presented in Tables 4 and 5 show that CFRS outperforms PRS and FRS for all ten experiment sets in terms of MAE and RMSE, respectively. Both FRS and CFRS are developed using collaborative filtering techniques with using additional user-item information and fuzzy logic.

Results presented in Table 6 give coverage of different recommendation methods for all ten experiment sets. The coverage value of CFRS is always higher than the PRS and FRS approaches for all ten experiment sets. The high coverage of the RS indicates the effectiveness of the proposed approach.

From the above-presented results, we found that the contextual recommender system always shows better performance than the PRS and FRS in terms of MAE, RMSE, and coverage.

We have compared the examined methods based on each experiment set, but in reality, the final effectiveness of a RS depends on its overall ability to generate effective recommendations. Therefore, Figs. 3, 4, and 5 depicts the graphical representation of the complete systems MAE, RMSE, and coverage, respectively. From

Table 4 Performance comparison of PRS, FRS, and CFRS in terms of MAE

Experiment set no.	PRS	FRS	CFRS
1	0.8447	0.5657	0.51
2	0.9087	0.534	0.493
3	0.9843	0.7857	0.7581
4	0.9944	0.6306	0.54
5	1.481	1.3059	0.9963
6	1.4636	1.3546	0.9969
7	0.6522	0.6422	0.621
8	0.8347	0.6574	0.5543
9	1.3091	0.9639	0.9078
10	1.2015	1.1107	0.954
Average	*1.0674*	*0.8550*	*0.7331*

Table 5 Performance comparison of PRS, FRS, and CFRS in terms of RMSE

Experiment set no.	PRS	FRS	CFRS
1	1.0955	0.6939	0.6402
2	1.0714	0.6919	0.6774
3	1.0078	0.9076	0.8856
4	1.2626	0.7938	0.7522
5	1.8696	1.3681	1.254
6	1.8758	1.8389	1.398
7	0.8007	0.7918	0.789
8	1.2033	0.7725	0.7201
9	1.735	1.2476	1.1211
10	1.422	1.3416	1.1966
Average	*1.3343*	*1.0447*	*0.9434*

Table 6 Performance comparison of PRS, FRS, and CFRS in terms of coverage

Experiment set no.	PRS	FRS	CFRS
1	0.3576	0.3793	0.4772
2	0.381	0.4062	0.4821
3	0.3102	0.3119	0.3554
4	0.5284	0.5323	0.541
5	0.5217	0.5072	0.5587
6	0.3125	0.25	0.3644
7	0.4286	0.4286	0.4663
8	0.4432	0.4462	0.6533
9	0.3415	0.3415	0.367
10	0.479	0.3902	0.4889
Average	*0.41037*	*0.39934*	*0.47543*

Fig. 3, we can infer that the contextual recommender system (CFRS) significantly outperforms compared to PRS and FRS in terms of MAE. Similarly, Fig. 4 compares the overall performance of all examined approaches in terms of RMSE.

Figure 5 shows the superiority of CFRS in terms of coverage compared to other approaches with notable margin. Moreover, the FRS method exposed improved
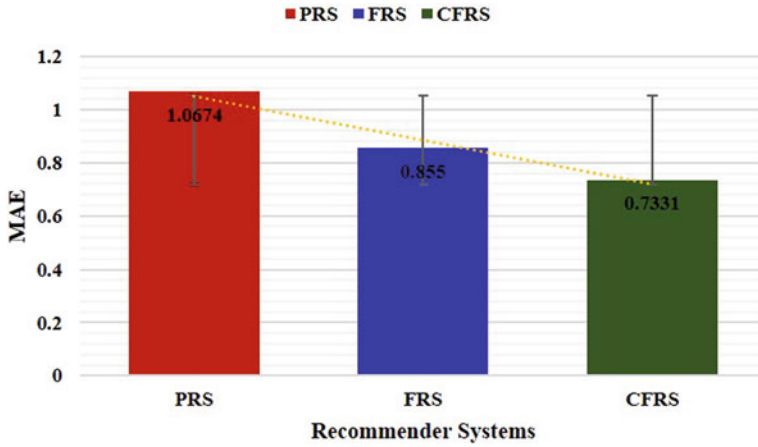
Fig. 3 Comparison of different RS on the basis of the average MAE of ten experiment sets
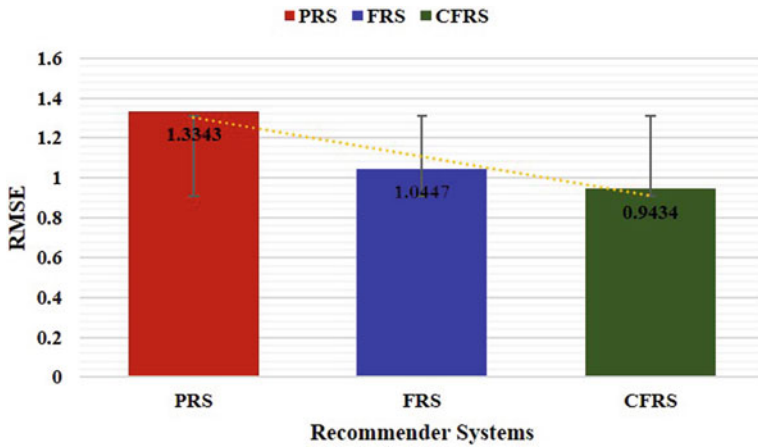

Fig. 4 Comparison of different RS on the basis of average RMSE of ten experiment sets

MAE and RMSE than PRS method, but it fails to maintain its superiority in terms of coverage of the system.

Overall, the results presented above reveal that the context-aware recommender system-based method has better performance in terms of MAE, RMSE, and coverage. Results also proved that the contextual features play an important role in enhancing the effectiveness of RS.
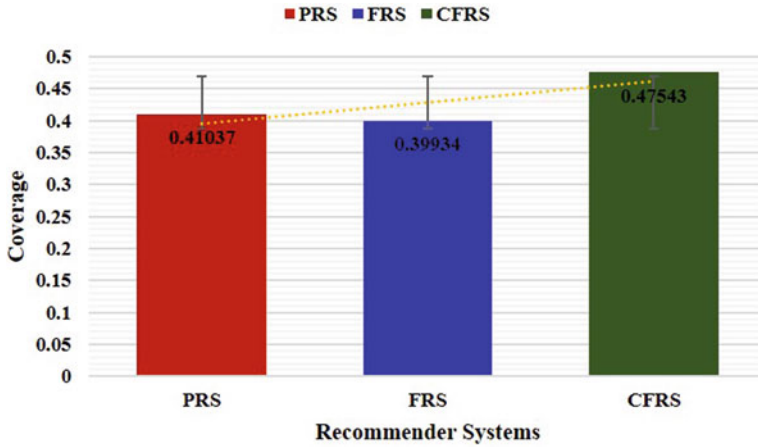
Fig. 5 Comparison of different RS on the basis of average coverage of ten experiment sets

5 Conclusion

The developed HRS framework is intended to enhance interaction by giving the patient better health-related recommendations. Increased user interaction and increased convenience are the direct benefits of providing just relevant recommendations. The framework for recommendations is based on patient data, and collaborative filtering is used to discover patients with comparable symptoms for certain health-related conditions. Hence, similar medications can be recommended to patients depending on their medical histories. A fuzzy set has been introduced to address the issue of ambiguity connected with a patient's condition and illness characteristics, and it has been utilized to create hybrid patient profiles. This enables patients to determine the most similar neighborhood for a more accurate recommendation. The experimental results demonstrate the importance of incorporating contextual information for enhancing the effectiveness in terms of MAE with a 46% improvement, RMSE with a 41% improvement, and coverage prediction accuracy with a 14% improvement. By observing the results, we can say that the patient modeling using diverse information improved the performance as the chosen data was highly sparse where disease ratings were relatively low compared to the total number of diseases. In future, the proposed framework can be tested on a real-world healthcare dataset with multimodal features, and one can extend it by designing the appropriate fuzzy sets for the contextual variables.

References

1. Bobadilla, J., Ortega, F., Hernando, A., Gutiérrez, A.: Recommender systems survey. Knowl. Based Syst. **46**, 109–132 (2013). https://doi.org/10.1016/j.knosys.2013.03.012
2. Anwar, K., Siddiqui, J., Sohail, S.S.: Machine learning-based book recommender system: a survey and new perspectives. Int. J. Intell. Inf. Database Syst. **13**, 231–248 (2020)
3. Adomavicius, G., Tuzhilin, A.: Toward the next generation of recommender systems: a survey of the state-of-the-art and possible extensions. IEEE Trans. Knowl. Data Eng. **17**, 734–749 (2005). https://doi.org/10.1109/TKDE.2005.99
4. Sohail, S.S., Siddiqui, J., Ali, R.: Classifications of recommender systems: a review. J. Eng. Sci. Technol. Rev. **10**, 132–153 (2017). https://doi.org/10.25103/jestr.104.18
5. Anwar, K., Siddiqui, J., Saquib Sohail, S.: Machine learning techniques for book recommendation: an overview. SSRN Electron. J., 1291–1297 (2019). https://doi.org/10.2139/ssrn.3356349
6. Yang, S., Zhou, P., Duan, K., et al.: emHealth: towards emotion health through depression prediction and intelligent health recommender system. Mob. Netw. Appl. **23**, 216–226 (2018). https://doi.org/10.1007/s11036-017-0929-3
7. Tran, T.N.T., Felfernig, A., Trattner, C., Holzinger, A.: Recommender systems in the healthcare domain: state-of-the-art and research issues. J. Intell. Inf. Syst. **57**, 171–201 (2021). https://doi.org/10.1007/s10844-020-00633-6
8. Chen, R.C., Chiu, J.Y., Batj, C.T.: The recommendation of medicines based on multiple criteria decision making and domain ontology – an example of anti-diabetic medicines. Proc. Int. Conf. Mach. Learn. Cybern. **1**, 27–32 (2011). https://doi.org/10.1109/ICMLC.2011.6016682
9. Mahmoud, N., Elbeh, H.: IRS-T2D: individualize recommendation system for type2 diabetes medication based on ontology and SWRL. In: International Conference on Informatics and Systems, INFOS 2016 ACM International Conference Proceeding Series, pp. 203–209. Association for Computing Machinery (2016). https://doi.org/10.1145/2908446.2908495
10. Doulaverakis, C., Nikolaidis, G., Kleontas, A., Kompatsiaris, I.: GalenOWL: ontology-based drug recommendations discovery. J. Biomed. Semantics. **3**, 14 (2012). https://doi.org/10.1186/2041-1480-3-14
11. Doulaverakis, C., Nikolaidis, G., Md, A.K., Kompatsiaris, I.: Panacea, a semantic-enabled drug recommendations discovery framework. CEUR Workshop Proc. **1061**, 1–6 (2013)
12. Stark, B., Knahl, C., Aydin, M., et al.: BetterChoice: a migraine drug recommendation system based on Neo4J. In: 2017 2nd IEEE International Conference on Computational Intelligence and Applications (ICCIA), pp. 382–386. IEEE (2017). https://doi.org/10.1109/CIAPP.2017.8167244
13. Nasiri, M., Minaei, B., Kiani, A.: Dynamic recommendation: disease prediction and prevention using recommender system. Int. J. Basic Sci. Med. **1**, 13–17 (2016). https://doi.org/10.15171/ijbsm.2016.04
14. Dharia, S., Jain, V., Patel, J., et al.: PRO-Fit: a personalized fitness assistant framework. Proc. Int. Conf. Softw. Eng. Knowl. Eng. SEKE, 386–389 (2016). https://doi.org/10.18293/SEKE2016-174
15. Zhang, Y., Chen, M., Huang, D., et al.: iDoctor: personalized and professionalized medical recommendations based on hybrid matrix factorization. Futur. Gener. Comput. Syst. **66**, 30–35 (2017). https://doi.org/10.1016/j.future.2015.12.001
16. Othman, M., Muhd Zain, N., Paidi, Z., Pauzi, F.A.: Framework of health recommender system for COVID-19 self-assessment and treatments: a case study in Malaysia. Int. J. Comput. Sci. Netw. Secur. **21**, 12 (2021)
17. Kuanr, M., Mohapatra, P., Mittal, S., et al.: Recommender system for the efficient treatment of COVID-19 using a convolutional neural network model and image similarity. Diagnostics. **12**, 2700 (2022). https://doi.org/10.3390/diagnostics12112700
18. Bhimavarapu, U., Chintalapudi, N., Battineni, G.: A fair and safe usage drug recommendation system in medical emergencies by a stacked ANN. Algorithms. **15**, 1–11 (2022). https://doi.org/10.3390/a15060186

19. Duan, L., Street, W.N., Xu, E.: Healthcare information systems: data mining methods in the creation of a clinical recommender system. Enterp. Inf. Syst. **5**, 169–181 (2011). https://doi.org/10.1080/17517575.2010.541287
20. Al-shamri, M.Y.H., Bharadwaj, K.K.: Fuzzy-genetic approach to recommender systems based on a novel hybrid user model. Expert Syst. Appl. **35**, 1386–1399 (2008). https://doi.org/10.1016/j.eswa.2007.08.016
21. Klir, G.J., Yuan, B.: Fuzzy Sets and Fuzzy Logic: Theory and Applications. Prentice Hall PTR, Upper Saddle River (1996)
22. Wasid, M., Ali, R.: Multi-criteria clustering-based recommendation using Mahalanobis distance. Int. J. Reason. Intell. Syst. **12**, 96–105 (2020). https://doi.org/10.1504/IJRIS.2020.106803
23. Al-Shamri, M.Y.H.: Similarity modifiers for enhancing the recommender system performance. Appl. Intell. **52**, 8534–8550 (2022). https://doi.org/10.1007/s10489-021-02900-7
24. Wasid, M., Ali, R.: A frequency count approach to multi-criteria recommender system based on criteria weighting using particle swarm optimization. Appl. Soft Comput. **112**, 107782 (2021). https://doi.org/10.1016/j.asoc.2021.107782
25. Resnick, P., Iacovou, N., Suchak, M., et al.: GroupLens: an open architecture for collaborative filtering of netnews. In: CSCW '94: Proceedings of the 1994 ACM Conference on Computer Supported Cooperative Work, pp. 175–186. ACM Press, New York (1997)

Prediction of Growth and Review of Factors Influencing the Transmission of COVID-19

Gyanendra K. Verma

1 Introduction

Coronavirus (SARS-CoV-2) broke out in China. It caused 1,521,252 confirmed contamination cases and 92,798 deaths as of April 10, 2020 (Fig. 1). The World Health Organization (WHO) declared COVID-19 a pandemic on March 11, 2020 due to the alarming spread of infection in more than 113 countries. COVID-19 is a member of a family of enveloped, non-segmented, positive series RNA viruses widely distributed in the clan of mammals, humans, and animals collectively known as the corona. Four of its ancestors have become mild to the extent that they merely cause the symptom of cough and cold. SARS, a severe acute respiratory disease caused by a coronavirus strain, first appeared in 2003. SARS peaked in the winter and began to subside in the summer.

The influenza season typically lasts from the start of October until the end of spring. Consequently, SARS did not deviate from the seasonal trend of influenza. Hence, it is partially known to our race. However, with an overall mortality rate of about 2%, COVID-19 is too mistaken to be one of the lines. The cause of concern is its infectiousness; its exponential spread makes it a genuine health hazard to the globe.

Certain studies [2–4] have created the perception that COVID-19 cannot survive in high temperatures. Hence, there is some misplaced pleasure that with the rise of mercury in months to come in India and similar tropical countries, and it will become self-limiting. We are afraid that this shifting sand of expectation may cause tragic consequences.

G. K. Verma (✉)
Department of Information Technology, National Institute of Technology Raipur, Raipur, India
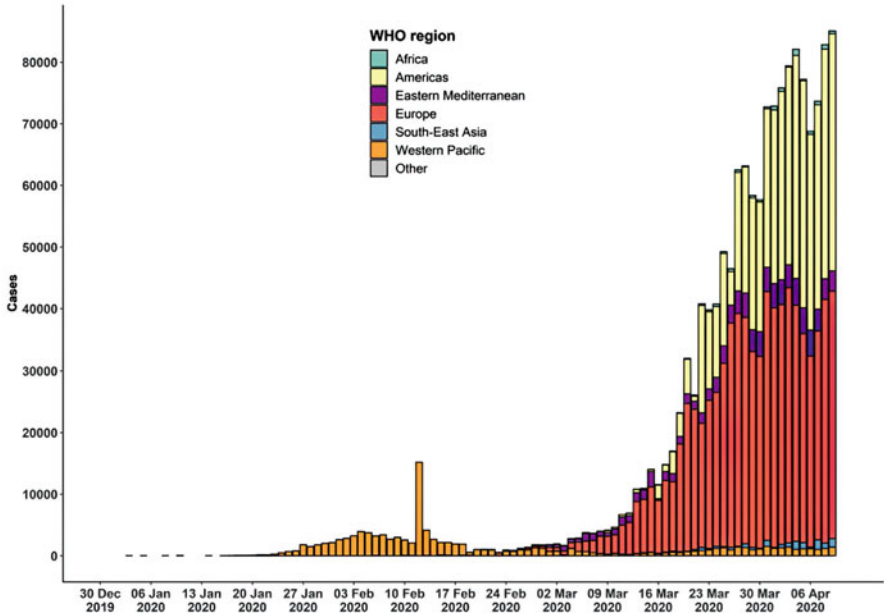e-mail: gkverma.it@nitrr.ac.in

Fig. 1 Globally confirmed case of COVID-19 as of now 10th April 2020 [1]

This endeavors to predict the likely infected cases and fatalities for different population sizes based on mathematical modeling with various permutations. Furthermore, we have reviewed the following factors influencing the transmission of COVID-19:

– Effect of temperature and humidity
– Effect of social distancing
– Effect of population density
– Effect of air pollution
– Other factors

Our submission is that even if high temperature and humidity dampen the reproductive ratio, it has no consequence on the transmission of COVID-19. On the contrary, social distancing is an effective measure to reduce the transmission of COVID-19. The aspect of various modes of social distancing remains unexplored.

The key contributions of this chapter are outlined below:

1. We have formulated the prediction of the exponential growth of infected cases of COVID-19 based on two parameters.
2. A detailed report on COVID-19 prediction methods based on Computational Intelligence is presented.

3. We have also reviewed the effect of temperature, humidity and social distancing, air pollution, population density, and other factors responsible for the spread of COVID-19.
4. The model is significant in reducing the transmission of COVID-19.

The rest of the chapter is organized as follows. In Sect. 2, we reviewed three factors influencing the transmission of COVID-19. A mathematical model is proposed in Sect. 3. Section 4 is dedicated to results, analysis, and discussions. We have summarized the findings in Sect. 5.

2 Review: Factors Influencing the Transmission of COVID-19

2.1 Effect of Temperature and Humidity

There are studies [5, 6] assigning the significant effect of temperature and humidity on the transmission of COVID-19. As per Fig. 2, the outbreak region of COVID-19 worldwide has been limited to a narrow east–west strip along 30–50 N approximately. The temperature and humidity in the very region range from 5–11°C and 47–79%, respectively. During the same period, the spread of COVID-19 is limited to countries adjacent to South China. The number of infected cases and the death toll are reported less in these adjacent regions. Mao Wang claims [5] that a 1°C rise in the average temperature (minimum and maximum) diminishes the infection by 0.83. At the same time, the cumulative number is decreased by a factor of 0.86 on a 1°C increase in minimum temperature in the single-factor model. Neeltje van Doremalen et al. [5] analyzed the aerosol and surface stability of HCoV-19 and found that COVID-19 can be viable in aerosols even after 3 h with reduced infectivity at room temperature. The stability of the same virus in plastic and steel is up to 72 h. K. H. Chan [2] reported the infectivity of SARS CoV (SARS coronavirus) was lost after heating at 56°C for 15 min. Araujo M. B. et al. [6] reported significant correlations between temperature and humidity and the outbreak of COVID-19. They established an inverse relationship between the incidence of coronavirus and humidity as SARCCoV incidences diminish quickly with the increase in temperature from 15°C to 29°C.

COVID-19 has a good chance of long-term survival in subtropical nations like Malaysia, Indonesia, and Thailand due to the favorable environmental conditions. The virus can remain infectious for up to two weeks in low-humidity environments, which could aid in the spread of the disease in a community like Hong Kong, which is located in a subtropical climate. We can see the increase in the temperature in April–June 2020 in subtropical regions. It is predicted that the number of infected cases will significantly increase in the coming days. In the meantime, the graph increases if we correlate the number of infected cases with the temperature. It clearly
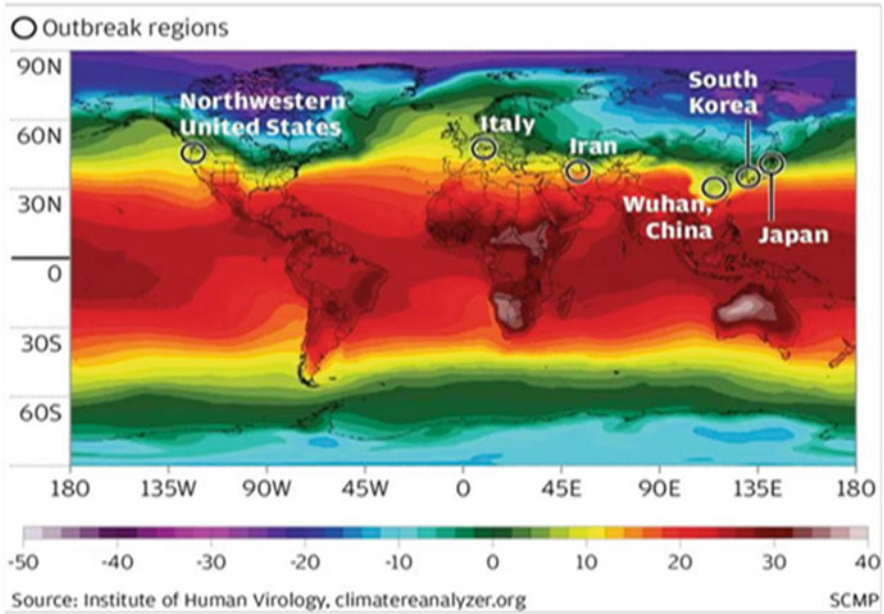
Fig. 2 COVID-19 outbreak regions [adopted from 9]

shows that the growth factor is increasing due to the physical interaction of a person with the infected person.

2.2 Effect of Population and Social Distancing

Their preventive measures, such as social distancing, may significantly influence the transmission of the COVID-19 pandemic. Social distancing removes all social contact with people in public areas. A complete social distancing is impossible, as people need various commodities for livelihood. The authorities can impose a complete or a partial lockdown to isolate contact among people. A report on Coronavirus [7] states that around 20% of the global population is under coronavirus lockdown.

The impact of social distancing depends upon the following factors:

1. How many infected people exhibit symptoms and whether they isolate themselves
2. The timing of isolation following the appearance of symptoms
3. The length of the infectious period prior to the onset of apparent symptoms

Early self-isolation for social distancing is vital if the symptoms are not severe [8]. These factors are linked to the transmission of COVID-19. A large number of coun-

tries imposed lockdowns to ban mass gatherings. For effective implementation, they also seal borders at providences and district levels. However, it seems ineffective as the supplies of essential articles are continued, and people need to obey the government's instructions in many places. A new high is likely if restrictions are eased after a few months to prevent a severe economic impact. These significant problems are to blame for the rapidly increasing frequency of COVID-19 infections.

2.3   Effect of Population Density

The pandemic's ability to spread is strongly influenced by population density. It measures the average number of people residing in an area of one kilometer (Number of persons/km^2) [9]. The more the population density, the faster diseases can spread. One crucial aspect affecting a location's susceptibility to the virus is likely population density. COVID-19 has spread over the world and has had a significant impact on a variety of venues. One kind is defined by sizable, crowded, superstar cities like New York and London, which draw massive numbers of tourists, have a diverse worldwide population, and have dense residential districts. A second category comprises industrial hubs linked by supply chains, such as Wuhan, Detroit, and Northern Italy. A third category includes popular tourist destinations worldwide, such as the ski resorts in France, Switzerland, and Italy. The virus has attacked nursing homes for the elderly, cemeteries, and offshore cities.

2.4   Effect of Air Pollution

Air pollution is one type of environmental pollution caused due to the presence of harmful particles and gases. Carbon dioxide, Carbon monoxide, and Sulfur oxide are significant contributors to air pollution. Before the COVID-19 pandemic in 2020, CO_2 emissions increased roughly 1% yearly. By early April 2020, daily worldwide CO_2 emissions were 17% (11 to 25%) lower than the mean levels of 2019, with decreases in surface transport responsible for just under half of this effect. When emissions were at their lowest, the average for each country fell by 26% [10].

2.5   Effect of Other Factors

Humans are impacted by the altitudes as well. People who live at higher altitudes are exposed to more sunlight, which is the primary source of vitamin D. Vitamin D is crucial for controlling innate and adaptive immune responses beyond its roles in maintaining bone and calcium homeostasis [11]. However, as the altitude rises,

atmospheric pressure falls, and oxygen in the air drops [12]. Above 2400 m, a lack of oxygen can worsen respiratory and viral illnesses [13].

3 Methods Based on Computational Intelligence to Predict COVID-19

3.1 Fuzzy Sets

Fuzzy sets are one of the main approaches in computational intelligence. It is based on mathematical set theory. Fuzzy sets have been successfully utilized in various applications. Many researchers have also used Fuzzy sets to predict COVID-19. This section throw light on some of the studies. A computerized behavioral model was developed by Lauraitis et al. [14] to forecast and compare the reaction conditions of HD patients and healthy people using Fuzzy logic and a neural network to develop a smartphone app. The neural network's backpropagation technique with a fuzzy logic system produced the best results [14].

Awotunde et al. [15] developed a fuzzy logic-based medical diagnostic system using prolog programming. They claimed improved system performance using statistical measures such as precision and recall. They established that a fuzzy-based system is more efficient for medical diagnostics. To forecast cholera, a fuzzy logic model was also created. The factors that contribute to cholera were investigated using this model. A forecasting algorithm was created to determine the chance of cholera illness and assist health personnel in making wise decisions [16].

3.2 Artificial Neural Networks

The study [17] presents an Artificial Neural Network to predict COVID-19 spread. The predictor was built using a traditional method with an "NAdam" optimizer for learning the training model. They used data from government agencies and open repositories for the training. In order to offer a potentially extensive range of values for the expected COVID-19 spread, prediction results were presented for both nations and regions. They claimed and demonstrated great accuracy, which sometimes exceeds 99%.

An ANN-based time series prediction of COVID-19 was presented by [18]. In all three scenarios, the article projects the numbers for the following day, or for April 21, and compares the outcomes to the values that were actually reported. India's deviation was found to be 6%, whereas it was less than 3.5% for the other three nations. The authors advise that the modified multilayer neural network (MMLNN) model be incorporated into the health policy of the nations battling the spread of the virus due to the high accuracy prediction capacity. The short-term forecasts of

the viral infection's spread, in particular, can be used to inform decisions on health measures like movement restrictions.

Peipel W. et al. [19] proposed a new hybrid model based on LSTM-CA for epidemic simulation and forecasting. They simulated the spatio-temporal epidemic propagation based on fine-grained actual patient location for the first time. They claimed improved accuracy with LSTM-CA against a single LSTM or CA model. The experiments were performed to analyze the effectiveness of their proposed LSTM-CA model for predicting the spread of COVID-19 in China.

The research proposed by [20] was to develop a hybrid system to predict COVID-19. An EEMD with ANN was used with the real-time COVID-19 time series data for the prediction. The dataset used in this study was from January to May 2020. The training of the system was done using denoised time series data.

This study [21] forecast COVID-19 using ARIMA models and polynomial functions. This study's key finding was to analyze a correlation between COVID-19 behavior and population in a particular area. These findings open up the possibility of developing more forecasting models to predict COVID-19 and factors influencing the behavior considering, among other things, variables like humidity, environment, and culture.

M. Pourhomayoun and M. Shakibi [22] proposed a prediction model using AI and ML as an essential building block for COVID-19 patients. Several Machine learning algorithms were utilized to predict the death rate in COVID-19 patients. Using a different dataset of COVID-19 patients, the model was assessed. The results were shown using the sensitivity and specificity of the proposed model and confusion matrix.

This research [23] suggests a convolutional neural network model to identify COVID-19 illness. A KNN classifier that considers the neighborhood labeling agreement replaces the final SoftMax CNN layer in the proposed technique to increase accuracy. The proposed evolutionary algorithm incorporates three potent evolutionary operators into the search process: Cauchy Mutation (CM), etc. This quickens convergence and strikes the ideal balance between the exploration and exploitation phases. The suggested evolutionary technique is then utilized to automatically acquire the best CNN hyperparameter values, resulting in a notable improvement in the classification accuracy of the proposed method.

3.3   Evolutionary Computing

The research [24] offers a prediction model that looks at how non-pharmaceutical treatments (NPIs) affect the development of COVID-19 and is based on the recurrent gated unit (GRU). Multi-population evolutionary algorithm, a meta-heuristics technique, was created to find the best mitigation tactics that limit COVID-19 cases while minimizing economic and other adverse effects. The MPEA-DE model's recommended mitigation tactics were compared to three standard search tactics.

This study [25] deals with a technique for calculating the development of the epidemiological parameters of an SIRD model (short for susceptible, infected, recovered, and deceased persons), which enables to assess the efficacy of the government's sanitary actions in controlling the COVID-19 epidemic in Spain. To reduce the square sum of errors, they only consider the number of fatalities among the several time series that measure the pandemic. The four sub-periods in the time series of fatalities under consideration, which spans from March to the end of September, illustrate the various forms of isolation employed by the Spanish government.

In order to identify COVID-19 situations, this study [26] proposes and creates a computational intelligence-based framework employing convolutional neural networks (CNNs) and genetic algorithms (GAs). A computational intelligence-based algorithm was proposed that utilizes the newest 5G mobile technology of multi-access edge computing and a novel CNN framework for identifying COVID-19. This method implies that the CNN-based automated COVID-19 identification tool should be accessible to everyone with a 5G device (such as a 5G mobile phone). The model incorporates a unique CNN structure with the genetic algorithm (GA) for hyperparameter adjustment as part of the suggested automated model.

3.4 Swarm Intelligence

For COVID-19, scientists use various prediction models to help them make educated judgments and enact effective control measures. The old models needed better accuracy since there were much uncertainty and insufficient essential data. BB Hazarika et al. [27] proposed a wavelet-based model to predict COVID-19. Modern support vector regression (SVR) and traditional RVFL were used for prediction. The data obtained from wavelet analysis were fed to the RVFL. The top 5 worst-hit countries' COVID data were utilized as input for the model. Their findings also include daily forecasting for the next 60 days.

This study [28] reviewed the dangerous aspects of COVID-19 using prominent ML algorithms. They utilized regression, SVM, and Least Absolute Shrinkage and Selection Operator (LASSO); they claimed that Exponential Smoothing outperformed followed by regression and LASSO, which are effective at forecasting the number of new confirmed cases, the death rate, and the percentage of patients who recover. At the same time, SVM performs poorly in all scenarios where predictions are made based on the currently available dataset.

Study [29] provides a co-evolutionary transfer learning (CETL) technique for predicting the requirements of a group of medical supplies, which is essential for COVID-19 prevention and management. The CETL recycles data from disasters that were both natural and artificial, as well as from other epidemics like the avian flu and SARS. The CETL uses a fuzzy deep Contractive Auto Encoder (CAE) for each prediction job. All prediction networks are cooperatively evolved via intra-

Table 1 COVID-19 prediction systems with the method used, modalities, and performance

Methods	Algorithms	Study	Modality
Fuzzy sets	Fuzzy logic	Awotunde et al. 2014 [15]	Prolog programming
	Fuzzy logic and NN	Lauraitis et al. [14]	Backpropagation
	Fuzzy logic	Aroyehun et al. [16]	Fuzzy logic model
Artificial neural networks	ANN	Wieczorek, M. [17]	NAdam optimizer
	MMLNN	Majhi, B. [18]	Modified multilayer neural network
	LSTM-CA	Wang, P. et al. [19]	Spatio-temporal propagation
	ANN time series	Hasan, N. [20]	Time series data
	AI and ML	Pourhomayoun, M. et al. [22]	ML building blocks
Evolutionary computing	MPEA-DR and GRU	Bi, L. et al. [24]	Gated recurrent unit
	Evolutionary DL	Jalali, S. M. J. et al. [23]	X-ray images
Swarm intelligence	GA	Hassan, M. R. et al. [26]	Genetic algorithm
	SIRD	Acosta-González et al. [25]	Epidemiological parameters
Others	Linear regression	Rustam, F. et al., 2020 [28]	Exponential smoothing
	SVR and RVFL	Hazarika, B. B. et al. [27]	Wavelet analysis
	ANIMA	Hernandez-Matamoros et al. [21]	ARIMA models

population and inter-population evolution to acquire task-specific knowledge within each domain and standard information shared across the domains.

Noticeable studies based on Computational Intelligence are summarized in Table 1.

4 Method to Predict Exponential Growth of Infected Cases

According to data [30], the number of cases is multiple of 1.15 to 1.25 to the number of previous days. If the number of given cases is N_d and the average number of people someone infected is exposed to each day is E, and each one of those people has a probability p of becoming a new infection. Then, the new cases on a given day can be given as

$$\Delta N_d = E.p.N_d \tag{1}$$

where ΔN_d is change over a day

$$\Delta N_{d+1} = N_d + E.p.N_d \tag{2}$$

$$N_{d+1} = (1 + E.p)N_d \tag{3}$$

If the number of new cases is proportional to the number of existing cases, it means that each day multiplies by a constant.

$$N_d = (1 + E.p)_d N_0 \tag{4}$$

For a random shuffling model,

$$p = 1 - \frac{N_d}{Population Size} \tag{5}$$

For N cases,

$$\frac{d_N}{d_t} = C \left(1 - \frac{N_d}{Population Size} \right) N \tag{6}$$

The growth rate is defined as

$$R = \frac{\Delta N_d}{\Delta N_{d-1}} \tag{7}$$

These two factors play a crucial role in the growth of newly infected cases.

5   Results and Discussions

We have considered the three population sizes of 10 million, 1 billion, and 10 billion. The reproductive ratio varies from country to country; therefore, we have divided the reproductive rate into two categories, i.e., slow ($R_0 = 1.8$) and high with $R_0 = 2.2$. The growth prediction for each category with different percentages of transmission is estimated. The prediction has its intrinsic limitation as various parameters that influence the transmission of COVID-19 might not be accounted for. The analyses also considered the different preventive measures taken by the different state agents after the outbreak alarm.

Our analysis is based on **(i)** no intervention, **(ii)** intervention after 30 days, and **(iii)** intervention after 60 days. It proved from existing studies [31] that the delay in adopting preventive measures results in excess mortality.

The preventive measures adopted by the countries are social distancing by imposing complete lockdown. It is impossible to achieve a 100% lockdown;

therefore, we have considered a standard 71% decrease in transmission during the lockdown. We have predicted the growth of COVID-19 without intervention, with results shown in Tables 2, 3, 4, 5, 6, 7. The reproductive rate is kept at 1.8 and 2.2 for three different population categories: Tables 2, 3 for 10 million populations, Tables 4, 5 for 1 billion populations, and Tables 6, 7 for 10 billion populations. The highest infection is 6.63% with $R_0 = 2.2$. The number of people infected with peak infection is 66 million, and the mortality will be 15 million in a population of 10 billion. In the same duration, approximately 12% of people are exposed to the disease.

The second analysis was carried out with preventive actions such as social distancing and lockdowns imposed by the authorities after 30 and 60 days of starting the pandemic. The total social distance includes removing all social contact other than the household. Generally, it is seen that essential services are in operation during the lockdown period; therefore, it is impossible to achieve sent percent social distancing. We assume that the transmission is decreased by 71% during social distancing. Partial dock down or social distancing is ineffective; it must be above 70% for an effective decrease in the transmission of a pandemic. The results show (Figs. 4–9a) the highest rate for three categories (exposed, infectious, and fatalities) for all sizes of the population (10M, 1B, and 10B) without adapting to preventive measures. These values are valid if the government or authorities take no preventive measures such as social distancing and lockdown. For the larger population and with the high reproductive rate, the highest infection rate will be 6.63% of the total population.

Our analysis is given under two categories: **(i)** intervention after 30 days and **(ii)** intervention after 60 days. The results show that the first category is very effective in bringing down the number of infected cases. With the high reproductive ratio, the number of infections is 16,705 under the first category in contrast to 652,771 under the second category. The number of infected cases significantly increased if the lockdown was imposed after 60 days. Figure 4(a) depicts a total population of 54.91% will be exposed, with 4.19% infected persons. Figure 4(b) and 4(c) shows intervention after 30 and 60 days with a total of 0.05% and 0.60% infected cases, respectively. As seen in Fig. 4(c), there is a sharp increment in infected cases and fatality rates. Therefore, rapid and quick social distancing is desirable within 1 month to reduce the number of infections and mortality significantly.

6   Findings and Conclusion

We have presented a mathematical model for the growth prediction of COVID-19. Since the spread varies with age and population, our analysis is based on three population sizes, i.e., 10 million, 1 billion, and 10 billion. The different reproductive rate has been evident for COVID-19; therefore, we have considered two reproductive rates, high and low. All the analysis is based on different population sizes and the two reproductive ratios. In this study, we showed that the number of infections and

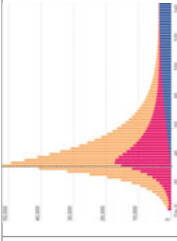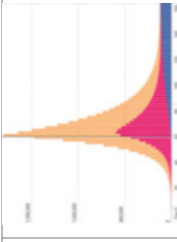**Table 2** Prediction of COVID-19 with 10 million populations ($R_0 = 1.8$)

Low reproductive ratio			
	Fig. 4(a) No intervention	Fig. 4(b) Intervention after 30 days	Fig. 4(c) Intervention after 60 days
Exposed	5,501,791 (54.91%)	11,112 (0.11%)	121,642 (1.21%)
Infectious	419,537 (4.19%)	5286 (0.05%)	60,280 (0.60%)
Fatalities	138,962 (1.39%)	1048 (0.01%)	12,045 (0.12%)

Table 3 Prediction of COVID-19 with 10 million populations ($R_0 = 2.2$)
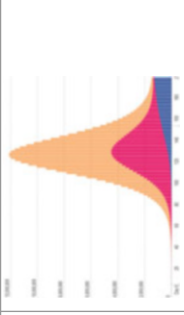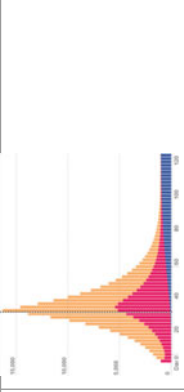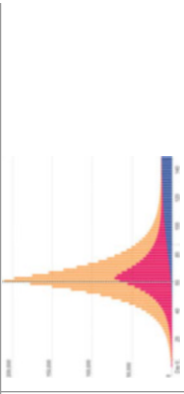
High reproductive ratio			
	Fig. 5(a) No intervention	Fig. 5(b) Intervention after 30 days	Fig. 5(c) Intervention after 60 days
Exposed	1,218,317 (12.16%)	36,633 (0.36%)	823,429 (8.22%)
Infectious	664,424 (6.63%)	16,475 (0.16%)	393,548 (3.93%)
Fatalities	165,846 (1.66%)	3543 (0.04%)	69,066 (0.69%)

Table 4 Prediction of COVID-19 with 1 billion populations ($R_0 = 1.8$)
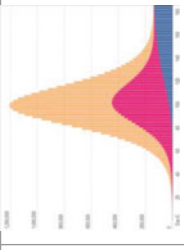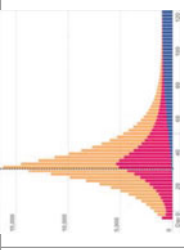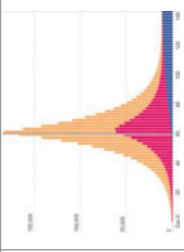
Low reproductive ratio			
	Fig. 6(a) No intervention	Fig. 6(b) Intervention after 30 days	Fig. 6(c) Intervention after 60 days
Exposed	7,696,264 (7.62%)	11,178 (0.1%)	144,532 (0.14%)
Infectious	4,236,004 (4.20%)	5315 (0.01%)	70,524 (0.07%)
Fatalities	1,283,473 (1.27%)	1058	13,981 (0.01%)

Table 5 Prediction of COVID-19 with 1 billion populations ($R_0 = 2.2$)
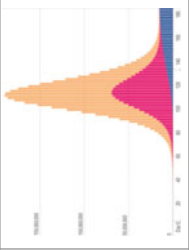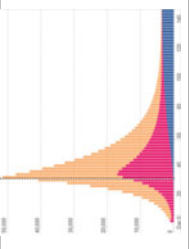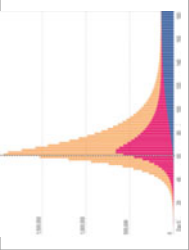
High reproductive ratio			
	Fig. 7(a) No intervention	Fig. 7(b) Intervention after 30 days	Fig. 7(c) Intervention after 60 days
Exposed	12,192,972 (12.08%)	36,589 (0.04%)	1,247,667 (1.24%)
Infectious	6,664,729 (6.60%)	17,151 (0.02%)	586,452 (0.58%)
Fatalities	1,631,372 (1.62%)	3744	8975 (.01%)

Table 6 Prediction of COVID-19 with 10 billion populations ($R_0 = 1.8$)
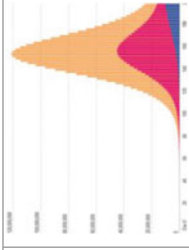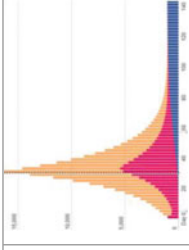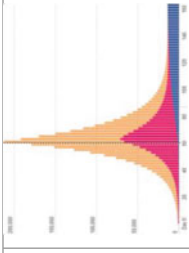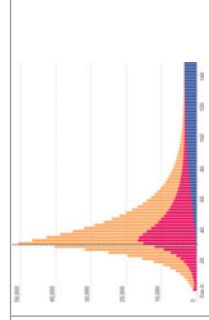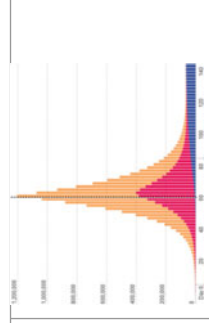
Low reproductive ratio			
	Fig. 8(a) No intervention	Fig. 8(b) Intervention after 30 days	Fig. 8(c) Intervention after 60 days
Exposed	76,555,035 (7.60%)	11,185	145,806 (0.01%)
Infectious	42,251,186 (4.2%)	5318	69,310 (0.01%)
Fatalities	10,174,714 (1.01%)	1058	13,940

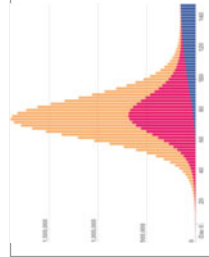**Table 7** Prediction of COVID-19 with 10 billion populations ($R_0 = 2.2$)

High reproductive ratio			
	Fig. 9(a) No intervention	Fig. 9(b) Intervention after 30 days	Fig. 9(c) Intervention after 60 days
Exposed	122,457,773 (12.16%)	36,167	1,370,618 (0.14%)
Infectious	66,740,886 (6.63%)	16,705	652,771 (0.06%)
Fatalities	15,703,234 (1.56%)	3649	141,033 (0.01%)

the probability of becoming a new infection significantly affect the transmission of COVID-19, irrespective of the temperatures and humidity. The temperature and humidity may affect it up to some extent. However, the transmission is proportional to the contact of humans with infected humans. The findings of this study are as follows:

– To end the pandemic COVID-19, we must reduce the R, which can only be possible by reducing the contact of humans with infected humans.
– More than 70% population must be isolated for a practical impact of social distancing to prevent the spread of the pandemic.
– The effect of temperature and humidity on the spread of COVID-19 is limited.
– The transmission of COVID-19 would not be limited during the April–June months of 2020 in high-temperature region countries like India, Pakistan, Sri Lanka, etc.

Several factors, including temperature and humidity, are responsible for the spread of COVID-19. However, we have established that understanding the relationship between two parameters, namely p and E, is essential for predicting the growth and end time of the pandemic COVID-19.

References

1. WHO.: Coronavirus disease (COVID 19) outbreak https://www.who.int/emergencies/diseases/novelcoronavirus. Accessed 25 Mar 2020
2. Chan, K.H., Peiris, J.S., Lam, S.Y., Poon, L.L.M., Yuen, K.Y., Seto, W.H.: The effects of temperature and relative humidity on the viability of the SARS coronavirus. Adv. Virol. (2011)
3. Wang, M., Jiang, A., Gong, L., Luo, L., Guo, W., Li, C., et al., Chen, Y.: Temperature significant change COVID-19 Transmission in 429 cities. medRxiv 2020a
4. Weather Report.: https://www.windy.com/articles/doesoutside-temperature-affect-the-spreading-ofcoronavirus-covid-19-11519?29.966,76.837,5. Accessed 25 Mar 2020a
5. Van Doremalen, N., Bushmaker, T., Morris, D.: Aerosol and surface stability of HCoV-19 (SARS-CoV-2) compared to SARS-CoV-1. medRxiv 2020. Basic science virology research
6. Araujo, M.B., Naimi, B.: Spread of SARSCoV-2 Coronavirus likely to be constrained by climate. medRxiv 2020
7. Report on Coronavirus.: https://www.theguardian.com/world/2020/mar/24/nearly-20-of-global-population-under-coronavirus-lockdown. Accessed 11 Apr 2020
8. Anderson, R.M., Heesterbeek, H., Klinkenberg, D., Hollingsworth, T.D.: How will country-based mitigation measures influence the course of the COVID-19 epidemic? Lancet **395**(10228), 931–934 (2020)
9. Liu, J., Zhou, J., Yao, J., Zhang, X., Li, L., Xu, X., et al., Zhang, K.: Impact of meteorological factors on the COVID-19 transmission: a multi-city study in China. Sci. Tot. Environ. **726**, 138513 (2020)
10. Rosenberg, M.: Population Density. Geography.about.com. March 2, 2011. Retrieved on December 10, 2011
11. Quéré, C., Jackson, R., Jones, M., et al., Peters, G.: Temporary reduction in daily global CO_2 emissions during the COVID-19 forced confinement. Nat. Clim. Change **10**, 647–653 (2020)
12. Chen, H., Goldberg, M.S., Villeneuve, P.J.: A systematic review of the relation between long-term exposure to ambient air pollution and chronic diseases. Rev. Environ. Health **23**(4), 243–297 2008

13. Peacock, A.J.: Oxygen at high altitude. Br. Med. J. (1998). PMC 1114067. PMID 9774298
14. Lauraitis, A., Maskeliunas, R., Damaševicius, R.: ANN and fuzzy logic based model to evaluate huntington disease symptoms. J. Healthc Eng. **2018**, 1–10 (2018)
15. Awotunde, J.B., Matiluko, O.E., Fatai, O.W.: Medical diagnosis system using fuzzy logic. Afr. J. Comput. ICT Ref. **7**, 99–106 (2014)
16. Aroyehun, A., Olabiyisi, S., Omidiora, E., Ganiyu, R., Idowu, P.: Development of a fuzzy logic model for predicting the likelihood of cholera disease. WJERT **4**, 340–363 (2018)
17. Wieczorek, M., Silka, J., Wozniak, M.: Neural network powered COVID-19 spread forecasting model. Chaos Solitons Fractals **140**, 110203 (2020)
18. Majhi, B.: A modified Artificial Neural Network (ANN)-based time series prediction of COVID-19 cases from multi-country data. J. Inst. Eng. India Ser. B, 1–16 (2023)
19. Wang, P., Liu, H., Zheng, X., Ma, R.: A new method for spatio-temporal transmission prediction of COVID-19. Chaos Solitons Fractals **167**, 112996 (2023)
20. Hasan, N.: A methodological approach for predicting COVID-19 epidemic using EEMD-ANN hybrid model. Internet Things **11**, 100228 (2020)
21. Hernandez-Matamoros, A., Fujita, H., Hayashi, T., Perez-Meana, H.: Forecasting of COVID-19 per regions using ARIMA models and polynomial functions. Appl. Soft Comput. **96**, 106610 (2020)
22. Pourhomayoun, M., Shakibi, M.: Predicting mortality risk in patients with COVID-19 using machine learning to help medical decision-making. Smart Health **20**, 100178 (2021)
23. Jalali, S.M.J., Ahmadian, M., Ahmadian, S., Hedjam, R., Khosravi, A., Nahavandi, S.: X-ray image based COVID-19 detection using evolutionary deep learning approach. Expert Syst. Appl. **201**, 116942 (2022)
24. Bi, L., Fili, M., Hu, G.: COVID-19 forecasting and intervention planning using gated recurrent unit and evolutionary algorithm. Neural Comput. Appl. **34**(20), 17561–17579 (2022)
25. Acosta-González, E., Andrada-Félix, J., Fernández-Rodríguez, F.: On the evolution of the COVID-19 epidemiological parameters using only the series of deceased. A study of the Spanish outbreak using Genetic Algorithms. Math. Comput. Simul. **197**, 91–104 (2022)
26. Hassan, M.R., Ismail, W.N., Chowdhury, A., Hossain, S., Huda, S., Hassan, M.M.: A framework of genetic algorithm-based CNN on multi-access edge computing for automated detection of COVID-19. J. Supercomput. **78**(7), 10250–10274 (2022)
27. Hazarika, B.B., Gupta, D.: Modelling and forecasting of COVID-19 spread using wavelet-coupled random vector functional link networks. Appl. Soft Comput. **96**, 106626 (2020)
28. Rustam, F., Reshi, A.A., Mehmood, A., Ullah, S., On, B.W., Aslam, W., Choi, G.S.: COVID-19 future forecasting using supervised machine learning models. IEEE Access **8**, 101489–101499 (2020)
29. Song, Q., Zheng, Y.J., Yang, J., Huang, Y.J., Sheng, W.G., Chen, S.Y.: Predicting demands of COVID-19 prevention and control materials via co-evolutionary transfer learning. IEEE Trans. Cybern. (2022)
30. WHO.: Coronavirus disease 2019 Situation reports. https://www.who.int/emergencies/diseases/novelcoronavirus-2019/situation-reports. Accessed 11 April 2020
31. Bootsma, M.C., Ferguson, N.M.: The effect of public health measures on the 1918 Influenza pandemic in US cities. Proc. Natl. Acad. Sci. **104**(18), 7588–7593 (2007)

COVID-19 Combating Strategies and Associated Variables for Its Transmission: An Approach with Multi-Criteria Decision-Making Techniques in the Indian Context

Debesh Mishra (ORCID) **and Mohamed Lahby** (ORCID)

1 Introduction

The 'Severe Acute Respiratory Syndrome Coronavirus (SARS-CoV-2)' was the pathogen's new designation as of February 11, 2020, according to the 'International Committee on Taxonomy of Viruses' [39], whereas COVID-19 was the label given to the outbreak by 'World Health Organization (WHO)'. The following stages of COVID-19 disease transmission include the following: A preliminary phylogenetic study of Stage-1 virus COVID-19 suggested that it may be zoonotic. Stage-2 includes the spreading of COVID-19 to people from animals [3]. Furthermore, the COVID-19 viruses have a 2- to 14-day period of incubation [3, 20, 71] and Stage-3 with the potential for human-to-human transmissions from coughing droplets, contaminated surfaces, or surroundings. Stage-4 will then follow with the COVID-19 epidemic and community transmission [116], and Stage-5 with COVID-19 progressively spreading globally and the number of active cases increasing exponentially [46]. Development of a novel virus suggests that knowledge of dissemination patterns and the related risk factors for infections will be restricted early in outbreaks [125]. Numerous scholarly works have examined COVID-19 prevalence, transmission among people with the disease, and prophylaxis among those patients' close contacts [72].

With the exception of Antarctica, more instances of the coronavirus (COVID-19) have been documented globally since incidences of the disease were first noted in Wuhan (China), in December 2019. The 'World Health Organization' classified

D. Mishra (✉)
Mechanical Engineering, IES University, Bhopal, India

M. Lahby
University Hassan II, Higher Normal School of Casablanca, Casablanca, Morocco
e-mail: lahby@ieee.org

233

COVID-19 as an epidemic as a result of the rate of increase exceeding the rate of patients [126]. The SARSCoV-2 is the virus responsible for COVID-19 with around 71,000,000 verified cases and 1,600,000 confirmed deaths worldwide as of December 15, 2020 [126]. When a person who is infected coughs, sniffles, or spits, the virus is discharged from their respiratory secretions. These droplets can infect other persons when they come into touch with them [102]. Most infections are frequently self-limited. In the elderly and those with existing medical conditions, it might lead to more severe sickness [128]. According to current data, fever is present in 88% of cases, exhaustion in 38%, dyspnoea in 18.7%, myalgias in 14.9%, and a dry-cough in 67% of cases at the time of illness's beginning [24, 25]. The most frequent consequence is pneumonia. A mortality rate of 2.3–5% is seen in extreme symptoms [128]. Other than supportive care, there are currently no confirmed particular therapies for people with the new virus. Many patients have obtained off-label and benevolent use medications in China, France, Italy, Turkey, Spain, and now the United States [126]. So far, a variety of strategies have been employed to combat the infection. Currently only few limited vaccines are utilized as the main approaches in India, while the efficacy of various medications is yet uncertain [34, 37, 74, 88].

The virus COVID-19 is regarded as infectious and has been classified as a pandemic. Each country is taking precautions to lessen the rate of transmission after the virus spread to several countries. International health organizations like the WHO routinely issue advisory recommendations urging rigorous action against the causes of COVID-19 transmission. Businesses are seeing the interruption to their supply chain and discrepancy between supply and demand for 'products and services' as a result of the COVID-19 worldwide outbreak. Due to travel restrictions and restricted borders, it is often difficult for enterprises to discover alternate transit and logistic networks. The only approach to identify efficient and secure therapies for COVID-19 and potential future outbreaks is through the quick and concurrent blending of supportive care and arbitrary control trials. The supporting systems that provide decision-makers with the details they need about the options and their attributes are known as 'decision-making models'. The total number of verified cases has recently begun to decline as a result of administrative interventions, enforced controls (like shutting down public transit), adjustments to standard personal hygiene practices (like always wearing a facemask and avoiding physical intimacy), and so on [131]. According to Schippers and Rus [105], resolving the COVID-19 issue might be seriously compromised by group thinking, a limited emphasis on the virus containment issue, and an increase in commitment. The predictions of different responsible factors associated with the pandemic can guide to take precautions accordingly [36, 115]. Despite the exponential global spread of COVID-19, the mortality rate is still manageable, allowing people everywhere to regain their faith in their ability to combat this pandemic collectively. However, only a small amount of scholarly research has examined the causes of the COVID-19 disease's spread among people in various nations [46]. In this situation, a variety of variables contribute to the individuals' COVID-19 infection spread. Therefore, by taking into account only a few variables, policymakers, health authorities, and

immunologists cannot determine the level of dissemination and therefore prepare for mitigation. As a result, policymakers and health authorities must conduct a thorough review of the variables contributing to COVID-19's transmission and take all of them into account when developing mitigation and preventative policies. Consequently, methods for 'multi-criteria decision-making (MCDM)' are most appropriate [70].

The following 'research-questions (R-Qs)' were briefly addressed in this chapter:

- R-Q1: What are the main preferences of COVID-19 vaccines among the Indian community?
- R-Q2: What are the essential variables that contribute to the spread of COVID-19?
- R-Q3: Which of them require immediate attention and are the most serious?
- R-Q4: In light of these variables, how should policymakers rank them?

Following is the arrangement for the remaining portion of this chapter. In Sect. 2, the current literature was discussed on COVID-19 vaccinations; COVID-19 transmission variables; and vaccination's reluctances in India. The research methodology used in this chapter was discussed in Sect. 3. In Sect. 4, the results related to the findings was given, which was followed by Sect. 5 with discussion. Finally, in Sect. 6, the conclusion of this chapter was presented.

2   Literature Review

In periods of crisis, the success of policymakers' decisions is highly dependent on their capacity to synthesize and understand information. Governments are faced with the challenging tasks of decision-making in the interests of public safety and health due to the COVID-19 issue. In essence, decision-makers act in response to potential threats whose scopes are unclear while operating under significant time constraints and uncertainties. However, the government should implement an appropriate set of strategies as soon as feasible given that the death rate for serious conditions has been found to be 10% [36]. In a numerical study of COVID-19, Bai et al. [11] analysed the features of the recovery and transmission rate and forecasted the future trend. Decision trees and prior algorithms have been used to analyse the COVID-19 virus's routing information [61], but there is still a potential that some data may be overlooked and more algorithms will need to be included to ensure system results. In a study [8], the spread of COVID-19 in China's Hubei region was anticipated and simulated, but the features of the population, such as the impact of age, the presence of other health issues, and the measures taken to avoid the spread, were not investigated. By using a time-series and kinetic-analysis model, Yichi et al. [129] have demonstrated how the Chinese government's emergency measures, such as its ban on individuals leaving the country, have a significant effect on the spread of the outbreak. As per experimental findings, deceased people's

body do not cause further infection, and those who have recovered get benefits from the developed antibodies already present in their systems, which help to avoid future virus replications. According to He et al. [47], the delayed diagnosis of the symptoms and the manufacture of Chinese medication have been identified as the variables leading to the abnormal dynamic characteristics of COVID-19.

Healthcare decision-making involves a sophisticated network of meaningful relationships between several stakeholders [92]. Currently, there are few mathematical models or methods utilized to facilitate the selection of an effective vaccine for combating pandemics and outbreaks. Literature on the variables that could influence a person's decision to accept or reject a vaccination among vaccine alternatives is limited. A clinical decision assistance system has been built using the 'analytic hierarchy process (AHP)' approach [59]. The 'BAILEY's model' was a quantitative decision-making tool utilized by Kumar and Roy [68] in the preclusion and management of COVID-19. Importantly, the criteria and methods for choosing a vaccination among vaccine options are hardly discussed in the literature. Therefore, it is crucial to create a discrete choice model to examine the many selection criteria for vaccines among the options available. The prevention and treatment of worldwide outbreaks all depend on scientific understanding. Some of this information may be condensed in plans for pandemic response and preparation (at both the national and global levels) or may be effectively acquired from panels of experts with knowledge in pertinent fields of study, such as virologists, communicable diseases data analysts, and sociologists [84]. In a catastrophe like the COVID-19 pandemic, the top-government policy experts have a serious decision-making challenge. When a novel infectious illness initially develops, policymakers may try to restrict spreading by quick actions to stop further dissemination. Before the pandemic, the infection was treated with a variety of medications and techniques. Evaluating COVID-19 treatment alternatives by using MCDM techniques have been claimed to be highly valuable because, to yet, no viable treatment option has been discovered and only success was obtained on case based [130]. The COVID-19 virus's properties, such as its virulence, transmissibility, and historical background, were unclear during the outbreak [9]. The dynamics of the system are unclear given the current state of information, which makes the effects of potential policy-actions like shutting institutions or donning masks in public. Policymakers can better appreciate the scope of an issue by considering the different levels of uncertainty, such as uncertainty about-models, across-models, and inside-models [44, 45, 75].

The comprehensive literature on COVID-19's vaccinations, transmission, and variables contributing to its transmission are presented and discussed in the following sections.

2.1 COVID-19's Vaccinations

The COVID-19 pandemic's epicentre has been moving from China to Europe and eventually the United States during the entire year 2020. India has become the new

location of the COVID-19 virus's epicentre as the second wave spreads throughout the nation. Since April 2021, India has recorded almost 3 lakh COVID-19 instances every day, which is a more dangerous, and ominous trend than the initial wave. The extremely infectious double mutated version of COVID-19, the simplicity of therapies, and people's careless behaviour are the key causes of this increase in COVID-19 cases [127]. Since COVID-19 (SARS-CoV-2) has a far greater infection rate than previous viruses like 'MERS-CoV and SARS-CoV', it can spread quickly around the world and result in a worldwide epidemic [23]. Droplets, aerosols, and fomites are the principal means of human-to-human COVID-19 transmission [122]. Additionally, according to certain research, COVID-19 dust might also spread via the air [97, 108, 110]. The COVID-19 pandemic's transmission channels, however, are the subject of a contentious disagreement among academics and experts, even if everyone in the globe abides by WHO norms. To prevent exposure to the virus, it is crucial to adopt preventative measures such hand washing, quick isolation of patient's with symptoms or diagnosed, social distance, and the use of sanitizers and masks [29]. Even with the aforementioned measures, this illness continues to have a high mortality rate and afflict all nations in the world [90]. The transmission of COVID-19 is attributed to a number of variables, including social distances [63], climate-related variables [55], safety- and hygiene-related variables [35], and cognitive variables [101]. Therefore, it is necessary to employ various preventatives and control techniques, both locally and globally.

There are about 30 vaccine contenders being developed in India, all at different levels. Two are at the most advanced level of these. These include 'COVAXIN' from the 'Indian Council of Medical Research (ICMR)' and alliance with 'Bharat Bio-tech', as well as 'COVISHIELD' from 'Serum Institute of India (SII)' [82, 96]. The 'National AIDS Research Institute (NARI)' in Pune and the ICMR are responsible for overseeing all studies. The 'Department of Biotechnology (DBT)' and the 'Department of Science and Technology (DST)' are funding other vaccine alternatives that are in various research stages [21, 78, 79]. Six of these potential vaccines are now undergoing clinical trials. The preclinical trial stage is being experienced by the remainder [119]. The 'COVISHIELD', 'COVAXIN', and 'Sputnik-V' are the leading contenders. A phase-III human clinical study for COVISHIELD, a non-replicating adenovirus type-5 vector-vaccine, is now taking place in India. A locally created complete virion inactivated vaccine called COVAXIN is also undergoing Phase III human clinical trials. On January 3, 2021, the 'Central Drugs and Standards Committee (CDSCO)' formally authorized both of these vaccination candidates [117, 119]. Sputnik-V vaccine began Phase-III in the first week of August 2020 after successfully completing the Phase-II study. This Russian-based vaccine, created by the 'Gamaleya Research Institute', is based on the common cold virus and has demonstrated the ability to stimulate the production of antibodies by the immune system [82]. Larger human studies are being conducted there, and this vaccine will also be produced there [83]. The subsequent creation of a successful and enhanced approach is largely dependent on the discovery of the

COVID-19's transmission variables. As a result, this chapter aims to identify and describe the potential sources of COVID-19 viral transmission through the existing literature.

2.2 COVID-19's Transmission Variables

According to research findings, it is crucial to keep COVID-19 from spreading by maintaining good cleanliness, safety, sensitivity, social, demographic, and psychological variables. In the next sub-sections, the major and significant COVID-19's transmission variables are elaborated.

2.2.1 Climate-Related Variables

Climate-related variables including air quality, temperature, wind speed, rainfall, humidity, and solar radiation help the new COVID-19 virus spread quickly [4, 67]. Relative humidity, temperature, and wind speed are significant determinants in the spread of COVID-19, according to an analysis by Chen et al. [24, 25] regarding the link between environmental conditions and the severity degree of transmission. According to Wang et al. [123], who studied how temperature affects COVID-19's transmission, low-temperature nations should enact strict control measures to stop COVID-19's transmission. In humid continental locations, warmth periodicity also promotes COVID-19's transmission favourably [95]. Furthermore, research shows that the COVID-19's transmission is influenced by the relative humidity and everyday temperatures [51]. A few studies, for example, found that low humidity may have facilitated COVID-19's transmission [10, 123]. For limiting the spread so that the heart and lungs can fight off the infections, the relatively high humidity (>95%) is recommended [65]. However, other investigations discovered that the rate of COVID-19's transfer and wind speed had an inverse association [13]. As a result, the transmitting rate is increased when the wind blows more slowly. In addition to transfer from person to person, Coccia [28] found that air pollution may speed up the spread of COVID-19.

2.2.2 Safety- and Hygiene-Related Variables

First and foremost, everyone who has had direct touch with a COVID-19 patient is at high infection risks [125]. According to recent studies, those who are infected with the COVID-19 virus but do not exhibit any symptoms (i.e. those who are asymptomatic) are also responsible for spreading the disease [50]. On February 17, 2020, 189 asymptomatic travellers out of 1723 travellers tested positive for the COVID-19 virus [85]. The 'personal protective equipment (P.P.E.)' such as 'masks and face-shields' help to safeguard medical professionals from COVID-19 patients,

while also protecting the general public [112]. The WHO has previously issued a warning on the serious disruptions of the availability of P.P.E. products on a worldwide scale and urges business and governments to enhance output by about 40% to satisfy the growing demand on a global scale. The COVID-19 illness can spread widely through the air and surfaces, in both 'intensive-care units (I.C.U.)' and to medical-ward designated COVID-19, according to Guo et al. [41], suggesting a significant potential danger of spreading among the physicians and medical staffs. Therefore, it is essential to have a sufficient and timely supply of P.P.E. to reduce the transmitting rates. Additionally, used tissues, masks, gowns, and gloves from households and hospitals that are medical wastes might potentially spread the dangerous COVID-19. As a result of routinely handling unlabelled wastes properly, the sanitation workers and rag pickers are vulnerable to COVID-19's infection.

2.2.3 Making Decisions with Attentiveness

Worldwide, significant behavioural-based intrusions have been made to slow the development of COVID-19 [64]. To slow the pace of transmission, some nations have issued full travel bans [40], lockdowns [66], and forced quarantines [94]. Due to decreased vehicle traffic and better air quality in several Indian cities, lockdown has had a considerable beneficial influence on lowering COVID-19 transmission and pollution levels [53]. In the provinces of Wuhan and Ezhou, China implemented a lockdown on January 23, restricting all public transportation and social activities. Many nations announced border control measures to stop visitors from China after the WHO designated COVID-19 a global health emergency on January 30, 2020. A 14-day obligatory quarantine period and a ban on international travellers from China, Hong Kong, and Macao were implemented by the Philippines on February 2, 2020 [31]. Impact of human travel and mobility on the transmission of the COVID-19 virus was examined and shown to be extensive by Gondauri and Batiashvili [38]. Additionally, delays in COVID-19 identification and quarantine have accelerated COVID-19 spread [124]. To prevent the spread of COVID-19 and increase response to the existing overburdened healthcare systems, governments in several nations are officially enforcing quarantines and travel restrictions.

2.2.4 Social- and Demographic-Variables

Social cohesion (mass assembling), density of population, and age range are the primary social- and demographic-variables [76]. Religious events, panic-related movements, worker interstate travel, and other conditions can cause large crowds, which can speed up the spread of COVID-19. For instance, in China, the COVID-19 epidemic occurred at the same time as the Lunar New Year celebrations. From Wuhan city, the COVID-19 epicentre, it was projected of five million people travelling to the world's various parts [24, 25]. From another occurrence, several pilgrims who had attended massive prayers in Iran and returned to Pakistan tested

positive for COVID-19, and amid the COVID-19 crisis, over 10,000 pilgrims congregated in Bangladesh for prayer. In Malaysia, there have been more than a hundred new COVID-19 infection cases since a large meeting in Kuala Lumpur in February 2020. According to statistics, the Sri Pentatig mass gathering was directly responsible for more than 35% of the COVID-19 cases in Malaysia [22]. Nearly 30% of COVID-19 cases in India were linked to large religious gatherings, according to studies. To prevent social gatherings, the majority of countries quickly closed places of worship, retail centres, workplaces, and cancelled sporting events. As a result, huge religious assemblies and religious tourism are among the major causes of COVID-19 spreading [86]. High population density may be another important demographic variable contributing to the COVID-19 virus spreading more quickly. Researchers discovered a link between the COVID-19 transfer rate and population density [107]. Mumbai is the most severely impacted city in India because of its dense population and most of its locations are quite susceptible to COVID-19 infection [57]. Using a mask and maintaining a distance from others are two self-protective behaviours that have been shown to reduce individual infection risk and stop the spread of disease [93]. Unfortunately, social distance regulations (such as suspending activities, shutting down companies and schools, and issuing orders to stay at home) have a terrible financial and societal impact [2, 17].

2.2.5 Psychological-Related Variables

Every pandemic has an impact on a person's psychology, and thus making people aware of them, providing health-related education, and taking preventative actions to minimize disease spread are crucial [56]. For instance, Ilesanmi and Alele (2020) investigated the impact of Ebola virus infection's knowledge, attitudes, and perceptions among Nigerians. Their findings indicate that the majority of the population lacked awareness and had a poor attitude about the viral spread. Similar to this, Roy et al. [103] conducted a survey of regular people to evaluate their awareness of, attitudes about, and practices related to the COVID-19 epidemic. According to their research, social isolation, knowledge of COVID-19, travel restrictions, quarantine, and hygiene precautions were crucial. The majority of participants concurred that taking these precautions and cultivating a positive outlook might aid in preventing the potential illness. Participants expressed anxiety and dread over the reintegration of recovering patients into society. As a result, the community's behaviour has been impacted by the dread and worry caused by the extremely contagious COVID-19. Ample public knowledge is thus required in order to influence people's attitudes toward recovering patients and prevents social discriminations [32].

2.3   Vaccination's Reluctances in India

The digital gap is more pronounced in India, where a sizeable section of the population lives in rural areas without access to formal schooling [19, 109, 118]. This suggests that vaccination reluctance may perhaps be more prevalent than previously assumed. According to a study, between 29% and 39% of Indians were unwilling to get vaccines at the beginning of 2021 [27]. Another longitudinal study conducted from January to June of 2021 indicated that 12.7% of adult Indians will not receive the COVID-19 vaccination [120]. Other studies have discovered that worries about the safety and adverse effects of the current vaccinations are the main causes of vaccine reluctance and rejection in India [30]. The COVID-19 vaccine awareness programmes and communication should be based on research, regionally targeted, culturally appropriate, multifaceted, and led by politicians, healthcare experts, dependable voices from the area, and role models. In the extremely varied India's population, researches need to be made on the best ways in spreading the benefits in receiving the COVID-19's vaccine, as well as to alleviate fears and eliminate misunderstandings and misleading facts [60, 104].

Nearly half of Indians have acquired at least single dose of the COVID-19 vaccination by October 2021 [91]. India will now have to deal with COVID-19 resistant and reluctant groups when vaccination rates stagnate [12, 111]. Government should see COVID-19 vaccine reluctance as a severe public health concern. Even a small percentage of vaccine scepticism in India might result in millions of COVID-19 vaccination-refusing citizens throughout the country, which would encourage the emergence of new variations and frequent outbreaks for a very long period.

3   Research Methodology

This research involved an exhaustive literature analysis, followed by interaction with healthcare specialists to identify the underlying vulnerabilities with the COVID-19 pandemic outbreak in Indian context. Moreover, in order to address the aforementioned global health issues, further in-depth investigation is needed to pinpoint and examine the causes of COVID-19's transmission globally. In this chapter, the decision-making model for vaccine's selection was made based on the appropriateness of the available vaccines for COVID-19 patients in the setting of India with various comorbidities. The experts evaluated the vaccine's suitability in terms of four criteria, including the following: vaccine's availability that relies on its ease of access and manufacturing-location; vaccine's effectiveness [77], which can increase the value of vaccine; the likelihood of vaccine-related adverse effects, which may be severe or moderate, and their frequency; and cost savings that include vaccine, transport, and storage costs; respectively [1].

Additionally, despite the fact that other MCDM methods have been established, or the discovery of criteria's estimates and picking in view of their proclivities, one

Table 1 Characteristics of expert participants

Healthcare expert's competence areas	Sexual orientation		Years of experience (average)
	Male	Female	
Pulmonologist	10	2	Beyond 20
Neurologist	6	3	Beyond 16
General physician	3	2	Beyond 23

of the most popular methods that utilize comparisons was already considered as the 'Best-Worst Method (BWM)' with even less data needs and more trustworthy comparability [98]. Rezaei et al. [100] observed that the BWM is suitable when there are fewer criterions to be taken into consideration and that it also produces more consistent findings with fewer pair-wise comparisons [80]. The 'SWARA (Step-wise Weight Assessment Ratio Analysis)' approach, another MCDM method that can handle a variety of criteria in any complicated situation, has also demonstrated its unique use for diverse decision-making processes [81, 134]. Additionally, various research has recommended combining MCDM methods to effectively manage more complex problems, such as SWARA and the 'complex proportional assessment (COPRAS) method' [133]; and SWARA and 'VlseKriterijumska Optimizacija I Kompromisno Resenje (VIKOR) analysis' [6]. However, there are not many researches that take complicated problems into account when integrating BWM and SWARA methods. Therefore, in this chapter, a novel effort was made by combining two MCDM methods, such as the BWM and SWARA methods in order to rank the significant variables that contribute to spreading of COVID-19.

Initially, considering the existing availability, the main preferences of COVID-19's vaccines, such as 'COVISHIELD', 'COVAXIN', and 'Sputnik-V' among the Indian community was done by the use of SWARA approach. Further, in order to rank the essential and significant variables that contribute in spreading COVID-19 and according to how best to prioritize them, the associated significant variables were ranked using the BWM technique. Further, the associated sub-variables were ranked using the SWARA approach, which took into account the variable's optimized-weight values when determining the final weight values of the corresponding sub-variables. The 26 experts who participated in the decision-making stages for the research are enumerated in Table 1, along with information about their typical years of experience, higher education, and sexual orientation.

3.1 The Associated Variables and Sub-variables Identification for the COVID-19 Pandemic Transmission

According to literature, and experts' views, the COVID-19's transmission variables and the corresponding sub-variables were identified as depicted in Table 2.

Table 2 Summary of COVID-19 pandemic transmission variables and the corresponding sub-variables

Sl. no.	Variables	Sub-variables	Source(s)
1	Climate-related variables (V1)	Air-quality ($SV1_1$) Temperature ($SV1_2$) Rainfall ($SV1_3$) Humidity ($SV1_4$) Wind-speed ($SV1_5$)	Ahmadi et al. [4]; Coccia [28]; Hossain [49]; Wang et al. [123]
2	Safety- and hygiene-related variables (V2)	Unawareness of hygiene ($SV2_1$) P.P.E.'s shortages ($SV2_2$) Spitting ($SV2_3$) COVID patient's waste disposals ($SV2_4$) Close contacts ($SV2_5$)	Ghernaout and Elboughdiri [35]; Sohrabi et al. [113]; Vordos et al. [121]
3	Making decisions with attentiveness (V3)	Quarantine-delay ($SV3_1$) Lockdown-delay ($SV3_2$) Travel-restrictions ($SV3_3$)	Chinazzi et al. [26]; Kludge et al. [62]; Nicola et al. [89]; Sohrabi et al. [113]
4	Social- and demographic-variables (V4)	Social-discrimination and -cohesiveness ($SV4_1$) Age-group ($SV4_2$) Population-density ($SV4_3$)	Ahmed and Memish [5]; Bavel et al. [14]; Chen et al. [24, 25]; Mufsin and Muhsin [87]
5	Psychological-related variables (V5)	Knowledge, attitude, and activities ($SV5_1$) Impulsive purchases ($SV5_2$) Concealing past travels ($SV5_3$)	Bavel et al. [14]; Chakraborty and Maity [18]; Ho et al. [48]; Zhong et al. [132]

The five sub-variables under 'Climate-related variables (V1)' included 'Air-quality ($SV1_1$); Temperature ($SV1_2$); Rainfall ($SV1_3$); Humidity ($SV1_4$); and Wind-speed ($SV1_5$)'. The five sub-variables identified under 'Safety- and hygiene-related variables (V2)' included 'Unawareness of hygiene ($SV2_1$); P.P.E.'s shortages ($SV2_2$); Spitting ($SV2_3$); COVID patient's waste disposals ($SV2_4$); and Close contacts ($SV2_5$)'. Similarly, three sub-variables identified under 'Making decisions with attentiveness (V3)' included 'Quarantine-delay ($SV3_1$); Lockdown-delay ($SV3_2$); and Travel-restrictions ($SV3_3$)'. The three sub-variables under 'Social- and demographic-variables (V4)' included 'Social-discrimination and -cohesiveness ($SV4_1$); Age-group ($SV4_2$); and Population-density ($SV4_3$)'. The three sub-variables under 'Psychological-related variables (V5)' included 'Knowledge, attitude and activities ($SV5_1$); Impulsive purchases ($SV5_2$); and Concealing past travels ($SV5_3$)'; respectively.

3.2   The Actions Undertaken in BWM

As noted by Rezaei [99], the following actions were portions of the BWM:

Action-1 A collection of decision-criteria was formed, comprising of 'n' distinct criteria as: $\{C_1, C_2, \ldots, C_n\}$, based on a literature review and the opinions of experts.

Action-2 From the most important or most enviable criterion and the least important or least enviable criterion, the 'worst-criteria (WC) and best-criteria (BC)' were selected.

Action-3 Using values between '1 and 9', it was decided that the BC should take precedence over all other factors. The resulting 'best-to-others (BTO)' vector was provided by: $A_{BC} = \{a_{BC1}, a_{BC2}, \ldots, a_{BCn}\}$, where, $a_{BCi} = $ BC's choice over j, and $a_{BCBC} = 1$.

Action-4 Similar to previous action, other criteria's choices over WC were obtained. The resulting 'others-to-worst (OTW)' vector was provided by: $A_w = \{a_{1W}, a_{2W}, \ldots, a_{nW}\}^T$, where, $a_{jWC} = $ j's choice over WC, and $a_{WCWC} = 1$.

Action-5 The 'optimized-weights (AI_W)' that were found were $\{WC_1^*, WC_2^*, \ldots, WC_n^*\}$.

Calculating AI_w for minimizing the greatest absolute-differences, that is, $\{|WC_{BC} - (a_{BCj}WC_j)|, |WC_j - (a_{jWC}WC_{WC})|\}$ for all j was the primary goal of this stage. The 'minimax-model' that resulted was as follows:

$$\text{Minimax } \left\{ \left| WC_{BC} - \left(a_{BCj}WC_j \right) \right|, \left| WC_j - \left(a_{jwc}WC_{WC} \right) \right| \right\}$$

Subject to,

$$\sum_j WC_j = 1, \{WC_j \geq 0 \text{ for all } j\} \tag{1}$$

Then, continuing with 'Model-(1)', the following linear model was developed:

$$\text{Minimax } \xi^*$$

Subjected to,

$$\left| WC_{BC} - \left[a_{BCj}WC_j \right] \right| \leq \xi^*, \quad \left| WC_j - a_{jwc}WC_{WC} \right| \quad \{\text{for all } j\}$$
$$\sum_j WC_j = 1, \quad \{WC_j \geq 0 \text{ for all } j\} \tag{2}$$

The aforementioned 'Model-(2)' was solved to determine AI_W as well as the 'optimized-value (ξ^*)'. A number 'closer to 0' was essential for evaluating the comparison's 'consistency (C_i^*)', which was another key consideration [100].

Table 3 Values of C_I in BWM

a_{BCWC}	9	8	7	6	5	4	3	2	1
C_I (Maximum ξ^*)	5.23	4.47	3.73	3.00	2.30	1.63	1.00	0.44	0

However, the C_I in Eq. (3) below helps to determine the C_i^*.

$$C_i^* = [\xi^*/C_I] \tag{3}$$

The values of 'consistency-index (C_I)' that were utilized, was as shown in Table 3.

3.3 The Stages Undertaken in SWARA

The subsequent stages, according to Stanujkic et al. [114], were used to prioritize more and less crucial factors.

Stage 1 Clustering the criteria according to order of importance

In this stage, experts evaluated the proportional weights assigned to each criterion to rate them. The more significant criterion was initially placed first, and only then was the less significant criterion added in the end destination.

Stage 2 Assessing how relevant typical values are in comparison

Depending on how important criterion (c_j) was in comparison to criterion (c_{j+1}), the relative-importance of 'average values (s_j)' was established beginning with the criterion that has been placed second.

Stage 3 Coefficients' (k_j) computation as given:

$$k_j = \begin{cases} 1, & j = 1 \\ s_j + 1, & j > 1 \end{cases} \tag{4}$$

Stage 4 Recalculated-weights' (q_j) calculation as stated below:

$$q_j = \begin{cases} 1, & j = 1 \\ \frac{q_{j-1}}{k_j}, & j > 1 \end{cases} \tag{5}$$

Stage 5 Final weights' (w_j) computation of the 'evaluation-criteria' for n number of criteria, as given:

$$w_j = \frac{q_j}{\sum_{k=1}^{n} q_k} \tag{6}$$

Table 4 w_j of available vaccines

Vaccines	Relative-importance of s_j	k_j	q_j	w_j	Rank based on w_j value
COVAXIN		1	1	0.396	1
COVISHIELD	0.21	1.21	0.826	0.327	2
Sputnik-V	0.18	1.18	0.700	0.277	3

4 Results

The ranking of the available vaccine's preferences in India and the COVID-19 transmission variables with the corresponding sub-variables was described in the following sub-sections.

4.1 Ranking of the Available Vaccine's Preferences in India

The w_j values of different available vaccines were obtained by using SWARA approach as illustrated in Table 4. It may be noted the experts' suggestion were taken for sorting the available vaccines according to their preferences. The ranking based on w_j values of different vaccines revealed the preference for COVAXIN at first level, which was followed by the subsequent preferences for COVISHIELD and Sputnik-V at second and third levels.

4.2 Ranking of the COVID-19 Transmission Variables and Corresponding Sub-variables

4.2.1 Variable's Ranking by BWM

The BC and WC were chosen based on the experts' opinion and the respective importance of each of the five selected Vs. Then, on a scale of '1 to 9', experts were interviewed to decide which variables were favoured as BC over all others. By using the same evaluation values, the opinions of other variables associated to the WC were also established. Additionally, the AI_w values for each of the criteria in addition to the C_i^* was derived using the 'BWM-Solver.xlsx software', and equation (ii) was used to finalize the preference scores for all five Vs.

The variable V2 was chosen as the BC and V2 as WC. Table 5 illustrated the comparisons of V2 to all Vs, while Table 6 illustrated the comparisons of all Vs to V5. Table 7 illustrated the AI_w values for each variable, such as $AI_{w1} = 0.229$; $AI_{w2} = 0.448$; $AI_{w3} = 0.114$; $AI_{w4} = 0.153$; and $AI_{w5} = 0.054$. Additionally, C_i^* was found to be 0.011, as shown in Table 7. Then, taking criterion on X-axis and values of AI_w on Y-axis, a graph was created as shown in Fig. 1. The AI_w

Table 5 The comparison of V2 to all Vs

BTO	V1	V2	V3	V4	V5
V2	2	1	4	3	8

Table 6 All Vs comparison to V5

OTW	V1	V2	V3	V4	V5
V5	4	8	2	3	1

Table 7 Vs' AI_w values

Vs	AI_w	C_i^*	Rank
V2	0.448	0.011	**1**
V1	0.229	**2**	
V4	0.153	**3**	
V3	0.114	**4**	
V5	0.054	**5**	
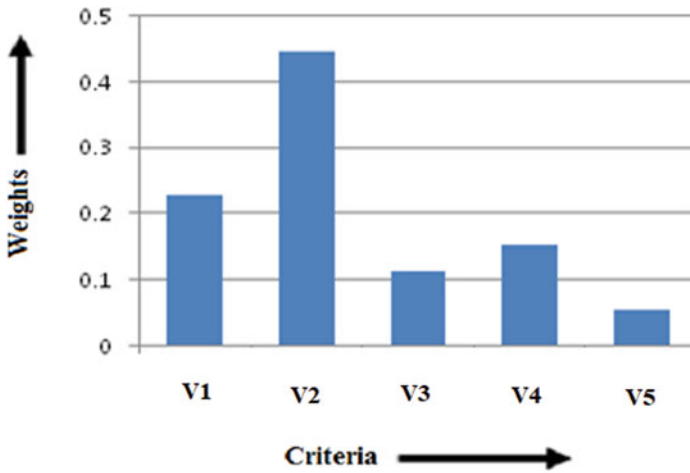
Fig. 1 Values of AI_w for all Vs

for different Vs revealed that 'Safety- and hygiene-related variables (V2)' to be rated in the first level, and was followed by 'Climate-related variables (V1); Social- and demographic-variables (V4); Making decisions with attentiveness (V3); and Psychological-related variables (V5)'; respectively.

4.2.2 Sub-variable's Ranking by SWARA

The 'final revised-weight (FRw_j) values' for each of the sub-variables under each of the different Vs were calculated using the AI_w of the various Vs found in BWM as presented in Tables 8, 9, 10, 11, and 12, respectively. The FRw_j of each sub-variable was calculated using the AI_w [58]. It should be mentioned that the experts'

Table 8 FRw_j of all sub-variables of V1

Sub-variables	Relative-importance of s_j	k_j	q_j	w_j	#FRw_j
SV1$_5$		1	1	0.269	0.061
SV1$_4$	0.20	1.17	0.854	0.229	0.052
SV1$_1$	0.18	1.18	0.724	0.194	0.044
SV1$_2$	0.19	1.19	0.608	0.163	0.037
SV1$_3$	0.15	1.15	0.529	0.142	0.032

#FRw_j of, SV1$_4$ = 0.229 × 0.229 = 0.052; SV1$_3$ = 0.142 × 0.229 = 0.032

Table 9 FRw_j of all sub-variables of V2

Sub-variables	Relative-importance of s_j	k_j	q_j	w_j	FRw_j
SV2$_1$		1	1	0.258	0.115
SV2$_5$	0.15	1.15	0.869	0.224	0.100
SV2$_4$	0.13	1.13	0.769	0.198	0.088
SV2$_2$	0.16	1.16	0.663	0.171	0.076
SV2$_3$	0.15	1.15	0.576	0.148	0.066

Table 10 FRw_j of all sub-variables of V3

Sub-variables	Relative-importance of s_j	k_j	q_j	w_j	FRw_j
SV3$_1$		1	1	0.390	0.044
SV3$_3$	0.19	1.19	0.840	0.327	0.037
SV3$_2$	0.16	1.16	0.724	0.282	0.032

Table 11 FRw_j of all sub-variables of V4

Sub-variables	Relative-importance of s_j	k_j	q_j	w_j	FRw_j
SV4$_3$		1	1	0.379	0.058
SV4$_1$	0.15	1.15	0.869	0.329	0.050
SV4$_2$	0.13	1.13	0.769	0.291	0.044

Table 12 FRw_j of all sub-variables of V5

Sub-variables	Relative-importance of s_j	k_j	q_j	w_j	FRw_j
SV5$_1$		1	1	0.384	0.020
SV5$_3$	0.17	1.17	0.854	0.328	0.017
SV5$_2$	0.14	1.14	0.749	0.288	0.015

Table 13 Final weight's summary

Variables and sub-variables	AI_w and FRw_j	Variable's ranking based on AI_w	Sub-variable's ranking based on FRw_j
V1	**0.229**	**2nd**	–
$SV1_1$	0.044	–	**10th**
$SV1_2$	0.037	–	**11th**
$SV1_3$	0.032	–	**12th**
$SV1_4$	0.052	–	**8th**
$SV1_5$	0.061	–	**6th**
V2	**0.448**	**1st**	–
$SV2_1$	0.115	–	**1st**
$SV2_2$	0.076	–	**4th**
$SV2_3$	0.066	–	**5th**
$SV2_4$	0.088	–	**3rd**
$SV2_5$	0.100	–	**2nd**
V3	**0.114**	**4th**	–
$SV3_1$	0.044	–	**8th**
$SV3_2$	0.032	–	**7th**
$SV3_3$	0.037	–	**11th**
V4	**0.153**	**3rd**	–
$SV4_1$	0.050	–	**9th**
$SV4_2$	0.044	–	**10th**
$SV4_3$	0.058	–	**7th**
V5	**0.054**	**5th**	–
$SV5_1$	0.020	–	**13th**
$SV5_2$	0.015	–	**15th**
$SV5_3$	0.017	–	**14th**

recommendations were followed regarding the respective importance of the sub-variables under the various Vs.

Following the above calculations, Table 13 provided a summary of the weights assigned to each relevant variables and sub-variables, together with their relative rankings in relation to the AI_w and FRw_j values. It was observed that the safety- and hygiene-related variables ranked at first level, which was followed by climate-related variables; social- and demographic-variables; making decisions with attentiveness; and psychological-related variables. The sub-variables in the descending order of ranking included the following: Unawareness of hygiene; Close contacts; COVID patient's waste disposals; P.P.E.'s shortages; Spitting; Wind-speed; both Lockdown-delay and Population-density; both Humidity and Quarantine-delay; Social-discrimination and -cohesiveness; both Air-quality and Age-group; both Temperature and Travel-restrictions; Rainfall; Knowledge, attitude and activities; Concealing past travels; and Impulsive purchases; respectively.

5   Discussion

As COVID-19 spreads, it poses a serious threat to government agencies and decision-makers worldwide [52, 54]. There is a pressing need for effective and safe vaccinations as a result of this continued growth [43]. Public health initiatives to encourage the usage of the vaccine as a means of putting an end to the deadly pandemic might be seriously undermined by external forces that have an influence on the vaccine approval process [16]. Consideration of several psychological and social variables is necessary for the recommended and widespread acceptance of vaccines [106]. Irrespective of vaccination effectiveness, it has been demonstrated that COVID-19's vaccine allocation for older persons (more than 60 years) resulted in subsequent decrease in mortality [33]. According to a study on the vaccination habits of nurses, nurses' COVID-19-related job demands were linked to greater work stress and, as a result, a larger intention to get the COVID-19's vaccine [69]. The COVID-19 pandemic highlights the difficulties that governments and international organizations have in deciding which feasible interventions will be most successful. The best available scientific data, which is often offered by expert opinions and relevant studies, would be combined to create the logical strategic decision [7, 15, 42].

The ideal course of action is for the decision-makers to consult vaccination experts in addition to experts in other disciplines, such as for analysing cost-analysis and social-factors. Depending on the characteristics of the system and other important factors, a decision may require a certain group of experts [73]. The choice of vaccination by the public can undoubtedly be influenced by media coverage, but decision-makers' views should not be impacted by it [1].

6   Conclusion

This chapter provided a novel hybrid MCDM framework to identify variables and sub-variables that are responsible for COVID-19's transmission. In order to rank the significant variables that contribute to spreading of COVID-19, an effort was made by combining both the 'Best-Worst-Method (BWM)' and 'Step-Wise Assessment and Ratio-Analysis (SWARA)' methods establishing a hybrid MCDM framework. Apart from this, it also analysed the existing available vaccines preferences among the Indian community. A 'safe and healthy' environment can be achieved by revising healthcare plans and policies in light of the results and underlying consequences. This work has several shortcomings despite these original contributions; thus, it provides some suggestions for further research. First of all, because COVID-19 is a novel virus that may transmit in a variety of ways, virology and observational studies are still in their infancy. The analysis can be repeated in the future with the addition of new variables and sub-variables that affect COVID-19's transmission.

References

1. Abdelwahab, S.F., Issa, U.H., Ashour, H.M.: A novel vaccine selection decision-making model (VSDMM) for COVID-19. Vaccine. **9**, 718 (2021). https://doi.org/10.3390/vaccines9070718

2. Adolph, C., Amano, K., Bang-Jensen, B., Fullman, N., Wilkerson, J.: Pandemic politics: timing state-level social distancing responses to COVID-19. J. Health Polit. Policy Law. **46**(2), 211–233 (2021)

3. Ahmad, T., Khan, M., Haroon, T.H.M., Nasir, S., Hui, J., Bonilla-Aldana, D.K., Rodriguez-Morales, A.J.: COVID-19: zoonotic aspects. Travel Med. Infect. Dis. **36**, 101607 (2020)

4. Ahmadi, M., Sharifi, A., Dorosti, S., Ghoushchi, S.J., Ghanbari, N.: Investigation of effective climatology parameters on COVID-19 outbreak in Iran. Sci. Total Environ. **729**, 138705 (2020)

5. Ahmed, Q.A., Memish, Z.A.: The cancellation of mass gatherings (MGs)? Decision making in the time of COVID-19. Travel Med. Infect. Dis. **34**, 101631 (2020)

6. Alimardani, M., Zolfani, S.H., Aghdaie, M.H., Tamošaitienė, J.: A novel hybrid SWARA and VIKOR methodology for supplier selection in an agile environment. Technol. Econ. Dev. Econ. **19**, 533–548 (2013)

7. Alsalem, M.A., Mohammed, R., Albahri, O.S., Zaidan, A.A., Alamoodi, A.H., Dawood, K., Alnoor, A., Albahri, A.S., Zaidan, B.B., Aickelin, U., Alsattar, H., Alazab, M., Jumaah, F.: Rise of multiattribute decision-making in combating COVID-19: a systematic review of the state-of-the-art literature. Int. J. Intell. Syst. **37**, 3514–3624 (2022). https://doi.org/10.1002/int.22699

8. Anastassopoulou, C., Russo, L., Tsakris, A., Siettos, C.: Databased analysis, modelling and forecasting of the novel coronavirus [2019-nCoV] outbreak. medRxiv. Preprint (2020). Available from: https://doi.org/10.1101/2020.02.11.20022186

9. Anderson, R.M., Heesterbeek, H., Klinkenberg, D., Hollingsworth, T.D.: How will country-based mitigation measures influence the course of the COVID-19 epidemic? Lancet. **395**, 931–934 (2020)

10. Auler, A.C., Cássaro, F.A.M., da Silva, V.O., Pires, L.F.: Evidence that high temperatures and intermediate relative humidity might favor the spread of COVID-19 in tropical climate: a case study for the most affected Brazilian cities. Sci. Total Environ. **729**, 139090 (2020)

11. Bai, Y., Yao, L., Wei, T., Tian, F., Jin, D.Y., Chen, L., Wang, M.: Presumed asymptomatic carrier transmission of COVID-19. JAMA. **323**(14), 1406 (2020)

12. Bansal, P., Raj, A., Shukla, D.M., Sunder, N.: COVID-19 vaccine preferences in India. Vaccine. **40**, 2242–2246 (2022). https://doi.org/10.1016/j.vaccine.2022.02.077

13. Bashir, M.F., Ma, B., Komal, B., Bashir, M.A., Tan, D., Bashir, M.: Correlation between climate indicators and COVID-19 pandemic in New York, USA. Sci. Total Environ. **728**, 138835 (2020)

14. Bavel, J.J.V., Baicker, K., Boggio, P.S., Capraro, V., Cichocka, A., Cikara, M., Crockett, M.J., Crum, A.J., Douglas, K.M., Druckman, J.N., Drury, J.: Using social and behavioural science to support COVID-19 pandemic response. Nat. Hum. Behav. **4**(5), 460–471 (2020)

15. Berger, L., Berger, N., Bosetti, V., Gilboa, I., Hansen, L.P., Jarvis, C., Marinacci, M., Smith, R.D.: Rational policymaking during a pandemic. Proc. Natl. Acad. Sci. **118**(4), e2012704118 (2021). https://doi.org/10.1073/pnas.2012704118

16. Bokemper, S.E., Huber, G.A., Gerber, A.S., James, E.K., Omer, S.B.: Timing of COVID-19 vaccine approval and endorsement by public figures. Vaccine. **39**, 825–829 (2021)

17. Briscese, G., Lacetera, N., Macis, M., Tonin, M.: Compliance with Covid-19 Social-Distancing Measures in Italy: The Role of Expectations and Duration, vol. 27. National Bureau of Economic Research, Cambridge, MA (2020)
18. Chakraborty, I., Maity, P.: COVID-19 outbreak: migration, effects on society, global environment and prevention. Sci. Total Environ. **728**, 138882 (2020)
19. Chakraborty, C., Ranjan, A., Bhattacharya, M., Agoramoorthy, G., Lee, S.S.: The current second wave and COVID-19 vaccination status in India. Brain Behav. Immun. **96**, 1–4 (2021). https://doi.org/10.1016/j.bbi.2021.05.018
20. Chan, J.F.-W., Yuan, S., Kok, K.-H., et al.: A familial cluster of pneumonia associated with the 2019 novel coronavirus indicating person-to-person transmission: a study of a family cluster. Lancet. **395**(10223), 514–523 (2020)
21. Chatterji, S.: Covid-19 vaccine diplomacy in India's outreach plan. Hindustan Times (2020)
22. Che Mat, N.F., Edinur, H.A., Abdul Razab, M.K.A., Safuan, S.: A single mass gathering resulted in massive transmission of COVID-19 infections in Malaysia with further international spread. J. Travel Med. **27**(3), taaa059 (2020)
23. Chen, J.: Pathogenicity and transmissibility of 2019-nCoV—a quick overview and comparison with other emerging viruses. Microbes Infect. **22**(2), 69–71 (2020)
24. Chen, N., Zhou, M., Dong, X., et al.: Epidemiological and clinical characteristics of 99 cases of 2019 novel coronavirus pneumonia in Wuhan, China: a descriptive study. Lancet. **395**(10223), 507–513 (2020a)
25. Chen, S., Yang, J., Yang, W., Wang, C., Bärnighausen, T.: COVID-19 control in China during mass population movements at New Year. Lancet. **395**(10226), 764–766 (2020b)
26. Chinazzi, M., Davis, J.T., Ajelli, M., Gioannini, C., Litvinova, M., Merler, S., et al.: The effect of travel restrictions on the spread of the 2019 novel coronavirus (COVID- 19) outbreak. Science. **368**(6489), 395–400 (2020)
27. Chowdhury, S.R., et al.: Covid-19 vaccine hesitancy: trends across states, over time (2021). Available at: https://www.ideasforindia.in/topics/human-development/covid-19-vaccine-hesitancy-trends-across-states-over-time.html
28. Coccia, M.: Factors determining the diffusion of COVID-19 and suggested strategy to prevent future accelerated viral infectivity similar to COVID. Sci. Total Environ. **729**, 138474 (2020)
29. Coşkun, H., Yıldırım, N., Gündüz, S.: The spread of COVID-19 virus through population density and wind in Turkey cities. Sci. Total Environ. **751**, 141663 (2021)
30. Danabal, K.G.M., Magesh, S.S., Saravanan, S., Gopichandran, V.: Attitude towards COVID 19 vaccines and vaccine hesitancy in urban and rural communities in Tamil Nadu, India–a community-based survey. BMC Health Serv. Res. **21**(1), 1–10 (2021)
31. de Bruin, Y.B., Lequarre, A.S., McCourt, J., Clevestig, P., Pigazzani, F., Jeddi, M.Z., et al.: Initial impacts of global risk mitigation measures taken during the combating of the COVID-19 pandemic. Saf. Sci. **128**, 104773 (2020)
32. Devakumar, D., Shannon, G., Bhopal, S.S., Abubakar, I.: Racism and discrimination in COVID-19 responses. Lancet. **395**(10231), 1194 (2020)
33. Foy, B.H., Wahl, B., Mehta, K., Shet, A., Menon, G.I., Britto, C.: Comparing COVID-19 vaccine allocation strategies in India: a mathematical modelling study. Int. J. Infect. Dis. **103**, 431–438 (2021)
34. Gao, J., Tian, Z., Yang, X.: Breakthrough: chloroquine phosphate has shown apparent efficacy in treatment of COVID-19 associated pneumonia in clinical studies. Biosci. Trends. **14**(1), 72–73 (2020)
35. Ghernaout, D., Elboughdiri, N.: Urgent proposals for disinfecting hospital wastewaters during COVID-19 pandemic. Open Access Libr. J. **7**(5), 1–18 (2020)
36. Ghosh, A., Roy, S., Mondal, H., Biswas, S., Bose, R.: Mathematical modelling for decision making of lockdown during COVID-19. Appl. Intell. **52**, 699–715 (2022). https://doi.org/10.1007/s10489-021-02463-7
37. Gilardin, L., Bayry, J., Kaveri, S.V.: Intravenous immunoglobulin as clinical immune-modulating therapy. Can. Med. Assoc. J. **187**(4), 257–264 (2015)

38. Gondauri, D., Batiashvili, M.: The study of the effects of mobility trends on the statistical models of the COVID-19 virus spreading. Electron. J. Gen. Med. **17**(6), em243 (2020)
39. Gorbalenya, A.E., Baker, S.C., Baric, R.S., de Groot, R.J., Drosten, C., Gulyaeva, A.A., Haagmans, B.L., Lauber, C., Leontovich, A.M., Neuman, B.W., Penzar, D.: Severe acute respiratory syndrome-related coronavirus: the species and its viruses–a statement of the Coronavirus Study Group. bioRxiv. (2020). https://doi.org/10.1101/2020.02.07.937862
40. Gössling, S., Scott, D., Hall, C.M.: Pandemics, tourism and global change: a rapid assessment of COVID-19. J. Sustain. Tour. **29**(1), 1–20 (2020)
41. Guo, Z.D., Wang, Z.Y., Zhang, S.F., Li, X., Li, L., Li, C., Cui, Y., Fu, R.B., Dong, Y.Z., Chi, X.Y., Zhang, M.Y.: Aerosol and surface distribution of severe acute respiratory syndrome coronavirus 2 in hospital wards, Wuhan, China, 2020. Emerg. Infect. Dis. **26**(7), 1586 (2020)
42. Gupta, R., Rathore, B., Srivastava, A., Biswas, B.: Decision-making framework for identifying regions vulnerable to transmission of COVID-19 pandemic. Comput. Ind. Eng. **169**, 108207 (2022). https://doi.org/10.1016/j.cie.2022.108207
43. Halilova, J.G., Fynes-Clinton, S., Green, L., Myerson, J., Wu, J., Ruggeri, K., Addis, D.R., Rosenbaum, R.S.: Short-sighted decision-making by those not vaccinated against COVID-19. Sci. Rep. **12**, 11906 (2022). https://doi.org/10.1038/s41598-022-15276-6
44. Hansen, L.P.: Nobel lecture: uncertainty outside and inside economic models. J. Polit. Econ. **122**, 945–987 (2014)
45. Hansen, L.P., Marinacci, M.: Ambiguity aversion and model misspecification: an economic perspective. Stat. Sci. **31**, 511–515 (2016)
46. Harapan, H., Itoh, N., Yufika, A., Winardi, W., Keam, S., Te, H., et al.: Coronavirus disease 2019 (COVID-19): a literature review. J. Infect. Public Health. **13**, 667–673 (2020)
47. He, X., Lau, E.H., Wu, P., Deng, X., Wang, J., Hao, X., Lau, Y.C., Wong, J.Y., Guan, Y., Tan, X., Mo, X.: Temporal dynamics in viral shedding and transmissibility of COVID-19. Nat. Med. **26**, 1–4 (2020)
48. Ho, C.S., Chee, C.Y., Ho, R.C.: Mental health strategies to combat the psychological impact of COVID-19 beyond paranoia and panic. Ann. Acad. Med. Singap. **49**(1), 1–3 (2020)
49. Hossain, M.A.: Is the spread of COVID-19 across countries influenced by environmental, economic and social factors? medRxiv (2020)
50. Hu, Z., Song, C., Xu, C., Jin, G., Chen, Y., Xu, X., et al.: Clinical characteristics of 24 asymptomatic infections with COVID-19 screened among close contacts in Nanjing, China. Sci. China Life Sci. **63**(5), 706–711 (2020)
51. Islam, A.R.M.T., Hasanuzzaman, M., Shammi, M., Salam, R., Bodrud-Doza, M., Rahman, M.M., et al.: Are meteorological factors enhancing COVID-19 transmission in Bangladesh? Novel findings from a compound Poisson generalized linear modeling approach. Environ. Sci. Pollut. Res. **28**(9), 11245–11258 (2021)
52. Issa, U., Balabel, A., Abdelhakeem, M., Osman, M.: Developing a risk model for assessment and control of the spread of COVID-19. Risks. **9**, 38 (2021)
53. Jadhav, V.R., Aher, J.S., Bhagare, A.M., Dhaygude, A.C.: COVID-19 era: what's impact of the lockdown on India's environment? J. Chem. Environ. Sci. Appl. **7**(1), 1–6 (2020)
54. Jaffé, R., Ortiz, M., Jaffé, K.: Globalized low-income countries may experience higher COVID-19 mortality rates. medRxiv (2020)
55. Jha, S., Goyal, M.K., Gupta, B., Gupta, A.K.: A novel analysis of COVID 19 risk in India incorporating climatic and socioeconomic Factors. Technol. Forecast. Soc. Change. **167**, 120679 (2021)
56. Johnson, E.J., Hariharan, S.: Public health awareness: knowledge, attitude and behaviour of the general public on health risks during the H1N1 influenza pandemic. J. Public Health. **25**(3), 333–337 (2017)
57. Kaushal, J., Mahajan, P.: Asia's largest urban slum-Dharavi: a global model for management of COVID-19. Cities. **111**, 103097 (2021)
58. Keršuliene, V., Zavadskas, E.K., Turskis, Z.: Selection of rational dispute resolution method by applying new step-wise weight assessment ratio analysis (SWARA). J. Bus. Econ. Manag. **11**, 243–258 (2010)

59. Khanmohammadi, S., Rezaeiahari, M.: AHP based classification algorithm selection for clinical decision support system development. Procedia Comput. Sci. **36**, 328–334 (2014)
60. Khubchandani, J., Sharma, S., Price, J.H., Wiblishauser, M.J., Sharma, M., Webb, F.J.: COVID-19 vaccination hesitancy in the United States: a rapid national assessment. J. Community Health. **46**(2), 270–277 (2021)
61. Kim, D., Hong, S., Choi, S., Yoon, T.: Analysis of transmission route of MERS coronavirus using decision tree and Apriori algorithm. In: 2016 18th International Conference on Advanced Communication Technology (ICACT), pp. 559–565. IEEE (2016)
62. Kludge, H.H.P., Jakab, Z., Bartovic, J., D'Anna, V., Severoni, S.: Refugee and migrant health in the COVID-19 response. Lancet. **395**(10232), 1237–1239 (2020)
63. Koo, J.R., Cook, A.R., Park, M., et al.: Interventions to mitigate early spread of SARSCoV-2 in Singapore: a modelling study. Lancet Infect. Dis. **20**, 678 (2020). https://doi.org/10.1016/S1473-3099(20)30162-6
64. Kraemer, M.U., Yang, C.H., Gutierrez, B., Wu, C.H., Klein, B., Pigott, D.M., Open COVID-19 Data Working Group†, Du Plessis, L., Faria, N.R., Li, R., Hanage, W.P.: The effect of human mobility and control measures on the COVID-19 epidemic in China. Science. **368**(6490), 493–497 (2020)
65. Kroumpouzos, G., Gupta, M., Jafferany, M., Lotti, T., Sadoughifar, R., Sitkowska, Z., et al.: COVID-19: a relationship to climate and environmental conditions? Dermatol. Ther. **33**(4), e13399 (2020)
66. Ku, P.K., Holsinger, F.C., Chan, J.Y., Yeung, Z.W., Chan, B.Y., Tong, M.C., Starmer, H.M.: Management of dysphagia in the patient with head and neck cancer during COVID-19 pandemic: practical strategy. Head Neck. **42**(7), 1491–1496 (2020)
67. Kulkarni, H., Khandait, H., Narlawar, U.W., Rathod, P., Mamtani, M.: Independent association of meteorological characteristics with initial spread of Covid-19 in India. Sci. Total Environ. **764**, 142801 (2021)
68. Kumar, A., Roy, R.: Application of mathematical modeling in public health decision making pertaining to control of COVID-19 pandemic in India. Epidemiol. Int. **5**(2), 23–26 (2020)
69. Kwok, K.O., Li, K.-K., Wei, W.I., Tang, A., Wong, S.Y.S., Lee, S.S.: Influenza vaccine uptake, COVID-19 vaccination intention and vaccine hesitancy among nurses: a survey. Int. J. Nurs. Stud. **114**, 103854 (2021)
70. Lakshmi Priyadarshini, S., Suresh, M.: Factors influencing the epidemiological characteristics of pandemic COVID 19: a TISM approach. Int. J. Healthc. Manag. **13**(3), 1–10 (2020)
71. Li, Q., Guan, X., Wu, P., et al.: Early transmission dynamics in Wuhan, China, of novel coronavirus-infected pneumonia. N. Engl. J. Med. **382**(13), 1199–1207 (2020)
72. Lipsitch, M., Swerdlow, D.L., Finelli, L.: Defining the epidemiology of Covid-19—studies needed. N. Engl. J. Med. **382**(13), 1194–1196 (2020)
73. Liu, H.W., Wang, G.J.: Multi-criteria decision-making methods based on intuitionistic fuzzy sets. Eur. J. Oper. Res. **179**(1), 220–233 (2007)
74. Lu, H.: Drug treatment options for the 2019-new coronavirus (2019-nCoV). Biosci. Trends. **14**(1), 69–71 (2020)
75. Marinacci, M.: Model uncertainty. J. Eur. Econ. Assoc. **13**, 1022–1100 (2015)
76. McCloskey, B., Zumla, A., Lim, P.L., Endericks, T., Arbon, P., Cicero, A., et al.: A risk-based approach is best for decision making on holding mass gathering events. Lancet. **395**(10232), 1256–1257 (2020)
77. McPhedran, R., Toombs, B.: Efficacy or delivery? An online Discrete Choice Experiment to explore preferences for COVID-19 vaccines in the UK. Econ. Lett. **200**, 109747 (2021)
78. Mint: For COVID vaccine distribution in India, govt boosting tracking mechanism. Mint (2020a)
79. Mint: For COVID vaccine delivery, govt to map out cold chain storage facilities. Mint (2020b)
80. Mishra, D., Satapathy, S.: MCDM approach for mitigation of flooding risks in Odisha (India) based on information retrieval. Int. J. Cognit. Inform. Nat. Intell. **14**, 77–91 (2020). https://doi.org/10.4018/IJCINI.2020040105

81. Mishra, D., Satapathy, S.: SWARA approach for ranking of agricultural supply chain risks of Odisha in India. Int. J. Inf. Decis. Sci. **13**, 85–109 (2021)

82. Mohammad, M., Pratishtha, S., Mohsina, P., Faheem, P., Rajiv, K., Rakesh, P.: Covid-19 vaccines available in India. Comb. Chem. High Throughput Screen. **25**(14), 2391 (2022). https://doi.org/10.2174/1386207325666220315115953

83. Mohanty, K., Das, A.: Coronavirus vaccine: how long before you can get a Covid-19 vaccine? Times of India (2020)

84. Morgan, O.: How decision makers can use quantitative approaches to guide outbreak responses. Philos. Trans. R. Soc. Lond. B Biol. Sci. **374**, 20180365 (2019)

85. Moriarty, L.F., Plucinski, M.M., Marston, B.J., Kurbatova, E.V., Knust, B., Murray, E.L., Pesik, N., Rose, D., Fitter, D., Kobayashi, M., Toda, M.: Public health responses to COVID-19 outbreaks on cruise ships—worldwide, February–March 2020. Morb. Mortal. Wkly Rep. **69**(12), 347 (2020)

86. Mubarak, N., Zin, C.S.: Religious tourism and mass religious gatherings—the potential link in the spread of COVID-19. Current perspective and future implications. Travel Med. Infect. Dis. **36**, 101786 (2020)

87. Mufsin, P.P., Muhsin, P.P.: Sociocultural and religious factors complicate India's COVID-19 response. The Diplomat (2020)

88. Mustafa, S., Balkhy, H., Gabere, M.N.: Current treatment options and the role of peptides as potential therapeutic components for Middle East Respiratory Syndrome (MERS): a review. J. Infect. Public Health. **11**(1), 9–17 (2018)

89. Nicola, M., Alsafi, Z., Sohrabi, C., Kerwan, A., Al-Jabir, A., Iosifidis, C., Agha, M., Agha, R.: The socio-economic implications of the coronavirus pandemic (COVID-19): a review. Int. J. Surg. **78**, 185–193 (2020)

90. Noorimotlagh, Z., Jaafarzadeh, N., Martínez, S.S., Mirzaee, S.A.: A systematic review of possible airborne transmission of the COVID-19 virus (SARS-CoV-2) in the indoor air environment. Environ. Res. **193**, 110612 (2020)

91. Our World in Data: Statistics and research: coronavirus (COVID-19) vaccinations-India (2021). Available at: https://ourworldindata.org/covid-vaccinations?country¼IND

92. Öztürk, N., Karacan, I., Tozan, H., Vayvay, Ö.: Defining criteria weights by AHP in health technology assessment. Value Health. **20**, A698 (2017)

93. Papageorge, N.W., Zahn, M.V., Belot, M., Van den Broek-Altenburg, E., Choi, S., Jamison, J.C., et al.: Socio-demographic factors associated with self-protecting behavior during the Covid-19 pandemic. J. Popul. Econ. **34**(2), 691–738 (2021)

94. Piguillem, F., Shi, L.: Optimal COVID-19 quarantine and testing policies. Econ. J. **132**(647), 2534–2562 (2022)

95. Pramanik, M., Udmale, P., Bisht, P., Chowdhury, K., Szabo, S., Pal, I.: Climatic factors influence the spread of COVID-19 in Russia. Int. J. Environ. Health Res. **32**(4), 723–737 (2022)

96. Press Information Bureau: Multilateral Cooperation Is the Key to Overcoming Global Challenges Such as COVID-19: Dr. Harsh Vardhan. Press Information Bureau, Government of India (2020)

97. Qu, G., Li, X., Hu, L., Jiang, G.: An imperative need for research on the role of environmental factors in transmission of novel coronavirus (COVID-19). Environ. Sci. Technol. **54**(7), 3730–3732 (2020). https://doi.org/10.1021/acs.est.0c01102

98. Rezaei, J.: Best-worst multi-criteria decision-making method. Omega. **53**, 49–57 (2015)

99. Rezaei, J.: Best-worst multi-criteria decision-making method: some properties and a linear model. Omega. **64**, 126–130 (2016)

100. Rezaei, J., Nispeling, T., Sarkis, J., Tavasszy, L.: A supplier selection life cycle approach integrating traditional and environmental criteria using the best worst method. J. Clean. Prod. **135**, 577–588 (2016)

101. Roger, F., Delabouglise, A., Roche, B., Peyre, M., Chevalier, V.: Origin of the Covid-19 virus: the trail of mink farming. The Conversation (2021)

102. Rothe, C., Schunk, M., Sothmann, P., et al.: Transmission of 2019-nCoV infection from an asymptomatic contact in Germany. N. Engl. J. Med. **382**(10), 970–971 (2020)
103. Roy, D., Tripathy, S., Kar, S.K., Sharma, N., Verma, S.K., Kaushal, V.: Study of knowledge, attitude, anxiety & perceived mental healthcare need in Indian population during COVID-19 pandemic. Asian J. Psychiatr. **51**, 102083 (2020)
104. Sallam, M.: COVID-19 vaccine hesitancy worldwide: a concise systematic review of vaccine acceptance rates. Vaccine. **9**(2), 160 (2021). https://doi.org/10.3390/vaccines9020160
105. Schippers, M.C., Rus, D.C.: Optimizing decision-making processes in times of COVID-19: using reflexivity to counteract information-processing failures. Front. Psychol. **12**, 650525 (2021). https://doi.org/10.3389/fpsyg.2021.650525
106. Schoch-Spana, M., Brunson, E.K., Long, R., Ruth, A., Ravi, S.J., Trotochaud, M., Borio, L., Brewer, J., Buccina, J., Connell, N., et al.: The public's role in COVID-19 vaccination: human-centered recommendations to enhance pandemic vaccine awareness, access, and acceptance in the United States. Vaccine. **39**(40), 6004–6012 (2020)
107. Selcuk, M., Gormus, S., Guven, M.: Impact of weather parameters and population density on the COVID-19 transmission: evidence from 81 provinces of Turkey. Earth Syst. Environ. **5**(1), 87–100 (2021)
108. Setti, L., Passarini, F., De Gennaro, G., Barbieri, P., Perrone, M.G., Miani, A.: Airborne transmission route of COVID-19: why 2 meters/6 feet of inter-personal distance could not be enough. Int. J. Environ. Res. Public Health. **17**(8), 2932 (2020). https://doi.org/10.3390/ijerph17082932
109. Shah, M.: India's digital divide is hampering its mass Covid-19 vaccination campaign (2021). Available at: https://www.scmp.com/week-asia/health-environment/article/3141180/indias-digital-divide-hampering-its-mass-covid-19
110. Shao, S., Zhou, D., He, R., Li, J., Zou, S., Mallery, K., et al.: Risk assessment of airborne transmission of COVID-19 by asymptomatic individuals under different practical settings. J. Aerosol Sci. **151**, 105661 (2021)
111. Sheth, J., Prasad, K., Puwar, T.: An objective overview of Covid-19 vaccine situation in India. Natl. J. Community Med. **13**(5), 342–345 (2022). https://doi.org/10.55489/njcm.1305202261
112. Sobel, D., Gn, M., O'Rourke Jr., T.K., Tucci, C., Pareek, G., Golijanin, D., et al.: Personal protective equipment for common urologic procedures before and during the United States COVID-19 pandemic: a single institution study. Urology. **141**, 1–6 (2020)
113. Sohrabi, C., Alsafi, Z., O'neill, N., Khan, M., Kerwan, A., Al-Jabir, A., Iosifidis, C., Agha, R.: World Health Organization declares global emergency: a review of the 2019 novel coronavirus (COVID-19). Int. J. Surg. **76**, 71–76 (2020)
114. Stanujkic, D., Karabasevic, D., Zavadskas, E.K.: A framework for the selection of a packaging design based on the SWARA method. Eng. Econ. **26**, 181–187 (2015)
115. Sungheetha, A.: COVID-19 risk minimization decision making strategy using data-driven model. J. Inf. Technol. Digit. World. **3**(1), 57–66 (2021). https://doi.org/10.36548/jitdw.2021.1.006
116. Tack, J., Schol, J., Geeraerts, A., Huang, I.H., Mori, H., Scarpellini, E., et al.: A survey on the impact of the COVID-19 pandemic on motility and functional investigations in Europe and considerations for recommencing activities in the early recovery phase. Neurogastroenterol. Motil. **32**, e13926 (2020)
117. The Hindu: India approves COVID-19 vaccines Covishield and Covaxin for emergency use. The Hindu (2021)
118. Thiagarajan, K.: Why is India having a covid-19 surge? BMJ. **373**, n1124 (2021). https://doi.org/10.1136/bmj.n1124
119. Times of India: COVID-19 vaccine India: 8 coronavirus vaccines at various trial stages in India: key details. Times of India (2020)
120. Umakanthan, S., Patil, S., Subramaniam, N., Sharma, R.: COVID-19 vaccine hesitancy and resistance in India explored through a population-based longitudinal survey. Vaccine. **9**(10), 1064 (2021)

121. Vordos, N., Gkika, D.A., Maliaris, G., Tilkeridis, K.E., Antoniou, A., Bandekas, D.V., et al.: How 3D printing and social media tackles the P.P.E. shortage during Covid-19 pandemic. Saf. Sci. **130**, 104870 (2020)
122. Wang, J., Du, G.: COVID-19 may transmit through aerosol. Ir. J. Med. Sci. (1971-). **189**(4), 1143–1144 (2020)
123. Wang, C., Pan, R., Wan, X., Tan, Y., Xu, L., McIntyre, R.S., et al.: A longitudinal study on the mental health of general population during the COVID-19 epidemic in China. Brain Behav. Immun. **87**, 40–48 (2020)
124. Wells, C.R., Townsend, J.P., Pandey, A., Moghadas, S.M., Krieger, G., Singer, B., et al.: Optimal COVID-19 quarantine and testing strategies. Nat. Commun. **12**(1), 1–9 (2021)
125. WHO: (2020). Retrieved from https://covid19.who.int/ on Nov 26 2022
126. World Health Organization: Situation updates on March 26, 2020 (2020). https://covid19.who.int/
127. Xu, S., Li, Y.: Beware of the second wave of Covid-19. Lancet. **395**(10233), 1321–1322 (2020)
128. Yi, Y., Lagniton, P.N.P., Ye, S., Li, E., Xu, R.-H.: COVID-19: what has been learned and to be learned about the novel coronavirus disease. Int. J. Biol. Sci. **16**(10), 1753–1766 (2020)
129. Yichi, L., Wang, B., Peng, R., Zhou, C., Zhan, Y., Liu, Z., Jiang, X., Zhao, B.: Mathematical modeling and epidemic prediction of COVID-19 and its significance to epidemic prevention and control measures. Ann. Infect. Dis. Epidemiol. **5**(1), 1–9 (2020)
130. Yildirim, F.S., Sayan, M., Sanlidag, T., Uzun, B., Ozsahin, D.U., Ozsah, I.: Comparative evaluation of the treatment of COVID-19 with multicriteria decision-making techniques. J. Healthc. Eng. **2021**, 1–11, 8864522 (2021). https://doi.org/10.1155/2021/8864522
131. Zhai, P., Ding, Y., Wu, X., Long, J., Zhong, Y., Li, Y.: The epidemiology, diagnosis and treatment of COVID-19. Int. J. Antimicrob. Agents. **55**, 105955 (2020)
132. Zhong, B.L., Luo, W., Li, H.M., Zhang, Q.Q., Liu, X.G., Li, W.T., et al.: Knowledge, attitudes, and practices towards COVID-19 among Chinese residents during the rapid rise period of the COVID-19 outbreak: a quick online cross-sectional survey. Int. J. Biol. Sci. **16**(10), 1745 (2020)
133. Zolfani, S.H., Bahrami, M.: Investment prioritizing in high tech industries based on SWARA-COPRAS approach. Technol. Econ. Dev. Econ. **20**, 534–553 (2014). https://doi.org/10.3846/20294913.2014.881435
134. Zolfani, S.H., Chatterjee, P.: Comparative evaluation of sustainable design based on step-wise weight assessment ratio analysis (SWARA) and best worst method (BWM) methods: a perspective on household furnishing materials. Symmetry. **11**, 74 (2019). https://doi.org/10.3390/sym11010074

Crisis Management, Internet, and AI: Information in the Age of COVID-19 and Future Pandemics

Karim Darban, Smail Kabbaj, and Khawla Esmaoui

1 Introduction

Social media applications help people around the world to connect, share moments, stay informed, and exchange information's almost instantly. One of the most important social trends of the past decade has been the launch and rise of the social media's Facebook and Twitter [6]. However, it also enables people to share and amplify fake news, kindle crises, and hold onto their beliefs, which are sometimes in opposition to reality, a psychological mechanism behind the current excesses of disinformation that might entail refuting scientific truths with little to no arguments, which explain the popularity of online-made communities like anti-vaxxers and flat-earthers [24]. Opinions like these have likely always been there, the only distinction is that they did not reach the broad and enormous audience that was reserved for the mass media because they were limited to small circles and their propagation was very slow. Social networks have democratized massification, making it less the exclusive domain of traditional media. From that point forward, the characteristics of "information" deviate from historical norms: In order to provide logical safeguards for the information spread, mass-information resulting in general opinion was shared by official sources and certified (public or private) professional media. Now, this is not the case, or more accurately, the traditional media have lost the relative monopoly they once had [31].

Unlike traditional media, social media operates under a different logic: With traditional media, the consumer could adopt one of two attitudes, depending on his preferences and affinities: to watch or not to watch said media. His capacity for choice expands thanks to social media in two ways: there are many more platforms

K. Darban (✉) · S. Kabbaj · K. Esmaoui
University Hassan II, Casablanca, Morocco
e-mail: dr.karim.darban@gmail.com; s.kabbaj@encgcasa.ma; khawlaesmaoui95@gmail.com

available, and he can create content on his own. This initially results in a dispersion of the offer, with each one trying to more or less mimic the norms of the traditional media. However, as the process develops, this tendency lessens to the point where consumers will cluster according to their shared interests and tolerate less and less "information" that contradicts their initial beliefs, this will be accomplished both manually, as the user will unfollow untolerated or uninteresting information, and vice versa, and automatically, as the algorithms of these social-apps keeps filtering the "likable" content for each user depending on the earlier manual information filtering [16].

Since its outbreak, the COVID-19 pandemic has been linked to the construct of an infodemic, in which misinformation fill knowledge gaps or serve as the counterpoint to a deluge of occasionally contradictory information coming from different sources, which causes mass confusion and nervousness [28]. Some authors of controversial but highly consumed and shared content over the internet (on the wearing of masks, treatments, or vaccinations) will even trespass the fence from digital to traditional media, like Didier Raoult, depicted in Fig. 1, author of more
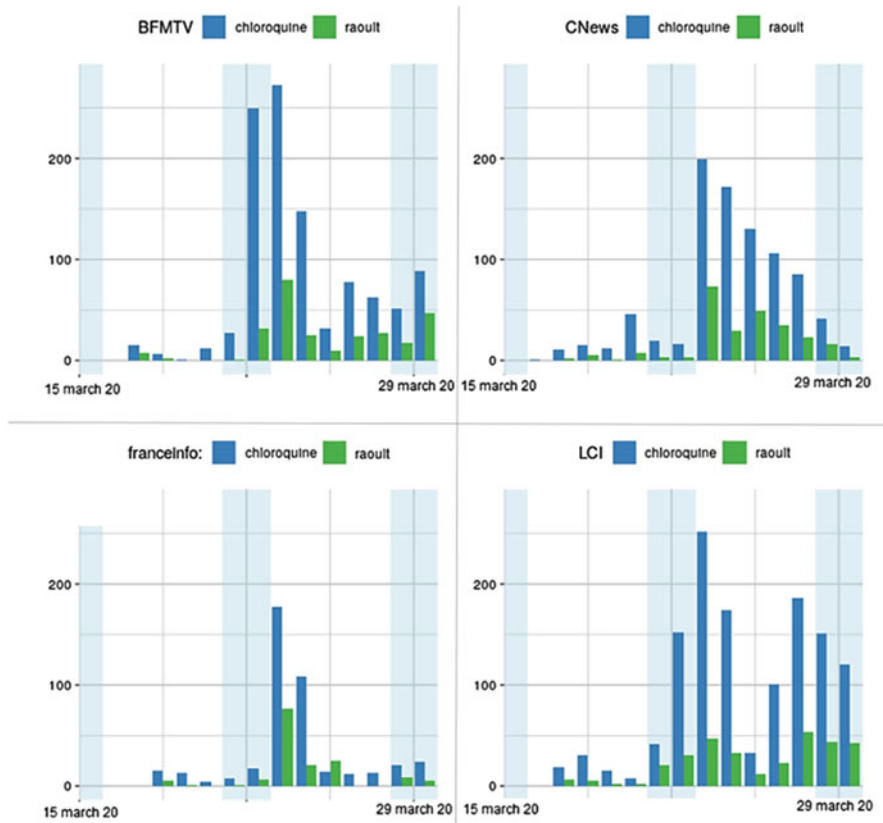
Fig. 1 Comparison of the number of pronunciations of the terms "chloroquine" promoted by Didier Raoult and "Raoult" on the major French news channels continuously for 2 weeks. (Source: French National Audiovisual Institute [14])

than a hundred YouTube videos with 400k to 4M views (by December 2022), making the internet and its social medias not only more consumed than traditional media [26] but a rudder that directs the content and the speakers of traditional media and thus the general opinion, a ruder that can, dangerously enough, be held by anyone in times of crisis.

2   Monitoring the Content: The Use of AI Against Internet Misinformation During COVID-19

The COVID-19 pandemic has had a significant impact on the way we communicate and access information. With lockdowns and social distancing measures in place, social media and other digital platforms have become an important way for people to stay connected and informed. At the same time, the rapid spread of misinformation about COVID-19 has made it difficult for people to distinguish between reliable and unreliable sources of information. Artificial intelligence (AI) has played a crucial role in monitoring and combating the spread of false information about COVID-19.

AI has been used in a number of ways to monitor and combat the spread of misinformation about COVID-19. One approach is the use of machine learning algorithms to detect and flag misinformation on social media platforms. Machine learning techniques involve the use of algorithms that can learn from data and improve their performance over time. These algorithms can be trained on large datasets of true and false information, allowing them to learn the characteristics of each. Once trained, these algorithms can be used to classify new pieces of information as true or false. One example of a machine learning technique is the use of support vector machines, which can be used to classify text or image data, so these algorithms will be able to analyze the text and images in a post, as well as the interactions and reactions of users, to determine whether it is likely to be misinformation. Once flagged, the post can be removed or labeled with a warning, reducing its visibility and impact. For example, as shown in Fig. 2, Facebook has used it to identify and remove false or misleading content related to COVID-19 [13]. It has also been used by Twitter to identify and remove accounts that are spreading misinformation about COVID-19 [29].

Another approach is the use of natural language processing (NLP) to identify and classify misinformation on social media platforms. NLP algorithms can analyze the text of a post and classify it as true, false, or partially true based on its content and context. This allows for the creation of fact-checking systems that can automatically identify and flag misinformation for further review [9, 10]. Artificial intelligence was also useful to track and analyze the spread of misinformation about COVID-19 on social media platforms. This can be done by analyzing the patterns of sharing and engaging with misinformation, as well as the sources and channels through which it is disseminated. This information can be used to identify and target misinformation at its source, and to develop strategies for mitigating its spread [8].
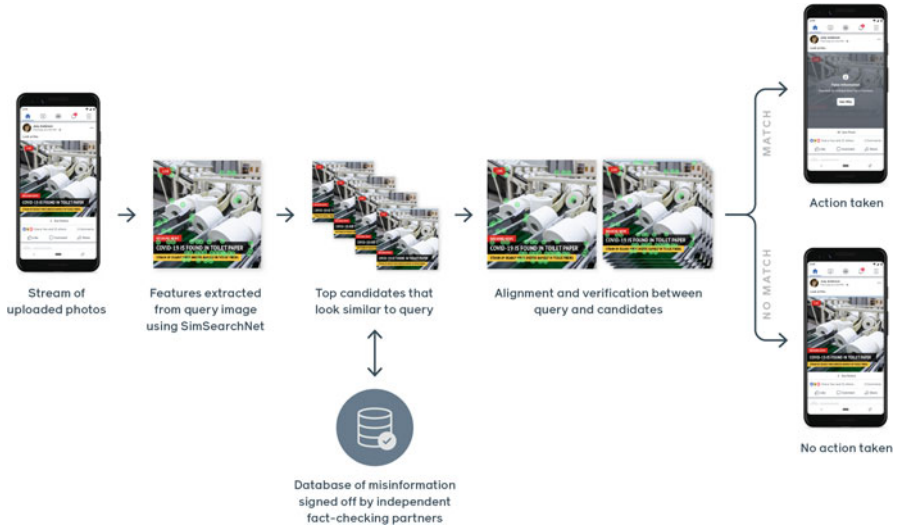
Fig. 2 Life cycle of Facebook images as they get matched against a database of certified misinformation. (Source: Facebook [13])

Researchers have also used AI to track the spread of misinformation about COVID-19 on social media platforms [4]. This has included identifying false or misleading content, as well as analyzing the way in which such content is shared and disseminated on social media. For instance, academics have used AI to analyze Twitter data to understand how people's attitudes toward COVID-19 and related policies have changed over time [11]. Pattern recognition techniques involve the use of algorithms to identify patterns and characteristics of false information. These algorithms can analyze the language, tone, and other features of a piece of content to determine whether it is likely to be true or false. One example of a pattern recognition technique is the use of sentiment analysis, which involves analyzing the emotional content of a piece of text to determine its overall sentiment.

Despite the potential of AI in monitoring and combating the spread of misinformation about COVID-19, there are a number of challenges and limitations to these approaches. One challenge is the need for high-quality training data to ensure the accuracy and effectiveness of machine learning algorithms. This can be difficult to obtain, especially in the context of rapidly evolving events such as the COVID-19 pandemic. This can also result in deleting safe content or falsely banning their authors. Another challenge is the issue of bias in AI systems. If the training data is biased, the algorithms will be biased as well, potentially leading to the amplification of misinformation or the suppression of accurate information. This issue has been particularly problematic in the context of social media platforms, where the algorithms used to identify and flag misinformation may be influenced by the biases of their creators. There are also still limitations to the ability of AI to understand and interpret the context and nuance of every language, which

can affect its accuracy in identifying and classifying misinformation. Additionally, AI systems can be vulnerable to manipulation and spoofing, making it easier for misinformation to evade detection. Finally, the constantly evolving nature of the COVID-19 pandemic, which requires the AI systems to be updated and refined on an ongoing basis, as new information becomes available and the spread of the virus changes, the algorithms need to be able to adapt and accurately identify misinformation related to the current situation.

AI has played a significant role in the effort to monitor and combat the spread of misinformation about COVID-19. However, it is important to recognize the challenges and limitations of these approaches, and to take steps to address them in order to effectively mitigate the impact of misinformation on public health.

3   Exploiting the Content: The Use of AI and Social Media to Manage Information in the Case of a Global Crisis

In recent years, social media has become an increasingly important source of information during crises and emergencies. From pandemics to natural disasters, individuals and organizations rely on platforms like Twitter, Facebook, and Instagram to stay informed and share updates in real time. However, the vast amount of data generated by social media can be overwhelming, making it difficult for crisis management teams to identify and prioritize relevant information. Artificial intelligence (AI) can be used to effectively sort and analyze social media data, providing crisis management teams with valuable insights and helping them make more informed decisions.

Internet and its social medias are frequently portrayed as an infrastructure that enables organizations such as governments, local authorities, and companies to communicate with citizens from top to bottom and, on the other hand, to increase citizen feedback information from the down to top to improve the observation of an event [27]. The research in the area of crisis informatics [25] has emphasized the changes brought about by social media and how individuals have used them to progressively communicate about an occurrence, inform themselves, and organize themselves to act. According to the academics, social networks have quickly emerged as a crucial channel for communication and information exchange. Karimiziarani et al. [21] and Interdonato et al. [19] demonstrated that crisis management organizations were already interested in extracting information from social network data, whether in the form of reports, "useful" sorting, or summaries of the information gathered. Even if the chance to use a fresh source of information to comprehend the crisis's theater and better respond to it is fully absorbed, the truth remains that its use might be expensive in terms of human resources, even when the circumstance calls for managers to act promptly. This is how a new aspect of the use of artificial intelligence (AI) in crisis management has opened up.

Table 1 Computer or artificial intelligence (AI)-assisted systems for social media content filtering

Tweedr	Twitris	ESA	AIDR	Twitcident
Ashktorab et al. [3]	Jadhav et al. [20]	Cameron et al. [7]	Imran et al. [17]	Abel et al. [1]

Based on a review of the literature, Imran et al. [18] list the typical use of data from social networks in crisis management: Binary classifications that determine whether the data is relevant or not, data segmentation that allows semantically similar tweets to be grouped together and reduces the amount of information that humans will ultimately have to read and interpret, automated generation of summaries that once again allows for a reduction in the amount of information that needs to be processed by humans, information verification, and named entity recognition that enables semantically enriched data are all examples of data analysis techniques.

One particular goal is persistent and has long been the primary one when leveraging AI data from social networks: situational awareness, which is described as "understanding the crisis situation" [15]. Concretely, the goal is to give the crisis management cells a shared understanding of the crisis situation (common operational picture – COP). A number of computer or artificial intelligence (AI) systems can be given as illustrated in Table 1.

Twitcident [1], for instance, is a structure for filtering and evaluating tweets that was developed by scientists from the Delft University of Technology to crowdsource data about crises. The system, whose architecture is described in Fig. 3, has been put through testing as a support program for the Dutch police and fire department in 2012. Their paper presents the results of an empirical study that sought to investigate the impact of Twitter on information diffusion in emergency situations. The results show that Twitter is an effective platform for quickly disseminating accurate information about emergency situations. The authors found that Twitter users are more likely to spread information quickly and accurately than traditional media outlets, and the accuracy of the information is largely unaffected by time, location, or the size of the network. Furthermore, the study revealed that Twitter users tend to spread both accurate and inaccurate information, with the accuracy of the information increasing over time. In conclusion, the authors suggest that Twitter could be an effective tool for disseminating accurate information during a crisis.

The authors explain the significance of going beyond situational awareness in [12, 32] and of providing, at the output of the AI processing module, data from social networks, information targeted to the specific needs of decision-makers. They discuss a comprehensive architecture for an actionable collaborative Common Operational Picture (COP) in crisis situations, powered by social media data. The architecture is composed of three layers: the knowledge layer, the interaction layer, and the communication layer. The knowledge layer is responsible for collecting and analyzing social media data, while the interaction layer is responsible for providing the collaboration functions such as group chat and audio/video conferencing. Finally, the communication layer is responsible for providing a secure
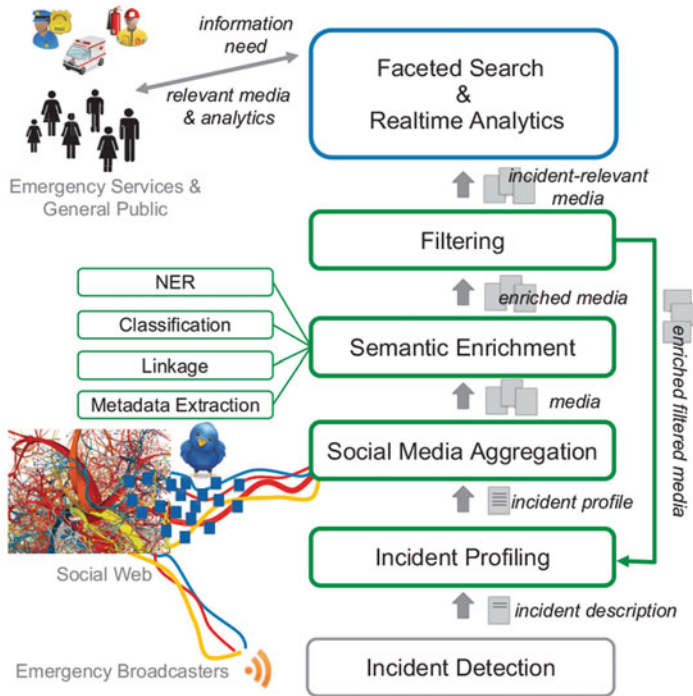
Fig. 3 Twitcident architecture [1]

communication infrastructure. They also present a prototype application based on the proposed architecture and its evaluation results.

We continue to acknowledge that social media's contribution to crisis management has both an organizational and an informational component: Informational in the sense that all of the released content serves as a source of pertinent data for assessing what is occurring in the present, and organizational in terms of working together to address the issue. The crisis is usually taking place in an exceptional setting, and while it may come as a surprise and be marked by uncertainty, it is still important to know how to respond appropriately and instantaneously. To achieve this, the so-called useful knowledge to be communicated to crisis supervisors must be tailored to their particular requirements and the situational constraints must be taken into consideration in the choice and deployment of the AI modules.

There have been a number of AI models created with regard to crisis management and Benaben et al. [5] recall the COSIMMA metamodel, designed to set up a cooperative reaction to a crisis (whose ideas mirror those of the BPMN2.0). The Collaborative Situation Metamodel for crisis management (COSIMMA) is structured in two layers: a core layer that describes concepts and relations of any collaborative situation and a specific layer dedicated to crisis management that inherits concepts from the core layer and adds more specific concepts related to

the domain. The specific layer is structured into four packages: Context, Partners, Objectives, and Behavior. The Context package includes concepts related to the environment and characteristics of the crisis situation, such as Good, People, Natural site, Civilian society, Territory, Danger, and Intrinsic risk. The Partners package includes concepts related to stakeholders and their resources and services, such as Actor, Resource on site, Service, Actor service, and Mediation service. The Objectives package includes concepts related to the goals and effects of the crisis management, such as Emerging risk, Effect, and Objective. The COSIMMA model along with social media can help crisis managers in multiple ways. First, they can provide real-time updates on the crisis, and can detect trends in the data, which can help managers make more informed decisions. Second, they can identify influencers and stakeholders, allowing managers to better target their communications and resources. Third, they can use the data to create and evaluate different scenarios, which can help managers better respond to the crisis. Finally, they can use the data to track the progress of the crisis, and make adjustments as needed.

The methodology used in Kropczynski et al. [22] is quite unique; after conducting discussions and examinations with offline crisis professionals, the authors aimed to identify the questions that 911 service representatives must try to answer for every operation. The 6 Ws came from the concept of the six questions: Who, What, When, Where, Why, and Weapons. The 6Ws can be used as an AI model to collect and analyze social media content related to a crisis. For example, the Who question can help identify who is responsible for the crisis, who is affected by it, and who is responding to it. The What question can be used to determine what is happening, what kind of content is being shared, and what type of crisis it is. The When question can help to determine when the crisis started, when new developments are occurring, and when the crisis is likely to end. The Where question can be used to identify where the crisis is occurring and where it is spreading. The Why question can be used to identify the root causes of the crisis and the motivations of the people involved.

Term frequency-inverse document frequency (TF-IDF) is a statistical measure used to evaluate the importance of a word in a document or a collection of documents [23]. It can be used by AI to monitor social media content in a similar way to how it is used by humans, by identifying the most important words or phrases in a piece of text and using them to track trends, identify key themes or topics, and understand the sentiment of users on social media. One way that AI can use TF-IDF to monitor social media content in case of crisis is by integrating it into a machine learning model. For example, a model could be trained on a large dataset of social media posts or comments, with the TF-IDF values of the words in each post or comment serving as features. The model could then be used to classify new posts or comments as positive, negative, or neutral based on their TF-IDF values. Another way that AI can use TF-IDF to monitor social media content is by using it as part of a natural language processing (NLP) system. By integrating TF-IDF into an NLP system, the system can identify the most important words or phrases in a piece of text and use them to understand the overall meaning and sentiment of the text. Al-Khateeb and Epiphaniou [2] used TF-IDF in their paper to find

potentially abusive language in social media posts, by comparing the frequency of certain words or phrases with that of other posts in the same corpus. The TF-IDF score indicates which words and phrases are more likely to be associated with abusive language. This can help law enforcement identify potential cyber-stalkers and online groomers, as well as provide a better understanding of the context in which such activities take place.

Graph theory can also be used as an AI algorithm to massively analyze the relationships and connections between social media users in the case of crisis [30]. A social media graph is a mathematical representation of the connections between users, with each user represented as a node and the connections between them represented as edges. One application of graph theory in social media monitoring is the identification of key influencers within a particular network. For example, if we were interested in understanding how a particular topic was being disseminated through a social media platform, we might look for users with high betweenness centrality, as they are likely to be key spreaders of information. Another application is the identification of communities within a social media platform. By analyzing the connections between users, it is possible to identify clusters of users who are more closely connected to each other than to users outside of their cluster. These clusters may represent communities of users who share similar interests or beliefs, and can be useful for understanding how certain ideas or topics are being created or discussed within different parts of a social media platform. However, there are also some limitations to this approach. One is the potential for privacy concerns, by analyzing the connections between social media users. Overall, the combination of AI and graph theory offers a powerful toolkit for organizations looking to effectively monitor and analyze social media data. By automating the process of extracting and classifying relevant information, as well as analyzing the connections between users, it is possible to gain valuable insights into the dynamics of social media platforms.

4   Conclusion and Future Research Recommendations

This chapter has analyzed the role of AI and social media in crisis management during the COVID-19 pandemic. Our findings show that AI and social media can be valuable tools for detecting and combating the spread of misinformation on social media platforms, as well as for facilitating communication and the flow of information during a crisis. We have explored various machine learning techniques, including support vector machines, named entity recognition, and graph theory, that can be used to analyze and monitor social media content during a crisis.

The use of AI and social media in the context of the COVID-19 pandemic illustrates the potential of these technologies to both facilitate and disrupt communication and the flow of information. On the one hand, AI and social media have provided a valuable way for people to stay connected and informed during the pandemic. On the other hand, the spread of misinformation has posed significant challenges, and the use of AI by social media platforms to combat this problem

has raised questions about the role of these platforms in moderating content and protecting users from misinformation. Our analysis has identified potential challenges, such as the potential for biased algorithms. There have been concerns that AI systems may reflect the biases of their creators or the data they are trained on, leading to discriminatory outcomes. In the context of crisis management, this could have serious consequences, as biased algorithms of such private organizations could result in the suppression of important information or the amplification of misinformation.

Despite these challenges, the use of AI and social media in crisis management has the potential to be highly beneficial. AI can help monitor and analyze social media activity in real time, providing valuable insights into the spread of misinformation and the effectiveness of crisis management.

Moving forward, our study suggests several future directions for research in this area. Some potential recommendations for future research include the following:

Incorporating real-time data from multiple sources: Future research could focus on ways to more effectively incorporate real-time data from a variety of sources, including traditional news outlets and government agencies, into AI and social media analysis. This could help crisis managers get a more comprehensive understanding of a crisis situation and make more informed decisions.

Enhancing the accuracy and precision of AI and social media analysis: While current techniques such as natural language processing, deep learning, and machine learning have shown promise in analyzing social media data during a crisis, there is still room for improvement in terms of accuracy and precision. Research could be conducted to identify ways to further refine these techniques and make them more effective in crisis situations.

Exploring the ethical and societal implications of using AI and social media in crisis management: As AI and social media become more prevalent in crisis management, it will be important to consider the ethical and societal implications of their use. Research could be conducted to identify and address any potential negative consequences of using these technologies in crisis situations.

Developing strategies for managing and mitigating misinformation: Misinformation can be a major issue during times of crisis, and research could be conducted on ways to effectively manage and mitigate the spread of false information through social media and other channels.

Overall, further research and development in these areas will be crucial for effectively utilizing AI, social media, and related technologies in crisis management in the future.

References

1. Abel, F., Hauff, C., Houben, G.J., Stronkman, R., Tao, K.: Twitcident: fighting fire with information from social web streams. In: Proceedings of the 21st International Conference on World Wide Web, pp. 305–308. Association for Computing Machinery, New York (2012)
2. Al-Khateeb, H.M., Epiphaniou, G.: How technology can mitigate and counteract cyber-stalking and online grooming. Comput. Fraud Secur. **2016**(1), 14–18 (2016)

3. Ashktorab, Z., Brown, C., Nandi, M., Culotta, A.: Tweedr: mining twitter to inform disaster response. In: Proceedings of ISCRAM, University Park, PA, USA, pp. 269–272, 18–21 May 2014

4. Balakrishnan, V., Zhen, N.W., Chong, S.M., Han, G.J., Lee, T.J.: Infodemic and fake news–a comprehensive overview of its global magnitude during the COVID-19 pandemic in 2021: a scoping review. Int. J. Disaster Risk Reduct. **78**, 103144 (2022)

5. Benaben, F., Fertier, A., Montarnal, A., Mu, W., Jiang, Z., Truptil, Lamothe, J.: An AI framework and a metamodel for collaborative situations: application to crisis management contexts. J. Contingencies Crisis Manag. **28**(3), 291–306 (2020)

6. Bentivegna, S., Rita, M., Anna, S.: The agenda-building power of Facebook and Twitter: the case of the 2018 Italian general election. In: Electoral Campaigns, Media, and the New World of Digital Politics, pp. 124–142. University of Michigan Press (2022)

7. Cameron, M., Yin, J., Karimi, S., Robinson, B.: ESA: emergency situation awareness via microbloggers. In: Proceedings of the 21st ACM International Conference on Information and Knowledge Management, pp. 2701–2703 (2012)

8. Chamola, V., Hassija, V., Gupta, V., Guizani, M.: A comprehensive review of the COVID-19 pandemic and the role of IoT, drones, AI, blockchain, and 5G in managing its impact. IEEE Access. **8**, 90225–90265 (2020)

9. Chen, Q., Leaman, R., Allot, A., Luo, L., Wei, C.H., Yan, S., Lu, Z.: Artificial intelligence in action: addressing the COVID-19 pandemic with natural language processing. Annu. Rev. Biomed. Data Sci. **4**, 313–339 (2021)

10. Chowdhary, K.: Natural language processing. In: Fundamentals of Artificial Intelligence, pp. 603–649. Springer (2020)

11. Cinelli, M., De Francisci Morales, G., Galeazzi, A., Quattrociocchi, W., Starnini, M.: The echo chamber effect on social media. Proc. Natl. Acad. Sci. **118**(9), e2023301118 (2021)

12. Coche, J., Montarnal, A., Tapia, A., Benaben, F.: Actionable collaborative common operational picture in crisis situation: a comprehensive architecture powered with social media data. In: Working Conference on Virtual Enterprises, pp. 151–162. Springer, Cham (2019)

13. Facebook: Using AI to detect COVID-19 misinformation and exploitative content (2020). Retrieved from https://ai.facebook.com/blog/using-ai-to-detect-covid-19-misinformation-and-exploitative-content/

14. French National Audiovisual Institute: ÉTUDE INA. Comment Didier Raoult et la chloroquine ont surgi dans le traitement médiatique du coronavirus (2020). Retrieved from https://larevuedesmedias.ina.fr/etude-coronavirus-covid19-traitement-mediatique-raoult-chloroquine

15. Gjøsæter, T., Radianti, J., Chen, W.: Understanding situational disabilities and situational awareness in disasters. In: Proceedings of the 16th ISCRAM Conference – València, Spain, May 2019

16. Gkikas, D.C., Tzafilkou, K., Theodoridis, P.K., Garmpis, A., Gkikas, M.C.: How do text characteristics impact user engagement in social media posts: modeling content readability, length, and hashtags number in Facebook. Int. J. Inf. Manage. Data Insights. **2**(1), 100067 (2022)

17. Imran, M., Castillo, C., Lucas, J., Meier, P., Vieweg, S.: AIDR: artificial intelligence for disaster response. In: Proceedings of the 23rd International Conference on World Wide Web, pp. 159–162. Association for Computing Machinery, New York (2014)

18. Imran, M., Castillo, C., Diaz, F., Vieweg, S.: Processing social media messages in mass emergency: survey summary. In: Companion Proceedings of the Web Conference 2018, pp. 507–511. Association for Computing Machinery, New York (2018)

19. Interdonato, R., Guillaume, J.L., Doucet, A.: A lightweight and multilingual framework for crisis information extraction from Twitter data. Soc. Netw. Anal. Min. **9**, 1–20 (2019)

20. Jadhav, A.S., Purohit, H., Kapanipathi, P., Anantharam, P., Ranabahu, A.H., Nguyen, V., et al.: Twitris 2.0: semantically empowered system for understanding perceptions from social data (2010)

21. Karimiziarani, M., Jafarzadegan, K., Abbaszadeh, P., Shao, W., Moradkhani, H.: Hazard risk awareness and disaster management: extracting the information content of twitter data. Sustain. Cities Soc. **77**, 103577 (2022)
22. Kropczynski, J., Grace, R., Coche, J., Halse, S., Obeysekare, E., Montarnal, A., et al.: Identifying actionable information on social media for emergency dispatch. In: Proceedings of the ISCRAM Asia Pacific, Wellington, New Zealand, pp. 428–438, Nov 2018
23. Liu, C.Z., Sheng, Y.X., Wei, Z.Q., Yang, Y.Q.: Research of text classification based on improved TF-IDF algorithm. In: 2018 IEEE International Conference of Intelligent Robotic and Control Engineering (IRCE), pp. 218–222. IEEE (2018)
24. Modgil, S., Singh, R.K., Gupta, S., Dennehy, D.: A confirmation bias view on social media induced polarisation during Covid-19. Inf. Syst. Front., 1–25 (2021). https://doi.org/10.1007/s10796-021-10222-9
25. Palen, L., Anderson, J., Bica, M., Castillos, C., Crowley, J., et al.: Crisis informatics: human-centered research on tech & crises: a guided bibliography developed by crisis informatics researchers. hal-02781763 (2020)
26. Richter, F.: The end of the TV era? Media use in the U.S. – Statista (2020). Retrieved from https://www.statista.com/chart/9761/daily-tv-and-internet-consumption-worldwide/
27. Rizza, C.: Social media contribution to the crisis management processes: towards a more accurate response integrating citizen-generated content and citizen-led activities. In: Handbook of Computational Social Science for Policy, pp. 421–436. Springer International Publishing, Cham (2023)
28. Starbird, K., Spiro, E., West, J.: This covid-19 misinformation went viral. Here's what we learned. The Washington Post. (2020)
29. Twitter: Twitter's response to COVID-19 (2021). Retrieved from https://blog.twitter.com/en_us/topics/company/2020/covid-19
30. Ucer, S., Ozyer, T., Alhajj, R.: Explainable artificial intelligence through graph theory by generalized social network analysis-based classifier. Sci. Rep. **12**(1), 1–17 (2022)
31. Workman, M.: An empirical study of social media exchanges about a controversial topic: confirmation bias and participant characteristics. J. Soc. Media Soc. **7**(1), 381–400 (2018)
32. Zade, H., Shah, K., Rangarajan, V., Kshirsagar, P., Imran, M., Starbird, K.: From situational awareness to actionability: towards improving the utility of social media data for crisis response. Proc. ACM Hum. Comput. Interact. **2**(CSCW), 1–18 (2018)

Index